Supported by 日本財団 THE NIPPON FOUNDATION

日 中 笹 川 医 学 奨 学 金 制 度

第３９期研究者研究報告会

研　究　報　告　集

2017 年 4 月～2018 年 3 月

公益財団法人　日中医学協会

２０１８　年　３　月　２９　日

日 本 財 団 ビ ル 大 会 議 室

目　次(発表順)

1 Influence Factors of the Radiolucent Line at Bone-Tibial component interface after Cemented Total Knee Arthroplasty
人工膝関節置換術における脛骨骨切除面での術後骨透亮像に関与する因子

京都大学大学院　顧　世忠　・・・・・・・・・　P.1

2 Comparison of the 7th and 8th editions of the UICC-TNM classification on stage 0-I lung adenocarcinoma
ステージ0-I肺腺癌におけるUICC-TNM分類の第7版および第8版の比較

東京大学医学部附属病院　王 黎明　・・・・・・・・・　P.6

3 Time-varying Pattern of Mortality and Recurrence from Papillary Thyroid Cancer: Lessons from a Long-Term Follow-Up
甲状腺乳頭癌で死亡と再発の時間によって変わるパターン:長期のフォローアップからの教訓

東京女子医科大学　董　文武　・・・・・・・・・　P.12

4 Hyperinflated lungs compress the heart during expiration in COPD patients: a new finding on dynamic-ventilation computed tomography
呼吸ダイナミックＣＴを用いた慢性閉塞性肺疾患における心臓断面積の呼吸時変化の検討

琉球大学大学院　徐　妍妍　・・・・・・・・・　P.18

5 Recreational drug use and sexual behaviors among men who have sex with men in Sichuan, China
中国四川省のMSM(men who have sex with men) におけるレクリエーショナルドラッグ使用と性行動

京都大学大学院　戴　映雪　・・・・・・・・・　P.28

6 Assessment of Mechanical Properties of WaveOne Gold NiTi Rotary Instruments
WaveOne Gold NiTiファイルの機械的特性の評価

東京医科歯科大学大学院　童　方麗　・・・・・・・・・　P.33

7 Thoracoscopic esophagectomy and lymphadenectomy in prone position followed by conduit gastric pull up in HALS
腹臥位胸腔鏡下食道切除術、HALS胃管再建術、頚部吻合術手術手技について

東北大学大学院　李　君鵬　・・・・・・・・・　P.37

8 Lactoferrin Bioconjugated Clarithromycin-Loaded Nanostructured Lipid Carriers: A New Drug Delivery System for Inflammatory Lung Diseases Therapy
ラクトフェリン結合クラリスロマイシン含有ナノ構造脂質キャリアの調製：炎症性肺疾患に対する新規薬物送達システム

名古屋市立大学大学院　趙　瑩　・・・・・・・・・　P.41

9 Development of a transitional care program for patients with chronic obstructive pulmonary disease
慢性閉塞性肺疾患患者のための移行ケアプログラムの開発

兵庫県立大学　焦　丹丹　・・・・・・・・・　P.48

10 Can Daikenchuto Benefit Enteral Nutrition Management in Critical Care Patients?
ICU患者の栄養療法における大建中湯の使用法

千葉大学大学院　石　箏箏　・・・・・・・・・　P.54

11 Characterization of niche cells in corneal limbus
角膜輪部におけるニッチ細胞の特性に関する研究

大阪大学大学院　黎　頴莉　・・・・・・・・・　P.60

12 Does the attitude toward the well-known Confucian maxim influence rumination and depression in China? A cross-sectional study
中国で孔子の名言に対する態度が反すうと抑うつに影響を与えるか:横断研究

京都大学大学院　劉　林林　・・・・・・・・・　P.67

13 Promotion of TGF-β1 monomer formation by Hydrogen sulfide contributes to its inhibitory actions on Ang II- and TGF-β-induced EMT in renal tubular cells
硫化水素によるTGF-β1単量体の形成は、Ang IIおよびTGF-β誘発した
腎尿細管上皮細胞間葉転換の阻害作用に寄与する

山梨大学大学院　黄　勇　・・・・・・・・・　P.74

14 Coronary accordion phenomenon and its OFDI characteristics
冠状動脈アコーディオン現象のOFDI影像特徴

湘南鎌倉総合病院　朱　舜明　・・・・・・・・・　P.81

15 Elucidation of the underlying mechanism by which prunella vulgaris exerts therapeutic effect on thyroiditis
夏枯草の抗甲状腺炎作用分子機構の解明

帝京大学　陳　飛　・・・・・・・・・　P.85

16 "A" elevation underlies the "X" overproduction in hydatidiform mole: an implication for the link between molar pregnancy and preeclampsia
胞状奇胎における“X”の過剰産生への“A”の関与について

東京大学医学部附属病院　王　冠　・・・・・・・・・　P.93

17 Comparison of Positioning for Preterm Infants between China and Japan
日中における早産児のポジショニングの比較

国立成育医療研究センター　夏　幸閣　・・・・・・・・・　P.98

18 Improvements in Cuff Techniques in A Lung Transplantation Model in Rats: Device Improvement and Procedure Modification
ラットの肺移植モデルにおけるカフ技術の改善：装置の改善および処置の変更

京都大学大学院　田　東　・・・・・・・・・　P.105

19 Long-term effects of antihypertensive therapy on cardiovascular events and new onset diabetes mellitus in high-risk hypertensive patients in Japan
カンデサルタンとアムロジピンが日本人ハイリスク高血圧患者の10年超の予後に及ぼす影響：CASE-J 10

京都大学大学院　劉　金梁　・・・・・・・・・　P.110

20 The Influence of Storage Temperature and Time Before Freeze Processing on Stem Cells Quality of Cord Blood Products
凍結処理前の貯蔵温度及び時間による臍帯血幹細胞の品質への影響

日本赤十字社　葉　盛　・・・・・・・・・　P.116

21 Direct reprogramming of patients' fibroblasts to neurons to understand neurodegenerative diseases
患者の線維芽細胞をニューロンに直接再プログラムした神経変性疾患の理解

大阪大学医学部附属病院　金　銀実　・・・・・・・・・　P.124

22 Topographic distribution influences the prognostic impact of CD68 and CD204 positive macrophages in non-small cell lung cancer
非小細胞癌浸潤マクロファージの臨床病理学意義；浸潤部位別の検討

秋田大学大学院　李　卓　・・・・・・・・・　P.131

23 18F-Sodium Fluoride Dynamic PET/CT in patients with intracranial tumors
18F- Sodium Fluoride ダイナミックPET/CT検査を用いた脳腫瘍評価に関する後向き研究

横浜市立大学大学院　劉　恩濤　・・・・・・・・・　P.138

24 Relationships between time pressure, relational coordination with nursing managers, and burnout in Japanese home-visiting nurses
日本人訪問看護師の時間圧力、看護管理者との関係調整、バーンアウトとの関係

東京大学大学院　曹　暁翼　・・・・・・・・・　P.144

資　料　日中笹川医学奨学金制度第39期研究者一覧　・・・・・・・・・　P.151

Influence Factors of the Radiolucent Line at Bone-Tibial component interface after Cemented Total Knee Arthroplasty

人工膝関節置換術における脛骨骨切除面での術後骨透亮像に関与する因子

研究者氏名　顧　世忠（第 39 期笹川医学研究者）
中国所属機関　中国医科大学附属第一医院骨科、運動医学/関節外科
日本研究機関　京都大学医学部附属病院整形外科
指導責任者　松田　秀一　教授，栗山　新一　助教

Abstract:

Because the importance of a radiograph for evaluation of total knee arthroplasty (TKA) aseptic loosening is obvious. The presence of radiolucent lines may result in micromotion between the bone-cement or implant-cement interface, usually leading to bone resorption or even aseptic loosening. The radiolucent lines have been described to occurred either immediately TKA or within 2 years of TKA. Our purpose of the study is to assess the influence factors of the radiolucent lines in the interface between tibial bone cutting and cement after the bi-surface of primary TKA on short term. One hundred thirty-four knees in 107 patients undergoing cemented primary total knee arthroplasty (TKA) between Dec 2010 and Jun 2015 were retrospectively examined at kyoto university department hospital. The mean age of patients at the time of surgery was 74.4 years. All patients were followed up at least 2 years, and the mean time to follow-up was 40.3 months (range, 24–72 months). The Bi-Surface Knee System (Japan Medical Material, Kyoto, Japan) was used in all patients. The composition of the tibial components is titanium (Ti) alloy. We assessed implant position and measured the width of the radiolucent lines for the zones 1 and 2 on the AP at the tibial bone-cement interface. The maximum depth of cement penetration in tibial bone was measured in postoperative zones 1，2，3M，3L and 5 on the AP view. Multiple regression analysis and Pearson's correlation analysis were used to correlation coefficients. This study will be contributed to a peer reviewed English journal. Therefore, we apologize that we can not describe the result and discussion sections in this study.

Keywords: cement, radiolucent lines, tibial component, total knee arthroplasty, zone, aseptic loosening

Introduction:

Total knee arthroplasty(TKA) as a very reliable and effective treatment of knee arthritis, can improve the patient's pain and function, quality of life, and satisfaction, with survival rates of over 90% at follow-up over 10 years [1–6]. As the quantity of primary TKA being operated increases every year, the quantity of revision TKA rising steadily, projected to increase by 601% from 2005 to 2030 [7]. Therefore, the good fixation component is a prior condition to achieve long-term success of the implant [8]. In other words, reducing or delaying revision TKA is also crucial. However, aseptic loosening is cited to be the most common reason of failure in the primary TKA and also the main reason for the revision TKA [6,9,10], as Sharkey et al [10] reported that aseptic loosening accounts for 39.9% of revisions in a 10-year update. To overcome the major postoperative complication, a lot of orthopedic surgeons use bone cement to fix the tibia interface.

Cementing techniques have been developed rapidly in recent decades. The fixation strength of tibial component can be improved by improving the fixation of tibia. The underlying mechanism of aseptic loosening is unknown and is

believed to have multiple causes. The aseptic loosening may be attributed to changes in bone morphosis after TKA. However the importance of a radiograph for evaluation of TKA aseptic loosening is obvious, in previous studies on the factors influencing the development of radiolucent lines and tibial component loosening, therefore the importance of radiolucent lines is known to all [11]. The radiolucent lines exist between implant and bone interface due to the radiolucent lines potential association with aseptic loosening. Radiolucent lines are defined as radiolucent intervals between the bone-cement or implant-cement interfaces [12]. The presence of radiolucent lines may result in micromotion between the bone-cement or implant-cement interface, usually leading to bone resorption or even aseptic loosening [13]. The radiolucent lines have been described to occurred either immediately TKA or within 2 years of TKA [14]. Some studies showed the postoperative appearance rates of radiolucent lines under the tibial component more evident than under the femoral component. We also noticed the occurrence of radiolucent lines in some patients' radiography under the tibial component during postoperative follow-up.

This time we studied the radiolucent lines through tibial bone-cement interface. Our purpose of the study is to assess the influence factors of the radiolucent lines in the interface between tibial bone cutting and cement after the bi-surface of primary TKA on short term to improve the longevity of the tibial component.

Materials and Methods:

One hundred thirty-four knees (right, 68 knees; left, 66 knees) in 107 patients (88 women, 19 men) undergoing cemented primary total knee arthroplasty (TKA) between Dec 2010 and Jun 2015 were retrospectively examined. The preoperative diagnosis was varus osteoarthritis in all knees. The mean age of patients at the time of surgery was 74.4 years (range, 58–86 years). Twenty-seven patients were operated with bilateral TKA, but not at the same time. The exclusion criteria were lost follow-up or information, with serious bone defects which require metal augmentation or bone grafting, postoperative high tibial osteotomy, and with infection after operation. The mean body mass index (BMI) at surgery was 26.0 kg/m² (range, 16.8–38.9 kg/m²). All patients were followed up at least 2 years, and the mean time to follow-up was 40.3 months (range, 24–72 months). The mean preoperative femorotibial angle (FTA) was 185.0° (range, 170.6–197.1°) (Table. 1).

The Bi-Surface Knee System (Japan Medical Material, Kyoto, Japan) was used in all patients. The composition of the tibial components is titanium (Ti) alloy. The lengths of Bi-Surface tibial keels were 42-48 mm. The high-viscosity cement (HVC) (Simplex P; Stryker, USA) was used for fixing the femoral and tibial components to femoral and tibial cut surface, respectively. The thickness of polyethylene inserts ranged from 9 to 17 mm was used. All patients underwent a same preparation of the tibia. In this study, it was evaluated the interface between tibial cutting surface and cement using intraoperative or early postoperative, 2 year postoperative anteroposterior (AP) radiographs.

In the radiographic evaluation, the tibial component was divided into five zones on the AP view [12,15]. We assessed implant position and measured the width of the radiolucent lines for the zones 1 (medial) and 2 (lateral) on the AP at the tibial cutting surface and cement interface [12] (Fig. 1), and calculated the difference between the early postoperative and 2 year postoperative radiographs. The tibial component was defined as radiographically loose if the radiolucent line was seen in all zones, or if the component had migrated. Also the early postoperative and 2 year postoperative AP view was reviewed to ensure that the tibial component was placed with underhang or overhang (Fig. 2, 3). Underhang and overhang were measured on both medial and lateral sides of the tibia and expressed as a positive and negative distance. The maximum depth of cement penetration in tibial bone was measured in postoperative zones 1 (medial)，2 (lateral)，3M，3L and 5 on the AP view calibrated to 0.1 mm (Fig. 4). The depth of cement penetration zones 3M, 3L and 5

represented the keel area. For the surgeon the maximum depth of cement penetration might be an easier parameter to measure than the mean penetration. The range of flexion was also measured using goniometer at 2 year postoperative follow-up. The mean postoperative hip-knee-ankle angle (HKA) was measured. Measurements were performed three times to minimize measurement errors by one surgeon in a computer imaging software.

Continuous variables were stated as mean ± standard deviation (SD) and range (minimum–maximum). Multiple regression analysis was used to identify correlations between the medial tibial radiolucent lines and age or BMI or sex. $P < 0.05$ results was considered as statistical significance. Pearson's correlation coefficient analysis was used to correlation coefficients. The depths of cement penetration were analyzed.

Results and Discussions:

This study will be contributed to a peer reviewed English journal. Therefore, we apologize that we can not describe the result and discussion sections in this study.

References:

[1] Abdeen AR, Collen SR, Collen SB, Vince KG. Fifteen-year to 19-year follow-up of the Insall-Burstein-1 total knee arthroplasty. J Arthroplasty 2010;25:173–8.

[2] Nakamura S, Ito H, Nakamura K, Kuriyama S, Furu M, Matsuda S. Long-Term Durability of Ceramic Tri-Condylar Knee Implants: A Minimum 15-Year Follow-Up. J Arthroplasty 2017;32:1874–9.

[3] Argenson J-NA, Parratte S, Ashour A, Saintmard B, Aubaniac J-M. The outcome of rotating-platform total knee arthroplasty with cement at a minimum of ten years of follow-up. J Bone Joint Surg Am 2012;94:638–44.

[4] Schwartz AJ, Della Valle CJ, Rosenberg AG, Jacobs JJ, Berger RA, Galante JO. Cruciate-retaining TKA using a third-generation system with a four-pegged tibial component: a minimum 10-year followup note. Clin Orthop 2010;468:2160–7.

[5] Nakamura S, Kobayashi M, Ito H, Nakamura K, Ueo T, Nakamura T. The Bi-Surface total knee arthroplasty: minimum 10-year follow-up study. The Knee 2010;17:274–8.

[6] Faris PM, Ritter MA, Davis KE, Priscu HM. Ten-Year Outcome Comparison of the Anatomical Graduated Component and Vanguard Total Knee Arthroplasty Systems. J Arthroplasty 2015;30:1733–5.

[7] Bozic KJ, Kurtz SM, Lau E, Ong K, Chiu V, Vail TP, et al. The epidemiology of revision total knee arthroplasty in the United States. Clin Orthop 2010;468:45–51.

[8] Pijls BG, Valstar ER, Nouta K-A, Plevier JW, Fiocco M, Middeldorp S, et al. Early migration of tibial components is associated with late revision: a systematic review and meta-analysis of 21,000 knee arthroplasties. Acta Orthop 2012;83:614–24.

[9] Srinivasan P, Miller MA, Verdonschot N, Mann KA, Janssen D. Strain shielding in trabecular bone at the tibial cement-bone interface. J Mech Behav Biomed Mater 2017;66:181–6.

[10] Sundfeldt M, Carlsson LV, Johansson CB, Thomsen P, Gretzer C. Aseptic loosening, not only a question of wear: a review of different theories. Acta Orthop 2006;77:177–97.

[11] Martin JR, Watts CD, Levy DL, Miner TM, Springer BD, Kim RH. Tibial Tray Thickness Significantly Increases Medial Tibial Bone Resorption in Cobalt–Chromium Total Knee Arthroplasty Implants. J Arthroplasty 2017;32:79–82.

[12] Meneghini RM, Mont MA, Backstein DB, Bourne RB, Dennis DA, Scuderi GR. Development of a Modern Knee

Society Radiographic Evaluation System and Methodology for Total Knee Arthroplasty. J Arthroplasty 2015;30:2311–4.

[13] Sherman RM, Byrick RJ, Kay JC, Sullivan TR, Waddell JP. The role of lavage in preventing hemodynamic and blood-gas changes during cemented arthroplasty. J Bone Jt Surg 1983;65:500–6.

[14] Hazelwood KJ, O'Rourke M, Stamos VP, McMillan RD, Beigler D, Robb WJ. Case series report: Early cement-implant interface fixation failure in total knee replacement. The Knee 2015;22:424–8.

[15] Scuderi GR, Bourne RB, Noble PC, Benjamin JB, Lonner JH, Scott WN. The New Knee Society Knee Scoring System. Clin Orthop 2012;470:3–19.

Table 1. Characteristics of patients.

Characteristics	
Female, N (%)	88 (82.2)
Age, years (SD)	74.4 (6.5)
Right Side, N (%)	68 (63.6)
BMI, kg/m² (SD)	26.0 (4.0)
Follow-up, months (SD)	40.3 (13.1)
Preoperative FTA, degree (SD)	185.0 (5.2)

Table 2. The depth of cement penetration in tibia on the AP.

Cement penetration	Mean(mm)	Range(mm)
Zone 1	2.5	0-7.7
Zone 2	3.6	0-17.7
Zone 3M	3.0	0-8.1
Zone 3L	3.2	0-9.6
Zone 5	5.2	0-33.5

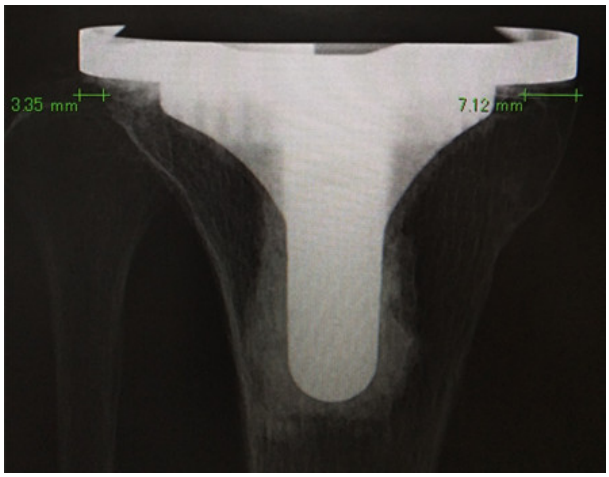

Fig 1. The width of the radiolucent lines for the zones 1 (medial) and 2 (lateral) on the AP.

Fig 2. Intraoperative or early postoperative (left) and 2 year postoperative medial tibia overhang (right).

Fig 3. Intraoperative or early postoperative (left) and 2 year postoperative medial tibia underhang (right).

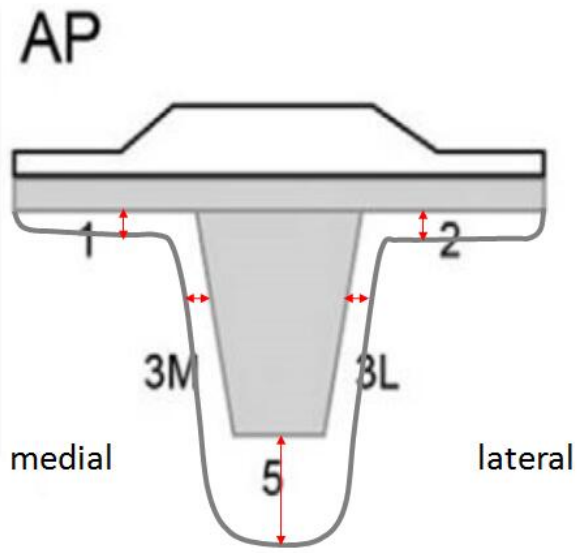

Fig 4. The cement penetration zones at tibia.

注：本研究は今後英文雑誌に投稿予定である。

作成日：2018 年 2 月 27 日

Comparison of the 7th and 8th editions of the UICC-TNM classification on stage 0-I lung adenocarcinoma

ステージ 0-I 肺腺癌における UICC-TNM 分類の第 7 版および第 8 版の比較

研究者氏名　王　黎明（第 39 期笹川医学研究者）
中国所属機関　中国医科大学附属第一医院胸部外科
日本研究機関　東京大学医学部附属病院呼吸器外科
指導責任者　中島　淳 教授

Abstract:

Objectives: Early lung adenocarcinoma has been more frequently found recently. The 8th edition of the UICC-TNM classification for lung cancer has been effective since January 2017. This study aims to elucidate advantages of the current classification for patients with stage 0-I lung adenocarcinoma, in comparison with the older one.

Methods: We retrospectively reviewed the data of clinical stage I (7th edition) lung adenocarcinoma patients who underwent surgery in our hospital from 2001 to 2015, and reclassified them by the 8th edition. Survival analysis was used to evaluate the impact of the two classifications on prognosis.

Results: We registered 386 cases. Clinical T-factors (8th) were significant prognostic factors for overall survival (P=0.002) and recurrence-free survival (P<0.001) by univariate analysis. However, those in the previous edition were not (P=0.948 and P=0.216 respectively). Pathological T-factors (8th) were the independent prognostic factors for overall survival (P<0.001) and recurrence-free survival (P<0.001) by multivariate analysis. In contrast, those in the previous edition were not (P=0.160 and P=0.717 respectively).

Conclusions: The 8th edition of the UICC-TNM classification predicts postoperative prognosis more precisely than the 7th one in both clinical and pathological stage 0-I lung adenocarcinoma. It probably because the stage distribution of the population which included in the research project the 8th edition based on has been changed, and the new edition develops a more accurate staging criteria for GGN, whose incidence has been increasing recently.

Key Words:

Lung cancer, adenocarcinoma, neoplasm staging, prognosis

Introduction:

Early lung adenocarcinoma has been more frequently found recently (1). The 8th edition of the UICC-TNM classification for lung cancer has been effective since January 2017. Comparing with the 7th edition, many changes had been made to stage I, and the 8th edition also initiated a new method of measuring tumor size of lung adenocarcinoma

showing GGN feature (2). In order to verify whether the new edition is better than the previous one in predicting the postoperative prognosis of the patients with stage 0-I lung adenocarcinoma and how is the accuracy of the new measuring method, we carried out this study.

Methods:

Study design and data

This is a retrospective and observational study. Lung adenocarcinoma patients with clinical stage I (according to the 7th edition of the UICC-TNM classification) who underwent surgery in our hospital from April 2001 to December 2015 were registered in the study. Preoperative HRCT and postoperative tumor-free surgical margin were required, and we excluded the patients whose pathological stage were stage II or more advanced according to the postoperative pathology, and also the ones lost during follow-up. We reassessed the data by CT images and pathology, and reclassified them according to the 8th edition of the UICC-TNM classification.

Statistical methods

We used univariate survival analysis to evaluate which factors were statistically significant on affecting the prognosis. Then these significant factors were included in the multivariate survival analysis. Finally, we got the conclusions by comparing the survival curves of the clinical and pathological T-factors between the 7th and 8th editions of the UICC-TNM classification, and by analyzing the results of multivariate survival analysis. The data were analyzed using SPSS (Version 16.0). The survival curves were estimated according to the Kaplan-Meier's method, and the differences between groups were compared using a log-rank test. Forward: LR approach was used in the Cox proportional hazard model for estimating the relative risk and finding the independent prognostic factors. A P value of less than 0.05 was considered statistically significant.

Results:

Patient characteristics (Table 1)

Relationships between the 7th and 8th classifications (Table 2 and Table 3)

Univariate survival analysis (Table 1)

From the results of the univariate survival analysis, the following factors: age, gender, smoking, obstructive disorder, restrictive disorder, vessel invasion, pleural invasion, clinical T-factor (8th), pathological T-factor (7th), and pathological T-factor (8th) affected both of the overall survival and recurrence-free survival. On the contrary, surgical procedure and clinical T-factor (7th) had relationship with neither of the two survivals.

Comparison of the clinical T-factors (Figure 1)

Comparison of the pathological T-factors (Figure 2 and Table 4)

From the results of the multivariate survival analysis showed in Table 4, the following factors: age, gender, restrictive disorder, and pathological T-factor (8^{th}) were the independent prognostic factors for both of the overall survival and recurrence-free survival. On the contrary, smoking, obstructive disorder, pleural invasion, and pathological T-factor (7^{th}) were the independent prognostic factors for neither of the two survivals.

Discussion:

In the 8^{th} classification, instead of the whole size of GGN on CT/ the size of lepidic growth in pathology, the solid components size on CT/ invasive size in pathology were used as the clinical/ pathological T descriptors (3,4). However, the 8^{th} classification is based on a worldwide database in which the size of the tumor was not defined as that of solid part/ invasive part. And some research concluded the opponent view (5). Then here comes the questions: Is the new measuring method really suitable for the GGN lung adenocarcinoma? And how is the accuracy? We can answer the questions by comparing the prognostic significance of clinical/ pathological T-factors between the 7^{th} and the 8^{th} editions, for they represent the old and the new measuring method respectively. From the results of our study (Figure 1 and Table 4), we can get the conclusions that the new measuring method is more accurate than the previous one. In another word, the 8^{th} edition of the UICC-TNM classification predicts postoperative prognosis more precisely than the 7^{th} one in both clinical and pathological stage 0-I lung adenocarcinoma.

The possible reasons are as follows: 1. The stage distribution of the population which included in the research project the 8^{th} edition based on has been changed. Early stages (stage 0-I) lung cancer are predominant now, especially in Asia and North America (1). So it will be more accurate when using the 8^{th} edition to evaluate the data of the lung cancer in early stage from Asia, and all the cases in our study are stage 0-I from Japan. 2. The special and precise staging criteria for GGN lung adenocarcinoma is supplemented in the 8^{th} edition. More and more lung adenocarcinomas showing GGN feature were found recently. So it will be more accurate when using the 8^{th} edition to evaluate the data of GGN lung adenocarcinoma, and there are 253 of 386 (65.54%) cases of pure/ part solid GGN lung adenocarcinomas in our study.

Table 1 Univariate survival analysis

Prognostic factor	Number of patients	Overall survival		Recurrence-free survival	
		Cumulative 5-year survival rate (%) ±SE	*P*-value	Cumulative 5-year survival rate (%) ±SE	*P*-value
Age (years)			<0.001		0.005
≤68	207 (53.6%)	95.4 ±1.6		86.2 ±2.5	
>68	179 (46.4%)	82.3 ±3.2		75.0 ±3.6	
Gender			<0.001		<0.001
Male	205 (53.1%)	84.7 ±2.8		75.1 ±3.3	
Female	181 (46.9%)	94.8 ±1.8		87.8 ±2.7	
Smoking			0.005		0.001
Yes	200 (51.8%)	87.2 ±2.6		77.1 ±3.2	
No	186 (48.2%)	92.0 ±2.2		85.4 ±2.8	
Obstructive disorder			0.042		0.008
Yes	111 (28.8%)	85.2 ±3.7		72.7 ±4.6	
No	275 (71.2%)	91.4 ±1.9		84.7 ±2.3	
Restrictive disorder			<0.001		<0.001
Yes	16 (4.1%)	49.9 ±13.8		46.0 ±13.2	
No	370 (95.9%)	91.2 ±1.6		82.7 ±2.1	
Surgical procedure			0.152		0.167
Lobectomy	261 (67.6%)	92.8 ±1.8		84.4 ±2.5	
Segmentectomy	23 (6.0%)	77.9 ±10.0		74.9 ±9.9	
Wedge resection	102 (26.4%)	83.5 ±3.9		74.4 ±4.6	
Vessel invasion			<0.001		<0.001
Yes	71 (18.4%)	76.4 ±5.6		53.6 ±6.3	
No	315 (81.6%)	92.4 ±1.7		87.4 ±2.0	
Pleural invasion			<0.001		<0.001
Yes	59 (15.3%)	78.8 ±5.7		54.7 ±6.7	
No	327 (84.7%)	91.8 ±1.6		86.5 ±2.0	
Clinical T-factor (7th)			0.948		0.216
cT1a	302 (78.2%)	89.2 ±2.0		82.6 ±2.4	
cT1b	72 (18.7%)	90.5 ±3.7		74.9 ±5.5	
cT2a	12 (3.1%)	90.9 ±8.7		81.8 ±11.6	
Clinical T-factor (8th)			0.002		<0.001
cTis	76 (19.7%)	95.6 ±2.5		94.0 ±2.9	
cT1mi	47 (12.2%)	93.6 ±4.6		91.0 ±5.2	
cT1a	108 (28.0%)	90.8 ±3.2		87.4 ±3.5	
cT1b	124 (32.1%)	82.0 ±3.8		66.7 ±4.5	
cT1c	25 (6.5%)	85.0 ±8.1		64.8 ±10.1	
cT2a	6 (1.6%)	80.0 ±17.9		40.0 ±29.7	
Pathological T-factor (7th)			<0.001		<0.001
pT1a	299 (77.5%)	91.4 ±1.8		87.4 ±2.1	
pT1b	27 (7.0%)	90.6 ±6.5		74.7 ±9.0	
pT2a	60 (15.5%)	79.2 ±5.6		55.5 ±6.7	
Pathological T-factor (8th)			<0.001		<0.001
pTis	59 (15.3%)	98.1 ±1.8		98.1 ±1.8	
pT1mi	120 (31.1%)	94.2 ±2.3		90.6 ±2.9	
pT1a	102 (26.4%)	89.0 ±3.5		82.8 ±4.1	
pT1b	41 (10.6%)	80.3 ±6.7		64.7 ±8.0	
pT1c	5 (1.3%)	—[a]		—[a]	
pT2a	59 (15.3%)	78.8 ±5.7		54.7 ±6.7	

[a], all patients were censored

Table 2 Relationship in the clinical T-factors

		8th edition						
		cTis	cT1mi	cT1a	cT1b	cT1c	cT2a	Sum
7th edition	cT1a	72	42	87	101	0	0	302
	cT1b	4	5	20	19	24	0	72
	cT2a	0	0	1	4	1	6	12
	Sum	76	47	108	124	25	6	386

Table 3 Relationship in the pathological T-factors

		8th edition						
		pTis	pT1mi	pT1a	pT1b	pT1c	pT2a	Sum
7th edition	pT1a	59	114	94	32	0	0	299
	pT1b	0	6	8	8	5	0	27
	pT2a	0	0	0	1	0	59	60
	Sum	59	120	102	41	5	59	386

Table 4 Multivariate survival analysis

Prognostic factor	Overall survival			Recurrence-free survival		
	P-value	RR	95.0% CI for RR	*P*-value	RR	95.0% CI for RR
Age	0.001	2.798	1.500 - 5.221	0.047	1.591	1.006 - 2.516
Gender	0.008	0.420	0.220 - 0.799	0.018	0.553	0.338 - 0.904
Smoking	0.502			0.531		
Obstructive disorder	0.574			0.212		
Restrictive disorder	0.004	0.287	0.122 - 0.678	0.029	0.427	0.198 - 0.919
Vessel invasion	0.113			0.004	0.473	0.283 - 0.790
Pleural invasion	0.231			0.622		
Pathological T-factor (7th)	0.160			0.717		
Pathological T-factor (8th)	<0.001			<0.001		
pT1mi to pTis	0.118	5.147	0.660 - 40.149	0.039	8.412	1.113 - 63.552
pT1a to pTis	0.065	6.947	0.885 - 54.540	0.020	11.067	1.466 - 83.535
pT1b to pTis	0.017	12.158	1.550 - 95.390	0.006	17.943	2.329 - 138.259
pT1c to pTis	0.975	0.000	0.000 - 0.000	0.974	0.000	0.000 - 0.000
pT2a to pTis	0.007	16.035	2.133 - 120.571	0.002	23.364	3.110 - 175.538

RR, relative risk; CI, confidence interval.

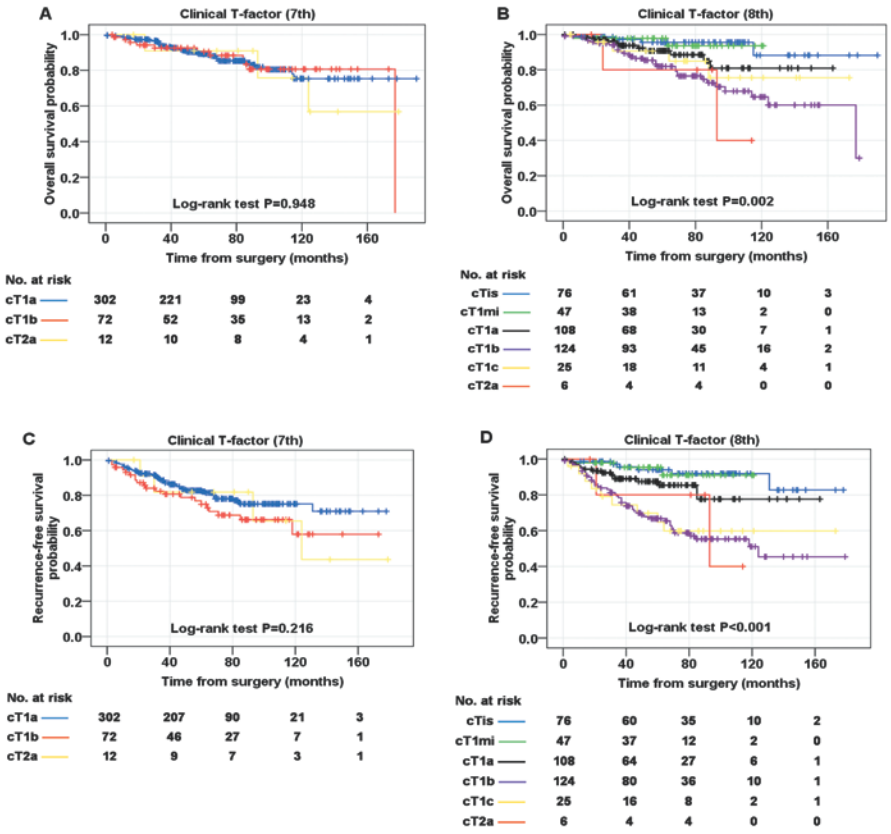

Figure 1 Comparison of clinical T-factors between the 7th and 8th editions of the UICC-TNM classification by univariate survival analysis. The overall survival curve of patients stratified with clinical T-factors (8th) (B) was more clearly separated than that of the 7th (A) (*P*=0.002 vs. *P*=0.948). The recurrence-free survival curve of patients stratified with clinical T-factors (8th) (D) was more clearly separated than that of the 7th (C) (*P*＜0.001 vs. *P*=0.216).

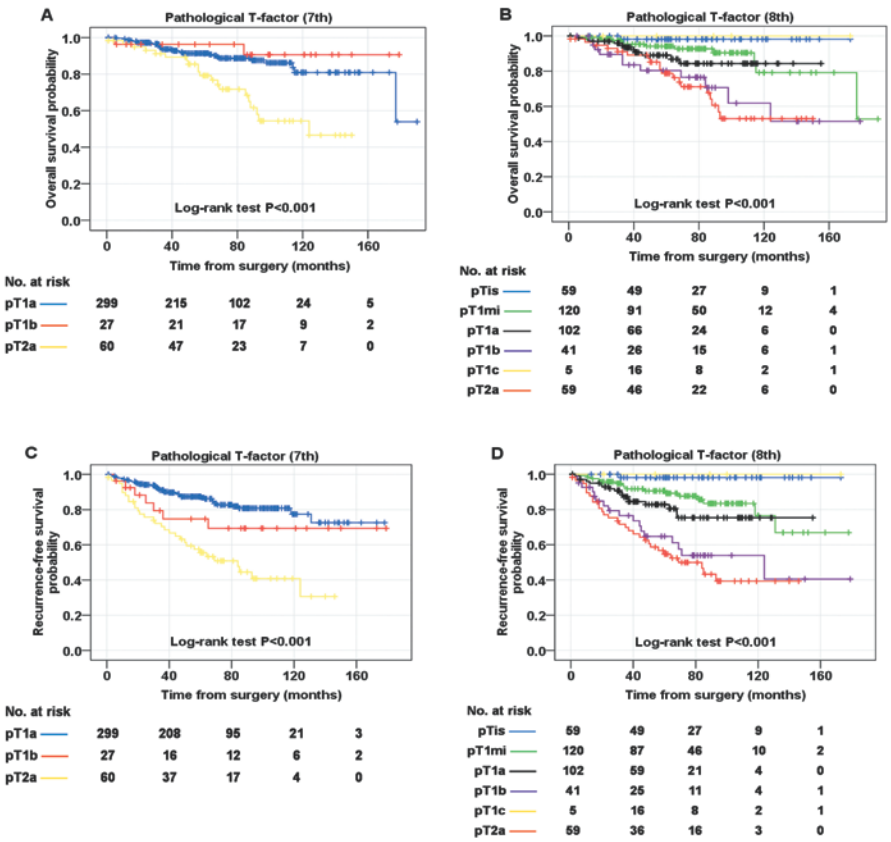

Figure 2 Comparison of pathological T-factors between the 7th and 8th editions of the UICC-TNM classification by univariate survival analysis. The overall and recurrence-free survival curves of patients stratified with pathological T-factors (7th and 8th) (A, B, C, D) were all clearly separated (all of the *P* values were less than 0.001).

References:

1. Rami-Porta R, Bolejack V, Giroux DJ, Chansky K, Crowley J, Asamura H, *et al*. The IASLC lung cancer staging project: the new database to inform the eighth edition of the TNM classification of lung cancer. J Thorac Oncol 2014;9:1618-24.

2. Brierley J, Gospodarowicz MK, Wittekind Ch. TNM classification of malignant tumours. 8th edition. Chichester, West Sussex, UK; Hoboken, NJ: John Wiley & Sons, Inc., 2017:106-12.

3. Travis WD, Asamura H, Bankier AA, Beasley MB, Detterbeck F, Flieder DB, et al. The IASLC Lung Cancer Staging Project: Proposals for Coding T Categories for Subsolid Nodules and Assessment of Tumor Size in Part-Solid Tumors in the Forthcoming Eighth Edition of the TNM Classification of Lung Cancer. J Thorac Oncol 2016;11:1204-23.

4. Wittekind Ch, Compton CC, Brierley J, Sobin LH. TNM supplement: a commentary on uniform use. 4th edition. Oxford: Wiley-Blackwell, 2012:6.

5. Song SH, Ahn JH, Lee HY, Lee G, Choi JY, Kang J, *et al*. Prognostic impact of nomogram based on whole tumour size, tumour disappearance ratio on CT and SUVmax on PET in lung adenocarcinoma. Eur Radiol 2016;26:1538-46.

注：本研究は第１１８回日本外科学会定期学術集会（２０１８年４月５日　東京都）にて発表予定である。

作成日：2018 年 2 月 14 日

Time-varying Pattern of Mortality and Recurrence from Papillary Thyroid Cancer: Lessons from a Long-Term Follow-Up

甲状腺乳頭癌で死亡と再発の時間によって変わるパターン：長期のフォローアップからの教訓

研究者氏名	董　文武（第 39 期笹川医学研究者）
中国所属機関	中国医科大学第一付属病院甲状腺外科
日本研究機関	東京女子医科大学乳腺内分泌外科
指導責任者	岡本　高宏 教授
共同研究者名	堀内　喜代美，　徳光　宏紀， 坂本　明子，　野口　英一郎， 植田　吉宣

Abstract:

Background: Little is known about annual hazard rates of cancer mortality and recurrence for papillary thyroid cancer (PTC). In this study we investigated the time-varying pattern of death and recurrence from PTC and independent prognostic factors for cause specific survival (CSS) and recurrence-free survival (RFS) of PTC.

Methods: This retrospective chart review enrolled 466 patients diagnosed with PTC who underwent curative initial surgery between April 1981 and December 1991 with a median follow-up of 18.4 years. Clinical characteristics, cancer mortality (primary endpoint) and recurrence (secondary endpoint) were ascertained. Survival curves were generated using Kaplan-Meier method and annual death/recurrence hazard was estimated using hazard function.

Results: The 10-year, 20-year and 30-year CSS rates were 97.3%, 93.8% and 91.4%, respectively. 11 (44.0%) cases of death occurred within the first 10 years, whereas 10 (40.0%) and 4 (16.0%) cases occurred within 10-20 years and 20-30 years after surgery, respectively. The 10-year, 20-year and 30-year RFS rates were 88.7%, 78.2% and 70.6%, respectively. 46 (54.8%) cases of recurrence occurred within the first 10 years, whereas 29 (34.5%), 7(8.3%) and 2(2.4%) cases occurred within 10-20 years, 20-30 years and ≥ 30 years after surgery, respectively. Age ≥ 55 years and presence of maximal extrathyroidal extension were independent prognostic factors for CSS. Age ≥ 55 years, male, tumor size > 4cm, presence of extranodal extension and pathological lymph node metastasis were independent prognostic factors for RFS. The annual hazard curve of cancer mortality presented a double-peaked distribution, with a first peak at the 10th year, and the second peak reaching the maximum at the 20th year after surgery for the entire population. The annual hazard curve of recurrence showed a triple-peaked pattern with surges at about 12, 22, and 29 years after surgery.

Conclusion: Patients with PTC harboring at least one of the prognostic characteristics may be at sustained risk of cancer mortality and recurrence even 10 or more years after initial treatment. Understanding the hazard rate of PTC is key to creating more tailored treatment and surveillance.

Key Words:

Papillary thyroid cancer, death risk, recurrence risk, hazard

Introduction

Papillary thyroid cancer (PTC) is an indolent disease and rarely behaves as aggressive tumors clinically with an excellent prognosis as evidenced by the extremely low 30-year disease-specific mortality (DSM) rate (less than 10%), but may

recur several years after initial treatment (1, 2). Risk of death or recurrence was generally described by survival curves rather than hazard functions when outcomes in patients diagnosed with thyroid cancer were reported. Survival curves focus on the cumulative time distribution of survival or recurrence-free, that is, the percentage of patients who remain survival or recurrence-free at a given time after initial treatment. However, the hazard function depicts the rate of failure (death or recurrence) at any instant among the remaining 'at risk' individuals. It describes not only the magnitude of the failure rate, but also how it changes over time. Time-varying pattern of death or recurrence for PTC has never been reported. In the present study we examined the time-varying pattern of death and recurrence of PTC and the time and site distribution of death and/or recurrence, along with risk factors predicting death and recurrence of PTC.

Materials and methods

Patients

A total of 466 patients with PTC who underwent curative initial surgery between April 1981 and December 1991 in the Department of Endocrine Surgery at Tokyo Women's Medical University were eligible for inclusion in this study. Patients with one or more of the following conditions were excluded: non-PTC types (follicular/medullary/ anaplastic/poorly differentiated), age ≤ 18 years, a history of previous thyroidectomy, presence of distant metastasis at the time of diagnosis, or never free of disease. Patients were categorized in three prognostic subgroups: low-risk (T1N0M0 in TNM classification), intermediate-risk, and high-risk patients (T > 5 cm, extrathyroidal extension to the mucosa of the trachea or esophagus, a large number of clinical lymph node metastases, lymph node metastasis > 3 cm, or the presence of distant metastasis). For this study, thyroidectomy were dichotomized into two groups: total thyroidectomy and less than total thyroidectomy (including subtotal, partial, enucleation, and Dunhill). This retrospective study was approved by the Ethical Committee of Tokyo Women's Medical University (No.4445), and the requirement to obtain informed consent was waived.

Statistical analysis

The survival distributions were estimated using the Kaplan-Meier method and compared using the log-rank test. Cox proportional hazards regression was used for multivariate analysis to determine independent prognostic factors for death and recurrence. For a graphical display of CSS and RFS, annual hazard rates were estimated using a Kernel-smoothing method (3-5). All statistical analyses were performed using the Stata statistical software package 9.0 (Stata Corporation Ltd, College Station, TX, USA). Differences were considered statistically significant if $P < 0.05$.

Results

General characteristics of the study population were summarized in Table 1. The sites of initial recurrence and the interval from initial treatment to recurrence were shown in Table 2.Time-varying pattern of death and recurrence were shown in Fig. 1. The 10-year, 20-year and 30-year CSS rates were 97.3%±0.8%, 93.8%±1.4% and 91.4%±1.8%, respectively. The 10-year, 20-year and 30-year RFS rates were 88.7%±1.6%, 78.2%±2.3% and 70.6%±3.5%, respectively.

Prognostic factors

Survival analysis of CSS and RFS was showed in Table 3, Table 4, Fig. 2 and Fig. 3.

Death hazard analysis

Annual death hazard rate for 466 patients with PTC was shown in Fig 4. The annual hazard curve of cancer mortality presented a double-peaked distribution, with a first minor peak at the 10th year, followed by a nadir at the 14th year and then a rapid rise reaching the major peak at the 20th year after surgery for the entire population.

Recurrence hazard analysis

Annual recurrence hazard rate for 466 patients with PTC was shown in Fig. 5. The annual hazard curve of recurrence for

the entire population presented a triple-peaked pattern with surges at about 12, 22, and 29 years after surgery.

Discussion

As far as we know, this study is the first retrospective analysis of postoperative death and recurrence pattern of thyroid cancer over time. We identified patients with PTC had a good long-term prognosis. Most of cancer mortality and recurrence occurred in the first 20 years, but there were still some patients who underwent such experience after 20 years postoperatively. Age at surgery ≥ 55 years was the only independent prognostic factor for both CSS and RFS. Another striking observation was that we revealed the double-peaked and triple-peaked time distribution of death and recurrence risk among PTC patients undergoing surgery, respectively. High-risk patients carried higher hazard rates of both cancer mortality and recurrence compared with the low- or intermediate-risk patients. Patients with stage III or IV had a higher death hazard rate than those with stage I or II.

In conclusion, we revealed the time distribution of cancer mortality and recurrence risk and independent prognostic factors for CSS and RFS of PTC. Armed with this information, we will be better able to formulate individual treatment and surveillance recommendations.

TABLE 1 SUMMARY OF PATIENT CHARACTERISTICS

Patient characteristics		*No. of patients (%)*
Age at surgery (years)	< 55	324 (69.5)
	≥ 55	142 (30.5)
Gender	Male	80 (17.2)
	Female	386 (82.8)
Tumor size(cm)	≤ 4	404 (86.7)
	> 4	62 (13.3)
Multifocality	Yes	71 (15.2)
	No	395 (84.8)
Extrathyroidal extension	ExT0	237 (50.9)
	ExT1	158 (33.9)
	ExT2	71 (15.2)
Extranodal extension	ExN0	447 (95.9)
	ExN1	19 (4.1)
PLNM	Yes	367 (78.8)
	No	99 (21.2)
Extent of thyroidectomy	Total thyroidectomy	75 (16.1)
	Less than total thyroidectomy	391 (83.9)
Extent of neck dissection	No	9 (1.9)
	Central compartment only	37 (7.9)
	Central and lateral compartments	420 (90.1)
Risk class	Low	135 (29.0)
	Intermediate	169 (36.3)
	High	162 (34.8)
TNM stage (8th edition)	I	346 (74.2)
	II	89 (19.1)
	III	24 (5.2)
	IV	7 (1.5)
RAI treatment	Yes	7 (1.5)
	for primary lesion	3 (0.6)
	for recurrent disease	4 (0.9)
	No	459 (98.5)

TABLE 2. SITE AND TIME OF INITIAL RECURRENCES

Specific recurrence site	*No. of patients (%)*	*Time[mean ± SD]*
Local	12 (14.3)	10.60±7.80
Regional	52 (61.9)	7.86±7.71
Distant	14 (16.7)	13.49±5.62
Both		
Local+Regional	4 (4.8)	5.14±4.51
Local+Distant	1 (1.2)	15.94
Regional+Distant	1 (1.2)	19.96
Total	84 (100.0)	9.41±7.69

TABLE 3. SURVIVAL ANALYSIS OF CAUSE SPECIFIC SURVIVAL IN 466 PATIENTS WITH PAPILLARY THYROID CANCER

Variable	*Univariate analysis*	*Multivariate analysis*	
	P	*HR (95% CI)*	*P*
Age at surgery (≥55 years vs. <55 years)	< 0.001*	6.899 (2.798-17.014)	< 0.001*
Gender (Male vs. Female)	0.002*	2.206 (0.973-5.003)	0.058
Tumor size (>4cm vs. ≤4cm)	< 0.001*	2.102 (0.891-4.957)	0.090
Multifocality (positive vs. negative)	0.103	1.772 (0.728-4.317)	0.208
Extrathyroidal extension	< 0.001*		
ExT1 vs. ExT0		1.488 (0.509-4.350)	0.468
ExT2 vs. ExT0		2.998 (1.033-8.701)	0.043*
Extranodal extension (ExN1 vs. ExN0)	0.205	2.177 (0.482-9.828)	0.312
PLNM (positive vs. negative)	0.007*	-	-

TABLE 4. SURVIVAL ANALYSIS OF RECURRENCE FREE SURVIVAL IN 466 PATIENTS WITH PAPILLARY THYROID CANCER

Variable	*Univariate analysis*	*Multivariate analysis*	
	P	*HR (95% CI)*	*P*
Age at surgery (≥55 years vs. <55 years)	< 0.001*	1.799 (1.086-2.980)	0.021*
Gender (Male vs. Female)	0.001*	2.659 (1.688-4.188)	< 0.001*
Tumor size (>4cm vs. ≤4cm)	< 0.001*	1.892 (1.159-3.299)	0.027*
Multifocality (positive vs. negative)	0.052	1.279 (0.770-2.124)	0.195
Extrathyroidal extension	0.003*		
ExT1 vs. ExT0		1.458 (0.848-2.507)	0.996
ExT2 vs. ExT0		2.198 (1.219-3.963)	0.148
Extranodal extension (ExN1 vs. ExN0)	0.003*	2.176 (0.928-5.104)	0.004*
PLNM (positive vs. negative)	< 0.001*	2.157 (1.319-3.527)	0.004*

ExT0, no extension; ExT1, extension to the sternothyroid muscle or perithyroid soft tissues; ExT2,

extension to subcutaneous soft tissues, larynx, trachea, esophagus, recurrent laryngeal nerve, or prevertebral fascia encasing the carotid artery or mediastinal vessels. ExN0, no extension; ExN1, extension to strap muscle, recurrent laryngeal nerve, trachea, or jugular vein. PLNM, pathological lymph node metastasis. RAI, radioactive iodine therapy. Recurrence was classified as follows: "local" if only the thyroid bed or residual thyroid gland tissue was involved; "regional" if the lymph nodes of the central or lateral compartments of the neck was involved; "distant" if disease was located in other sites, including the lungs, live, bones, and brain. HR, hazard rate. CI, confidence interval. * Statistically significant at $P < 0.05$.

Death time	*No. of patients (%)*
< 5 years	0(0)
5-10 years	11(44.0)
10-20 years	10(40.0)
20-30 years	4(16.0)
≥ 30 years	0(0)
Total	25(100.0)

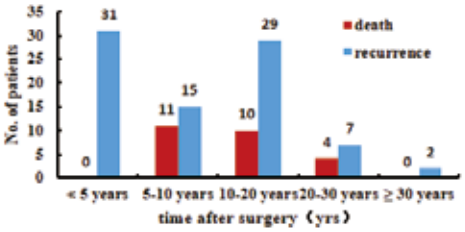

Recurrence time	*No. of patients (%)*	*L*	*R*	*D*	*L+R*	*L+D*	*R+D*
< 5 years	31(36.9)	3	25	0	3	0	0
5-10 years	15 (17.9)	3	9	3	0	0	0
10-20 years	29(34.5)	4	14	8	1	1	1
20-30 years	7(8.3)	2	2	3	0	0	0
≥ 30 years	2(2.4)	0	2	0	0	0	0
Total	84(100.0)	12	52	14	4	1	1

L, local; R, regional; D, distant.

FIG. 1. Time-varying pattern of death and recurrence in 466 patients with papillary thyroid cancer.

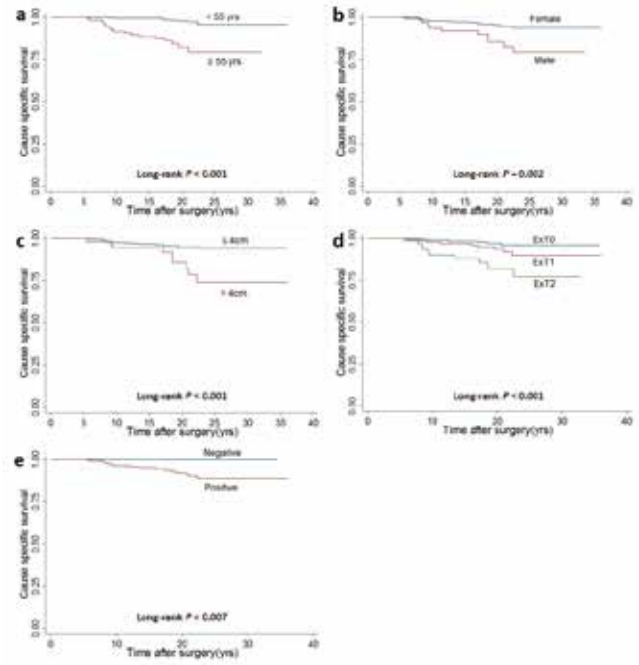

FIG. 2. Kaplan-Meier curves for cause specific survival in 466 patients with papillary thyroid cancer according to clinicopathological characteristics. (a) age; (b) gender; (c) tumor size; (d) extrathyroidal extension; (e) pathological lymph node metastasis.

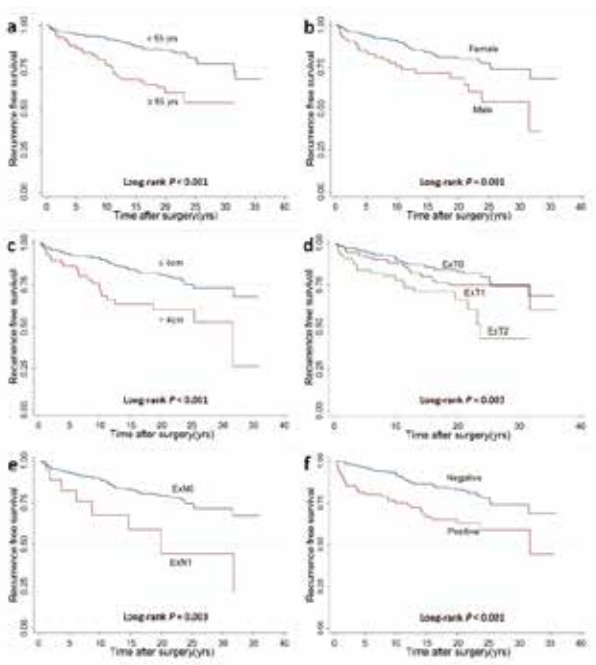

FIG. 3. Kaplan-Meier curves for recurrence free survival in 466 patients with papillary thyroid cancer according to clinicopathological characteristics. (a) age; (b) gender; (c) tumor size; (d) extrathyroidal extension; (e) nodal extension; (f) pathological lymph node metastasis.

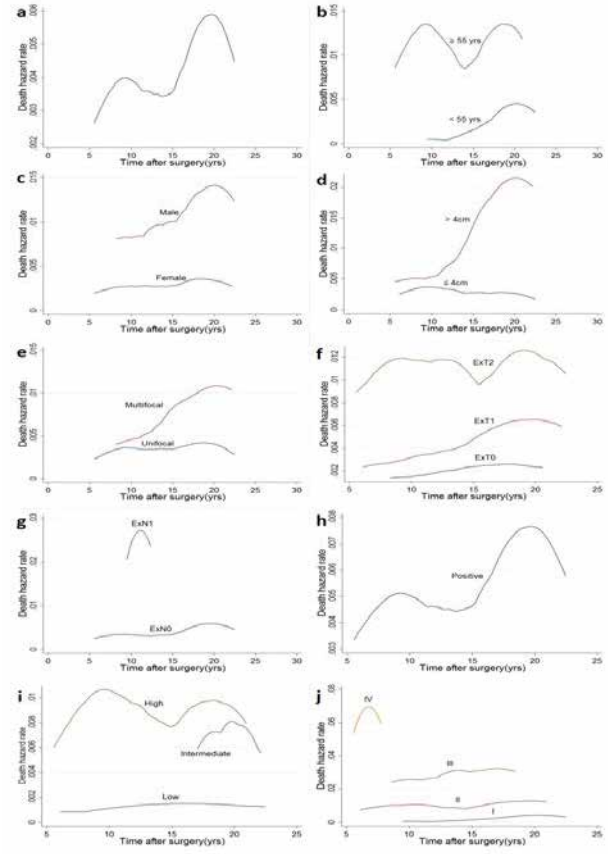

FIG. 4. Annual death hazard rate for 466 patients with papillary thyroid cancer. (a) the entire population; (b) age; (c) gender; (d) tumor size; (e) multifocality; (f) extrathyroidal extension; (g) nodal extension; (h) pathological lymph node metastasis; (i) Risk class; (j) AJCC staging.

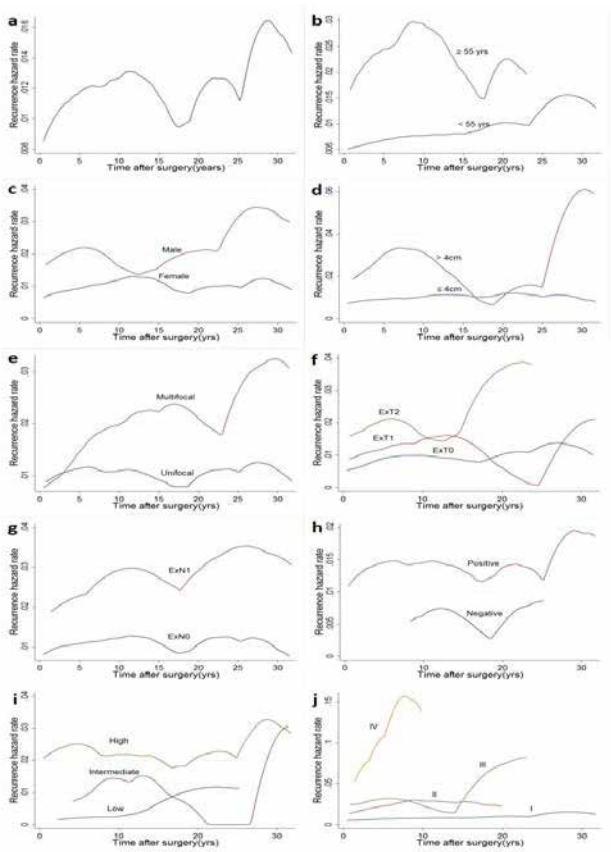

FIG. 5. Annual recurrence hazard rate for 466 patients with papillary thyroid cancer. (a) the entire population; (b) age; (c)gender; (d) tumor size; (e) multifocality; (f) extrathyroidal extension ; (g) nodal extension; (h) pathological lymph node metastasis; (i) Risk class; (j) AJCC staging.

References

1. Mazzaferri EL, Jhiang SM 1994 Long-term impact of initial surgical and medical therapy on papillary and follicular thyroid cancer. Am J Med **97**:418-428.

2. Grogan RH, Kaplan SP, Cao H, Weiss RE, DeGroot LJ, Simon CA, Embia OM, Angelos P, Kaplan EL, Schechter RB 2013 A study of recurrence and death from papillary thyroid cancer with 27 years of median follow-up. Surgery **154**:1436-1447.

3. Ramlau-Hansen H 1983 Smoothing counting process intensities by means of kernel functions. Ann Stat:**4**53-466.

4. Yin W, Di G, Zhou L, Lu J, Liu G, Wu J, Shen K, Han Q, Shen Z, Shao Z 2009 Time-varying pattern of recurrence risk for Chinese breast cancer patients. Breast Cancer Res Treat **114**:527-535.

5. Feng X-Y, Chen Y-B, Wang W, Guan Y-X, Li Y-F, Chen S, Sun X-W, Li W, Xu D-Z, Zhan Y-Q 2013 Time-varying pattern of recurrence risk for gastric cancer patients. Med Oncol **30**:514.

作成日：2018 年 2 月 15 日

Hyperinflated lungs compress the heart during expiration in COPD patients: a new finding on dynamic-ventilation computed tomography

呼吸ダイナミックＣＴを用いた慢性閉塞性肺疾患における心臓断面積の呼吸時変化の検討

研究者氏名　徐　妍妍　（第 39 期笹川医学研究者）
中国所属機関　中日友好病院放射線科
日本研究機関　琉球大学医学部放射線診断治療学講座
指導責任者　村山　貞之　教授，山城　恒雄　講師
共同研究者名　森谷　浩史　医師，椿本　真穂　助教

Abstract:

Purpose: The aims of this study were to evaluate dynamic changes in heart size during the respiratory cycle using four-dimensional computed tomography (CT) and to understand the relationship of these changes to airflow limitation in smokers.

Materials and methods: A total of 31 smokers, including 13 with COPD, underwent four-dimensional dynamic-ventilation CT during regular breathing. CT data were continuously reconstructed every 0.5 s, including maximum cross-sectional area (CSA) of the heart and mean lung density (MLD). Concordance between the cardiac CSA and MLD time curves was expressed by cross-correlation coefficients（CCCs）, and spearman rank correlation analysis was used to evaluate associations between the CCCs and the forced expiratory volume in 1 s ($FEV_{1.0}$) relative to the forced vital capacity (FVC). The CT-based cardiothoracic ratio at inspiration and expiration was also calculated. Comparisons of the CT indices between COPD patients and non-COPD smokers were made using the Mann–Whitney test.

Results: Cardiac CSA at both inspiration and expiration was significantly smaller in COPD patients than in non-COPD smokers (P<0.05). The cross-correlation coefficient between cardiac CSA and MLD during expiration significantly correlated with FEV1.0/FVC (ρ=0.63, P<0.001), suggesting that heart size decreases during expiration in COPD patients. The change in the cardiothoracic ratio between inspiration and expiration frames was significantly smaller in COPD patients than in non-COPD smokers (P<0.01).

Conclusion: Patients with COPD have smaller heart size on dynamic-ventilation CT than non-COPD smokers and have abnormal cardiac compression during expiration.

Keywords: heart, COPD, computed tomography, ventilation, emphysema

Introduction:

COPD is a heterogeneous disorder with significant extrapulmonary effects that contribute to disease severity.[1–5] Obstruction of expiratory airflow and loss of lung elasticity lead to lung hyperinflation and elevated intrathoracic pressure, causing various cardiovascular sequelae.[6–8] Increased intrathoracic pressure reduces venous return and thus reduces right ventricular output.[9–13] Furthermore, hyperinflation is associated with reduced ventricular filling, reduced stroke volume, and lower cardiac output.[14–18] In addition, Watz et al[15] found that severe COPD is associated with smaller cardiac size on echocardiography.

It has previously been reported that, in patients with severe COPD or emphysema, the heart appears narrowed on chest radiography.[19] However, dynamic changes in heart size throughout the respiratory cycle are unknown. Tomita et al[20] reported that the cardiac cross-sectional area (CSA) is significantly larger on expiratory computed tomography (CT) than on inspiratory CT in patients without severe airflow limitation and that the increase in heart size from the inspiratory to expiratory phase is correlated with the degree of expiration and the upward movement of the diaphragm. Patients with COPD have increased intrathoracic pressure during expiration,[21] which is tightly correlated with decreased venous return, decreased cardiac transmural filling pressure, and decreased cardiac output.[7–18] Furthermore, both decreased compliance of the pulmonary parenchyma and increased pulmonary vascular resistance due to hyperinflation can reduce cardiac output.[22,23] In addition, respiratory muscle insufficiency, including flattened diaphragms due to pulmonary hyperinflation, can reduce the inward recoil forces of the thoracic cage and thereby decrease cardiovascular pumping action in patients with COPD.[24,25]

Based on these observations and physiological theories, we hypothesized that changes in heart size throughout the respiratory cycle would differ between COPD patients and non-COPD subjects and that these differences would correlate with the severity of COPD (ie, airflow limitation). Recently, 320-row and 256-row multi-detector CT scanners have been developed that can continuously scan the thorax under normal breathing conditions, allowing visualization of thoracic respiratory movements.[26,27] Although dynamic-ventilation CT cannot cover the entire lung (≤160 mm in the z-axis), continuous mean lung density (MLD) values of the scanned lung can be obtained. A strong correlation between MLD and lung volume has previously been reported.[28,29] Thus, changes in MLD reflect pulmonary ventilation movements and can be used as an index of ventilation status.

The aims of this study were 1) to compare changes in heart size during the respiratory cycle in smokers with and without COPD using four-dimensional dynamic-ventilation CT and 2) to evaluate abnormal cardiac movements during ventilation in patients with COPD and determine the association of these abnormalities with the severity of obstructive lung disease.

Materials and methods

This retrospective study was approved by the institutional review board at Ohara General Hospital. Dynamic-ventilation CT was performed as part of routine clinical care at Ohara Medical Center, based on the need to observe parietal pleural invasion/adhesion by resectable thoracic neoplasms or to monitor excessive dynamic airway collapse in COPD patients. Based on the Ethical Guidelines for Medical and Health Research Involving Human Subjects, enacted by the Ministry of Health, Labor and Welfare of the Japanese Government, the institutional review board at Ohara General Hospital waived written informed consent from enrolled patients for this retrospective study. All CT data and patient information were anonymized and stored for analyses. This study was also arranged as part of the Area-detector Computed Tomography for the Investigation of Thoracic Diseases (ACTIve) Study, an ongoing multicenter research alliance in Japan.

Subjects

A total of 46 subjects underwent both conventional and dynamic-ventilation CT scans. After previewing the dynamic-ventilation CT images, 15 patients were excluded from the study due to insufficient cardiac scanning fields (cranial scanning field settings). Ultimately, 31 smokers (15 ex-smokers and 16 current smokers; five females and 26 males; mean age 72±10 years) were included in the study (Table 1). All subjects had undergone spirometry and chest CT scans at Ohara Medical Center at the Ohara General Hospital. None of the patients had a diagnosis of heart failure. Among the 31 subjects, 13 had previously been included in a different research study.[27] The results presented in this study do not overlap with the results presented in the previous report.

CT scans

All patients were scanned on a 320-row CT scanner (Aquilion ONE; Toshiba Medical Systems, Otawara, Japan) for both conventional (static) and dynamic-ventilation CT studies. Dynamic scanning was performed at a fixed point without bed movement (non-helical scanning), resulting in fluoroscopic images of 160 mm in length.[26,27] Scanning and reconstruction parameters for the dynamic-ventilation CT were as follows: tube current =40 mA (n=27) or 20 mA (n=4); tube voltage =120 kVp; rotation time =0.35 s; total scanning time =4.5–6.5 s; scanning field of view (FOV) =320 (medium, n=12) or 400 mm (large, n=19); imaging FOV =320 mm; collimation =0.5 mm; slice thickness =1 mm; reconstruction kernel = FC15 (for mediastinum); reconstruction interval =0.5 s/frame (total 9–13 frames); reconstruction method = half reconstruction. Scan data were converted to CT images using an iterative reconstruction method (adaptive iterative dose reduction using three-dimensional processing [AIDR3D], mild setting). Before the dynamic-ventilation scan, patients were coached on continuous deep breathing. Radiologic technologists monitored patients' respiratory movements and confirmed that expiratory movement from the peak inspiratory phase to the peak expiratory phase was included during the scanning. Radiation dose assessment for dynamic-ventilation CT was as follows: for CT scans with a tube current of 40 mA, the dose–length product (DLP) value for a single rotation was 20.4 mGy·cm (medium FOV) or 22.5 mGy·cm (large FOV). For adjusted CT scans with a tube current of 20 mA, the DLP value for a single rotation was 10.2 mGy·cm (medium FOV) or 11.3 mGy·cm (large FOV). The total estimated radiation exposure for dynamic-ventilation CT scans of 4.5–6.5 s varied from 2.7 to 6.1 mSv (mean 5.3 mSv).

A conventional static chest CT was also performed using helical scanning to image the entire thorax. Parameters for the conventional chest CT were as follows: tube currents = automatic exposure control (AEC); tube voltage =120 kVp; scanning method = helical scanning; rotation time =0.35 s; beam pitch =0.828; imaging FOV =320 mm; collimation = 0.5 mm ×80 rows; slice thickness =1 mm; reconstruction kernel = FC17 (for mediastinum); iterative reconstruction = AIDR3D (mild setting).

Image analysis: continuous lung density measurement

Using commercially available software (Lung Volume Measurement; Toshiba Medical Systems), the MLD was measured automatically in each frame, and a time curve for the MLD on the dynamic-ventilation scans was created. The peak inspiratory frame was defined as the lowest MLD on the time curve, and the peak expiratory frame was defined as the highest MLD. Thus, the expiratory phase was defined as occurring during the peak inspiratory to peak expiratory frames on the MLD curve.

Image analysis: continuous measurement of cardiac CSA

At each frame of the dynamic-ventilation CT, the cardiac CSA was measured semi-automatically by research software that had the same function as the CT scanner console. Based on a previously published method,[20] the following process was repeated in each subject: first, a threshold was set using Hounsfield units (HU) to exclude the pericardial fat pad (from 0 to 300 HU); second, at each time frame, all images that contained the heart were identified and the maximum cardiac CSA was determined; third, the boundary of the heart was traced and the maximum cardiac CSA was recorded. The CSAs measured at the peak inspiratory and peak expiratory frames were labeled as CSA_{insp} and CSA_{exp}.

Image analysis: CT-based cardiothoracic ratio (CTR) measurement

Employing the same research software used for the cardiac CSA measurements, the maximum transverse cardiac diameter and the maximum transverse diameter of the lungs on the peak inspiratory and peak expiratory frames were manually measured. Similar to previous studies that calculated the CT-based CTR,[20,30] the CTR was defined as the maximum transverse cardiac diameter divided by the maximum transverse lung diameter. For each patient, inspiratory

CTR, expiratory CTR, and the difference between inspiratory and expiratory CTR (ΔCTR = expiratory CTR − inspiratory CTR) were obtained.

Image analysis: emphysema and lung volume measurement on conventional chest CT

On the conventional helical CT scans, an emphysema measurement was performed using commercially available software (Lung Volume Measurement). The percent low attenuation volume (LAV%, <−950 HU) and the lung volume of the entire lung were automatically obtained.

Spirometry

All subjects performed spirometry, including forced expiratory volume in 1 s ($FEV_{1.0}$) and forced vital capacity (FVC), according to the American Thoracic Society standards.5 The spirometric values of the study participants are summarized in Table 1. Spirometry was performed within 15 days of the chest CT. Based on the criteria by the American Thoracic Society, 13 subjects were diagnosed with COPD. The other 18 smokers did not meet the criteria for COPD (non-COPD smokers).

Statistical analysis

Continuous variables are expressed as mean ± standard deviation. Comparisons of continuous variables, including CT indices of COPD patients versus non-COPD smokers, were made by the Mann–Whitney test. Cross-correlation coefficients (CCCs; $-1 \leq R \leq 1$) were calculated between the MLD and cardiac CSA time curves. If the two time curves had similar shapes and directions over time, the coefficient approached 1.[26,27] Thus, if the cardiac CSA became larger during expiration (ie, during MLD increase), the CCC contained some positive values. Spearman rank correlation analysis was used to evaluate the associations between CT indices and FEV1.0/FVC. A P-value of <0.05 was considered significant. All statistical analyses were performed using JMP 12.0 software (SAS Institute Inc., Cary, NC, USA).

Results

CT indices from conventional helical CT

The LAV% was significantly larger in COPD patients than in non-COPD smokers ($P<0.001$; Table 2), and significantly correlated with $FEV_{1.0}$/FVC ($\rho=-0.78$, $P<0.0001$). Lung volume, particularly the value adjusted for by the body surface area,[31] was significantly larger in COPD patients than in non-COPD smokers, suggesting that the lungs were hyperinflated in COPD patients.

Maximum cardiac CSA on peak inspiratory and expiratory frames

On the maximum cardiac CSA time curve, the CSA was significantly smaller in COPD patients than in non-COPD patients on both the peak inspiratory and peak expiratory frames ($P<0.05$; Table 2). Interestingly, the mean value of the maximum cardiac CSA slightly decreased from the peak inspiratory to the peak expiratory frame in COPD patients (69.1 cm^2 at inspiration, 68.2 cm^2 at expiration), whereas it increased in non-COPD smokers (Figure 1). The expiratory/inspiratory ratio of the maximum cardiac CSA demonstrated a moderate correlation with $FEV_{1.0}$/FVC ($\rho=0.55$, $P<0.01$), suggesting that a smaller maximum cardiac CSA on the peak expiratory frame correlated with more severe airflow limitation.

CCC between the maximum cardiac CSA and MLD time curves

The CCC between the maximum cardiac CSA and MLD time curves during the entire cycle (9–13 frames) significantly correlated with $FEV_{1.0}$/FVC (ρ=0.56, P<0.01), suggesting that subjects with increasing heart size during expiration/decreasing heart size during inspiration have less airflow limitation. Interestingly, the CCC between the maximum cardiac CSA and MLD time curves during the expiratory frames only (5–12 frames) demonstrated a higher correlation with FEV1.0/FVC (ρ=0.63, P<0.001) than the CCC during the entire cycle. Nine of 13 (69%) patients with COPD demonstrated a negative CCC during the expiratory phase, suggesting that these patients had a decreasing heart size during expiration, in contrast to normal physiological phenomena (Table 3, Figure 1).

CT-based CTR measurements

Although inspiratory CTR was not significantly different between COPD patients and non-COPD smokers, expiratory CTR and ΔCTR were significantly smaller in COPD patients than in non-COPD smokers.

Discussion

In this study, we found that 1) the maximum cardiac CSA was significantly smaller in patients with COPD than in non-COPD smokers on the peak inspiratory/expiratory frames on dynamic-ventilation CT, 2) the expiratory/inspiratory ratio of the CSA correlated with airflow limitation, 3) the maximum cardiac CSA often decreased during expiration in COPD patients, in contrast to normal physiological movements, and 4) this contrasting pattern of respiratory changes in heart size and respiratory movements of the lung correlated with airflow limitation. The observations described earlier can be briefly summarized as follows: in COPD patients, the heart size is smaller throughout the ventilation cycle, the change in the heart size between the peak inspira-tory and peak expiratory phases is smaller in non-COPD subjects, and abnormal cardiac compression (reduction in heart size) during expiration is frequently observed in COPD patients and does not occur in non-COPD subjects. These data suggest that, in COPD patients, respiratory lung movements have an abnormal influence on cardiac motion and may be related to impaired cardiac function in patients with COPD. When observing the dynamic-ventilation CT of severe COPD patients in this study, we frequently noticed that severe emphysematous lower lung regions, which would have extensive air trapping, did not decrease in volume and directly compressed the heart during expiration (Figure 1D-F), which was in contrast to non-COPD subjects (Figure 1A-C). Although this study did not assess cardiac output, these findings may improve our understanding of depressed cardiac function in patients with COPD and help create a comprehensive cardiopulmonary model of COPD.

Although no previous publications have used dynamic-ventilation CT to observe heart size, “small heart in severe emphysema or COPD” has been observed in previous studies using different imaging modalities, including echocardiography, radiography, and magnetic resonance imaging (MRI).[9–11,15,32,33] The smaller heart size in patients with COPD is associated with lung hyperinflation. In patients with COPD, lung hyperinflation is caused by a decrease in the elastic recoil of the lung parenchyma and dynamic air trapping during successive breaths. Lung hyperinflation leads to greater end-expiratory lung volume and increased intrathoracic pressure.[14–16,34] Increased intrathoracic pressure decreases venous return to the heart, which decreases cardiac preload, and impairs the compliance of the intrathoracic vascular bed.[9–11,16,17] Furthermore, external compression from hyperinflated lungs increases end-diastolic pressure.[10,15,35] Consequently, cardiac size and function is compromised in patients with COPD and/or severe emphysema.

Previous studies of heart size in COPD patients have been based on static images during a single respiratory phase, or on cardiac imaging without assessment of the respiratory cycle. Little attention has been paid to dynamic cardiac changes during the respiratory cycle, or the influence of ventilation phase on heart size, in patients with COPD. In the current study, we used dynamic-ventilation CT to demonstrate that smokers without obvious airflow limitation have an incremental change in heart size during expiration, consistent with previous reports of non-COPD patients.[20] In subjects

without airflow limitation, a rapid reduction in intrathoracic pressure during inspiration leads to an increase in venous return and an increase in right-sided cardiac volume. Meanwhile, reduced pulmonary venous return due to blood pooling in the lung parenchyma causes a reduction in left-sided cardiac volume.[36] In contrast, in subjects with significant airflow limitation, intrathoracic pressure rapidly increases during expiration, leading to increased left-sided cardiac volume and decreased right-sided cardiac volume. In addition, ventricular interdependence may cause changes in cardiac volume.[37,38] The complex geometric changes of the cardiac chambers make it difficult to speculate about the exact change in cardiac volume during ventilation. However, changes in heart size may also be explained by chest wall movement: during inspiration, the ribcage expands and the diaphragm moves downward, which stretches the pericardium in the craniocaudal direction, leading to a "thinner" heart shape on radiography and reconstructed coronal CT images.[20] Lung inflation during inspiration might also restrict the transverse movement of the heart. In contrast, during expiration, the diaphragm moves upward, slightly compressing the heart in the craniocaudal direction, resulting in a "pear-shaped" heart with a larger cardiac CSA than during inspiration.[20] Hence, in subjects without airflow limitation (ie, without lung hyperinflation), the cardiac CSA decreases during inspiration and increases during expiration.

While this physiological phenomenon was observed in non-COPD smokers in the current study, the situation appeared to be very different in patients with COPD. In these patients, the maximum cardiac CSA frequently decreased during expiration and the heart size was smaller during expiration than during inspiration. Although it is difficult to speculate about the pathophysiological mechanisms that underlie this observation, several factors may lead to paradoxical cardiac movement during expiration in patients with COPD. One factor is increased intrathoracic pressure, particularly during expiration.[21,39] Changes in intrathoracic pressure influence juxtacardiac pressure,[18] which may, in turn, change cardiac morphology. Intrathoracic pressure is greatly elevated during expiration in COPD patients[21] and may impair cardiac filling by reducing venous return to the thorax and by physically compressing the heart and pulmonary vessels.[10,19] A second factor is decreased compliance of the pulmonary parenchyma and increased pulmonary vascular resistance due to hyperinflation.[22,23] Decreased compliance of pulmonary tissue decreases lung distortion during ventilation, and increased vascular resistance reduces pulmonary venous return during expiration, resulting in decreased heart expansion during expiration. A third factor is the combination of hyperinflated lungs and a flattened diaphragm. Although COPD patients exhale by increasing their intrathoracic pressure, the hyperinflated lungs do not rapidly change size. The combination of elevated intrathoracic pressure and hyperinflated lungs may result in direct compression of the heart. Furthermore, the dysfunctional, flattened diaphragm in patients with severe COPD does not move upward/downward during ventilation, which may prevent the "physiological" increase in heart size that is normally caused by diaphragm elevation during expiration. Finally, exaggerated ribcage motion during expiration may affect heart size. Overall, these factors may explain the reduction in cardiac CSA during expiration that we observed in patients with severe COPD.

This study has several limitations. First, pulmonary function was only assessed using spirometric values, and other functional parameters, such as plethysmography and diffusion capacity, were not included. Second, cardiopulmonary exercise data were not evaluated in this study. Third, we did not evaluate cardiac function. Fourth, esophageal pressure, which is often used as an index of intrathoracic pressure, was not measured. Fifth, the study population was small. Sixth, the dynamic-ventilation CT could not scan the entire thorax. Although MLD is a reliable method for estimating lung volume, true respiratory changes in lung volume could not be measured. Sixth, cardiac performance might be influenced by body position,6and our measurements were obtained in the supine position only. Finally, the influence of heat rate on cardiac CSA was not assessed. In some patients, the maximum cardiac CSA time curve was uneven due to heartbeat. Our future studies will address each of these issues.

Conclusion

We used dynamic-ventilation CT to determine that heart size is significantly smaller in patients with COPD than in non-COPD smokers. Heart size decreased during expiration in most patients with COPD, which is in contrast to the non-COPD population. Dynamic-ventilation CT that exclusively observes respiratory motions of the lung and heart may provide further knowledge regarding cardiovascular dysfunction in COPD.

References

1. Mannino DM. The natural history of chronic obstructive pulmonary disease. Pneumonol Alergol Pol. 2011;79(2):139–143.

2. Sin DD, Man SF. Chronic obstructive pulmonary disease as a risk factor for cardiovascular morbidity and mortality. Proc Am Thorac Soc. 2005;2(1):8–11.

3. Roversi S, Fabbri LM, Sin DD, Hawkins NM, Agustí A. Chronic obstructive pulmonary disease and cardiac diseases. An urgent need for integrated care. Am J Respir Crit Care Med. 2016;194(11):1319–1336.

4. Falk JA, Kadiev S, Criner GJ, Scharf SM, Minai OA, Diaz P. Cardiac disease in chronic obstructive pulmonary disease. Proc Am Thorac Soc. 2008;5(4):543–548.

5. Vestbo J, Hurd SS, Agusti AG, et al. Global strategy for the diagnosis, management, and prevention of chronic obstructive pulmonary disease: GOLD executive summary. Am J Respir Crit Care Med. 2013;187(4):347–365.

6. Robotham JL. Cardiovascular disturbances in chronic respiratory insufficiency. Am J Cardiol. 1981;47(4):941–949.

7. Cournand A, Motley HL, Werko L, Richards DW. Physiological studies of the effects of intermittent positive pressure breathing on cardiac output in man. Am J Physiol. 1948;152(1):162–174.

8. Cournand A, Motley HL, Werko L. Mechanism underlying cardiac output change during intermittent positive pressure breathing (IPP) Fed Proc. 1947;6(1 pt 2):92.

9. Hutsebaut J, Scano G, Garcia-Herreros P, Degré S, De Coster A, Sergysels R. Hemodynamic characteristics in chronic obstructive lung disease as related to cardiac size. Respiration. 1981;41(1):25–32.

10. Jörgensen K, Müller MF, Nel J, Upton RN, Houltz E, Ricksten SE. Reduced intrathoracic blood volume and left and right ventricular dimensions in patients with severe emphysema: an MRI study. Chest. 2007;131(4):1050–1057.

11. Yamada T, Takeda J, Satoh M, Koyama K, Hashiguchi S, Yokoi M. Effect of positive end-expiratory pressure on left and right ventricular diastolic filling assessed by transoesophageal Doppler echocardiography. Anaesth Intensive Care. 1999;27(4):341–345.

12. Izumi S, Moriyama K, Kobayashi S, et al. Phasic venous return abnormality in chronic pulmonary diseases: pulsed Doppler echocardiography study. Intern Med. 1994;33(6):326–333.

13. Whittenberger JL, McGregor M, Berglund E, Borst HG. Influence of state of inflation of the lung on pulmonary vascular resistance. J Appl Physiol. 1960;15:878–882.

14. Barr RG, Bluemke DA, Ahmed FS, et al. Percent emphysema, airflow obstruction, and impaired left ventricular filling. N Engl J Med. 2010;362(3):217–227.

15. Watz H, Waschki B, Meyer T, et al. Decreasing cardiac chamber sizes and associated heart dysfunction in COPD: role of hyperinflation. Chest. 2010;138(1):32–38.

16. Tschernko EM, Gruber EM, Jaksch P, et al. Ventilatory mechanics and gas exchange during exercise before and after lung volume reduction surgery. Am J Respir Crit Care Med. 1998;158(5 pt 1):1424–1431.

17. Jörgensen K, Houltz E, Westfelt U, Nilsson F, Scherstén H, Ricksten SE. Effects of lung volume reduction surgery on left ventricular diastolic filling and dimensions in patients with severe emphysema. Chest. 2003;124(5):1863–1870.

18. Takata M, Mitzner W, Robotham JL. Influence of the pericardium on ventricular loading during respiration. J Appl Physiol. 1990;68(4):1640–1650.

19. Collins J. Diseases of the airways. In: Juhl JH, Crummy AB, Kuhlman JE, editors. Paul and Juhl's Essentials of Radiologic Imaging. 7th ed. Philadelphia: Lippincott-Raven Publishers; 1998. pp. 937–954.

20. Tomita H, Yamashiro T, Matsuoka S, Matsushita S, Kurihara Y, Nakajima Y. Changes in cross-sectional area and transverse diameter of the heart on inspiratory and expiratory chest CT: correlation with changes in lung size and influence on cardiothoracic ratio measurement. PLoS One. 2015;10(7):e0131902.

21. Nigro CA, Prieto JE, Kleinert MM, Rhodius EE. Effect of inhaled salbutamol on dynamic intrinsic positive end-expiratory pressure in spontaneously breathing patients with stable severe chronic obstructive pulmonary disease. Med Sci Monit. 2005;11(11):181–185.

22. Wrobel JP, Thompson BR, Williams TJ. Mechanisms of pulmonary hypertension in chronic obstructive pulmonary disease: a pathophysiologic review. J Heart Lung Transplant. 2012;31(6):557–564.

23. Harris P, Segel N, Green I, Housley E. The influence of the airways resistance and alveolar pressure on the pulmonary vascular resistance in chronic bronchitis. Cardiovasc Res. 1968;2(1):84–92.

24. Sciurba FC, Rogers RM, Keenan RJ, et al. Improvement in pulmonary function and elastic recoil after lung-reduction surgery for diffuse emphysema. N Engl J Med. 1996;334(17):1095–1099.

25. Similowski T, Yan S, Gauthier AP, Macklem PT, Bellemare F. Contractile properties of the human diaphragm during chronic hyperinflation. N Engl J Med. 1991;325(13):917–923.

26. Yamashiro T, Tsubakimoto M, Nagatani Y, et al. Automated continuous quantitative measurement of proximal airways on dynamic ventilation CT: initial experience using an ex vivo porcine lung phantom. Int J Chron Obstruct Pulmon Dis. 2015;10(1):2045–2054.

27. Yamashiro T, Moriya H, Tsubakimoto M, Matsuoka S, Murayama S. Continuous quantitative measurement of the proximal airway dimensions and lung density on four-dimensional dynamic-ventilation CT in smokers. Int J Chron Obstruct Pulmon Dis. 2016;11(1):755–764.

28. Yamashiro T, Matsuoka S, Bartholmai BJ, et al. Collapsibility of lung volume by paired inspiratory and expiratory CT scans: correlations with lung function and mean lung density. Acad Radiol. 2010;17(4):489–495.

29. Kundu S, Gu S, Leader JK, et al. Assessment of lung volume collapsibility in chronic obstructive lung disease patients using CT. Eur Radiol. 2013;23(6):1564–1572.

30. Gollub MJ, Panu N, Delaney H, et al. Shall we report cardiomegaly at routine computed tomography of the chest? J Comput Assist Tomogr. 2012;36(1):67–71.

31. Du Bois D, Du Bois EF. A formula to estimate the approximate surface area if height and weight be known 1916. Nutrition. 1989;5(5):303–311.

32. Hellebrandová L, Chlumský J, Vostatek P, Novák D, Rýznarová Z, Bunc V. Airflow limitation is accompanied by diaphragm dysfunction. Physiol Res. 2016;65(3):469–479.

33. Wigh RE. On defining microcardia: application in pulmonary emphysema. South Med J. 1978;71(2):150–154.

34. De Troyer A. Effect of hyperinflation on the diaphragm. Eur Respir J. 1997;10(3):708–713.

35. Camiciottoli G, Diciotti S, Bigazzi F, et al. Is intrathoracic tracheal collapsibility correlated to clinical phenotypes and sex in patients with COPD? Int J Chron Obstruct Pulmon Dis. 2015;10(1):843–852.

36. Guyton AC. Textbook of Medical Physiology. 5th ed. Philadelphia: WB Saunders; 1976.

37. Taylor RR, Covell JW, Sonnenblick EH, Ross J. Dependence of ventricular distensibility on filling of the opposite ventricle. Am J Physiol. 1967;213(3):711–718.

38. Janicki JS, Weber KT. The pericardium and ventricular interaction, distensibility, and function. Am J Physiol. 1980;238(4):H494–H503.

39. Yamauchi Y, Kohyama T, Jo T, Nagase T. Dynamic change in respiratory resistance during inspiratory and expiratory phases of tidal breathing in patients with chronic obstructive pulmonary disease. Int J Chron Obstruct Pulmon Dis. 2012;7(1):259–269.

Table 1. Clinical characteristics of the 31 study subjects

	mean±SD	range
Gender (female: male)	(5 : 26)	-
Age (years)	72 ± 10	(39 to 86)
Smoking status (ex-smoker : current smoker)	(15 : 16)	-
Smoking index (pack-years)	47 ± 11	(2 to 100)
$FEV_{1.0}$/FVC	0.71 ± 0.13	(0.41 to 0.92)

Abbreviations: $FEV_{1.0}$, forced expiratory volume in the first second; FVC, forced vital capacity; SD, standard deviation.

Table 2. CT-based indices in COPD patients versus non-COPD smokers

CT indices	COPD patients	Non-COPD smokers	P-value
Dynamic-ventilation CT			
Cardiac CSA_{Insp} (cm^2)	69.1±10.3	78.7±8.2	<0.05
Cardiac CSA_{Exp} (cm^2)	68.2±15.0	84.6±10.2	<0.01
CTR_{Insp} (%)	46.7±4.4	49.7±4.9	NS
CTR_{Exp} (%)	47.9±4.7	54.3±4.5	<0.001
ΔCTR (%)	1.2±2.0	4.6±2.7	<0.01
E/I ratio – CTR	1.03±0.04	1.10±0.06	<0.01
Helical CT			
LAV%	23.9±16.9	4.5±5.2	<0.001

Note: Data are expressed as mean ± SD.

Abbreviations: CSA, cross-sectional area; CT, computed tomography; CTR, cardiothoracic ratio; ΔCTR, difference between CTR_{Exp} and CTR_{Insp}; E/I, expiratory/inspiratory; Exp, expiratory; Insp, inspiratory; LAV%, percent low attenuation volume; NS, not significant; SD, standard deviation.

Table 3:CCC between the maximum cardiac CSA and MLD on dynamic-ventilation CT

CCC measurements	CCC between cardiac CSA and MLD		Correlation with $FEV_{1.0}$/FVC	
	Mean ± SD	Range	Coefficient (ρ)	*P*-value
Entire respiratory phase	0.14±0.62	−0.87 to 0.99	0.56	<0.01
Expiratory phase only	0.25±0.57	−0.79 to 0.94	0.63	<0.001

Note: The expiratory phase was defined from the peak inspiratory frame to the peak expiratory frame on the continuous MLD curve (5–12 frames).

Abbreviations: CCC, cross-correlation coefficient; CSA, cross-sectional area; CT, computed tomography; $FEV_{1.0}$, forced expiratory volume in 1 s; FVC, forced vital capacity; MLD, mean lung density; SD, standard deviation.

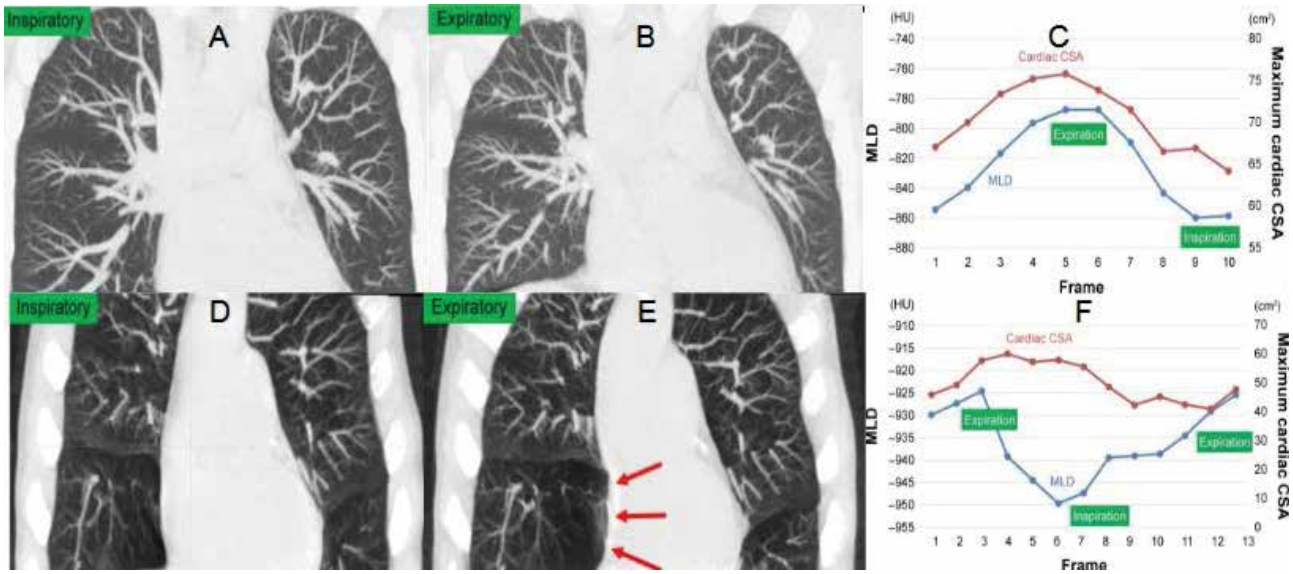

Figure A-C 39-year-old male current smoker without COPD. **Notes:** His $FEV_{1.0}$/FVC was 0.92. Inspiratory (A) and expiratory phases (B) (both shown in coronal view, MIP images) demonstrated an increase in heart size during expiration, mainly due to diaphragm elevation. Time curves of MLD and maximum cardiac CSA (C) showed similar motion trend , suggesting that cardiac CSA decreased with inspiration and increased with expiration (CCC of all frames =0.987).

Figure D-F 70-year-old male with COPD underwent dynamic-ventilation CT to evaluate central airway abnormalities. **Notes:** His FEV1.0/FVC was 0.55. The shape of the right atrium was normal during the inspiratory phase (D) but was severely compressed (arrows) during the expiratory phase, probably due to the emphysematous right middle lobe (E).Time curves of MLD and maximum cardiac CSA demonstrated almost opposite shapes (F), suggesting that the heart size increased during inspiration and decreased during expiration. The CCC of the entire cycle was −0.392, and that of the expiratory frames (frame no. 6–13 in this case) was −0.723.

Abbreviations: CT, computed tomography; FEV1.0, forced expiratory volume in 1 s; FVC, forced vital capacity; MIP, maximum intensity projection.CCC, cross-correlation coefficient; CSA, cross-sectional area; CT, computed tomography; HU, Hounsfield unit; MLD, mean lung density.

注：本研究は 2017 年 10 月 26 日「International Journal of Chronic Obstructive Pulmonary Disease 」という雑誌より発表しました。

作成日：2018 年 1 月 29 日

Recreational drug use and sexual behaviors among men who have sex with men in Sichuan, China

中国四川省の MSM(men who have sex with men) における レクリエーショナルドラッグ使用と性行動

研究者氏名　戴　映雪（第 39 期笹川医学研究者）
中国所属機関　成都市疾病予防控制中心感染病防制科
日本研究機関　京都大学社会健康医学系専攻社会疫学
指導責任者　木原　正博 教授
共同研究者　木原　雅子 准教授, Patou Masika Musumari 助教

Abstract

Background: Recreational drug use is associated with human immunodeficiency virus (HIV), sexually transmitted infections (STIs), and a range of risky sexual behaviors among men who have sex with men (MSM) in China, it is unclear to what extent these behaviors and outcomes differ between lifetime single-drug users and polydrug users in China. This research gap is addressed in the current study.

Methods: This is a cross-sectional study conducted from July 2016 to September 2016 among MSM in Sichuan Province, China. Participants were recruited in community-based organizations (CBOs), using convenient sampling. Multinomial logistic regression was applied.

Results: A total of 1122 participants were included. Overall, 12.7% reported HIV infection and 13.3% reported a history of STI. Twenty-eight percent of MSM have ever used recreational drugs, of whom 64.0% were lifetime single-drug users, and 36.0% were polydrug users. Factors associated with both single-drug and polydrug use included self-reported HIV (single-drug use: adjusted odds ratio [AOR] = 1.76, 95% confidence interval [CI]: 1.02–3.02; polydrug use: AOR = 3.19, 95% CI: 1.62–6.26), self-reported history of STIs (AOR = 1.86, 95% CI: 1.08–3.21; AOR = 3.32, 95% CI: 1.77–6.26), and ever had group sex (AOR = 2.23, 95% CI: 1.28–3.87; AOR = 4.68, 95% CI: 2.41–9.08).

Conclusion: We found that both lifetime single-drug and polydrug use were associated with risky sexual behaviors and outcomes (HIV/STIs), with a magnitude of the associations higher among polydrug users. Our findings suggest the urgent need for HIV prevention programs among MSM in China to integrate strategies that tackle recreational drug use.

Keywords

Recreational drug, polydrug, risky behavior, MSM, HIV

Introduction

Men who have sex with men (MSM) remain one of the populations with the highest burden of HIV. Sichuan, a southwest province of China and the setting of the present study, has one of the highest prevalence of HIV among MSM in the country [1], estimated 11.1% [2]. Substance use, including non-injection drug use, has been documented as one of main factors amplifying the risk of HIV in MSM.

The use of recreational drugs is pervasive among MSM in many parts of the world [3-6]. In China, recreational drugs, also referred to as “new-type drugs” include a wide range of substances such as rush popper, crystal meth, ecstasy, “happy water” and “magu” [7]. A national online survey indicated that 77.3% of Chinese MSM reported having ever used

recreational drugs [8].

The link between recreational drugs and risky sexual behaviors is extensively documented in many settings [3, 4, 9]. Emerging evidence suggest that polydrug use (defined as the use of more than one drug at the same time or within the same time period) may be associated with higher risk than the use of a single drug [3, 4, 10, 11]. Studies reporting the prevalence of recreational polydrug use [9, 12] or its association with risky sexual behaviors are remarkably scarce in China [13]. The current study addresses the above gap by investigating the prevalence of recreational drug use, and its relationship with socio-demographic factors, sexual behaviors, and HIV/STIs among MSM in three non-capital cities of Sichuan Province, China.

Methods

Study design, participants, and setting

This is a cross-sectional survey conducted from July to September 2016 in Sichuan Province, China. The population of interest was MSM, aged at least 18 years, and currently living in the selected cities. The participants of this study were recruited among those visiting community-based organizations (CBOs) for Voluntary Counseling & Testing (VCT).

Data collection

Data were collected using an anonymous self-administered structured questionnaire. The main outcome of this study was "lifetime recreational drug use", Those who ever used only one type were classified as "lifetime single drug" users, while those who reported more than one type were characterized as "lifetime polydrug users". Recreational drug listed in the questionnaire included rush popper, capsule zero (or 5-MEO-DIPT, foxy), crystal meth, ecstasy, magu, ketamine, happy water, GHB (gamma-hydroxybutyrate), cannabis, bath salt (or cathinone), red crystal meth (extracts from methamphetamine) and heroine. Participants were asked to specify the drug's name in case it was not listed.

Ethics statement

The current study was granted ethical clearance by the Ethics Board of the People's Hospital of Chengdu Tianfu New Area.

Statistical analysis

Data were double input with Epi-data version 3.0, and imported into SPSS 17 for Windows (SPSS Inc., Chicago, Illinois, USA) for statistical analysis. Multinomial logistic regression was applied to examine the linked factors.

Results

Characteristic of the participants

The analytical sample of this study consisted of 1122 participants. The majority of the participants were at least 25 years of age (67.6%), unmarried (78.0%), local residents (75.3%), had an employment (76.2%), and a monthly income of ≥ 3000 CNY (about 450 USD) (60.0%). Most participants reported having had two or more male sexual partners in the previous 12 months (75.7%). The proportion of condomless sex in the previous 12 months with "regular sex partner" and with "non-regular sex partner" was 54.6% and 36.3% respectively. In our sample, 12.7% of participants had self-reported HIV infection and 13.3% had self-reported history of STIs.

Recreational drug use

In total, 27.7% of the participants ever used recreational drugs, of whom 64.0% were lifetime single drug users. The reported recreational drugs among single drug users were rush popper (89.0%), crystal meth (8.5%), and capsule zero (2.5%).

Correlates of recreational drug use

In the adjusted model, alcohol use, sexual role preference, seeking partners mainly by Internet, ever had group sex, self-reported STIs, and self-reported HIV infection were independently associated with both single drug and polydrug use. Marital status, residential status and having regular sex partner were only associated with polydrug use, while sexual orientation was only associated with single drug use. Overall, the proportions of risky behaviors were higher when comparing polydrug users to non-drug users than when comparing single drug users to non-drug users.

In terms of risky behaviors, participants who reported ever engaged in a group sex were more likely to be single drug users (AOR=2.23, 95% CI: 1.28-3.87) and polydrug users (AOR=4.68, 95% CI: 2.41-9.08) compared to non-drug users.

HIV positive status was associated with increased odds of single-drug use (AOR=1.76, 95% CI: 1.02-3.02) and polydrug use (AOR=3.19, 95% CI: 1.62-6.26). The same trend was noted for self-reported STIs, with higher odds among single drug users (AOR=1.86, 95% CI: 1.08-3.21) and polydrug users (AOR=3.32, 95% CI: 1.77-6.26).

In addition, "receptive sexual role" was associated with increased odds of both single drug use (AOR=1.79, 95% CI: 1.05-3.07) and polydrug use (AOR=6.00, 95% CI: 2.54-14.17). Factors only associated with polydrug use included having regular sex partners in the previous 12 months (AOR=2.07, 95% CI: 1.18-3.64) and migration (AOR=2.26, 95% CI: 1.22-4.20).

Discussion

The relationship between HIV infection and history of STIs with recreational drug use was found in many previous studies [4, 9, 13, 14], and explained by the high prevalence of unprotected sex and other risky sexual behavior (such as group sex, multiple sex partnerships) among MSM populations who engage in recreational drugs [4, 13]. This is consistent with our results showing that a high proportion of lifetime single drug and polydrug users reported condomless sex either with regular or non-regular sex partners. In addition, we found that the proportion of "ever had group sex" was significantly higher in lifetime polydrug users and lifetime single drug users; respectively six times and three times higher than in non-recreational drug users. Recreational drugs are often used during group sex to extend sexual feeling and duration, maximizing sexual pleasure in gay subculture [15]. For example, crystal meth, one of the popular group sex drugs [16], can prolong sexual activity to last up to 10-12 hours [17]. This may explain the reason for the particularly higher prevalence of group sex among polydrug users observed in our study.

We also found that being a migrant (not officially registered in the local city) was associated with polydrug use. Migration from rural to urban areas is a common phenomenon in China, and is mostly fueled by economic reasons [18] and, specifically for MSM, searching for peer friendship [19]. Studies have shown that internal migrants in China are exposed to multiple stressors including, for example, poor work conditions, limited access to social security and medical benefits, and discrimination. The stressors lead to adverse mental health outcomes including depression, anxiety and substance use [20]. Moreover, migrant MSM may particularly be vulnerable to risky behaviors such as recreational drug use as a result of the sense of freedom from family and social norms in their original settings, and the need to assimilate into local gay subculture [19].

The interaction of being MSM and using recreational drugs can significantly amplify the risks of HIV/STIs. In our study, although the prevalence of HIV and history of STIs was already high among non-drug users (9.2% for HIV, 9.2% for STIs), it substantially increased among single drug users (15.6% for HIV, 16.7% for STIs) and polydrug users (32.1% for HIV, 37.5% for STIs). In China, most HIV/STIs prevention interventions among substance users have mainly focused

on people who inject drugs [21]. Our finding highlights the urgent need for appropriate HIV/STIs prevention strategies among MSM who use recreational drugs. In addition, the prevalence of risky behaviors was highest among recreational polydrug users, however, the prevalence among single drug users was no less alarming; suggesting that both groups warrant the attention of targeted strategies to reduce the risks of substance use and risky sexual behaviors.

References

1. Zhang, L., et al., *HIV prevalence in China: integration of surveillance data and a systematic review.* The Lancet Infectious Diseases, 2013. **13**(11): p. 955-963.
2. Liang, L., et al., *Infection status of HIV and its influence factors among men who have sex with men in Sichuan province.* Chin J Prev Med, 2014. **48**(11): p. 980-984.
3. Daskalopoulou, M., et al., *Recreational drug use, polydrug use, and sexual behaviour in HIV-diagnosed men who have sex with men in the UK: results from the cross-sectional ASTRA study.* The Lancet HIV, 2014. **1**(1): p. e22-e31.
4. Hidaka, Y., et al., *Substance use and sexual behaviours of Japanese men who have sex with men: a nationwide internet survey conducted in Japan.* BMC Public Health, 2006. **6**: p. 239.
5. Schmidt, A.J., et al., *Illicit drug use among gay and bisexual men in 44 cities: Findings from the European MSM Internet Survey (EMIS).* Int J Drug Policy, 2016. **38**: p. 4-12.
6. Suguimoto, S.P., et al., *Changing patterns of HIV epidemic in 30 years in East Asia.* Curr HIV/AIDS Rep, 2014. **11**(2): p. 134-45.
7. Ding, Y., N. He, and R. Detels, *Circumstances of initiation into new-type drug use among adults in Shanghai: are there differences by types of first new-type drug used?* Drug Alcohol Depend, 2013. **131**(3): p. 278-83.
8. Zhao, P., et al., *Recreational Drug Use among Chinese MSM and Transgender Individuals: Results from a National Online Cross-Sectional Study.* PLoS One, 2017. **12**(1): p. e0170024.
9. Chen, X., et al., *Club Drugs and HIV/STD Infection: An Exploratory Analysis among Men Who Have Sex with Men in Changsha, China.* PLoS One, 2015. **10**(5): p. e0126320.
10. Mimiaga, M.J., et al., *Polysubstance use and HIV/STD risk behavior among Massachusetts men who have sex with men accessing Department of Public Health mobile van services: implications for intervention development.* AIDS Patient Care STDS, 2008. **22**(9): p. 745-51.
11. Sewell, J., et al., *Poly drug use, chemsex drug use, and associations with sexual risk behaviour in HIV-negative men who have sex with men attending sexual health clinics.* Int J Drug Policy, 2017. **43**: p. 33-43.
12. Zhang, H., et al., *Poppers use and risky sexual behaviors among men who have sex with men in Beijing, China.* Drug Alcohol Depend, 2016. **160**: p. 42-8.
13. Duan, C., et al., *Recreational drug use and risk of HIV infection among men who have sex with men: A cross-sectional study in Shenzhen, China.* Drug Alcohol Depend, 2017. **181**: p. 30-36.
14. Zhang, C., et al., *Sexual Behaviors Linked to Drug and Alcohol Use Among Men Who Have Sex With Men in China.* Subst Use Misuse, 2016. **51**(14): p. 1821-30.
15. Hirshfield, S., et al., *Drug Use, Sexual Risk, and Syndemic Production Among Men Who Have Sex With Men Who Engage in Group Sexual Encounters.* Am J Public Health, 2015. **105**(9): p. 1849-58.
16. Phillips, G., C. Grov, and B. Mustanski, *Engagement in group sex among geosocial networking mobile application-using men who have sex with men.* Sex Health, 2015. **12**(6): p. 495-500.

17. Ding, Y. and N. He, *Club drugs and HIV/STI infection: A new public health concern in China.* Fuda Univ J Med Sci, 2012. **39**(6).
18. Wu, Z., et al., *HIV and syphilis prevalence among men who have sex with men: a cross-sectional survey of 61 cities in China.* Clin Infect Dis, 2013. **57**(2): p. 298-309.
19. Egan, J.E., et al., *Migration, neighborhoods, and networks: approaches to understanding how urban environmental conditions affect syndemic adverse health outcomes among gay, bisexual and other men who have sex with men.* AIDS Behav, 2011. **15 Suppl 1**: p. S35-50.
20. Meyer, S.R., et al., *Workplace and security stressors and mental health among migrant workers on the Thailand-Myanmar border.* Soc Psychiatry Psychiatr Epidemiol, 2016. **51**(5): p. 713-23.
21. UNAIDS. *HIV in Asia and the Pacific*. 2013 31st Oct 2017]; Available from: http://www.unaids.org/sites/default/files/media_asset/2013_HIV-Asia-Pacific_en_0.pdf.

作成日：2018 年 2 月 23 日

Assessment of Mechanical Properties of WaveOne Gold NiTi Rotary Instruments
WaveOne Gold NiTi ファイルの機械的特性の評価

研 究 者 氏 名　童　方麗（第 39 期笹川医学研究者）
中国所属機関　南方医科大学の口腔病院
日本研究機関　東京医科歯科大学大学院医歯学総合研究科
指 導 責 任 者　興地　隆史 教授，海老原　新 助教
共同研究者名　牧圭　一郎，木村　俊介，西条　美紀，時田　大輔

Abstract:

The purpose of this study was to compare the cyclic fatigue, stress, and flexibility of Wave One Gold files (WOG; Dentsply Maillefer, 25/0.07, 25mm) with Wave One files(WO; Dentsply Maillefer, 25/0.08, 25mm)　and Reciproc files (RE; VDW, 25/0.08, 25mm).

Key words:

Mechanical properties, WaveOne, WaveOne gold, Reciproc, cyclic fatigue, cantilever bending test; screw- in force

Introduction:

It has been reported that reciprocating motion reduced the risk of cyclic fatigue in nick-titanic rotary instruments caused by tension and compression in proportion to that of rotation motion. However, the single-file instrument would be subject to high stresses by shaping root canals with only one file. Therefore, it is crucial for clinicians to be aware of the mechanical properties of different instruments and their effect on instrument performance to decrease the potential risk of fracture.

Methods:

Rotary instruments including 30 WOG, 30 WO and 30 RE were randomly divided into 3 groups (n=10 each) for cyclic fatigue test, cantilever bending test, and torque/force analysis, respectively. A custom-made three-pin device with a 38° curvature and 5 mm radius was used for cyclic loading. Time to fracture and fractured length was recorded. Bending loads were measured at deflection of 0.5 mm and 2.0 mm during the loading process. An automated root canal instrumentation and torque/force analyzing system was used to prepare resin canals and detect torque and apical force generated during preparation. Maximum torque and apical force values were recorded.

Results:

In the cyclic fatigue test, time taken for WOG, WO, and RE to fail was 236.11 ± 17.30, 107.20 ± 33.59, and 274.22 ± 63.26 seconds, respectively. WOG and RE took significantly longer time to fracture compared with WO ($P<0.05$, one

way ANOVA and Turkey test), while no statistical difference was found between WOG and RE ($P>0.05$). Mean length of the fractured part of the file was not significantly different among all groups ($P>0.05$). In the bending test, WOG showed the smallest load values among all groups whether at deflection of 0.5 mm or 2mm ($P<0.05$, Kruskal Wallis test and Mann-Whitney U Test). In the torque/force analysis, both maximum upward apical force and maximum counterclockwise torque values in WOG and WO were significantly lower than those in RE ($P<0.05$, Kruskal Wallis test and Mann-Whitney U Test), while no difference between WOG and WO was detected ($P>0.05$).

Discussions:

WOG showed higher cyclic fatigue resistance compared with WO, and higher flexibility compared with WO and RE. WOG generated significantly lower maximum torque and may have advantages in reducing stress generation caused by screw-in forces, when compared with RE; while no advantages when compared with WO.

Reference:

1. Capar ID, Ertas H, Ok E, Arslan H, Ertas ET. Comparative study of different novel nickel-titanium rotary systems for root canal preparation in severely curved root canals. Journal of endodontics 2014;40(6):852-856.
2. Adiguzel M, Capar ID. Comparison of Cyclic Fatigue Resistance of WaveOne and WaveOne Gold Small, Primary, and Large Instruments. Journal of endodontics 2017;43(4):623-627.
3. De-Deus G, Moreira EJ, Lopes HP, Elias CN. Extended cyclic fatigue life of F2 ProTaper instruments used in reciprocating movement. International endodontic journal 2010;43(12):1063-1068.
4. Capar ID, Arslan H. A review of instrumentation kinematics of engine-driven nickel-titanium instruments. International endodontic journal 2016;49(2):119-135.
5. Elnaghy AM, Elsaka SE. Assessment of the mechanical properties of ProTaper Next Nickel-titanium rotary files. Journal of endodontics 2014;40(11):1830-1834.
6. Gao Y, Gutmann JL, Wilkinson K, Maxwell R, Ammon D. Evaluation of the impact of raw materials on the fatigue and mechanical properties of ProFile Vortex rotary instruments. Journal of endodontics 2012;38(3):398-401.
7. Keskin C, Inan U, Demiral M. Effect of interrupted motion on the cyclic fatigue resistance of reciprocating nickel-titanium instruments. International endodontic journal 2017.
8. Elsaka SE, Elnaghy AM, Badr AE. Torsional and bending resistance of WaveOne Gold, Reciproc and Twisted File Adaptive instruments. International endodontic journal 2017;50(11):1077-1083.
9. Topcuoglu HS, Duzgun S, Akti A, Topcuoglu G. Laboratory comparison of cyclic fatigue resistance of WaveOne Gold, Reciproc and WaveOne files in canals with a double curvature. International endodontic journal 2017;50(7):713-717.
10. Tokita D, Ebihara A, Miyara K, Okiji T. Dynamic Torsional and Cyclic Fracture Behavior of ProFile Rotary Instruments at Continuous or Reciprocating Rotation as Visualized with High-speed Digital Video Imaging. Journal of endodontics 2017;43(8):1337-1342.

Table 1. Time to Fracture and Length of Fractured Fragments of Instruments Subjected to Cyclic Fatigue Test

Group	time（seconds）	length (mm)
WOG	236.11 ± 18.25[a]	6.20 ± 0.24[c]
WO	107.20 ± 33.59[b]	5.78 ± 1.80[c]
RE	274.22 ± 66.63[a]	7.26 ± 0.18[c]

Values are mean ± standard deviation.

N = 10 in each group.

Mean values with different superscript letters in a column are significantly different (P < .05).

Table 2. Load Values of Cantilever Bending Test at the Defection of 0.5 mm and 2 mm

	Load (N)	
Group	0.5 mm	2 mm
WOG	0.34 ± 0.19[a]	2.09 ± 0.26[c]
WO	1.26 ± 0.16[b]	4.48 ± 0.36[d]
RE	1.10 ± 0.15[b]	4.00 ± 0.55[e]

Values are mean ± standard deviation.

N = 10 in each group.

Mean values with different superscript letters in a column are significantly different (P < .05).

Table 3. Maximum Apical Force and Maximum Torque Values in Two Directions

	Apical force (N)		**Torque (N•m)**	
Group	Upward	Downward	Counter-clockwise	Clockwise
WOG	-3.56 ± 0.53[a]	2.51±0.94[c]	-12.95±2.52[d]	3.64±1.33[f]
WO	-3.39±0.49[a]	2.41±1.85[c]	-11.87±3.10[d]	6.63±2.61[g]
RE	-7.26±1.49[b]	1.86±0.77[c]	-25.86±3.14[e]	9.54±3.64[g]

Values are mean ± standard deviation.

N = 10 in each group.

Mean values with different superscript letters in a column are significantly different (P < 0.05).

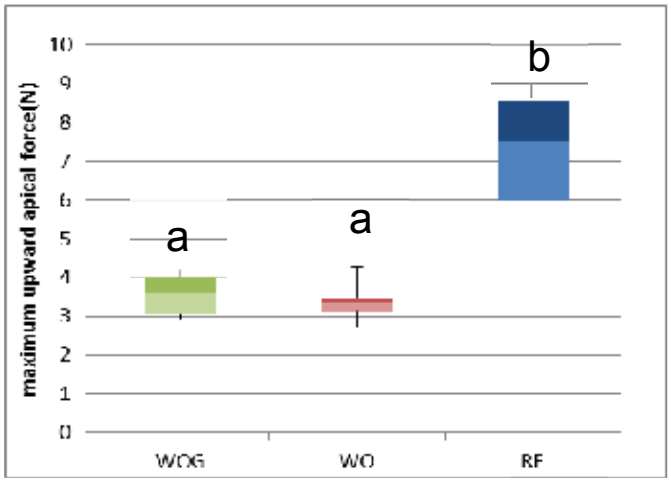

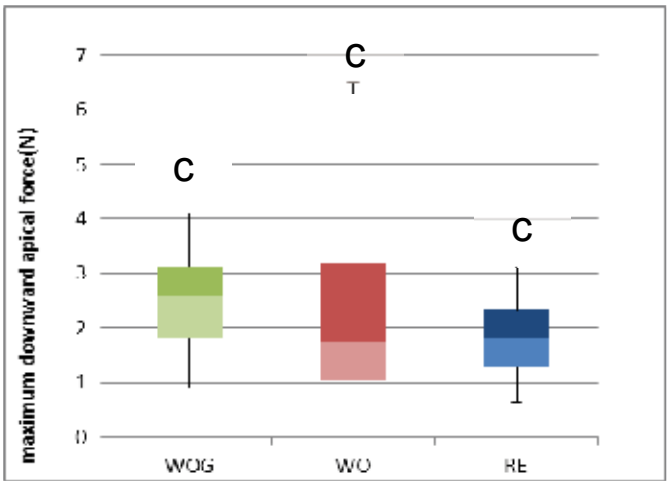

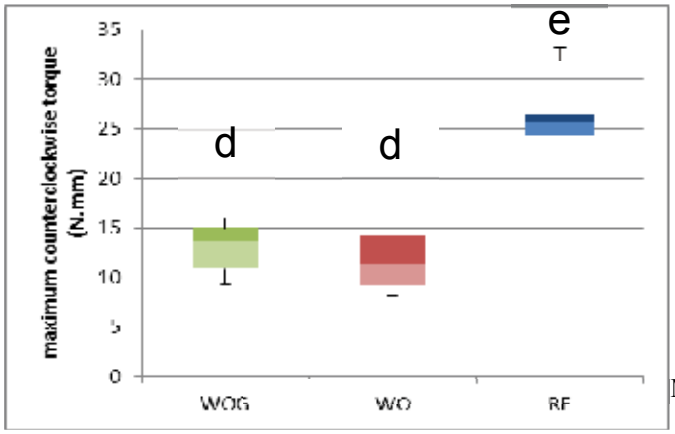

M

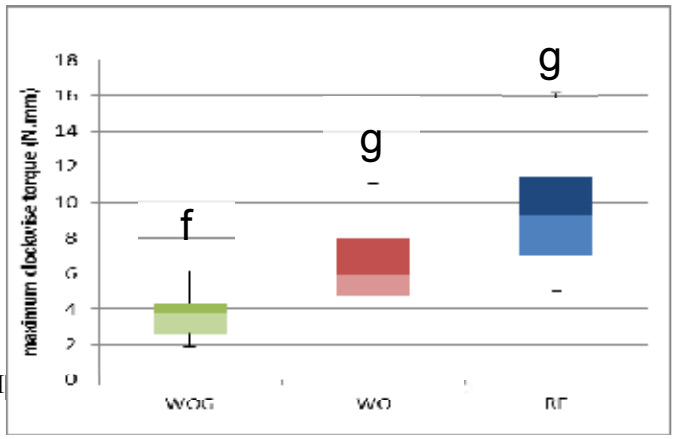

注：本研究は 2017 年 10 月 25 日「第 147 回日本歯科保存学会 2017 年度秋季学術大会」にて口演発表。

作成日：2018 年 2 月 13 日

腹臥位胸腔鏡下食道切除術、HALS 胃管再建術、頚部吻合術手術手技について

Thoracoscopic esophagectomy and lymphadenectomy in prone position followed by conduit gastric pull up in HALS

研 究 者 氏 名　　李　君鵬（第 39 期笹川医学研究者）
中国所属機関　　吉林省人民病院救急外科
日本研究機関　　東北大学病院移植・再建・内視鏡外科
指 導 責 任 者　　亀井　尚　教授

[はじめに]

食道癌、胃癌に代表される上部消化管疾患の治療は手術治療法、各種放射線療法、化学療法がある。しかし、胃癌、食道癌の治癒を目指す場合に最も確実な治療方法は現在でも切除手術である。代表的な疾患として、食道癌に対する根治切除術は胸部、腹部、頸部の 3 か所に手術操作が及び、高度侵襲を伴う上、周術期合併症、栄養や呼吸に関連する問題点も多い。胸腔鏡下食道切除術は手術の低侵襲化に寄与するものであり、日本では 1994 年に開始された。現在は日本全国で広く普及しているが、私の研究機関は日本で初めての胸腔鏡下食道切除手術を行った、この領域のオピニオンリーダーである。私が留学した２０１７年から８０例以上の腹臥位胸腔鏡下食道切除術を見学した。その手術手技について報告する。

[キーワード]

腹臥位胸腔鏡下食道切除術、HALS 胃管再建術、頚部吻合術、腸瘻造設、頚部リンパ節郭清、反回神経麻痺、Gambee1 層縫合法

[手術手技]

一、腹臥位胸腔鏡下食道切除術：

１、体位、人工気胸 - 右上肢をクロール状に挙上した左半腹臥位にベッドローテーションを加えて体位を作成している。ポート配置は後腋窩線を中心に第３、５、７、９肋間に 5 ポートを基本として留置するが、ここに 6-8ｍmHg の CO2 による人工気胸を加える。これにより右肺は虚脱し、縦隔が展開されるため、食道切除の術野が広く確保される。助手にょる肺の圧排が不要なため、簡便であり、肺圧排に関連した侵襲が低減できるメリットがある。

２、病変の確認 - ポートの挿入がすめば、人工気胸下で胸腔内の観察を行い病変を確認する。肺癒着がある場合には癒着剥離を行っておく。

３、奇静脈弓切離 - 食道背側の縦膈胸膜を切開し、頭側に進めていき、奇静脈弓をリネアステイプラーにて切離する。その背側断端にかけた支持糸を肋間から体外に誘導して牽引することで、同部位の展開が広く行われる。ここには右気管支動脈、胸管が存在しているが、これらは腫瘍の浸潤を受けていない限り温存する。

４、右反回神経周囲リンパ節郭清 - 右迷走神経に沿って頭側に縦膈胸膜を切開し、右鎖骨下動脈に到達する。右鎖骨下動脈と NO.106recR の組織の間を剥離して、右反回神経を同定し、これを確実に温存する。気管前方に連続する NO.106recR を可急的に頭側深部で切離することで郭清の上限を決定する。次いで脂肪組織と一塊になった NO.106recR を気管から剥離、切離することで郭清が完成する。106recR は食道癌リンパ節転移の最も重要な部位（好発部位）で、本手術の要点の一つである。反回神経麻痺を防止するために、術中リアルタイムに神経刺激を行うデバイス（NIM）が用いられる。

５、中下縦膈リンパ節郭清 - 食道の腹側で心嚢の背側を広く剥離する。気管分岐部尾側に気管支下、分岐部リンパ節 NO.107,109 リンパ節が存在する。このリンパ節の郭清は、組織を食道につけるように行い、確実に止血を行いながら処理する。右気管支動脈の末梢がこの部分にあることが多く、出血しやすいので注意が必要である。次いで、食道を牽引しながら、下行大動脈との剥離をすすめ、固有食道動脈を処理しながら、下縦膈リンパ節郭清（NO.111,NO.112aoA,NO.112pul）を行う。

６、左反回神経周囲リンパ節郭清 - 上部食道の背側を十分に剥離を行っておくと、後の郭清操作が容易となる。食道を全周性に剥離して、ガーゼで食道を背側に吊り上げ牽引、固定する。左反回神経は大動脈弓を反回し、頭側に向かうが比較的長い距離がある。まず、気管左側から神経とリンパ節が一塊になった組織を剥離した後、周りの薄い組織を少しずつ剥離しながら、左反回神経を同定する。これにも NIM を使用し、神経の同定、麻痺を防止する手技を徹底する。左反回神経の食道枝を切離しながら、左反回神経を患者左側に剥離温存し、気管左側壁から 106recL を含む脂肪組織を背側に剥離し、可及的頭側まで剥離することで郭清が完成する。

７、食道仮切離-食道を自動縫合器リネアステイプラーで切離する。再建の胃管を胸腔に誘導し、後縦隔経路で消化管再建するために、食道の両断端に糸をかける。先に郭清した下縦膈リンパ節は取り残さないように食道に付する。最後、胸腔に出血、副損傷などの異常がないかどうか確認する。ドレーンを入れ、閉創する。

二、HALS(Hand Assisted Laparoscopic Surgery)胃管再建術：

１、体位 - 体位は開脚仰臥位で行っている。上腹部に７CM 縦小開腹を置く。

２、胃結腸間膜の直視処理 - Alexis を縦小開腹創縁に固定し、胃と横行結腸を創外に脱転する。超音波凝固切開装置で胃結腸間膜を可及的に凝固切離する。

３、小網の直視処理 - 胃の用手把持が容易するために、超音波凝固切開装置で小網を肝臓寄りで凝固切離し、左手を挿入できるようにしておく。

４、ポート配置と気腹 - 臍左側にカメラポート、左肋弓下外側に術者用ポート、右下腹部に助手用ポートを留置する。

５、腹腔鏡下胃結腸間膜の処理 - 術者は患者の脚間に位置する。左手を挿入したあと、10mmHg の CO2 で気腹をして腹腔鏡下で手術を開始する。術者は左手の指で胃結腸間膜を丁寧に把持して頭腹側方向に移動する

ことにより胃結腸間膜のテンションが得られるようにする。脾臓下極に向かって超音波凝固切開装置で胃結腸間膜を剥離する。

６、左胃大網動静脈の切離 - 脾臓下極まで処理したところで、脾臓の位置を確認する。脾臓の損傷を防ぐために癒着は丁寧に処理する。左胃大網動脈の拍動を確認して血管を剥離露出し、クリップにて処理する。

７、短胃動静脈の処理 - 胃を把持している左手の動きによって、胃脾間膜のテンションをつくる。短胃動静脈を超音波凝固切開装置で十分に凝固切離して、脾臓上極に進む。膵臓と脾臓を損傷しないように丁寧に処理する。

８、左横隔膜脚の露出 - 胃穹窿を背側から処理し,めぐりあげるようにする。左下横隔膜動脈を確認して切離すると左横隔膜脚が露出される。左横隔膜脚を剥離しつつ腹部食道に至る。

９、腹部食道の剥離 - 気腹圧の低下を防ぐために横隔食道間膜の開放を行わずに腹部食道の腹側を処理することを先行させる。

１０、膵上縁のリンパ節郭清 - 胃全体を把持し、これを腹側に牽引し、胃膵ヒダを展開する。助手はガーゼ越しに鉗子で膵を尾側へ転がすことにより、この部位の十分なテンションが得られる。以降の操作で NO.７，９リンパ節を郭清する。

１１、左胃動静脈の切離 - 牽引された胃膵ヒダの漿膜を切離し、左胃動脈の拍動を確認しながら血管を露出する。左胃静脈、左胃動脈の順にクリップ処理する。この操作で NO.７，９リンパ節を含む脂肪組織は胃側に付くことになるため、充分に郭清される。

１２、腹部食道の全周性剥離 - 胃後壁から食道後壁にかけて、横隔膜脚に沿って脂肪組織を剥離し、横隔食道膜を切離し全周性に横隔膜脚を剥離する。この全周性の剥離のあと、胸部食道および食道に付着したリンパ節を腹腔内に引き出す。食道裂孔が約４横指分開大していることを確認する。裂孔が狭い場合は、消化管再建に備えて十分な広さを保つように横隔膜の一部を切離することもある。

１３、小開腹創からの引き出しと胃管作製の操作 - 胃管形成は体外で行う。幽門より口側に５ｃｍ程度離れた、右胃動脈支配部を最初の切離部位とする。大弯側より４ｃｍ幅でマーキングをし、胃管をデザインする。胃下部小弯から自動縫合器を用いて胃壁を伸展しながらマーキングに沿って切離し、胃管を作成する。胃管の癒着防止、縫合不全予防目的にステープル断端は漿膜筋層縫合を追加する。また、無血管野に糸をかけ、縫合予定部の目安としておく。

１４、腸瘻造設 - 術後の栄養補助のために、空腸上部にチューブ腸瘻を造設する。Treitz 靭帯から約 15ｃｍの空腸を引き出し、近位側と遠位側を確認する。腸内容を移動させて腸管を虚脱させる。空腸間膜対側の漿膜と漿膜筋層の間に生塩水を注射する。メスで空腸の漿膜筋層を切開するが、長さ約６CM である。肛門側のチューブ予定入口部に巾着縫合をおく。腸管壁の入口部に小切開をおき、腸瘻チューブ先端を遠側位腸管内に挿入し、約３５ｃｍ進めて巾着縫合を結び、固定する。腸瘻チューブ両側の腸管壁を軽く合わせるよ

うにして結節縫合を行い、トンネルを作成するが、いわゆる Witzel 法である。腸瘻チューブが挿入された空腸を腹壁に約６ｃｍの長さで固定、小切開をおいて腸瘻チューブを体外に引き出す。空腸と腹壁の腹膜を縫合して固定する。

三、頚部リンパ節郭清 - 胸部上部（Ｕｔ）中部（Ｍｔ）の胸部食道癌については、頚部リンパ節郭清を行う。胸部下部（Ｌｔ）の胸部食道癌については、術前画像診断で頚部あるいは NO.106rec リンパ節に転移を認めた場合は頚部リンパ節郭清を行う。頚部リンパ節郭清の操作は腹部操作と同時に別のチームで進行している。手順は NO.101R リンパ節郭清、NO.104R リンパ節郭清、NO.101L リンパ節郭清、NO.104L リンパ節郭清、という順番で行っている。基本的に頸横動脈は温存している。

四、胃管の頚部への挙上と頚部食道胃管吻合 - 頚部郭清を終了後、後縦隔経路に胃管を頚部までに挙上する。残食道胃管吻合は 4-0PDS で Gambee1 層縫合法、手縫いで行っている。食道胃管吻合終了後、左右頚部にドレーンを挿入して閉創する。食道裂孔にヘルニアを防ぐために腹部から横隔膜脚に胃管を固定する。異常がなければ腹部閉創する。

[考察および結語]

本術式は非常に低侵襲であるとともに手術手技として合理的であると考える。症例によって状況が異なるため、術式の手順や方法が変わる時もあるが、平均出血量 50ｍｌ、多くの症例が手術翌日から歩行可能である。術後長期の成績については今後の検討項目であるが、本研究室で約 300 例を行った時点での 5 年生存率は pStageI で 90%、IIA 71.1% IIB 51.2% III 41.0% IV でも 23.4%。と日本の全国平均を大きく上回っている。中国の食道癌手術もいずれこの術式になっていくものと思われる。

作成日：2018 年 2 月 20 日

Lactoferrin Bioconjugated Clarithromycin-Loaded Nanostructured Lipid Carriers: A New Drug Delivery System for Inflammatory Lung Diseases Therapy

ラクトフェリン結合クラリスロマイシン含有ナノ構造脂質キャリアの調製：炎症性肺疾患に対する新規薬物送達システム

研究者氏名　趙　瑩（第 39 期笹川医学研究者）

中国所属機関　広東省嘉応学院

日本研究機関　名古屋市立大学大学院　薬学研究科

指導責任者　尾関　哲也 教授

共同研究者名　田上　辰秋 講師

Abstract:

Purpose: Clarithromycin (CLM) is the commonly used anti-inflammatory and immunomodulatory drug for treatment of various respiratory infections, but existing CLM formulations could not transport drug to respiratory system directly and efficiently. The aim of this study is to construct a novel drug carrier for benefiting delivery of CLM to respiratory system for effective therapy of lung infection diseases.

Methods: Novel nanostructured lipid carriers (NLCs) loading of CLM were prepared using solvent diffusion method and decoration of Lactoferrin onto the surface of NLCs was achieved via carbodiimide method. Evaluation of these lipid nanoparticles was performed by DLS, FTIR, Bradford assay techniques. The stability study was investigated by monitoring the size and polydispersity index variation during three months storage time.

Results: Lf was successfully conjugated to the surface of CLM-loaded NLCs and the Lf-conjugation was confirmed both by qualitative and quantitative determination. Compared of FTIR spectra of C-NLCs and Lf-C-NLCs, characteristic peaks of amide bond presented on Lf-C-NLCs, and this finding can verify Lf has conjugated onto CLM-loaded NLCs. The C-NLCs and Lf-C-NLCs possessed appropriate size distribution with average size of 201.1 and 241.0 nm, respectively. The size of their freeze-dried powders decreased slightly. Moreover, result of stability study revealed that C-NLCs and Lf-C-NLCs can keep stable during three months tested time, especially their powders.

Conclusion: The resulting Lf bioconjugated CLM-loaded NLCs could be an efficient anti-inflammatory drug delivery system and could be potentially developed for pulmonary infection therapy due to their high stability and desired particle size for inhalation administration.

Key Words:

Clarithromycin, Nanostructured lipid carriers, Lactoferrin conjugation, Pulmonary infection

Introduction:

Clarithromycin(CLM) is a semisynthetic macrolide antibiotic by Japan' Taisho Pharmaceutical Company successful development, and differs from erythromycin only by methylation of the hydroxyl group at the 6 position(Fig.1), which makes clarithromycin more acid stable than erythromycin [1]. Clarithromycin possesses anti-inflammatory and immunomodulatory properties for treatment of various respiratory infections, including pneumonia, chronic obstructive pulmonary disease, pharyngitis, and tonsillitis due to inhibition of inflammatory cytokine and chemokine production. But Clarithromycin is mainly administered in oral dosage forms, such as tablets, capsules and suspensions. Pharmacokinetics study indicates that the absolute bioavailability of oral administration is just 50% [2]. In addition, Clarithromycin is classified as Biopharmaceutical Classification System (BCS) class 2 which is practically insoluble in water. Typical

problems associated with the poorly water-soluble drug are very low oral bioavailability and erratic absorption due to very low saturation solubility and dissolution velocity. The poor dissolution behavior brings about further limited absorption of clarithromycin [3,4]. To improve the disadvantage of macrolide antibiotic application, researchers concerned about developing new CLM formulations for intravenous administration [5-7] during recent decades.

However, there is not any report about direct respiratory administration of CLM due to the existing CLM formulations could not meet the requirements of good stability and suitable particle size for entering the respiratory system efficiently. Therefore, the major task in developing a new CLM delivery system for inflammatory lung diseases therapy is to define inhalable drug formulation with sufficient stability and appropriate size [8,9].

One of the most promising drug delivery systems for pulmonary administration is nanostructured lipid carriers (NLCs) [10]. For pulmonary administration, NLC dispersions can be nebulized without any significant change in mean particle size, and NLC powders could be used in a dry powder inhaler (DPI) [11]. Treating lung diseases locally avoids first-pass metabolism and deposits directly at the site of the disease. Furthermore, nanosized particles adhere to the mucosal surface of the lung for a longer period of time compared to larger particles due to the small and desirable size[12].

In this study, CLM-loaded NLCs were conducted for the first time for rational design, optimization and physicochemical characterization of novel respirable nanoparticles for systemic delivery. Furthermore, utilizing Lactoferrin (Lf) for surface modification, in order to enhance the anti-inflammatory efficacy of macrolide antibiotic, and contribute to drug delivery. Lactoferrin is a multifunctional protein which is an essential part of the respiratory tract antimicrobial defense system[13] with antimicrobial activity[14], and it was previously reported that it could benefit the transport of drug to bronchial epithelial cell[15]. However, it has not been exploited to conjugate with nanostructured lipid carriers. In present research, Lactoferrin-appended CLM loaded NLCs were developed as a promising new drug delivery system for treatment of pulmonary infection diseases.

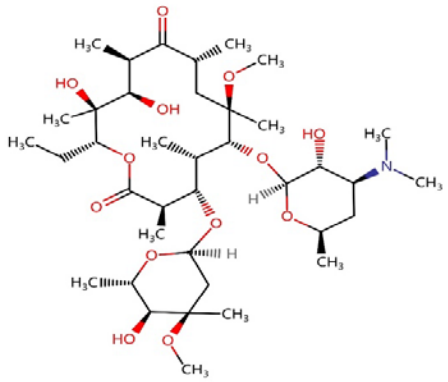

Fig.1. The chemical structure of Clarithromycin.

Methods:

Materials

Lactoferrin and Oleic Acid were generously provided by Wako Pure Chemical Industries, Ltd. (Osaka, Japan). Precirol ATO 5 was obtained from Gattefossé SAS (Saint-Priest, France). Poloxamer 188 was purchased from BASF Chemical Company (Ludwigshafen, Germany). 1-(3-Dimethylaminopropyl) -3-ethylcarbodiimide(EDC) and N-Hydroxysuccinimide(NHS) were purchased from Tokyo Chemical Industry Co., Ltd. (Tokyo, Japan). Phosphate Buffered Salts(PBS) was obtained from Takara Bio Inc. (Shiga, Japan). All other reagents and solvents used were of reagent grade.

Preparation of CLM-loaded nanostructured lipid carriers (CLM-loaded NLCs)

CLM-loaded NLCs(C-NLCs) were obtained using solvent diffusion method. CLM, Precirol ATO 5, and oleic acid were dissolved in a 1mL solvent mixture of ethanol and acetone by bath sonication, then kept on a water bath maintained at 70℃ to obtain lipid phase. At the same time, a surfactant solution was prepared and heated to the same temperature. The lipid phase was then injected into hot surfactant solution under mechanical agitation of 750 rpm. The CLM-loaded NLCs dispersion were stirred at 750rpm at room temperature until complete liberation of organic solvent. Next, the resulting suspension was filtered through a 0.8 μm membrane to remove precipitates, and lyophilized for further utilizing by Freeze dryer (Tokyo Rikakikai Co., Ltd., Japan).

Conjugation of Lf onto CLM-loaded NLCs

Lactoferrin (Lf) was conjugated on surface of CLM-loaded NLCs using carbodiimide chemistry method [16]. The carboxylic acid group of the lipid contained in CLM-loaded NLCs under the activation of EDC and NHS was utilized to connected with the amine group of Lf. In brief, EDC and NHS (3:1, w/w) were added to CLM-loaded NLCs dispersion in PBS for activating the carboxylic acid group for 2h. Then, Lf solution in PBS was added to these NLCs with stirring for 6h. EDC and NHS were removed using ultracentrifugation (14 000 g, 4°C, 30 min).

Qualitative determination of Lf-conjugation

The Fourier transform infrared (FTIR) spectra of Lf bioconjugated CLM-loaded NLCs(Lf-C-NLCs) was analyzed by means of a FTIR spectrophotometer (Shimadzu 8400S, Kyoto, Japan). The samples were prepared by the potassium bromide disk method and measurements were attempted with the accumulation of 20 scans and a resolution of 4 cm^{-1} over the range of 3800–600 cm^{-1}.

Quantitative determination of Lf-conjugation

The quantification of Lf conjugation on the surface of the C-NLCs was done using Bradford assay [17]. Briefly, the unbound Lf was separated by centrifugation, and mixed with the Bradford reagent in 96-well plate for 20 min at room temperature. The absorbance of Lf was measured at 595 nm using Multilabel Counter (PerkinElmer 1420, Tokyo, Japan) and compared with that of blank containing the same amount of Bradford reagent. Conjugation efficiency was calculated using the following formula:

$$\text{Conjugation efficiency } (\%) = \frac{\text{Weight of feeding Lf} - \text{Weight of unbound Lf}}{\text{Weight of feeding Lf}} \times 100\%$$

Measurement of particle size and distribution

The particle size, polydispersity index of different NLCs were measured using dynamic light scattering instrument in a Zetasizer Nano-ZS (Malvern Instruments, Malvern, UK). Before the measurement, the samples were diluted appropriately with distilled water. All of the measurements were performed in triplicate.

Stability studies of NLCs

The stability of C-NLCs, Lf-C-NLCs and their freeze-dried powders stored at 4°C for three months was investigated by monitoring the size and polydispersity index variation at 1 day, 30 days, 60 days and 90 days. The changes were used to evaluate the stability of the system.

Results:

Preparation of C-NLCs

CLM-loaded NLCs were successfully prepared using solvent diffusion method. Process variables and formulation variables (Table 1) were optimized to get C-NLCs of suitable particle size and uniform distribution. Optimized formulation was obtained with 5mg CLM, 100 mg of lipid of Precirol ATO 5 and Oleic Acid (10:9, w/w), 0.5% w/v of Poloxamer 188, and the ratio of solvent mixture of ethanol and acetone was 1:1(v/v). After the lipid phase injected into

surfactant solution, the NLCs dispersion was kept heating for 10 min continually, then stirred at room temperature for 12h. Precirol ATO 5 and oleic acid were used to provide free carboxylic group on the surface of C-NLCs for charge connecting with Lactoferrin.

Table 1. Investigation of process and formulation factors for preparation of C-NLCs.

Surfactant	Ethanol : Acetone(v/v)	Lipid		Heating Time (min)	Stirring Time (h)
		Solid	Liquid		
0.5% Tween80	1:1	Stearic Acid	Oleic Acid	5	2
0.5% DDAB	2:1	Precirol ATO 5	Cremophor ELP	10	4
0.5% Poloxamer 188	1:2	DSPC		30	12
1% Poloxamer 188		Stearylamine		60	24

Conjugation of Lf onto C-NLCs

Lf was successfully modified on the surface of C-NLCs using carbodiimide method(Fig.2) and the Lf-conjugation was confirmed both qualitatively and quantitatively.

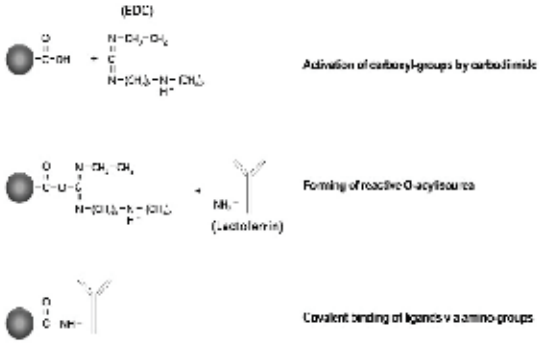

Fig.2. The reaction mechanism of Lf conjugating to C-NLCs.

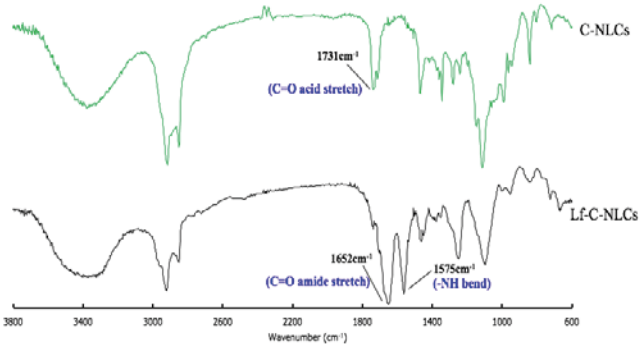

Fig.3. FTIR spectra of C-NLCs and Lf-C-NLCs.

Qualitative determination of Lf-conjugation

Fourier transform infrared spectroscopic (FTIR) analysis was carried out to evaluate the surface group interaction between amine group of Lf and carboxylic group of lipid in NLCs (Fig.3). FTIR spectra of C-NLCs showed a strong peak at 1731 cm^{-1} suggested the free carboxylic acid group of lipid present on C-NLCs. The spectra of Lf-C-NLCs depicted a characteristic peak of a C=O stretch of the amide linkage (–CONH) at 1652 cm^{-1} which indicates the formation of conjugate between C-NLCs and Lf. The peak at 1575 cm^{-1} (-NH bend) further confirmed the conjugation.

Quantitative determination of Lf-conjugation

Lf conjugation on C-NLCs surface was proved using FTIR as mentioned above. Lf conjugation was quantitatively detected using Bradford assay. The bioanalytical methods were successfully developed with good accuracy and precision. The calibration graphs plotted were linear with a correlation coefficient of 0.999. The conjugation efficiency was found to be 47.20% approximately.

Particle size and distribution

The mean diameter and polydispersity index of different NLCs were measured and summarized in Table 2. The particle size of NLCs without drugs was 194.7 nm. With the loading of drugs, the size increased a little, to 201.1 nm. It was also found that Lf-C-NLCs having the larger particle size (241.0 nm) than C-NLCs (201.1 nm) due to the surface Lf decoration. After the freeze-dried powder was redispersed in water, comparing to the previous dispersion, distribution of particles

became wide, but particle size decreased slightly(Fig.4). Polydispersity index of different NLCs was between 0.1 and 0.3, demonstrated that the particle of NLCs was homogeneous.

Table 2. Particle size and PDI of different NLCs.

	Blank NLCs	C-NLCs	C-NLCs powder	Lf-C-NLCs	Lf-C-NLCs powder
Particle size (nm)	194.7±2.6	201.1±1.4	182.2±2.9	241.0±3.3	226.8±2.1
PDI	0.153±0.022	0.184±0.012	0.257±0.016	0.253±0.019	0.284±0.027

Notes: C-NLCs powder and Lf-C-NLCs powder are detected using their redispersion in water. Values represent mean ± standard deviation (n=3).

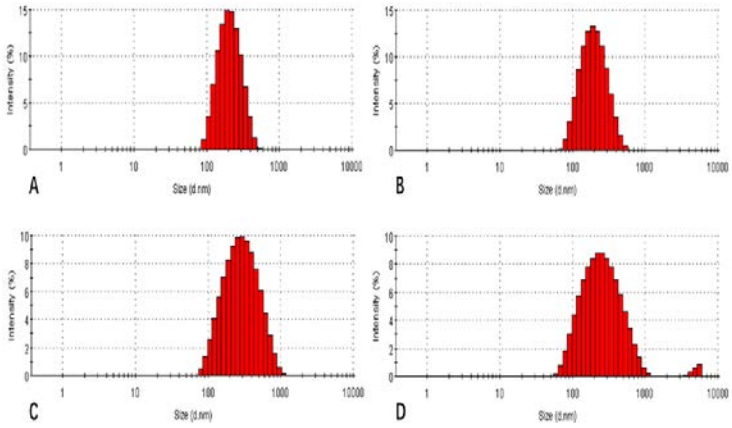

Fig.4. Comparison of different NLCs distribution by DLS.

Notes: A. C-NLCs, B. C-NLCs powder, C. Lf-C-NLCs, D. Lf-C-NLCs powder. C-NLCs powder and Lf-C-NLCs powder are detected using their redispersion in water.

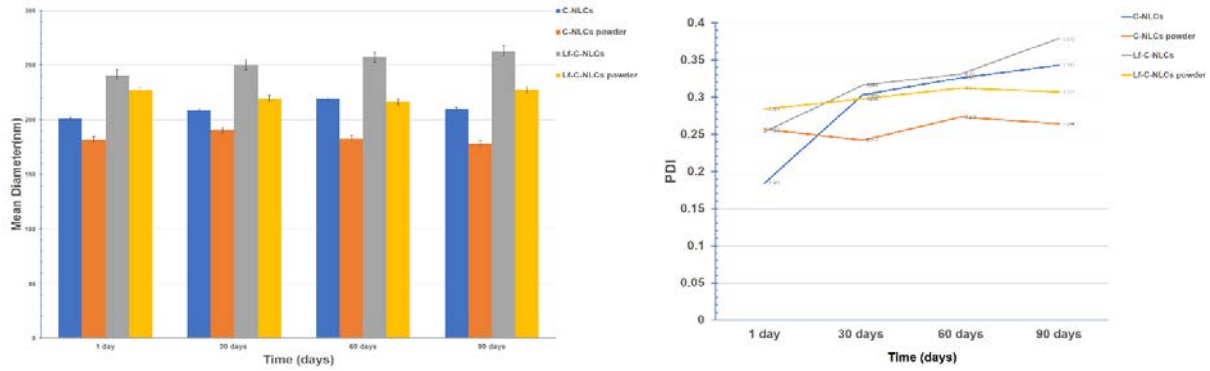

A B

Fig. 5. Stability studies of NLCs over a storage time of 3 months.

Notes: A. Particle size variation of different NLCs. B. Polydispersity index variation of different NLCs. C-NLCs powder and Lf-C-NLCs powder are detected using their redispersion in water. Data are presented as the mean ± SD (n=3).

Stability of NLCs

The variation of the mean diameter of NLCs was analyzed in Figure 5. The mean diameter of C-NLCs, Lf-C-NLCs and their freeze-dried powders remained stable during three months tested time, but the changes of PDI of C-NLCs and Lf-

C-NLCs were more remarkable than their powders.

Discussion:

In present study, Lactoferrin was successfully conjugated to nanostructured lipid carriers of loading of Clarithromycin. As known from other literature, more than 30% conjugation efficiency considered to be satisfactory [18]. However, the conjugation efficiency was found to be 47.20% approximately from this investigation, which is considerably higher than previously reported result of Lf on surface conjugated nanoparticles.

Nanostructured lipid carriers (NLCs), composed of solid and liquid lipids and surfactants, as the second lifetime lipid-based nanoparticles, compared to solid lipid nanoparticles(SLNs) which was appeared first, the advantages of NLCs are as follows: a disordered crystal structure, which can help load with both hydrophobic and hydrophilic drugs with a wide range of drug-loading properties; the carrier material is biodegradable and exhibits low in vivo toxicity [19]. NLCs can also be surface-modified[20]. The physical and chemical properties of NLCs particles are stable. Particle adhesion, accumulation and retention in the lung can lead to enhanced and sustained therapeutic effects and therefore result in a longer dosing interval and better patient compliance [21].

As result of this research, the size of C-NLCs and Lf-C-NLCs was between 180 and 240 nm, which could lead to an increased drug deposition in lung regions. In addition, C-NLCs, Lf-C-NLCs and their freeze-dried powders can keep stable during three months storage time, especially NLCs powders. The high stability provides support for future dry powder inhaler applications of CLM formulation for pulmonary administration.

Based on these result, it can be concluded that the formulation developed in this work may be considered as a promising effective anti-inflammatory drug delivery for the treatment of lung infection diseases. Next, further in vitro and in vivo studies will be carried out continually.

References:

1. Nakagawa Y, Itai S, Yoshida T, et al. Physicochemical properties and stability in the acidic solution of a new macrolide antibiotic, clarithromycin, in comparison with erythromycin. Chem Pharm Bull (Tokyo). 1992;40:725–728.

2. Chu SY, Deaton R, Cavanaugh J. Absolute bioavailability of clarithromycin after oral administration in humans. Antimicrob Agents Chemother. 1992;36:1147–1150.

3. Esfandi E′, Ramezani V, Vatanara A, et al. Clarithromycin Dissolution Enhancement by Preparation of Aqueous Nanosuspensions Using Sonoprecipitation Technique. Iran J Pharm Res IJPR. 2014;13:809–818.

4. Shahbaziniaz M, Foroutan SM, Bolourchian N. Dissolution Rate Enhancement of Clarithromycin Using Ternary Ground Mixtures: Nanocrystal Formation. Iran J Pharm Res IJPR. 2013;12:587–598.

5. Lovell MW, Johnson HW, Hui H-W, et al. Less-painful emulsion formulations for intravenous administration of clarithromycin. Int J Pharm. 1994;109:45–57.

6. Mohammadi G, Nokhodchi A, Barzegar-Jalali M, et al. Physicochemical and anti-bacterial performance characterization of clarithromycin nanoparticles as colloidal drug delivery system. Colloids Surf B Biointerfaces. 2011;88:39–44.

7. LingHao Q, Wei L. Formulation and evaluation of less-painful clarithromycin lipid microspheres. Arch Pharm Res.

2007;30:1336–1343.

8. Liu J, Gong T, Fu H, et al. Solid lipid nanoparticles for pulmonary delivery of insulin. Int J Pharm. 2008;356:333–344.

9. Dailey LA, Jekel N, Fink L, et al. Investigation of the pro inflammatory potential of biodegradable nanoparticle drug delivery systems in the lung. Toxicol Appl Pharmacol. 2006;215:100–108.

10. Han Y, Zhang Y, Li D, et al. Transferrin-modified nanostructured lipid carriers as multifunctional nanomedicine for codelivery of DNA and doxorubicin. Int J Nanomedicine. 2014;9:4107–4116.

11. Courrier HM, Butz N, Vandamme TF. Pulmonary drug delivery systems: recent developments and prospects. Crit Rev Ther Drug Carrier Syst. 2002;19:425–498.

12. Paranjpe M, Müller-Goymann CC. Nanoparticle-Mediated Pulmonary Drug Delivery: A Review. Int J Mol Sci. 2014;15:5852–5873.

13. Drago-Serrano ME, Campos-Rodríguez R, Carrero JC, et al. Lactoferrin: Balancing Ups and Downs of Inflammation Due to Microbial Infections. Int J Mol Sci. 2017;18(3):501.

14. Tomita M, Takase M, Bellamy W, et al. A review: the active peptide of lactoferrin. Acta Paediatr Jpn Overseas Ed. 1994;36:585–591.

15. Pandey V, Gajbhiye KR, Soni V. Lactoferrin-appended solid lipid nanoparticles of paclitaxel for effective management of bronchogenic carcinoma. Drug Deliv. 2015;22:199–205.

16. DeSilva NS, Ofek I, Crouch EC. Interactions of surfactant protein D with fatty acids. Am J Respir Cell Mol Biol. 2003;29:757–70.

17. Bradford MM. A rapid and sensitive method for the quantitation of microgram quantities of protein utilizing the principle of protein-dye binding. Anal Biochem. 1976;72:248–54.

18. Manoochehri S, Darvishi B, Kamalinia G, et al. Surface modification of PLGA nanoparticles via human serum albumin conjugation for controlled delivery of docetaxel. Daru 2013;21:58–67.

19. Liu C-H, Wu C-T. Optimization of nanostructured lipid carriers for lutein delivery. Colloids Surf Physicochem Eng Asp. 2010;353:149–156.

20. Zhang W-L, Gu X, Bai H, et al. Nanostructured lipid carriers constituted from high-density lipoprotein components for delivery of a lipophilic cardiovascular drug. Int J Pharm. 2010;391:313–321.

21. Patlolla RR, Chougule M, Patel AR, et al. Formulation, characterization and pulmonary deposition of nebulized celecoxib encapsulated nanostructured lipid carriers. J Control Release Off J Control Release Soc. 2010;144:233–241.

作成日：2018 年 2 月 23 日

Development of a transitional care program for patients with chronic obstructive pulmonary disease
慢性閉塞性肺疾患患者のための移行ケアプログラムの開発

研究者氏名　焦　丹丹（第 39 期笹川医学研究者）
中国所属機関　河南科技大学第一附属医院 呼吸内科
日本研究機関　兵庫県立大学地域ケア開発研究所
指導責任者　増野　園惠 教授

Abstract:

Background: When patients with chronic obstructive pulmonary disease (COPD) return home from the hospital, continuous care is needed to help these patients with self-management. Transitional care programs have the potential to equip patients who have COPD with the necessary skills for self-management and participation in their care. However, strong evidences on interventional programs are insufficient in China. The aim of this study, therefore, was to develop a transitional care program for patients with COPD. **Methods:** A literature review was conducted, along with ascertaining the operational process of the collaboration system in a Japanese hospital, and information gathering in China on Chinese community nursing. **Results:** A 3-month, nurse-led, transitional care program for patients with COPD and family caregivers was developed. Meanwhile, forms of evaluation for patients' education, a discharge plan, and a diary for recording patient illness at home were provided. **Discussion:** The developed program will be implemented in a tertiary hospital in the Henan province of China to test and verify its effectiveness.

Keywords:

Chronic obstructive pulmonary disease, transitional care

Introduction:

Chronic obstructive pulmonary disease (COPD) is a progressive disease marked by a slow decline in physical ability over time. According to World Health Organization estimates, more than 3 million people died of COPD in 2005, which contributed to 5% of all deaths globally. More than 53 million people aged 40 years or over have COPD in Japan (Fukuchi et al., 2004), in China, the prevalence of COPD is 8.2% (Zhong et al., 2007).

COPD is characterized by frequent recurrence and hospital readmission. In the hospital, patients with COPD and their family caregivers can obtain professional care, skills, and knowledge to manage the disease. The patients' ability to self-manage, however, gradually disappears after discharge from the hospital (Lainscak et al., 2013), which may lead to poor self-management at home and recurrence of COPD. Patients who experience difficulties with self-management are unable to deal with unpredicted acute deterioration of symptoms. Furthermore, existing evidence shows that a poor transition of patients and their family caregivers from the hospital to home is linked to high readmission rates (Naylor, 2003; Vinson, Rich, Sperry, Shah, & McNamara, 1990).

Transitional care is defined as sets of actions designed to ensure the coordination and continuity of healthcare as

patients transfer between different locations or different levels of care within the same location (e.g., hospitals, the patient's home, long-term care facilities) (Naylor, 2003). Further, it has been proven to be effective in reducing readmission rates (Hamar et al., 2016; Linden & Butterworth, 2014) and improving the health-related quality of life of patients with chronic disease (Li et al., 2014; Yu et al., 2015).

Both in Japan and the United States, the department of social workers or case managers in hospitals connect with healthcare providers in the community and other settings, coordinating patient care for those who have been discharged from the hospital. In China, unlike in developed countries, home nursing services are still in the initial stages; therefore, a research program that focuses on providing seamless, continuous care between Chinese hospitals and home settings is needed.

In implementing transitional care, the engagement of caregivers (e.g., family members, partners, friends, neighbors) is a required part of care strategy, which should be considered in the future (Naylor et al., 2017). Studies show that people who were living with a spouse or caregiver improved their adherence to COPD treatment as a result of receiving support and encouragement from partners (Bourbeau & Bartlett, 2008; Nici et al., 2006).

Additionally, while transitional care is necessary in China, there is still, to date, uncertainty about the type of care model that should be adopted. It has been suggested that choosing the proper, most effective care model, would be based on the actual healthcare situation and care facilities, in order to achieve good health outcomes (Coleman & Min, 2015).

Methods:

Design

In order to establish a basis for the development of a transitional care program, we used PubMed, PsychINFO, and CINANL to conduct a literature review. Information on the community collaboration model was gathered in a hospital in Japan. In addition, in China, resources for patients caring in community nursing, connections between hospitals and communities for home nursing services, and the feasibility of implementing the program in the hospital were ascertained.

Ethical considerations

A confidential agreement has been signed when the researcher participated in procedures of the community collaboration system in the Japanese hospital.

Results:

1. Bases for the program

The literature review identified two main transitional care models: one is the Transitional Care Model (TCM) developed by Mary Naylor (Naylor et al., 2009), and another one is the Care Transitions Intervention (CTI) developed by Eric A. Coleman (Coleman, 2013). The TCM emphasizes a nurse-led hospital plan and follow-up visits for patients at home including a health assessment and teaching patients how to manage their disease(Hirschman, Shaid, McCauley, Pauly, & Naylor, 2015). The CTI includes hospital visits, home visits, and telephone follow-up with a trained coach, such as an advanced practice nurse or social worker, to assist patients with taking medication, calling the physician, and

identifying personal potential risks (Coleman, 2013). The care concept arising from the two transitional care models is one of partnership, involving patients and their family caregivers, in addition to healthcare providers. This program, therefore, intended to merge the components of the two existing models to include the following: a nurse-implemented plan, in-hospital education, and patient follow-ups, as well as the partnership as mentioned above.

Understanding the community collaboration system of the hospital in Japan provided the idea for identifying key family members that help manage disease for patients with COPD. Within Chinese home nursing services, there is a gap (Zhao & Wong, 2009) and lack of coordination (Kashiwagi, Tamiya, Sato, & Yano, 2013) between hospitals and communities. In line with addressing these weaknesses, the appropriate transitional care program for COPD patients in a Chinese setting is determined. In addition, the possibility of implementing the project is confirmed.

2. Interventions

A 3-month, nurse-led transition care program centered on COPD patients and key family caregivers was developed, comprising two stages (in-hospital and at home). The care program framework is organized as follows:

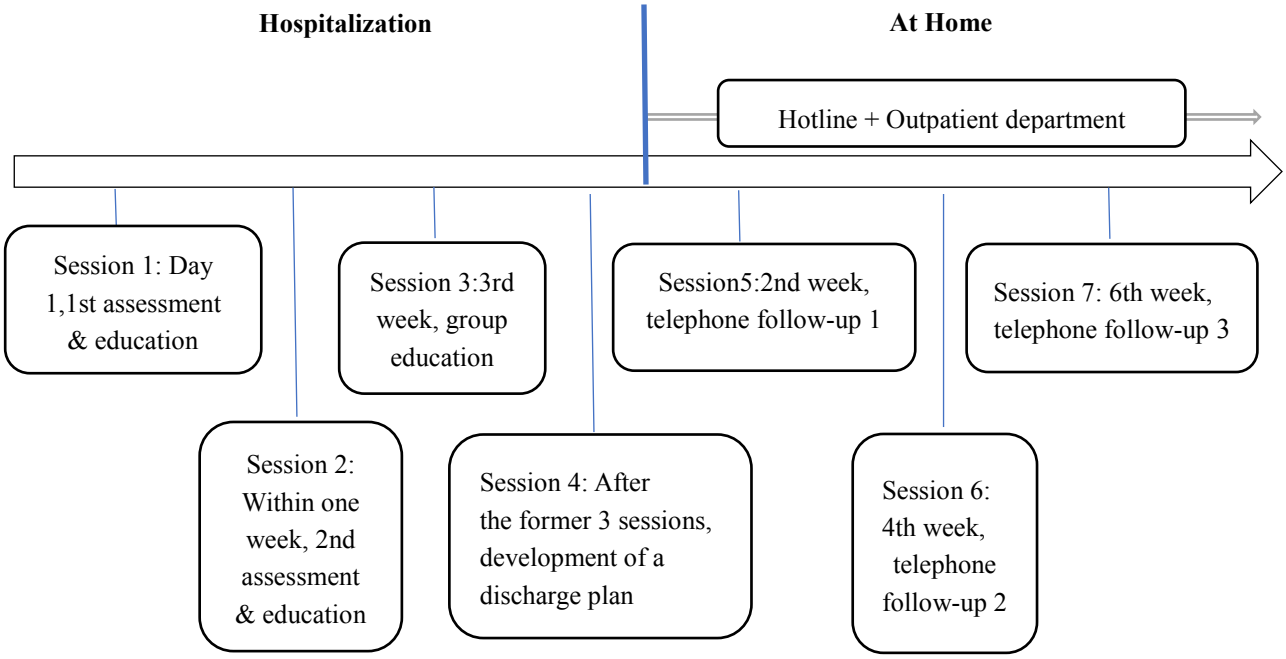

Fig. 1 The program framework

Stage 1: In hospital

During hospitalization, patients and family members will participate in establishing a discharge plan, as well as four sessions: one individual assessment, two individual educational sessions, and one group education session. All sessions are carried out according to certain standards for patients and their family members.

(1) Session 1: first assessment and education for individuals

This is completed on the day of admission by the nurse on duty. The nurse carries out patient assessments to identify personal information, risk factors of COPD, main symptoms, and severity of disease. Individual education aims to assist patients learning about and adjusting to the ward environment. Simple treatment information is also conveyed to patients to help them acquire skills and knowledge, such as the method of nebulization, the function of medication,

and precautions for laboratory examination. Session 1 is completed according to items from the evaluation form at admission.

(2) Session 2: second assessment and education for individuals

Within the first week after admission, the primary nurse assesses patients' previous knowledge about COPD, current symptoms, emotion, medication, dietary habits, family support, and ability to perform physical activity. The nurse provides corresponding management skills and instructions based on the two assessments. Session 2 is completed based on information from the second evaluation and education forms.

(3) Session 3: group health education

In the third week, group patient education is conducted by multidisciplinary professionals (the skilled nurse, physician, nutritionist, and pharmacist) in the ward, providing knowledge of disease, nutrition, medication, and exercise.

(4) Session 4: discharge planning development and implementation

After finishing the first 3 sessions, the primary nurse, together with the patient and family members, develop the individual discharge plan, which is designed to manage disease at home and is based on previous assessments. Additionally, the plan is accompanied by written material, and patients are encouraged to record diary entries under supervision of the family members living with them.

Further, on the day before leaving the hospital, the primary nurse will review the patient's discharge plans, inquire about and address patient questions, and emphasize major problems relevant to the individual's situation (e.g., precautions for long-term oxygen therapy, medication adherence, nutrition).

Stage 2: At-home stage

After discharge, 3 follow-up telephone calls will be provided for intervention patients at home.

(5) Sessions 5-7: telephone call

A ward nurse skilled in the care of patients with COPD calls patients by telephone on the 2nd, 4th, and 6th weeks after discharge. During the follow-up calls, the nurse will check patients' conditions according to the diary items regardless of whether patients recorded changes in illness. During the calls, patients are also permitted to express their other health status concerns. Additionally, the nurse will encourage patients to either visit the outpatient department or call the ward at any time whenever they feel uncomfortable.

(6) Consultation at the outpatient department

When patients feel uncomfortable or they undergo periodical physical examinations, they are encouraged to visit the outpatient department. At the outpatient department, the physician will first check the patient's diary to identify risk factors, inquire about the patient's current symptoms, and prescribe medication or another form of treatment depending on the patient's situation. The nurse then provides individual treatment instructions for the patient.

3. Program products

Forms related to the following were designed and printed: (1) patient evaluation and education, (2) the discharge plan, and (3) the patient's diary notes for recording changes of illness at home.

Discussion:

The primary difference between the Japanese community collaboration system and the transitional care model presented in this report, is the involvement of healthcare providers who give continuous care to patients after discharge. In this transitional care program, a hospital is responsible for continuous disease management for patients; however, in the Japanese community collaboration system, patients are referred to home visiting programes to be provided with healthcare services.

Further, one of the strong points of the transitional care program is community collaboration; specifically, the program identifies and meets the needs of the key family caregivers, and includes a conference for support plan development. Individuals attending the conference include a ward nurse, a nurse from the regional collaboration department, a care manager from the home visiting institution which is approved by the patient and family in advance, a medical facility provider (if possible) and a key family member. During the conference, all the participants discuss and develop the support plan together. The key family member is the crucial person who is responsible for caregiving, despite possibly having poor knowledge or difficulty in implementing the caring role. Therefore, it is essential to meet the caregiver-related needs of the key family member who lives with the patient who has COPD.

Further planning is needed to test and verify the effectiveness of this 3-month, nurse-led quasi-experimental transitional care program for patients with COPD and family caregivers. Two respiratory wards in a tertiary hospital in the Henan province of China are expected to be allocated to the control group and experimental group, with 75 patients in each group. The primary predicted outcome is improvement of health-related quality of life, and the secondary outcomes are reduced hospital readmission rates and number of visits to the clinic. It is hoped that the findings of the study will provide strong evidences for COPD management. If successful, this transition program could potentially be implemented as part of the routine care provided to patients with COPD, and its application to other chronic conditions can be explored.

References:

Bourbeau, J., & Bartlett, S. J. (2008). Patient adherence in COPD. *Thorax, 63*(9), 831-838. doi: 10.1136/thx.2007.086041

Coleman, E. A., & Min, S. J. (2015). Patients' and Family Caregivers' Goals for Care During Transitions Out of the Hospital. *Home Health Care Serv Q, 34*(3-4), 173-184. doi: 10.1080/01621424.2015.1095149

Fukuchi, Y., Nishimura, M., Ichinose, M., Adachi, M., Nagai, A., Kuriyama, T., . . . Zaher, C. (2004). COPD in Japan: the Nippon COPD Epidemiology study. *Respirology, 9*(4), 458-465. doi: 10.1111/j.1440-1843.2004.00637.x

Hamar, B., Rula, E. Y., Wells, A. R., Coberley, C., Pope, J. E., & Varga, D. (2016). Impact of a scalable care transitions program for readmission avoidance. *Am J Manag Care, 22*(1), 28-34.

Hirschman, K. B., Shaid, E., McCauley, K., Pauly, M. V., & Naylor, M. D. (2015). Continuity of Care: The Transitional Care Model. *Online J Issues Nurs, 20*(3), 1.

Kashiwagi, M., Tamiya, N., Sato, M., & Yano, E. (2013). Factors associated with the use of home-visit nursing services covered by the long-term care insurance in rural Japan: a cross-sectional study. *BMC Geriatr, 13*, 1. doi: 10.1186/1471-2318-13-1

Lainscak, M., Kadivec, S., Kosnik, M., Benedik, B., Bratkovic, M., Jakhel, T., . . . Farkas, J. (2013). Discharge coordinator intervention prevents hospitalizations in patients with COPD: a randomized controlled trial. *J Am Med Dir Assoc, 14*(6), 450 e451-456. doi: 10.1016/j.jamda.2013.03.003

Li, Jia-Mei, Cheng, Shou-Zhen, Cai, Wei, Zhang, Zhao-Hui, Liu, Qiong-Hui, Xie, Bi-Zhen, & Wang, Mu-Dan. (2014). Transitional care for patients with chronic obstructive pulmonary disease. *International Journal of Nursing Sciences, 1*(2), 157-164. doi: 10.1016/j.ijnss.2014.05.004

Linden, A., & Butterworth, S. (2014). A comprehensive hospital-based intervention to reduce readmissions for chronically ill patients: a randomized controlled trial. *Am J Manag Care, 20*(10), 783-792.

Naylor, M. D. (2003). Nursing intervention research and quality of care: influencing the future of healthcare. *Nurs Res, 52*(6), 380-385.

Naylor, M. D., Feldman, P. H., Keating, S., Koren, M. J., Kurtzman, E. T., Maccoy, M. C., & Krakauer, R. (2009). Translating research into practice: transitional care for older adults. *J Eval Clin Pract, 15*(6), 1164-1170. doi: 10.1111/j.1365-2753.2009.01308.x

Naylor, M. D., Shaid, E. C., Carpenter, D., Gass, B., Levine, C., Li, J., . . . Williams, M. V. (2017). Components of Comprehensive and Effective Transitional Care. *J Am Geriatr Soc*. doi: 10.1111/jgs.14782

Nici, L., Donner, C., Wouters, E., Zuwallack, R., Ambrosino, N., Bourbeau, J., . . . Troosters, T. (2006). American Thoracic Society/European Respiratory Society statement on pulmonary rehabilitation. *Am J Respir Crit Care Med, 173*(12), 1390-1413. doi: 10.1164/rccm.200508-1211ST

Vinson, J. M., Rich, M. W., Sperry, J. C., Shah, A. S., & McNamara, T. (1990). Early readmission of elderly patients with congestive heart failure. *J Am Geriatr Soc, 38*(12), 1290-1295.

Yu, D. S., Lee, D. T., Stewart, S., Thompson, D. R., Choi, K. C., & Yu, C. M. (2015). Effect of Nurse-Implemented Transitional Care for Chinese Individuals with Chronic Heart Failure in Hong Kong: A Randomized Controlled Trial. *J Am Geriatr Soc, 63*(8), 1583-1593. doi: 10.1111/jgs.13533

Zhao, Y., & Wong, F. K. (2009). Effects of a postdischarge transitional care programme for patients with coronary heart disease in China: a randomised controlled trial. *J Clin Nurs, 18*(17), 2444-2455. doi: 10.1111/j.1365-2702.2009.02835.x

Zhong, N., Wang, C., Yao, W., Chen, P., Kang, J., Huang, S., . . . Ran, P. (2007). Prevalence of chronic obstructive pulmonary disease in China: a large, population-based survey. *Am J Respir Crit Care Med, 176*(8), 753-760. doi: 10.1164/rccm.200612-1749OC

作成日：2018 年 2 月 21 日

Can Daikenchuto Benefit Enteral Nutrition Management in Critical Care Patients?
ICU 患者の栄養療法における大建中湯の使用法

研 究 者 氏 名　石 箏箏（第 39 期笹川医学研究者）
中国所属機関　北京中医医院　重症医学科
日本研究機関　千葉大学附属病院　救急科· 集中治療部
指 導 責 任 者　織田　成人　教授
共同研究者名　大島　拓 助教

Abstract: *Background:* Gastrointestinal (GI) dysmotility is commonly observed in critically ill patients, and becomes a real challenge for the clinicians as it can lead to feeding intolerance during enteral nutrition (EN). Feeding intolerance occurred frequently in ICU patient with EN and was also associated with reduced calorie and protein delivery, as well as poorer clinical outcomes. Daikenchuto (DKT), a Kampo medicine, has been known to enhance gut motility, and has been proposed as a potential treatment for GI dysmotility. But its use in critically ill patients has not been well described. *Aim:* Therefore, we sought to investigate the efficacy of DKT for promoting EN delivery in critically ill patients. *Method:* We conducted a literature search for clinical studies on the prokinetic effect of DKT that published within the last 10 years. We selected studies that focused on ICU and post-operative settings. We excluded the studies without bowel movement or post-operative ileus as their study endpoints. Some other endpoints such as adverse effect were studied individually. *Findings:* 9 studies were included in our analysis. All studies were conducted in the post-operative phase, and not specifically in the ICU setting. Among the 9 studies, 8 studies had bowel movement, and 5 studies had postoperative ileus as their study endpoint. 4 out of 8 studies showed DKT significantly promoted bowel movement. By contrast, none of the 5 studies demonstrated that DKT significantly prevented post-operative ileus. Meanwhile, 7 out of 9 studies reported DKT was associated with limited incidence of diarrhea, vomiting and abnormal blood tests as adverse event. In some individual studies, DKT was shown to enhance gastric emptying and colonic motility in the early postoperative period of total gastrectomy. DKT also promoted stool formation and frequency with patients underwent total gastrectomy or colectomy and promoted nutrition support in patients who underwent hepatectomy. *Conclusion:* DKT enhances GI motility in post-operative settings, and the same effect can also be expected in critically ill patients. Clinical trails to study the effect of DKT to reduce feeding intolerance and enhance EN delivery in the ICU settings are warranted.

Key Words: Daikenchuto, critically ill patients, enteral nutrition, feeding intolerance, post-operative ileus

Introduction:

Gastrointestinal (GI) dysmotility is commonly observed in critically ill patients, and becomes a real challenge for the clinicians as it can lead to feeding intolerance during enteral nutrition (EN).[1] According to the etiology classification, GI dysmotility could be divided into two types. Primary dysmotility refers to visceral myopathies or neuropathies and may result in distinct phenotype as a megacystis, microcolon and hypoperitalsis syndrome[2]. GI dysmotility in ICU settings usually occurs as a secondary dysmotility, caused by toxic, metabolic, or infectious stress related to the critical illness affecting the enteric nerves, smooth muscles, or interstitial cell of Cajal.[3]

The symptoms of GI dysmotility, such as high gastric residual volume, vomiting, abdominal bloating, constipation or diarrhea could lead to feeding intolerance. Reignier et al[4] reported early EN was associated with cumulative incidences of vomiting (34%), diarrhea (36%), bowel ischemia (2%) as well as acute colonic pseudo-obstruction (1%) among adult shock patients, and early EN did not reduce the mortality or ICU length of stay. Furthermore, a Canadian retrospective study[5] showed feeding intolerance occurred in 30% of mechanically ventilated ICU patients with EN, and feeding intolerance was associated with reduced calorie and protein delivery, poorer clinical outcomes as well.

Small bowel feeding and prokinetic agents are common solutions to overcome EN intolerance. However, the nasojejunal tube is not always available, as placement of the tube requires skilled staff, and endoscopic or fluoroscopic placement are recommended.[6] A systematic review suggested that there was moderate-quality evidence that prokinetic agents reduce feeding intolerance in critically ill patients compared to placebo or no intervention. However, whether it could promote the mortality and ICU length of stay remained unclear.[7] In addition, the available promotility agents such as motilin receptor agonists (Erythromycin) or 5-HT4 receptor agonists (Metoclopramide) are associated with limited overall efficacy, poor tolerability, and troublesome adverse reactions,[8] which may preclude the use of promotility agents. Therefore, the ideal medication to enhance gut motility is in demand.

Daikenchuto (DKT) is one of most frequently prescribed Kampo medicine in Japan which derived from an ancient Chinese medicine textbook *Jingui Yaolue*.[9] Kampo has been integrated into biomedicine by the Japanese physicians to transform the use of which into a more practical form.[10] Nowadays, DKT has been proposed as a potential treatment for GI dysmotility. It is composed of defined ratios of processed Ginger, Japanese pepper, Asian Ginseng and maltose powder. In recent years, both basic and clinical studies have been carried out to study the efficacy of DKT for promoting gastrointestinal motility. Basic studies suggested DKT has local vasodilator effect in intestinal blood vessels via calcitonin gene-related peptide.[11] DKT relieved colonic blood ischemia via endogenous adrenomedullin,[12] and it enhanced small bowel movement through the elevation of neurotransmitters such as acetylcholine and nitric oxide.[13] Endo et al.[14] reported DKT reduced post-operative ileus (POI) in mice models through its anti-inflammatory effects. DKT has been prescribed to treat chronic consitipation.[15] Some case reports suggested DKT contributed to the resolution of POI.[16,17] Several RCTs have been conducted to test the effectiveness of DKT for the prevention and treatment of POI.[18-20] Nonetheless, the use of DKT in critically ill patients has not been well described. Therefore, we sought to investigate the efficacy of DKT for promoting EN delivery in critically ill patients.

Methods:

We conducted a literature search in Pubmed for clinical studies regarding the prokinetic effects of DKT published within the period from January of 2008 to January of 2018. Studies are included if: (1) study design was a RCT or a prospective study; (2) studies that focused on ICU or post-operative adults; (3) the full text of the studies is available. We included the studies with bowel movement or POI as their study endpoints. Some other endpoints such as adverse effect were studied individually.

Results:

Nine studies were selected. All the studies were conducted in the post-operative phase in Japan, not in the ICU setting. As for the study design, 7 are RCTs,[18,19,21-25] 2 are prospective studies.[26,27] The sample size varied between 18 subjects[26] in the smallest study and 336 subjects[25] in the largest. Among the 9 studies, 4 studies involved patients who underwent colon or colorectal cancer surgery,[18,24,25,27] 2 involved patients who underwent surgery for gastric cancer,[19,22] 1 involved patients who underwent surgery for pancreatic tumors,[23] and 2 enrolled patients with hepatectomy due to liver cancer.[21,26] Six studies introduced the formula 15g/day[18,19,21,23,25,26] and 3 introduced a half dose of 7.5 g/day.[22,24,27] The duration of the administration varied between 5 days[24] as the shortest and 17 days[23] as the longest. The details of the 9 studies are summarized in Table 1.

As shown in Table 2, eight out of 9 studies had bowel movement or flatus as their endpoint,[18,19,21-23,25-27] and 4 showed DKT significantly promoted the first post-surgical bowel movement or flatus.[19,21,26,27] Five out of 9 studies had incidence of POI as their main study endpoint,[19,22-25] and none demonstrated that DKT significantly prevented post-operative ileus. Three of the 9 studies reported the use of DKT in promotion of defecation quality, and all 3 studies indicated DKT modulated the post-surgical stool formation or frequency.[19,22,25] Meanwhile, 7 out of 9 studies reported that DKT was associated with limited incidence of diarrhea, vomiting and blood test abnormalities as adverse events, and the adverse effects observed in DKT group was equivalent to the control group.[18,19,21-23,25,26]

DKT was shown to enhance gastric emptying and colonic motility in the early postoperative period of total gastrectomy.[18,19] DKT significantly reduced intestinal gas volume in the patients underwent total gastrectomy.[22] DKT also promoted nutrition support by allowing for the increase in postoperative dietary intake of patients after hepatectomy.[26]

Discussion:

In this literature search, we included 7 RCT studies and 2 prospective studies. All of the studies enrolled the patients who underwent abdominal surgeries, and evidence regarding the use of DKT in ICU patients is lacking. Our literature review indicated that DKT promoted GI motility as well as nutrition delivery in some specific populations of post-operative patients, but might not prevent POI. Nevertheless, DKT was usually well tolerated and can be considered potentially harmless.

GI dysmotility in ICU and post-operative settings has been shown to share similar pathogenesis.[28] Some features of POI, including respective mechanisms, contributing factors as well as management strategies, overlaps with the features of GI dysmotility in critically ill patients. Symptoms resulting from GI dysfunction, such as dysporia, high gastric residual volume, abdominal bloating and inadequate nutrition delivery frequently occur during EN. DKT could help overcome feeding intolerance in ICU patients.

A recent meta-analysis showed perioperative administration of DKT significantly reduced the occurrence of POI in patients with GI cancer sugery.[29] The intestinal manipulation during open abdominal surgeries could induce ileus, while in ICU settings, sepsis, trauma, mechanical ventilation and certain medical agents (such as opioid agonists) are the common contributing factors for paralytic ileus.[30] Thus, the efficacy of DKT in preventing or resolving paralytic ileus in critically ill patients requires to be determined by the future studies.

Kampo patterns classification is a unique diagnostic method that emphasizes match of patterns and formulas. The physician observes the symptoms and conducts physical examination of the patients to identify specific physical features such as yin-yang, cold-heat, and deficiency-excess, to determine the indication of a certain Kampo formula. DKT was originally indicated for abdominal pain caused by coldness; the presentation of symptoms including cold

limbs or abdomen, watery stool, abdominal pain or bloating, powerlessness or lassitude, leads to the selection of DKT. Watanabe[31] suggested the current clinical research with DKT has not taken patterns classification into account, and it could be considered while planning a future study.

As conclusion, we have found that DKT enhanced GI motility in post-operative settings, and the same effect can also be expected in critically ill patients. Therefore, clinical trials to study the effect of DKT to promote GI motility and enhance EN delivery in the ICU settings are warranted.

References:

1. Ritz MA, Fraser R, Tam W, Dent J. Impacts and patterns of disturbed gastrointestinal function in critically ill patients. Am J Gastroenterol 2000;95:3044-52.
2. Moreno CA, Metze K, Lomazi EA, et al. Visceral myopathy: Clinical and molecular survey of a cohort of seven new patients and state of the art of overlapping phenotypes. Am J Med Genet A 2016;170:2965-74.
3. Schappi MG, Staiano A, Milla PJ, et al. A practical guide for the diagnosis of primary enteric nervous system disorders. J Pediatr Gastroenterol Nutr 2013;57:677-86.
4. Reignier J, Boisrame-Helms J, Brisard L, et al. Enteral versus parenteral early nutrition in ventilated adults with shock: a randomised, controlled, multicentre, open-label, parallel-group study (NUTRIREA-2). Lancet 2017.
5. Gungabissoon U, Hacquoil K, Bains C, et al. Prevalence, risk factors, clinical consequences, and treatment of enteral feed intolerance during critical illness. JPEN J Parenter Enteral Nutr 2015;39:441-8.
6. Schlein K. Gastric Versus Small Bowel Feeding in Critically Ill Adults. Nutr Clin Pract 2016;31:514-22.
7. Lewis K, Alqahtani Z, McIntyre L, et al. The efficacy and safety of prokinetic agents in critically ill patients receiving enteral nutrition: a systematic review and meta-analysis of randomized trials. Crit Care 2016;20:259.
8. Diamond SJ, Omer E, Kiraly L. In Search of the Ideal Promotility Agent: Optimal Use of Currently Available Promotility Agents for Nutrition Therapy of the Critically Ill Patient. Curr Gastroenterol Rep 2017;19:63.
9. Katayama K, Yoshino T, Munakata K, et al. Prescription of kampo drugs in the Japanese health care insurance program. Evid Based Complement Alternat Med 2013;2013:576973.
10. Yakubo S, Ito M, Ueda Y, et al. Pattern classification in kampo medicine. Evid Based Complement Alternat Med 2014;2014:535146.
11. Kono T, Koseki T, Chiba S, et al. Colonic vascular conductance increased by Daikenchuto via calcitonin gene-related peptide and receptor-activity modifying protein 1. J Surg Res 2008;150:78-84.
12. Kono T, Omiya Y, Hira Y, et al. Daikenchuto (TU-100) ameliorates colon microvascular dysfunction via endogenous adrenomedullin in Crohn's disease rat model. J Gastroenterol 2011;46:1187-96.
13. Kito Y, Suzuki H. Effects of Dai-kenchu-to on spontaneous activity in the mouse small intestine. J Smooth Muscle Res 2006;42:189-201.
14. Endo M, Hori M, Ozaki H, Oikawa T, Hanawa T. Daikenchuto, a traditional Japanese herbal medicine, ameliorates postoperative ileus by anti-inflammatory action through nicotinic acetylcholine receptors. J Gastroenterol 2014;49:1026-39.
15. Horiuchi A, Nakayama Y, Tanaka N. Effect of Traditional Japanese Medicine, Daikenchuto (TJ-100) in Patients With Chronic Constipation. Gastroenterology Res 2010;3:151-5.
16. Ogino H. Usefulness of Kampo medicine in enteral nutrition-From the standpoint of a pharmacist' view. Journal of Japanese Society for Parenteral and Enteral Nutrition 2017;32 (2017) 946-50.
17. Minoru Yagi HK, Nobuyuki Saikusa, Shinji Ishii, Motomu Yoshida, Naoki Hashizume, Suguru Fukahori, Kimio

Asagiri, Yoshiaki Tanaka. Introduction of Kampo medicine to clinical nutrition. The Journal of Japanese Society for Parenteral and Enteral Nutrition 2017;32:939-41.

18. Katsuno H, Maeda K, Ohya M, et al. Clinical pharmacology of daikenchuto assessed by transit analysis using radiopaque markers in patients with colon cancer undergoing open surgery: a multicenter double-blind randomized placebo-controlled study (JFMC39-0902 additional study). J Gastroenterol 2016;51:222-9.

19. Yoshikawa K, Shimada M, Wakabayashi G, et al. Effect of Daikenchuto, a Traditional Japanese Herbal Medicine, after Total Gastrectomy for Gastric Cancer: A Multicenter, Randomized, Double-Blind, Placebo-Controlled, Phase II Trial. J Am Coll Surg 2015;221:571-8.

20. Itoh T, Yamakawa J, Mai M, Yamaguchi N, Kanda T. The effect of the herbal medicine dai-kenchu-to on post-operative ileus. J Int Med Res 2002;30:428-32.

21. Shimada M, Morine Y, Nagano H, et al. Effect of TU-100, a traditional Japanese medicine, administered after hepatic resection in patients with liver cancer: a multi-center, phase III trial (JFMC40-1001). Int J Clin Oncol 2015;20:95-104.

22. Akamaru Y, Takahashi T, Nishida T, et al. Effects of daikenchuto, a Japanese herb, on intestinal motility after total gastrectomy: a prospective randomized trial. J Gastrointest Surg 2015;19:467-72.

23. Okada K, Kawai M, Hirono S, et al. Evaluation of the efficacy of daikenchuto (TJ -100) for the prevention of paralytic ileus after pancreaticoduodenectomy: A multicenter, double-blind, randomized, placebo-controlled trial. Surgery 2016;159:1333-41.

24. Yamada T, Matsumoto S, Matsuda MKA, et al. The effect of Daikenchuto on postoperative intestinal motility in patients with right-side colon cancer. Surg Today 2017;47:865-71.

25. Katsuno H, Maeda K, Kaiho T, et al. Clinical efficacy of Daikenchuto for gastrointestinal dysfunction following colon surgery: a randomized, double-blind, multicenter, placebo-controlled study (JFMC39-0902). Jpn J Clin Oncol 2015;45:650-6.

26. Hanazaki K, Ichikawa K, Munekage M, Kitagawa H, Dabanaka K, Namikawa T. Effect of Daikenchuto (TJ-100) on abdominal bloating in hepatectomized patients. World J Gastrointest Surg 2013;5:115-22.

27. Yoshikawa K, Shimada M, Nishioka M, et al. The effects of the Kampo medicine (Japanese herbal medicine) "Daikenchuto" on the surgical inflammatory response following laparoscopic colorectal resection. Surg Today 2012;42:646-51.

28. Caddell KA, Martindale R, McClave SA, Miller K. Can the intestinal dysmotility of critical illness be differentiated from postoperative ileus? Curr Gastroenterol Rep 2011;13:358-67.

29. Ishizuka M, Shibuya N, Nagata H, et al. Perioperative Administration of Traditional Japanese Herbal Medicine Daikenchuto Relieves Postoperative Ileus in Patients Undergoing Surgery for Gastrointestinal Cancer: A Systematic Review and Meta-analysis. Anticancer Res 2017;37:5967-74.

30. Adike A, Quigley EM. Gastrointestinal motility problems in critical care: a clinical perspective. J Dig Dis 2014;15:335-44.

31. Watanabe K, Matsuura K, Gao P, et al. Traditional Japanese Kampo Medicine: Clinical Research between Modernity and Traditional Medicine-The State of Research and Methodological Suggestions for the Future. Evid Based Complement Alternat Med 2011;2011:513842.

注：本研究は２０１８年１月２０日「第１３７０回千葉医学会例会　第３２回千葉集中治療研究会」にて口演発表

Table 1 Characteristics of the studies

Source	Design	No. of individuals	Population	Intervention Groups (daily dose, duration, control group)
Okada, 2016	RCT	273	Pancreatico-duodenectomy/ pancreatic tumors	15g, preoperative day 3- POD14, VS placebo
Yamada, 2017	RCT	88	Colectomy/right colon cancer	7.5g, POD 1-5, VS control
Yoshikawa, 2015	RCT	195	Total gastrectomy/gastric cancer	15g, POD 1/2-10, VS placebo
Akamaru, 2015	RCT	81	Total gastrectomy/gastric cancer	7.5g, POD 1- ,VS water
Katsuno, 2015	RCT	71	Open surgery/sigmoid cancer	15g, POD 2-8, VS placebo
Katsuno, 2015	RCT	336	Colectomy/colon cancer	15g, POD 2-8, VS placebo
Shimada, 2014	RCT	209	Hepatic resection/liver cancer	15g, preoperative day 3- POD 10, VS placebo
Yoshikawa, 2011	Prospective	30	Colectomy/colorectal cancer	7.5g/d, POD 1-7, VS control
Hanazaki, 2013	Prospective	18	Hepatectomy/liver cancer	15g/d, preoperative day 3-POD 10, VS lactulose+DKT

POD postoperative day; RCT randomized controlled trial

Table 2 Main endpoints of the 9 studies

Source	First flatus/ First faeces	Post-operative ileus	Stool formation/ Stool frequency	Adverse effects related to DKT
Okada, 2016	NS	NS	N/A	diarrhea, blood test abnormal
Yamada, 2017	N/A	NS	N/A	N/A
Yoshikawa, 2015	P=0.051	NS	P=0.026	diarrhea, nausea, ALB ↓ , AMY ↑
Akamaru, 2015	NS	NS	P=0.037	None
Katsuno, 2015	N/A	N/A	N/A	diarrhea
Katsuno, 2015	NS	N/A	P=0.016	diarrhea, vomiting, abdominal pain
Shimada, 2014	P=0.047	NS	N/A	TBA ↑ , diarrhea
Yoshikawa, 2011	P=0.02	N/A	N/A	N/A
Hanazaki, 2013	P≤0.05	N/A	N/A	None

ALB albumin; AMY amylase; DKT Daikenchuto; GI gastrointestinal; NS not significantly difference; N/A not applicable; TBA total bile acid

作成日：2018 年 2 月 22 日

Characterization of niche cells in corneal limbus
角膜輪部におけるニッチ細胞の特性に関する研究

研究者氏名　黎　顕莉（第 39 期笹川医学研究者）
中国所属機関　南方医学大学深圳病院
日本研究機関　大阪大学医学部眼科
指導責任者　西田　幸二　教授
共同研究者　林　竜平　教授

Abstract:

Corneal epithelial stem cells are localized in the limbus, which is the transitional tissue located between cornea and conjunctiva. The limbal epithelial stem cells (LSCs) maintain the corneal epithelial tissue homeostasis by providing their daughter cells into the central cornea. Limbal niche is a special microenvironment, which is critical for the homeostasis and activation of limbal stem cells. However, there are few studies on limbal niche. In this study, we have investigated nature limbal niche and presumed human induced pluripotent stem (iPS) cells induced limbal niche cells (iLNCs). We found that limbal niche existed in adult and child human corneal limbus, but not in adult mouse cornea. We also demonstrated that hLNCs expressed SSEA-4, OCT3/4, and N-cadherin, and these stem cell markers could support the proliferation capability of LSCs. We further found that Vimentin-positive fibroblast-like cells were detected in the differentiated human iPS cells, which formed self-formed ectodermal autonomous multi-zone (SEAM). These putative iPS cell-derived LNCs (iLNCs) could be purified by fluorescence-activated cell sorting (FACS) and amplified by cell passaging. The cultivated iLNCs expressed SSEA-4 and OCT3/4 as stem cell markers. Further investigation will be needed regarding the function of iLNCs.

Keywords: limbal niche, limbal niche cells, limbal stem cells, iPS cells

Introduction:

The corneal epithelium is believed to be maintained by limbal epithelial stem/progenitor cells (LSCs) located in the anatomical palisades of Vogt and to reside within a niche called limbal crypts in humans. These LSCs in the limbal basal layer exhibit a slow-cycling label-retaining property and high proliferative potential. They can differentiate into transient amplifying cells, which migrate toward the central cornea. The limbal stem cell niche, as similar to stem cells niches of other tissues, is a special microenvironment composed of niche cells, extracellular components including specialized extracellular matrix (ECM) and secreted molecules, and has been proposed to have a key role in the maintenance of LSCs in an undifferentiated state[1]. In our previous research, we have found some VIM^+ cells which anatomically associated with LSCs in the basement layer of the limbus, and demonstrate its ability to support LSCs[2]. These cells are presumed to be human limbal niche cells (hLNCs). Identification and characterization of stem cell niche cells are helpful for understanding niche regulation of stem cell self-renewal and fate decisions and have substantial potential for clinical application of stem cells in regenerative medicine.

iPS cells hold great promise in ocular surface regenerative medicine. Hayashi et.al have recently reported the generation of a self-formed ectodermal autonomous multi-zone (SEAM) of ocular cells from human iPS cells[3]. The SEAM contains four concentric zones of cells, each of which has the characteristic of a particular ocular cell lineage or lineages. In some

respects, the concentric SEAM mimics whole-eye development. Cells in SEAM zone-3 most closely resemble those of the presumptive ocular surface. We found that Vimentin positive (VIM^+) fibroblast-like cells were detected in the zone-3 and they seemed to be co-localized with $\Delta Np63^+$ epithelial cells at eight weeks of differentiation culture. Considering the anatomical location of nature hLNCs and LSCs, we suspect that these VIM^+ fibroblast-like cells were iLNCs. In this research, we have performed the characterization of nature limbal niche and the putative iLNCs.

Method:

Isolation of LSCs and hLNCs

After the removal of the central cornea for penetrating keratoplasty, the limbal tissues were treated with 2.4 U/ml Dispase (BD Biosciences, Bedford, MA) for 1h at 37°C and 0.02% EDTA solution (Nacalai Tesque, Kyoto, Japan) for 2min at room temperature. The limbal epithelial cells were mechanically scraped and incubated with 0.25% trypsin-EDTA (Thermo Fisher scientific, Grand Island, NY) for 15min at 37°C. For the culture of primary limbal epithelial cells, the scraped cells were suspended in keratinocyte culture medium (KCM) consisted of Dulbecco's modified eagle medium and Ham's F12 medium (DMEM/F12, 3:1), 5%FBS (Thermo Fisher scientific), 1nM cholera toxin (Calbiochem, La Jolla, CA), 2nM triiodothyronine (Takeda, Osaka, Japan), 0.4μg/ml hydrocortisone (Kowa, Tokyo, Japan), 1% insulin-transferrin-selenium supplement (Thermo Fisher scientific), 20ng/ml keratinocyte growth factor (KGF, Wako, Osaka, Japan), 100U/ml penicillin and 100 μg/ml streptomycin (Thermo Fisher scientific). For the culture of hLNCs, the scraped limbal cells were suspended in modified embryonic stem cell medium (MESCM) consisted of DMEM/F-12 (1:1) supplemented with 10% knockout serum, 5μg/mL insulin, 5μg/mL transferrin, 5ng/mL sodium selenite, 4ng/mL bFGF, 10ng/mL hLIF , and 1% penicillin-streptomycin solution.

Ocular cell differentiation from human iPS cells

Human iPS cell line 201B7 was used in this experiment. The differentiation culture for human iPS cells was performed as previously described[4]. Differentiated human iPS cells in CEM were dissociated using Accutase (Thermo Fisher scientific) and resuspended in ice-cold MESCM medium. The harvested cells were filtered with a cell strainer (40 μm, BD Biosciences, San Diego, CA) and then stained with PE-conjugated anti-factor-A, FITC-conjugated anti-factor-B, and Alexa 647-conjugated anti-factor-C antibodies for 1 h on ice. After being washed twice with PBS, stained cells underwent cell sorting with a FACS Aria II instrument (BD Biosciences). In all of the experiments, cells were stained with non-specific isotype IgG or IgM as controls (Biolegend). The data were analyzed using the BD FACSDiva Software (BD Biosciences).

3D Matrigel Culture

Matrigel with different thicknesses was prepared by adding the plastic dish with 5% diluted Matrigel, 200μL of 50% diluted Matrigel (all in ESCM) per square centimeter, respectively, by incubation at 37°C for 1 hour before use. On coated or 3D Matrigel, hLNCs and iLNCs were seeded at a density of $5x10^3 cells/cm_2$ or $1\ x10^4 cells/cm_2$ in MESCM.

Preparation of feeder layers

hLNCs and 3T3 cells were mitotically inactivated by incubation with 8 μg/ml of mitomycin C (MMC; Kyowa, Japan) for 2h at 37°C. The cells were washed thoroughly and reseeded in 6 well plates at 1×10^4 $cells/cm_2$ (3T3 cells were prepared at $2\times10^4 cells/cm_2$) as feeder layers.

Colony-forming assay

Primary limbal epithelial cells were seeded at a density of 1,000 cells per well of 6-well plate on MMC-treated various feeder layers and incubated for 10 days as previously described. The colonies were fixed with 10% neutral buffered formalin and stained with 1% rhodamine B (Wako, Osaka, Japan).

Histology and immunofluorescence staining

Cornea tissues (adult human cornea donor, 3years child cornea donor, and 18m adult mouse cornea) were embedded in OCT for immunofluorescence staining. For Immunofluorescence staining, sections and cells were fixed with 4% paraformaldehyde (PFA) at 4℃ for 30 min followed by blocking in 5% non-fat milk and 0.3% Triton X-100 in PBS for 1 h at room temperature. The samples were then incubated overnight at 4℃ with the following primary antibodies including anti-Keratin 3 (AE5) (1:200; Progen Biotechnik, Heidelberg, Germany), anti-P63 (4A4) (1:200; Santa Cruz), anti-SSEA-4 (1:66.5; Abcam), anti-N-cadherin (1:200; Santa Cruz), anti-Keratocan (1:200; Millipore) and anti-Vimentin (1:200; Bioss, Woburn, MA). After washing with PBS, the samples were incubated for 1 h with Alexa 568 or FITC-conjugated secondary antibody (1:200; Thermo Fisher scientific). The same concentration of corresponding normal, non-specific IgG was used as negative control.

Results

LNCs existed in adult and child human limbal tissues, but not in human central cornea and mouse cornea.

Immunofluorescence staining was performed on adult and child human corneal limbal tissues, as well as adult mouse corneal tissues. The results showed that the limbal tissue contained the typical stratified epithelium and underlying high cellularity region in the limbal stromal area and LSCs ($\Delta Np63^+$ cells) were distributed in the basal layer of the limbal epithelium. hLNCs ($VIM^+/\Delta Np63^-$ cells) were located close to the basal epithelial cells in the limbal crypts in adult and child human corneal limbal tissues (Fig. 1A, B, arrows), but not found in human central cornea and adult mouse cornea and limbus (Fig. 1C, D).

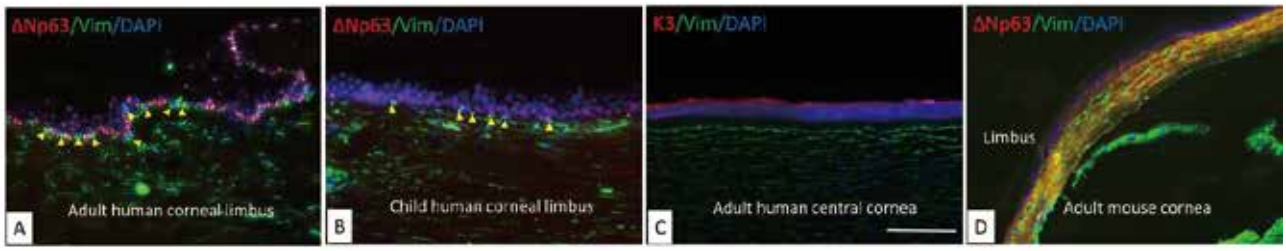

Fig.1 Identification of LNCs in adult, child human and adult mouse corneal tissue. (A, B) Both adult and child human limbal tissues maintained the typical stratified epithelium and the underlying high cellularity region in the limbal stroma.; $\Delta Np63^+$ LSCs and $VIM^+/\Delta Np63^-$ hLNCs (arrows) coexisted in the basal epithelial layer of the limbal crypts. (C) In the central cornea, epithelium was separated from stroma by Bowman's membrane. (D) Limbal crypts and $VIM^+/\Delta Np63^-$ niche cells were not observed in the basement layer of adult mouse corneal and limbal epithelium. Bars:100 μm.

hLNCs expressed Vimentin and several stem cell markers at the basal layer of the corneal limbal epithelium

Human limbal tissue contained the typical stratified epithelium and underlying stromal cell layers. $\Delta Np63^+$ LSCs and $VIM^+/\Delta Np63^-$ hLNCs (Fig. 2A, arrows) were co-localized in the limbal epithelial crypt. The VIM^+ / $p63^-$ hLNCs also

expressed SSEA-4 (Fig. 2B, arrows), OCT3/4 (Fig.2C, arrows) and N-cadherin (Fig. 2D, arrows) as stem cell markers but no stromal cell marker Keratocan (Fig. 2E).

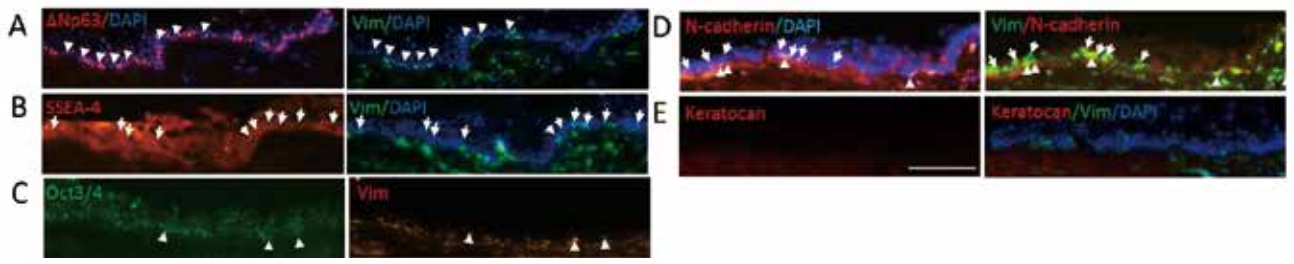

Fig.2 Identification of hLNCs in nature human limbal tissue *in situ*. Frozen sections of nature human limbal tissue showed that hLNCs (arrows) located in the basal epithelial layer of the limbal epithelium, and expressed Vimentin and stem cell markers such as SSEA-4 (B), OCT3/4 (C) and N-cadherin (D), but no ΔNp63 (A) and Keratocan (E). Bars: 100 μm.

Isolation and cultivation of hLNCs

We checked the existence of hLNCs in the cytospin samples prepared from the primary limbal cell suspension. The immunofluorescence staining showed that $\Delta Np63^+$ LSCs and $\Delta Np63^-$, VIM^+, $SSEA\text{-}4^+$, $OCT3/4^+$, $N\text{-}cadherin^+$ hLNCs were co-collected in limbal cell suspensions (Fig.3A-E). Moreover, no expression of Keratocan indicated that corneal stromal cells were not isolated by this method (Fig.3E). For the culture of hLNCs, the limbal cell suspension was seeded on 5%Matrigel coated cell culture plate and cultivated in the MESCM medium. Epithelial cells seemed to be disappeared and hLNCs were selectively proliferated after 7-10 days (Fig.4A). The hLNCs cultivated in 3D-Matrigel formed spheroids (Fig.4B, C). Passaged hLNCs cultivated in the MESCM still expressed stem cell markers *in vitro* (Fig.4D).

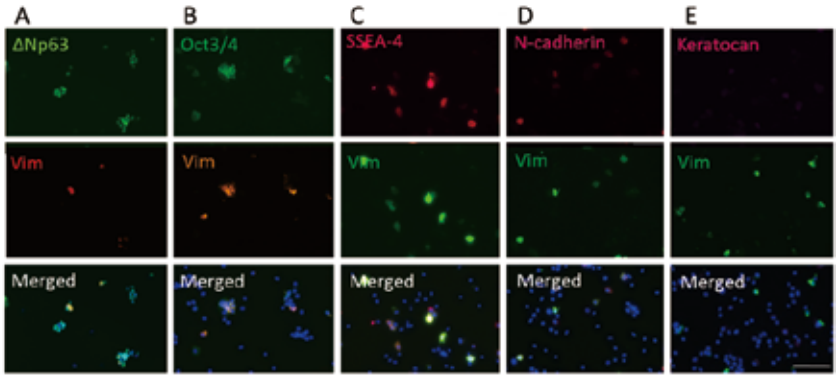

Fig.3 Identification of hLNCs in limbal cells suspension after enzymatic and scraping treatment. Immunostaining showed that collected limbal cells expressed LSCs marker $\Delta Np63^+$ (A), presumed hLNCs cell markers, VIM (A), OCT3/4 (B), SSEA-4 (C) and N-cadherin (D), but no stromal cell marker Keratocan (E). Bars: 100 μm.

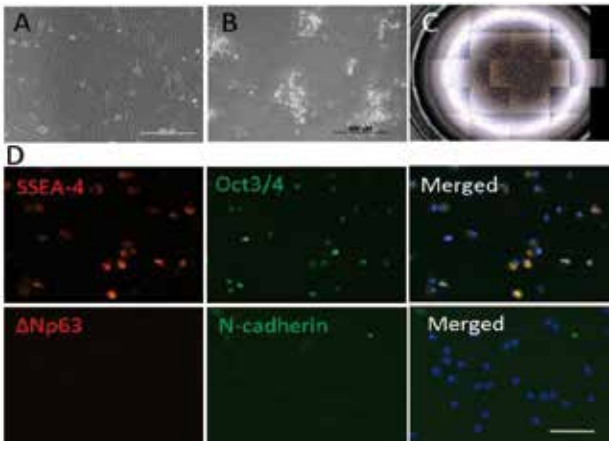

Fig4. Identification of *in vitro* proliferated hLNCs. (A) hLNCs cultured on Matrigel-coated plate showed fibroblast-like morphology. (B, C) hLNCs cultured on 3D-Matrigel formed spheres. (D) Immunofluorescence staining of 3rd generation hLNCs showed positive expression of SSEA-4, OCT3/4 and N-cadherin stem cell markers, but negative for ΔNp63. Bars:100 μm.

hLNCs supported proliferation of LSCs

Colony-forming assay was performed using hLNCs and 3T3 cells as feeder layers. The primary limbal epithelial cells formed typical cell colonies on both feeder layers after 10-13 days of culture. Moreover, immunofluorescence staining demonstrated that the co-culture of limbal epithelial cells with hLNCs and 3T3 feeder cells showed positive staining for cell proliferation marker, Ki67 (Fig.5). These results indicated that hLNCs support the proliferation capability of LSCs.

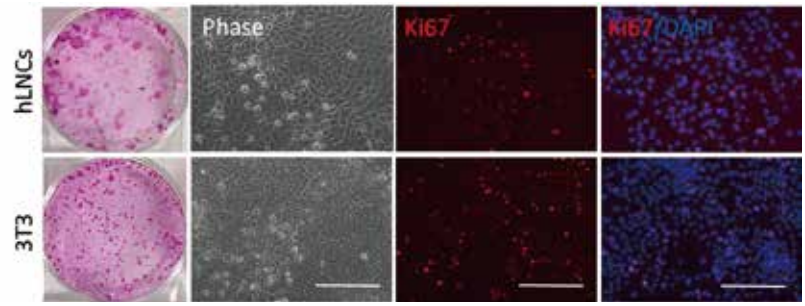

Fig.5 Colony-formation assay for LSCs co-cultivated with hLNCs and 3T3 feeder layers. Primary LSCs formed typical cell colonies on the hLNCs and 3T3 feeder layers after 10-13 days of culture and expressed cell proliferation marker, Ki67. Bars: 200 μm.

Isolation of presumed iLNCs from iPS cells differentiated ocular cells

Human iPS cells cultivated in differentiation medium at 8th week had formed typical SEAM structure with four identifiable concentric zones (Fig.6 A, B). Cells in zone-3 are deemed to be anlages of the ocular surface epithelium. VIM^+ fibroblast-like cells appeared in the $p63^+$ zone- 3 at eight weeks were considered as putative iLNCs (Fig.6 C). These cells proliferated during further cultivation (Fig.6 D). After the removal of zones-1 and -2 from the SEAM by manual pipetting, the cells that remained (that is, those in zone-3 and some in zone-4) were subjected to FACS to isolate the presumed iLNCs. The sorted $Facor\text{-}A^+/Factor\text{-}B^-/Factor\text{-}C^-$ cells were then seeded on Matrigel-coated six-well plate and cultured with the MESCM medium. Cytospin of the sorted cells showed that iLNCs (VIM^+ cells), $p63^+$cells and $VIM^-/p63^-$ cells were detected in zone-3, after further cultivation and cell passaging, homogeneous fibroblast-like iLNCs were expanded from the sorted cells (Fig.6 F). Immunofluorescence staining result showed that putative iLNCs express SSEA-4 and OCT3/4, but no N-cadherin, and $p63^+$cells (Fig6 G).

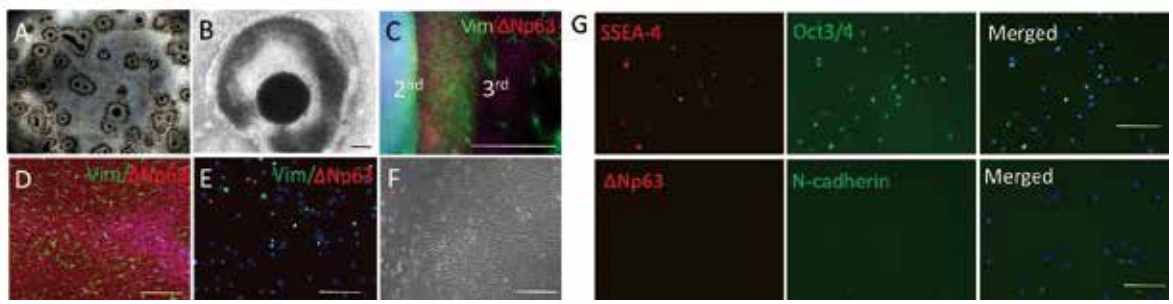

Fig.6 Isolation and identification of presumed iLNCs. (A) iPS cells cultivated in differentiation medium formed typical SEAM at 8th week. (B) SEAM formed with four identifiable concentric zones. (C) VIM^+ fibroblast-like cells appeared in the $p63^+$ zone- 3 at eight weeks; (D) The population of VIM^+ presumed iLNCs was increased in 14th week. (E) Sorted $Facor\text{-}A^+/Factor\text{-}B^-/Factor\text{-}C^-$ cells contain presumed iLNCs, $p63^+$ cells and other $VIM^-/p63^-$ cells (F) After cell passaging homogeneous fibroblast-like presumed iLNCs were obtained in MESCM culture system. (G) Immunofluorescence staining results showed that expanded iLNCs expressing SSEA-4 and OCT3/4, but no N-cadherin and ΔNp63 (Fig6 G). Bars: 200 μm.

Discussion

Firstly, we investigated nature limbal niches in different species, and adult or child corneal limbus. Grieve et.al found that radially oriented crypts extending beneath the scleral roof were found in humans and pigs but not in mice[5]. And in mouse, stem cells are distributed in a limbal trough close to the epithelial surface as well as distributed throughout the central cornea[6]. Our results also showed that VIM^+ LNCs were found in both adult and child human corneal limbal crypts, but not in the adult mouse cornea and limbus. It suggests that limbal niche might be a special structure for longer lifespan species. However, we only compared human and mouse cornea, therefore more species should be considered in the future study. This also indicates that we cannot investigate the development of LNCs using mouse embryonic eyes. Human iPS cells-derived SEAM highly mimicking the development of human developmental eyes, might be a good tool for investigating limbal niche cell *in vitro*.

In our previous research, we have isolated some VIM^+ cells anatomically associated with LSCs in the basement layer of limbus, which were different from limbal stromal cells and showed its ability to support LSCs. These cells are presumed to be hLNCs. This time, we did immunofluorescence staining for the hLNCs in nature limbal niche and have confirmed that these hLNCs expressed stem cell markers such as SSEA-4, OCT3/4, and N-cadherin, but not expressed stromal cell marker, Keratocan. These hLNCs can be isolated and purified *in vitro* culture. Even after the cultivation, hLNCs still expressed these stem cell markers, and maintained the ability to support proliferation ability of LSCs. The putative iLNCs were detected in the population of $Factor\text{-}A^+/Factor\text{-}B^-/Factor\text{-}C^-$cells by flow-cytometric analysis. The results showed that the putative iLNCs were isolated by FACS. The proliferated putative iLNCs showed a fibroblast-like cell morphology and expressed SSEA-4 and OCT3/4, but no N-cadherin. These presumed iLNCs showed similar characteristics to hLNCs in cell morphology and the expression of stem cell markers. However, we need further investigation about the function as a niche cell for LSCs. Therefore, in the future study, niche cell function assay and microarray analysis should be done to demonstrate whether functional iLNCs can be induced from human iPS cells.

In conclusion, in this study we showed some characterization for hLNCs, and demonstrated the putative iLNCs were induced from human iPS cells, which had similar characteristics to hLNCs. The iLNCs might be a promising cell source for ocular surface regeneration medicine for treating the patients and the research for limbal stem cell niche as well.

Reference:

1. Li W, Hayashida Y, Chen YT, Tseng SCG. Niche regulation of corneal epithelial stem cells at the limbus. Cell research 2007; 17:26-36.
2. Li YL, Inoue T, Takamatsu F, et al. Differences Between Niche Cells and Limbal Stromal Cells in Maintenance of Corneal Limbal Stem Cells. Investigative ophthalmology & visual science 2014; 55:1453-1462.
3. Hayashi R, Ishikawa Y, Sasamoto Y, et al. Co-ordinated ocular development from human iPS cells and recovery of

corneal function. Nature 2016; 531:376-380.
4. Hayashi R, Ishikawa Y, Katori R, et al. Coordinated generation of multiple ocular-like cell lineages and fabrication of functional corneal epithelial cell sheets from human iPS cells. Nature protocols 2017; 12:683-696.
5. Grieve K, Ghoubay D, Georgeon C, et al. Three-dimensional structure of the mammalian limbal stem cell niche. Experimental eye research 2015; 140:75-84.
6. Majo F, Rochat A, Nicolas M, Jaoude GA, Barrandon Y. Oligopotent stem cells are distributed throughout the mammalian ocular surface. Nature 2008; 456:250-254.

作成日：2018 年 2 月 27 日

Does the attitude toward the well-known Confucian maxim influence rumination and depression in China? A cross-sectional study.

中国で孔子の名言に対する態度が反すうと抑うつに影響を与えるか：横断研究

研 究 者 氏 名　劉　林林（第 39 期笹川医学研究者）
中国所属機関　天津精神保健センター
日本研究機関　京都大学医学部健康増進行動学
指 導 責 任 者　古川　壽亮 教授
共同研究者名　渡辺　範雄 准教授，小川　雄右 助教

Abstract：

Objectives: To examine: (1) if the attitude toward the well-known Confucian maxim “I daily examine myself on three points” may be different between depressive people and healthy people in China, (2) if the attitude is related to rumination and depression, (3) if there are relationships between the maxim and cognitive emotion regulation styles which have relationship with depression. Methods: This is a cross-sectional study using self-report questionnaires among convenience samples of patients with depression and healthy people in China. In total 55 depressive patients and 52 healthy people took part in the research, and 52 participants in each group completed all assessments. The attitude toward the maxim, ruminative response scale (RRS), self-rated depression scale (SDS) and cognitive emotion regulation questionnaire (CERQ) were used. Results: There was no significant difference in the attitude toward the well-known Confucian maxim between depressed group and healthy group (Z value=-0.16, P value=0.88, Mann-Whitney test). There was no correlation between the attitude toward the maxim and rumination or depression in each group. Positive reappraisal correlated with both the attitude toward the maxim and depression in healthy people (r=0.44, P<0.01; r=-0.28, P<0.01, respectively). Conclusions: The attitude toward the maxim does not influence rumination and depression, but it may have some indirect relationship with depression in healthy people through positive reappraisal.

Keywords:

Rumination, Culture, Depression, Emotion Regulation

Introduction:

According to the response styles theory, rumination is a mode of responding to distress that involves repetitively and passively focusing on symptoms of distress and on the possible causes and consequences of these symptoms (Nolen-Hoeksema, 1991; Nolen-Hoeksema, Wisco, Lyubomirsky, 2008). Nowadays, the concept of rumination has broadened and many theorists define rumination as the process of thinking perseveratively about one’s feelings and problems rather than in terms of the specific contents of thoughts (Nolen-Hoeksema, Wisco, Lyubomirsky, 2008). Indeed, rumination is strongly and consistently related to depressive symptoms (Mor & Winquist, 2002).

If rumination is not good for people, why do people still ruminate? One reason may be that they have positive beliefs in rumination (Papageorgiou & Wells, 2001a). People may think rumination is a helpful strategy for gaining insight, identifying causes and triggers of depression, solving problems, preventing future mistakes and failures, and prioritizing important tasks (Papageorgiou & Wells, 2001b, 2004). There is some research to show that positive beliefs about

ruminative thinking were associated with rumination (Kubiak, Zahn & Siewert, 2014) and subsequent depression (Watkins & Moulds, 2005).

The thinking style akin to rumination and positive beliefs about such a thinking style seem familiar in the traditional Chinese culture (GUO & WU, 2011). There is an old well-known maxim in China, which states "I daily examine myself on three points." This proverb is taken from a very famous ancient book <The Analects of Confucius>. Most people who have received junior high school education in China know this maxim. This proverb is mentioned by 20570 papers in China National Knowledge Internet (CNKI), the biggest database in China, as of December 2017. According to Confucius's disciple Tsang, the three points is whether, in transacting business for others, I may have been not faithful; whether, in intercourse with friends, I may have been not sincere; whether I may have not mastered and practiced the instructions of my Master. However, the explicit contents have been forgotten by most people, and the meaning has broadened indistinctly. It approximately means that self-examination should be practiced on a daily basis or many times, and people need to examine themselves to improve themselves.

It is widely believed that the culture and the psychological process influence each other (Lehman, Chiu, & Schaller, 2004). The expression, experience and conceptualization of mental disorders are associated with the culture (Marsella & Yamada, 2010). Different countries have different group characteristics. Chinese normative samples of Depression Scale in both MMPI and MMPI-2 were found to be consistently higher than the American norms (Cheung, Song & Zhang, 1996). Asian Americans were found to ruminate more, but their rumination had less association with depression than European Americans (Chang & Edward, 2010). As for Confucius, the Master must have wanted to teach us something useful, but it is unclear what cultural influence about his teaching has had on people. Some researchers (Zhang & Wang, 2015; GUO & WU, 2011) thought there may be something related between the maxim or culture and rumination, but to date no relevant research exists.

This study therefore aims to examine the following three associations. The first hypothesis is that depressive people have higher affinity with the maxim "I daily examine myself on three points" than healthy people. The second hypothesis is that the maxim is related with rumination and depression both among the depressed people and among the healthy people. The third hypothesis is that there are some relationships between the maxim and cognitive emotion regulation styles (Garnefski, Kraaij & Spinhoven, 2001) which have been shown to have some relationship with depression directly (Garnefski & Kraaij, 2006) or indirectly (Min & Yu, 2013).

Methods

This study is a cross-sectional study which assessed the attitude toward the maxim, rumination, and cognitive emotional regulation styles among people with or without major depression.

Result

In total 55 depressive patients and 52 healthy people took part in the research, and 52 participants in each group completed all assessments. Table 1 shows participants' characteristics.

Table 1. Baseline characteristics of participants in two groups

Characteristic	Depressed Group (n=52)	Healthy Group (n=52)	*P* value
Age, mean(SD), y	36.6(12.8)	35.2(8.7)	0.50
Sex, No.(%)			
Male	17(32.7)	23(44.2)	0.23
Female	35(67.3)	29(55.8)	
School education, No.(%)			
Junior high school	5(9.6)	5(9.6)	<0.001
Senior high school	7(13.5)	7(13.5)	
Undergraduate	32(61.5)	16(30.8)	
Postgraduate	8(15.4)	24(46.2)	
Marriage, No.(%)			
Unmarried	16(30.8)	15(28.8)	0.11
Married	32(61.5)	37(71.2)	
Divorced	4(7.7)	0	
Living area, No.(%)			
Rural	5(9.6)	6(11.5%)	0.75
City	47(90.4)	46(88.5%)	
Major depression, No.(%)			
Single	26(50%)	0	
Recurrent	26(50%)	0	

Abbreviations:RRS, ruminative response scale; SDS, self-rated depression scale; CERQ, cognitive emotion regulation questionnaire.

As can be seen from Table 2, the attitude toward the maxim were similar in the two groups. There was no statistically significant difference in Mann-Whitney test (*Z* value is -0.16, *P* value=0.88).With regard to other measurements, as expected, the depressed group scored significantly higher in SDS, RRS and some of CERQ scales than the healthy group.Table 3 shows that the attitude toward the maxim had no significant correlation with rumination or depression in both groups. As shown in Tables 4, the attitude toward the maxim was not related with any cognitive coping and depression at all in the depressed group. In contrast, the attitude toward the maxim correlated with self-blame, positive refocusing and especially positive reappraisal in the healthy group. Among the three coping, only positive reappraisal had negative correlation with depression

Table 3. The correlations between the attitude toward the maxim and RRS or SDS in both depressed group and Healthy group.

	Attitude toward the maxim	
	Depressed group	Healthy group
RRS total score	-0.01	0.15
Brooding factor	0.12	0.10
Reflection factor	0.09	0.12
SDS	0.05	0.08

Table 2. Psychological characteristics of the two groups

	Depressed Group (n=52)	Healthy Group (n=52)	*P* value
Attitude toward the maxim	2.63(0.93)	2.60(0.98)	0.88
SDS	65.19(13.02)	40.50(8.28)	<0.001
RRS			
Total scores	53.29(10.20)	35.08(5.52)	<0.001
Brooding Factor	13.29(2.52)	9.44(1.90)	<0.001
Reflection Factor	10.58(2.35)	7.44(1.71)	<0.001
CERQ			
Self-blame	14.12(2.47)	11.54(2.41)	<0.001
Acceptance	14.79(2.73)	13.38(2.70)	0.01
Focus on thought/Rumination	14.23(3.17)	9.69(2.87)	<0.001
Positive refocusing	11.06(2.91)	11.83(2.96)	0.18
Refocus on planning	13.19(3.43)	13.75(3.20)	0.39
Positive reappraisal	12.15(3.74)	14.15(3.77)	<0.01
Putting into perspective	11.23(2.00)	9.85(2.71)	<0.01
Catastrophizing	12.17(3.65)	7.38(2.32)	<0.001
Blame others	11.27(3.17)	9.21(3.04)	0.01

Abbreviations:RRS, ruminative response scale; SDS, self-rated depression scale; CERQ, cognitive emotion regulation questionnaire.

Table 4. The correlation between the attitude toward the maxim and CERQ and SDS in both depressed group and healthy group.

	Depressed Group		Healthy Group	
	Maxim	SDS	Maxim	SDS
Self-blame	0.27	0.02	**0.29***	0.12
Acceptance	0.13	-0.25	-0.00	-0.32*
Focus on thought/Rumination	0.21	0.45**	0.12	0.30*
Positive refocusing	0.26	-0.09	**0.32***	0.01
Refocus on planning	0.05	-0.03	0.25	-0.09
Positive reappraisal	0.27	-0.31*	**0.44****	**-0.28***
Putting into perspective	0.23	0.27	0.05	0.10
Catastrophizing	-0.07	0.58**	-0.50	0.60**
Blame others	-0.11	0.33*	-0.00	0.54*
SDS	0.05	1	-0.08	1

Abbreviations: Maxim: I daily examine myself on three points; SDS, self-rated depression scale;

*: $P<0.05$; **: $P<0.01$.

Discussion

This is the first study to compare the attitude toward the famous Confucian maxim "I daily examine myself on three points" between depressed people and healthy people. The results showed that there was no difference in the attitude toward the maxim between the depressed group and the healthy group, and the maxim was not related to either rumination or depression in each group. The first two of our hypotheses were therefore not supported by the data. As regards our third hypothesis, the attitude toward the maxim was correlated with some cognitive coping styles only among the healthy people.

Previous research has shown that the positive attitude toward rumination as measured by Positive Beliefs about Rumination Scale (PBRS) (Papageorgiou and Wells, 2001b) was closely linked to rumination in Chinese Hongkong people (Roger & Bhugra, 2008). By contrast, the maxim "I daily examine myself on three points" represents a deep-seated Chinese belief. Some authors (Zhang & Wang, 2015；GUO & WU, 2011) think it emphasizes self-reflection, self-analysis, recognition of shortcomings, summary of experience for self-growth and better moral. Self-reflection and self-rumination may be considered as adaptive and maladaptive aspects of self-conscious attention (Trapnell & Campbell, 1999). A research showed that self-reflection was associated with a lower level of depression and self-rumination with a higher level of depression (Takano & Tanno, 2009).

Unfortunately, definitional confusion of self-related terms exists in the field, including self-examination, introspection, self-awareness, or self-focus (Morin, 2017). It is therefore not easy to identify which of these various aspects of self-conscious attention the maxim recommends. We need to study finer details of beliefs represented by the maxim in order to distinguish between its adaptive and maladaptive aspects.

When examined in view of the cognitive coping styles for emotion regulation, the maxim was related with self-blame, positive refocusing, and positive appraisal. These aspects seem to be consistent with the meaning of the maxim discussed above, including reflecting self, recognizing shortcomings and summarizing for self-growth. However, these associations were observed only in the healthy group, but not in the depressed group. It is possible that self-blame and negative approach to refocusing or appraisal are symptoms of depression disorder, and the relationships were confounded by depression in the depressed people.

On the other hand, positive reappraisal was negatively associated with depression in the healthy group, as had been shown by many researches (Webb, Miles & Sheeran, 2012; Aldao, Nolen-Hoeksema & Schweizer, 2010; Martin & Dahlen, 2005). The maxim may therefore be protective against depression through positive reappraisal in the healthy people.

There are several limitations for this study. The biggest limitation is that the participants were recruited by convenience sampling, so bias might exist. For example, the healthy group had higher percentage of post-graduates than the depressed group, but if undergraduates and postgraduates are combined into higher education, there no longer existed significant difference. Secondly, depression in this research was measured by self-report scales and not by an objective method.

In conclusion, the attitude toward the well-known Confucian maxim "I daily examine myself on three points" is not different between the depressed and the healthy people. It was not associated with either rumination or depression.

Advocating this maxim therefore may not lead to depression. By contrast, it was associated with positive reappraisal which may prevent depression among the healthy people.

References

Aldao, A., Nolen-Hoeksema, S., & Schweizer, S. (2010). Emotion regulation strategies across psychopathology: A meta-analytic review. Clinical Psychology Review, 30, 217-237

Chang, Edward C., et al. (2010). Examining the relations between rumination and adjustment: Do ethnic differences exist between Asian and European Americans? Asian American Journal of Psychology, Vol 1(1), Mar, 46-56

Cheung, F. M., Song, W. Z., & Zhang, J. X. (1996). The Chinese MMPI–2: Research and applications in Hong Kong and the People's Republic of China. In J. N. Butcher (Ed.). International adaptations of the MMPI–2: A handbook of research and applications, 137-161

Dai Qin, Feng Zhengzhi, Xu Shuang, et al. (2015). The reliability and validity of the Chinese version Ruminative Response Scale(RRS) in Undergraduates. China Journal of Health Psychology, Vol 23(5): 753-758

Garnefski, N., Kraaij, V., & Spinhoven, P. (2001). Negative life events, cognitive emotion regulation and depression. Personality and Individual Differences, 30, 1311-1327

Garnefski, N., & Kraaij, V. (2006). Relationships between cognitive emotion regulation strategies and depressive symptoms: A comparative study of five specific samples. Personality and Individual Differences, 40, 1659-1669

GUO Suran, WU Xinchun. (2011). Rumination: Theories , Mechanism and Scales. Chinese Journal of Special Education, 3(129): 89-93

Lehman, D. R. , Chiu , C. & Schaller , M. (2004). Psychology and culture . Annual Review of Psychology, 55, 689-714

Kubiak,T., Daniela Zahn,D., Siewert,K., et al, (2014). Positive Beliefs about Rumination Are Associated with Ruminative Thinking and Affect in Daily Life: Evidence for a Metacognitive View on Depression. Behavioral and Cognitive Psychotherapy, 42, 568-576

Marsella, A. J., & Yamada, A. M. (2010). Culture and psychopathology: Foundations, issues, and directions. JOURNAL OF PACIFIC RIM PSYCHOLOGY Volume 4, Issue 2: 103-115

Martin, R. C., & Dahlen, E. R. (2005). Cognitive emotion regulation in the prediction of depression, anxiety, stress, and anger. Personality and Individual Differences, 39: 1249-1260

Min J, Yu JJ, Lee C, Chae J, et al. (2013). Cognitive emotion regulation strategies contributing to resilience in patients with depression and/or anxiety disorders. Comprehensive Psychiatry, Volume 54, Issue 8, November: 1190-1197

Morin, A. (2017). Self-related Terms. Frontiers in psychology, February, 8, 280: 1-9

Mor, N., & Winquist, J. (2002). Self-focused attention and negative affect: A meta-analysis. Psychological Bulletin, 128: 638-662

Nolen-Hoeksema, S. (1991). Responses to depression and their effects on the duration of depressive episodes. Journal of Abnormal Psychology, 100: 569-582

Nolen-Hoeksema, S., & Morrow, J. (1991). A prospective study of depression and posttraumatic stress symptoms after a natural disaster: The 1989 Loma Prieta earthquake. Journal of Personality and Social Psychology, 61(1), 115-121

Nolen-Hoeksema S, Wisco BE, Lyubomirsky S. (2008). Rethinking Rumination. Perspect Psychol Sci. 3: 400-24

Papageorgiou, C., & Wells, A. (2001a). Positive beliefs about depressive rumination: development and preliminary validation of a self-report scale. Behavior Therapy, 32: 13-26

Papageorgiou, C., & Wells, A. (2001b). Metacognitive beliefs about rumination in recurrent major depression. Cognitive and Behavioral Practice, 8: 160-164

Papageorgiou, C., & Wells, A. (2004). Depressive Rumination Nature, Theory and Treatment: 47

Roger M.K. Ng., & Dinesh Bhugra. (2008). Relationship between filial piety, meta-cognitive beliefs about rumination and response style theory in depressed Chinese patients. Asian Journal of Psychiatry 1, 28-32

Takano K1, Tanno Y. (2009). Self-rumination, self-reflection, and depression: self-rumination counteracts the adaptive effect of self-reflection. Behav Res Ther. Mar, 47(3): 260-264

Trapnell, P. D., & Campbell, J. D. (1999). Private self-consciousness and the Five-Factor Model of personality: distinguishing rumination from reflection. Journal of Personality and Social Psychology.76, 284-304

Treynor W, Gonzalez R, Nolen-Hoeksema S. (2003). Rumination reconsidered: a psychometric analysis. Cogn Ther Res. 27(3): 247-259

Wang Xiangdong, WANG Xilin, MA Hong. (1999). Rating scales for mental health. Chinese Mental Health Journal 12:444-451; 479-485; 393-396

Watkins, E., & Moulds, M. (2005). Positive beliefs about rumination in depression: A replication and extension. Personality and Individual Differences, 39(1), 73-82

Webb, T. L., Miles, E., & Sheeran, P. (2012). Dealing with feeling: A meta-analysis of the effectiveness of strategies derived from the process model of emotion regulation. Psychological Bulletin, 138, 775-808

World Medical Association. (2013). World Medical Association Declaration of Helsinki Ethical Principles for medical research involving human subjects. JAMA.310: 2191-2194

Zhang Kuo, Wang Xinjian. (2015). Advancements and Prospects of the Research on Depressive Rumination. Nankai Journal (Philosophy, Literature and Social Science Edition), 3, 108-118

Zhu Xiongzhao, Randy P., Auerbach, Shuqiao Yao, et al. (2008). Psychometric properties of the Cognitive Emotion Regulation Questionnaire: Chinese version. Cognition and emotion, 22(2): 288-307

作成日：2018 年 2 月 26 日

Promotion of TGF-β1 monomer formation by hydrogen sulfide contributes to its inhibitory actions on Ang II- and TGF-β-induced EMT in renal tubular cells

硫化水素によるTGF-β1単量体の形成は、Ang IIおよびTGF-β誘発した腎尿細管上皮細胞間葉転換の阻害作用に寄与する

研究者氏名　黄　勇（第39期笹川医学研究者）
中国所属機関　江西中医薬大学附属病院腎臓内科
日本研究機関　山梨大学医学部先端応用医学講座
指導責任者　姚　建 准教授

Abstract:

Hydrogen sulfide (H_2S), a vasodilative gas mediator with multifaceted biological functions, have been shown to be effective in attenuation of renal sclerosis in several different models of chronic renal diseases. However, the mechanisms involved have not been completely elucidated. Given that angiotensin II (Ang II)- and transforming growth factor-β (TGF-β)-induced epithelial-mesenchymal transition (EMT) in renal tubular epithelial cells is a pivotal cellular event contributing to renal sclerosis, we tested whether H_2S could intervene the processes of EMT induced by these factors and explored the potential mechanisms. 1) Exposure of cultured renal tubular epithelial cells to Ang II resulted in an increase in mesenchymal marker alpha smooth muscle actin (α-SMA) and a decrease in epithelial marker epithelial cadherin (E-cadherin), indicating an induction of EMT. 2) This effect of Ang II was associated with an increased activity of TGF-β. Blockade of TGF-β signaling with TGF-β receptor kinase inhibitor abolished, whereas exogenous TGF-β reproduced the EMT-promoting effect of Ang II, indicative of a mediating role of TGF-β. 3) In the presence of H_2S donor sodium hydrosulfide hydrate (NaHS), the EMT-inducing action of Ang II was largely prevented, which was associate with a reduced level of active TGF-β. 4) Further analysis revealed that H_2S caused a shift of band of TGF-β from a 25kDa dimeric structure to 12.5 kDa monomer in Western blot, which was similar to DTT (a reducing chemical that disrupts disulfide bond in proteins), suggesting a cleavage of the disulfide bond in TGF-β. This effect of H_2S and DTT was associated with a loss of its activity, as revealed by changes in TGF-β bioassay, Smad2 phosphorylation and EMT markers. 5) H_2S also suppressed Ang II-induced early ERK activation and TGF-β production in glomerular mesangial cells. It prevented the formation of hillock, an in vitro model of MC sclerosis. Collectively, these results indicate that H_2S counteracts Ang II- and TGF-β-induced EMT in renal tubular epithelial cells. This effect of H_2S was, at least in part, attributable to its induction of inactive TGF-β monomer formation. Our study thus provides novel mechanistic insight into the actions of H_2S and suggests that it could be used to treat certain renal sclerotic diseases.

Key Words:

Hydrogen sulfide; epithelial-mesenchymal transition; disulfide bond; TGF-β; Ang II

Introduction:

Renal interstitial fibrosis is the hallmark of chronic kidney disease (CKD) and is the most damaging process contributing to renal function decline (1). Many pathogenic factors have been identified to be involved in initiation and development of renal fibrosis. Among them, angiotensin II (Ang II) is one of the most extensively investigated one. Ang II is a potent vasoactive peptide that constricts blood vessels and increases blood pressure. Ang II also directly

regulates many cellular processes, including cell proliferation, migration, differentiation and matrix production. It also induces epithelial-mesenchymal transition (EMT; a cellular event by which injured renal tubular cells transform into mesenchymal cells) and promotes renal tubulo-interstitial fibrosis in chronic renal diseases (2, 3).

Hydrogen sulfide (H_2S) is a gaseous vasodilator synthesized from cysteine primarily by the enzymes cystathionine β-synthase and cystathionine-γ-lyase through the trans-sulfuration pathway. It has multifaceted biological functions. As a potent vasodilator, it counteracts many vascular actions of Ang II in vivo. It prevents renal fibrosis in diabetic and hypertensive rats (4-8). In vitro, H2S inhibits Ang II-induced cell proliferation and matrix production (9). Currently, the molecular mechanisms involved have not been completely understood.

Protein S-sulfhydration is a post-translational modification of specific cysteine residues in proteins. It alters enzymatic activity, protein stability, localization, and protein-protein interaction. S-sulfhydration of functional proteins by H_2S have been reported to be involved in many pathophysiological actions of H_2S, including its vasodilative, neuroprotective, anti-oxidative, anti-inflammatory, and ER stress-relieving actions (10-12). Given that the activation of the Ang II-TGF-β1 pathway has an important role in renal EMT and that the dimeric structure of TGF-β1 is stabilized by an inter-chain disulfide bond (13, 14). We speculated that H_2S might modify the disulfide bond of TGF-β1 and inhibit Ang II-induced renal EMT. Therefore, we sought to address this hypothesis.

Here, we present our results showing that H_2S attenuated Ang II-induced renal EMT through modification of the disulfide bond in TGF-β1. Our study thus provides novel mechanistic insight into the action of H_2S and suggests that H_2S could have potential therapeutic benefit in prevention and treatment of renal fibrosclerosis.

Methods and Methods:

1. Materials: NaHS and Ang II were purchased from Sigma-Aldrich (Saint Louis, USA). Recombinant Human TGF-β1 was obtained from PeproTech (New Jersey, USA). Antibodies against the α-SMA, TGF-β, phospho-Smad2 was obtained from Cell Signaling Technology (Beverly, MA). E-cadherin antibody was obtained from BD Biosciences (San Jose, CA). TGF-β type I receptor kinase inhibitor HTS466284 were obtained from Calbiochem (San Diego, CA, USA).
2. Cells: The rat renal tubular epithelial cell line NRK-52E was purchased from American Type Culture Collection (Manassas, VA). Cells were maintained in Dulbecco's modified Eagle's medium/Ham's F-12 (Gibco-BRL, Gaithersburg, MD) supplemented with 5% FBS. Experiments were performed in the presence of 0.5% FBS.
3. Western blot analysis: Equal amounts of cell lysates were separated with 10% SDS-polyacrylamide gels and electrotransferred onto 0.4 μm polyvinylidene difluoride membranes. The membranes were firstly incubated with 5% nonfat milk in PBS for 30 ~ 60 mins to reduce the nonspecific binding, and then incubated with the first antibodies (1:1000 dilution) in the same solution. After that, the membranes were washed with PBS containing 0.05% Tween 20 and probed with horseradish peroxidase-conjugated sheep anti-rabbit IgG or horse anti-mouse IgG (1:2000 dilution, Cell Signaling Technology). Immunoreactivity was detected with ECL (Amersham Biosciences). The chemiluminescent signal was captured with a Fujifilm luminescent image FAS-4000 analyzer (Fujifilm, Tokyo, Japan). Densitometric analysis of the intensity of the bands was done using NIH ImageJ software (http://rsb.info.nih.gov/ij/).
4. Measurement of TGF-β activity in vitro: TGF-β activity was assayed using MFB-F11 cells that were stably transfected with a reporter plasmid containing 12 CAGA boxes (Smad binding element) fused to a secreted alkaline phosphatase (SEAP) reporter gene, as described previously by (15). Briefly, MFBF11 cells at the density of 1×10^4cells/well in 96-well were exposured to a series of diluted TGF-β, collected conditioned media, or H_2S -treated TGF-β. Activity of SEAP was evaluated using the Great EscAPe Detection Kit (BD Bioscience), following the protocol

provided by the manufacturer. The intensity of chemiluminescent signal was determined by a luminometer (Gene Light 55; Microtech Nition, Chiba, Japan).

5. Statistical analysis: Data were expressed as mean ± SE (n = 4). A comparison of two populations was made using Student's t-test. For multiple comparisons with a single control, one-way analysis of variance (ANOVA) followed by Dunnett's test was employed. $p < 0.05$ was considered to indicate a statistically significant difference.

Results:

1. H_2S inhibits Ang II-induced EMT in renal tubular epithelial cells

Treatment of tubular epithelial NRK-52E cells with Ang II caused EMT, as indicated by the incensement of mesenchymal marker alpha smooth muscle actin (a-SMA) and loss of epithelial marker E-cadherin. This effect of Ang II was concentration-dependent (Fig. 1A). In the presence of 1000 μM NaHS, a H_2S donor, the EMT-promoting effect of Ang II was largely prevented (Fig. 1B). These results indicate that H_2S inhibits Ang II-induced EMT.

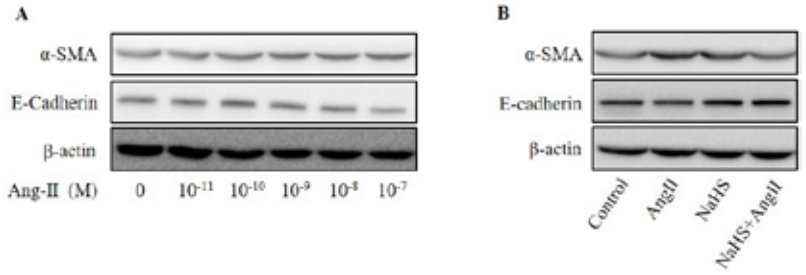

Fig.1. H_2S inhibits Ang II-induced EMT in renal tubular epithelial cells. (A) Effects of Ang II on the expression of α-SMA and E-cadherin. (B) Effects of H_2S on the expression of α-SMA and E-cadherin induced by Ang II.

2. Ang II-induced EMT associated with TGF-β

Previous studies have implicated TGF-β in Ang II-induced many biological actions, including EMT (16, 17). To determine the role of TGF-β in the EMT-inducing action of Ang II, we blocked TGF-β signaling with TGF-β receptor I kinase inhibitor HTS466284 and found that it completely blocked EMT-promoting action of Ang II, as manifested by the decreased expression of α-SMA and increased expression of E-cadherin (Fig. 2A). In further support of a role of TGF-β, Ang II treatment indeed caused an elevation in TGF-β activity in culture medium (Fig. 2B). Consistently, Western bot analysis revealed an increased level of TGF-β protein (Fig. 2C). Moreover, addition of exogenous TGF-β indeed induced EMT in our experimental settings (Fig. 2D). These results indicate that TGF-β mediates Ang II-induced EMT.

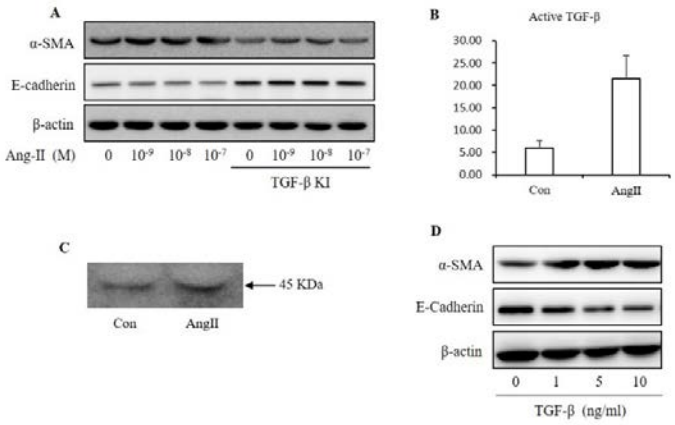

Fig.2. Ang II-induced EMT associated with TGF-β. (A) Effects of TGF-β receptor kinase inhibitor on Ang II-induced EMT in NRK-52E cells. (B) Effects of Ang II on the active TGF-β in NRK-52E cells. (C) Effects of Ang II on the secretion of TGF-β in NRK-52E cells. (D) Effects of TGF-β on EMT in NRK-52E cells.

3. H_2S inhibits TGF-β-induced EMT

Given that TGF-β mediated Ang II-induced EMT, we therefore focused on the effects of H_2S on TGF-β. Fig.3A shows that, in the presence of H_2S, the level of active TGF-β was largely suppressed under both basal and Ang II-stimulated conditions, as determined by TGF-β bioassay, whereas it did not greatly affect total TGF-β activity (Fig. 3B). Furthermore, pre-incubation of TGF-β with H_2S donor NaHS greatly reduced the its capacity in activation of p-Smad2 (Fig. 3C and D). Moreover, the structurally different H_2S donor sodium sulfide (Na_2S) and GYY 4137 also displayed the similar effects (Fig. 3E). DTT, a reducing agent that disrupt disulfide bond in proteins, also potently suppressed TGF-β activity. These results indicate that H_2S suppresses the biological activities of TGF-β.

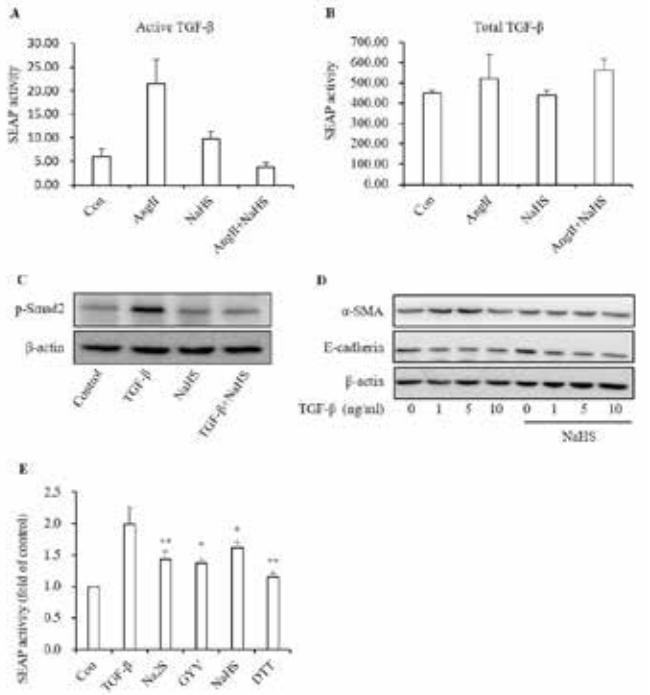

Fig.3. H_2S inhibits TGF-β-induced EMT. (A) Effects of H_2S on the active TGF-β induced by Ang II. (B) Effects of H_2S on the total TGF-β activity induced by Ang II. (C) Effects of H_2S on the expression of p-Smad2 induced by TGF-β. (D) Effects of H_2S on EMT induced by TGF-β. (E) Effects of different H_2S donor on the activity of TGF-β.

4. H_2S promotes TGF-β monomer formation

Given that the active TGF-β is a dimeric structure consisting of two monomers linked by disulfide bond and that disruption of disulfide bond results in a loss of TGF-β activity (13, 14), we speculated that H_2S might affect the structure of TGF-β vis modification of the disulfide bond. To test this speculation, TGF-β was pretreated with NaHS or DTT (a thiol reducing agent used for cleaving protein disulfide bonds). Afterwards, it is dialyzed against culture medium to remove the remaining NaHS, DTT and their metabolites. Bioactivity assay using MFB-F11 xxx cells revealed that H_2S- and DTT-treatment caused a significant reduction in TGF-β activity (Fig. 4A). Consistently, the ability in activating SMAD-2 signaling (Fig. 4B). Western blot analysis revealed that, different from the active TGF-β, which appeared as one band at the location of 25 kDa, H_2S treatment caused an appearance of an additional band that was localized at the same position of DTT-treated TGF-β, with a molecular weight at about 12.5 kDa, suggesting a cleavage of the disulfide bond (Fig. 4C). This effect of H_2S was concentration-dependent, being observable at the

concentration of 250 μM (Fig. 4D). Collectively, these observations suggest that H_2S disrupts the disulfide bond in TGF-β, leading to a loss of TGF-β activity.

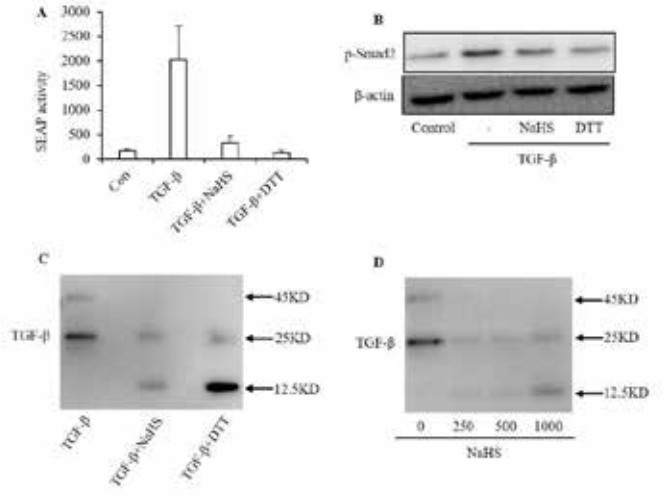

Fig.4. H_2S promotes TGF-β monomer formation. (A) Effects of H_2S on the activity of TGF-β. (B) Effects of H_2S on p-Smad2 induced by TGF-β in dialysis condition. (C) Effects of H_2S and DTT on the disulfide bond of TGF-β. (C) Effects of different concentration of H_2S on the disulfide bond of TGF-β.

Discussion:

In this study, we demonstrated, for the first time, that H_2S inhibited TGF-β production, promoted TGF-β monomer formation, and blunted Ang-II-induced EMT in cultured renal tubular epithelial cells. Our study thus provides novel mechanistic insights into the actions of H_2S and suggests it could be used for prevention and treatment of certain renal sclerotic diseases.

H_2S is one of the major vasodilators, which counteracts many vascular actions of Ang II. It downregulated Ang II /AT1R pathway and inhibited renal renin-angiotensin activity in renovascular hypertensive and diabetic rats (6, 19) . It also directly counteracted Ang II-induced hypertension and renal damage in rats (4, 8, 9). In this study, we demonstrated that H_2S directly suppressed Ang II-induced EMT in cultured renal tubular epithelial cells. There are also reports documenting a direct inhibition of Ang II-induced cell proliferation and matrix production by H_2S in cultured vascular smooth muscle cells (9). Given that abnormal cell proliferation, matrix production and EMT are characteristic pathological changes in several different types of renal diseases, H_2S may protect the kidney from Ang II-induced deleterious effects through both pressure-dependent and -independent mechanisms.

EMT, characterized by a phenotypic conversion from epithelial cells to fibroblast-like morphology, contributes to renal fibrosis and progression to end-stage kidney disease. Ang II and TGF-β are two major growth factors involved in stimulation of EMT in renal tubule epithelia cells (20, 21). They share many similar cellular responses and participate in almost every step of EMT. Many studies have shown that TGF-β mediates Ang II-induced renal fibrosis. Ang II induces TGF-β production and activates TGF-β signaling pathway. In line with these previous reports (3, 17, 22), we demonstrated that Ang II stimulated TGF-β activities and that blockade of TGF-β signaling with receptor kinase inhibitor abolished EMT-promoting action of Ang II. Our study thus provides additional evidences supporting a pivotal role of TGF-β in Ang II-induced EMT. In this context, it is conceivable that the protective effect of H_2S on EMT was most likely through its regulation on TGF-β. In support of this notion, H_2S donor indeed effectively blunted TGF-β induced EMT.

How did H_2S influence TGF-β-induced EMT? Theoretically, it could be due to its regulation on TGF-β activity or TGF-β signaling. In this study, we demonstrated that H_2S suppressed the activity of TGF-β without great influence on total activity of TGF-β, implying a possible regulation on TGF-β activation. Most of the biological action of H_2S have been shown to be related to its modification on cysteine residues in target proteins. Intriguingly, TGF-β1 has a dimeric structure consisting of two monomers linked by an inter-chain disulfide bond. Disruption of the disulfide bond causes a complete loss of its activity (13, 14). In this study, incubation of TGF-β with H_2S promoted the formation of TGF-β monomer in a way similar to the reducing chemical DTT, indicative of a cleavage of the disulfide bond. It was associated with a reduced bioactivity. We speculated that this could be one of the presently unrecognized mechanisms behind the anti-sclerotic effects of H_2S.

Of note, apart from its direct effect on TGF-β structure, H_2S could also affect Ang II- and TGF-β-induced EMT through other alternative mechanisms. Previous studies have demonstrated the existence of disulfide bonds in many important proteins that are involved in the biological actions of Ang II and TGF-β. These molecules should also be affected by H_2S. It is likely that the effect of H_2S, as observed in this investigation, could be a result of the combined effects of H_2S on many different molecules.

Our study could have significant implication. First, our study provides novel mechanistic insights into the actions of H_2S. Up to date, most of the proteins known to be modified by H_2S are intracellular molecules (10, 12) . Our study indicates that direct modification of the important extracellular proteins, such as cytokines and growth factors, could be important, but presently unrecognized mechanism underlying the biological actions of H2S. Second, our study provides an additional evidence supporting a mediating role of TGF-β in Ang II-induced EMT. The complete inhibition of Ang II and TGF-β-induced EMT suggest that H_2S could be a promising agent for prevention and treatment of certain sclerotic renal diseases.

In conclusion, our study demonstrated that H_2S alleviates Ang II and TGF-β-mediated induction of EMT, which was, at least in part, attributable to its effect on cleavage of disulfide bond in TGF-β. H_2S could be used to treat renal sclerotic diseases.

References:

1. Brosius FC. New insights into the mechanisms of fibrosis and sclerosis in diabetic nephropathy. Reviews in Endocrine and Metabolic Disorders. 2008;9(4):245.
2. Gray MO, Long CS, Kalinyak JE, Li H-T, and Karliner JS. Angiotensin II stimulates cardiac myocyte hypertrophy via paracrine release of TGF-β1 and endothelin-1 from fibroblasts. Cardiovascular research. 1998;40(2):352-63.
3. Shihab FS, Bennett WM, Tanner AM, and Andoh TF. Angiotensin II blockade decreases TGF-β1 and matrix proteins in cyclosporine nephropathy. Kidney international. 1997;52(3):660-73.
4. Al-Magableh MR, Kemp-Harper BK, and Hart JL. Hydrogen sulfide treatment reduces blood pressure and oxidative stress in angiotensin II-induced hypertensive mice. Hypertension Research. 2015;38(1):13.
5. Huang J, Wang D, Zheng J, Huang X, and Jin H. Hydrogen sulfide attenuates cardiac hypertrophy and fibrosis induced by abdominal aortic coarctation in rats. Molecular medicine reports. 2012;5(4):923-8.
6. Liu S-Y, Duan X-C, Jin S, Teng X, Xiao L, Xue H-M, and Wu Y-M. Hydrogen Sulfide Improves Myocardial Remodeling via Downregulated Angiotensin II/AT1R Pathway in Renovascular Hypertensive Rats. American

journal of hypertension. 2016;30(1):67-74.
7. Meng G, Zhu J, Xiao Y, Huang Z, Zhang Y, Tang X, Xie L, Chen Y, Shao Y, and Ferro A. Hydrogen sulfide donor GYY4137 protects against myocardial fibrosis. Oxidative medicine and cellular longevity. 2015;2015(
8. Zhou X, Feng Y, Zhan Z, and Chen J. Hydrogen sulfide alleviates diabetic nephropathy in a streptozotocin-induced diabetic rat model. Journal of Biological Chemistry. 2014;289(42):28827-34.
9. Zhao X, Zhang L-k, Zhang C-y, Zeng X-j, Yan H, Jin H-f, Tang C-s, and Du J-b. Regulatory effect of hydrogen sulfide on vascular collagen content in spontaneously hypertensive rats. Hypertension Research. 2008;31(8):1619.
10. Kabil O, and Banerjee R. Redox biochemistry of hydrogen sulfide. Journal of Biological Chemistry. 2010;285(29):21903-7.
11. Kimura H. Hydrogen sulfide: its production, release and functions. Amino acids. 2011;41(1):113-21.
12. Kimura H, Shibuya N, and Kimura Y. Hydrogen sulfide is a signaling molecule and a cytoprotectant. Antioxidants & redox signaling. 2012;17(1):45-57.
13. Lichtenberger FJ, Montague CR, Hunter M, Frambach G, and Marsh CB. NAC and DTT promote TGF-β1 monomer formation: demonstration of competitive binding. Journal of Inflammation. 2006;3(1):7.
14. Shi M, Zhu J, Wang R, Chen X, Mi L, Walz T, and Springer TA. Latent TGF-β structure and activation. Nature. 2011;474(7351):343.
15. Tesseur I, Zou K, Berber E, Zhang H, and Wyss-Coray T. Highly sensitive and specific bioassay for measuring bioactive TGF-β. BMC cell biology. 2006;7(1):15.
16. Rosenkranz S. TGF-β1 and angiotensin networking in cardiac remodeling. Cardiovascular research. 2004; 63(3):423-32.
17. Schultz JEJ, Witt SA, Glascock BJ, Nieman ML, Reiser PJ, Nix SL, Kimball TR, and Doetschman T. TGF-β1 mediates the hypertrophic cardiomyocyte growth induced by angiotensin II. The Journal of clinical investigation. 2002;109(6):787-96.
18. Sterzel R, Lovett D, Foellmer H, Perfetto M, Biemesderfer D, and Kashgarian M. Mesangial cell hillocks. Nodular foci of exaggerated growth of cells and matrix in prolonged culture. The American journal of pathology. 1986;125(1):130.
19. Ahmad FUD, Sattar MA, Rathore HA, Abdullah MH, Tan S, Abdullah NA, and Johns EJ. Exogenous hydrogen sulfide (H2S) reduces blood pressure and prevents the progression of diabetic nephropathy in spontaneously hypertensive rats. Renal failure. 2012;34(2):203-10.
20. Sun C-Y, Chang S-C, and Wu M-S. Uremic toxins induce kidney fibrosis by activating intrarenal renin–angiotensin–aldosterone system associated epithelial-to-mesenchymal transition. PloS one. 2012;7(3):e34026.
21. Zavadil J, and Böttinger EP. TGF-β and epithelial-to-mesenchymal transitions. Oncogene. 2005;24(37):5764.
22. Uhal BD, Kyong Kim J, Li X, and Molina-Molina M. Angiotensin-TGF-β1 crosstalk in human idiopathic pulmonary fibrosis: autocrine mechanisms in myofibroblasts and macrophages. Current pharmaceutical design. 2007;13(12):1247-56.

作成日：2018 年 2 月 20 日

Coronary accordion phenomenon and its OFDI characteristics
冠状動脈アコーディオン現象の OFDI 影像特徴

研究者氏名　朱　舜明（第 39 期笹川医学研究者）
中国所属機関　陝西省人民病院　循環器内科
日本研究機関　湘南鎌倉総合病院　循環器内科
指導責任者　齋藤　滋 教授

Abstract:

Accordion phenomenon is a transient angiographic multifocal filling defect observed mostly during percutaneous coronary intervention, mainly in tortuous vessels. A mechanical alteration during maneuvering of devices in tortuous coronary arteries frequently induces vessel wall shortening and coronary pseudo-stenosis, referred as accordion phenomenon. Subtraction of the devices normally leads to the entire resolution of the lesions. But this manipulation carries the risk of removing the guidewire from an actual dissection or lesion. Thus, additional imaging modalities such as optical coherence tomography (OCT)/ optical frequency domain imaging (OFDI) and intravascular ultrasound (IVUS) may be necessary for diagnosis as well as to guide treatment decisions. Here we report a case of accordion phenomenon confirmed by OFDI and try to illuminate the possible performance of this phenomenon.

Key words:

Accordion phenomenon, intravascular imaging, optical coherence tomography, optical frequency domain imaging, intravascular ultrasound

Case history:

A 72-year-old woman diagnosed as unstable angina was admitted for elective PCI. Half year ago, she received stent implantation in the proximal left descending artery due to acute myocardial infarction. The patient had a history of hypertension and dyslipidemia. Physical examination revealed a mild systolic murmur at the apex and her blood pressure was 145/85 mmHg. Electrocardiogram (ECG) showed abnormal Q wave in V1-V4. The lab tests were between normal ranges expect the eGFR was 47.7 mL/min/1.73 m^2. Two-dimensional echocardiography showed hypokinesis of the anterior and lateral wall with normal ejection fraction and mild mitral regurgitation. Direct PCI was done. A 6 French Slender Glidesheath was used via the left princeps pollicis artery. A 6 French SAL 1.0 SH guiding catheter was engaged in RCA. At the beginning of the procedure, the patient received 6,000 IU of heparin and the activated clotting time (ACT) was 287 seconds. Coronary angiography demonstrated severe tortuosity and significant stenosis in the middle portion of RCA (Fig 1, A). Runthrough Extra-floppy guidewire was advanced into the distal RCA. IVUS was done and the target lesion was decided. Svelte stent 3.5*23mm was inflated at 16 atmosphere for 30 seconds. Unfortunately, distal edge dissection was suspected after stenting. IVUS examination was done. But IVUS imaging was insufficient to illuminate the distal portion due to the lower resolution. Thus, high resolution OFDI was done. Distal edge dissection was confirmed and additional Svelte stent 3.5*23mm was deployed at 16 atmosphere for 30 seconds to cover the dissection (Fig 1, B). Good expansion and apposition were confirmed by both IVUS and OFDI. But, another abnormal narrowing was found in the distal edge of the second stent, suggesting a diagnosis of dissection, spasm, thrombosis or accordion phenomenon. OFDI imaging (Fig 2.) revealed the lumen contour gradually turned elliptical, and the vessel wall seemed to protrude into the lumen, mimicking intussusception and creating severe stenosis. By replacing the guidewire to a Finecross micro catheter, this narrowing lesion disappeared and thus we confirmed this pseudo-stenosis lesion was accordion phenomenon. Final angiography showed good results (Fig 1, C).

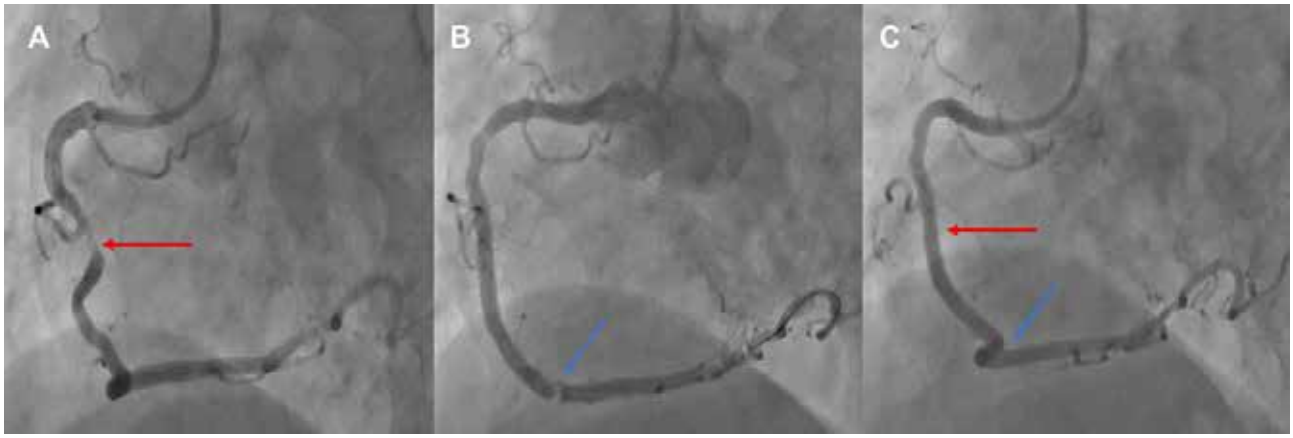

Figure 1. Coronary angiography of tortuous RCA. **A.** Severe stenosis in the middle portion of RCA (red arrow). **B.** After stenting, significant narrowing was found in the distal edge of the stent (blue arrow). **C.** After confirming of accordion phenomenon by OFDI, guidewire was removed, and the final angiography showed the fully cover of stent in the diseased middle RCA segment (red arrow) and the disappearance of stent edge stenosis (blue arrow).

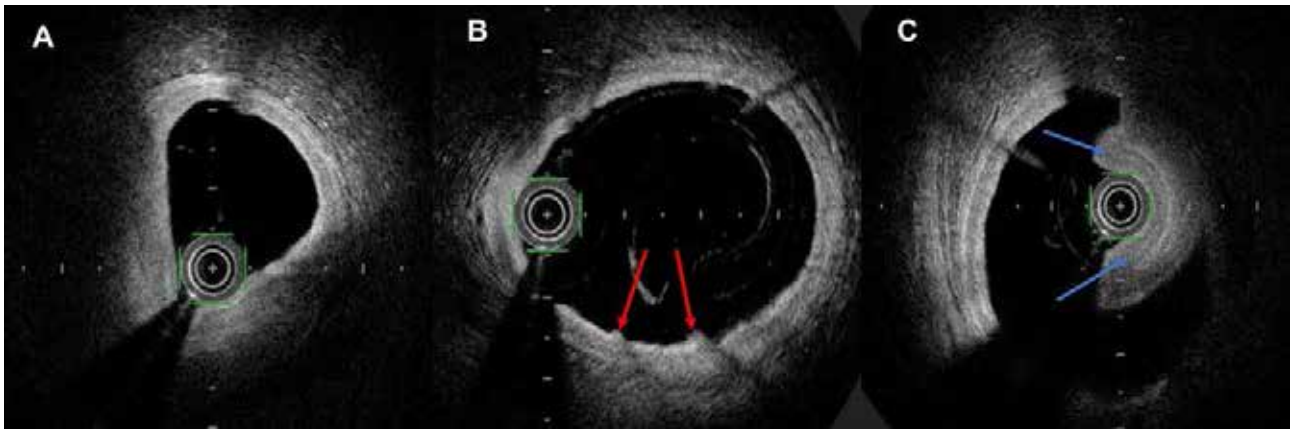

Figure 2. OFDI imagings of the pseudo-stenosis portion. A. Lumen contour was turning elliptical gradually and the medial layer was turning to be thickening on a flattened coronary wall. B. The intimal crumpling and protruding were demonstrated in OFDI imaging (red arrow), considering one of the typical appearance of accordion phenomenon. C. Image of a double-lumen mimicking a coronary dissection. Medial thickening (blue arrow) was also found due to the eccentric constrictions of the tortuous coronary artery.

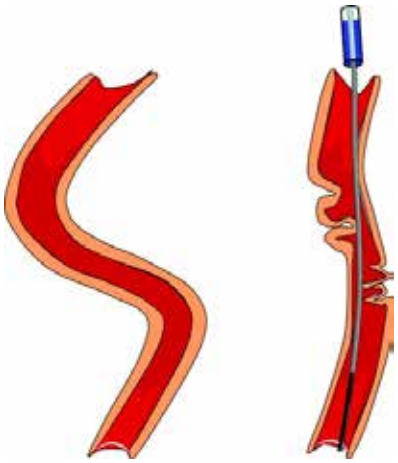

Figure 3. Schema of the accordion phenomenon. A tortuous artery is stretched by the guidewire, inducing folds of the vessel wall. These protruding folds induce several consecutive tight stenosis[1].

Discussion:

The accordion phenomenon is the appearance of pseudo-lesions after the advancement of stiff devices, including guidewires or stents, in a tortuous coronary artery, and it is caused simply by the invagination of the straightened arterial wall along its long axis[1] (Fig 3.). During PCI, mechanical reasons may induce angiographic defects, eccentric constrictions, attributed to the accordion phenomenon. It is produced by vessel wall shortening of tortuous segments, attributed to crumpling, invagination or intussusception with accordion-like appearance. The accordion effect or pseudo-narrowing may cause myocardial ischemia due to the shifting of the intima against the media layer of the vessel wall, with the resulting arterial folding. Theoretically, during the accordion effect there could be some arterial damage with platelet activation, clotting formation and subsequent intimal proliferation. Grewe et al[2] initially described this effect in an internal mammary graft during PTCA of the native LAD. The reported incidence of accordion effect is about 0.4%[3].The right coronary artery is thought to be predominately prone to develop this effect because this artery is entrenched in the epicardial fat tissue and courses rather freely in the atrioventricular groove.

This effect remains a challenge for physicians, because the differential diagnosis includes dissection, spasm, and thrombus. Distinguishing pseudo-lesions from these other conditions prevents unnecessary intervention. As has already been pointed out, this is not only an interesting angiographic finding but there are also important therapeutic implications: 1) differential diagnosis should be made with spasm, thrombosis and dissection; 2) it could be associated with impaired coronary flow accompanied with angina and electrocardiographic ischemic changes; 3) the crumpled coronary artery is not affected by the vasodilators; 4) the only therapeutic option is to pull back the intracoronary wire until the floppy tip lies across the engaged segment; and 5) interventional therapy for these pseudo-lesions must be avoided.

Previously, accordion phenomenon was reported as an elliptic-shaped lumen narrowing and a characteristic three-layered pattern of intimal thickening on a flattened coronary wall overlying a hypoechogenic space in IVUS examination[4]. These oval-shaped narrowing and attenuated findings look like vulnerable plaque. Although OCT/OFDI studies of this phenomenon in the literature were rare, we believe that the described tissue protrusion overlying the signal-free area most likely corresponds to the intussusception as already described in IVUS series[5]. In addition, the gradual crumpling of the walls visualized with OFDI was not mentioned in the IVUS study, presumably due to their very small size (< 100 mm, the axial resolution of IVUS)[6]. At the sites where the phenomenon was observed, the lumen contour gradually turned elliptical, and the vessel wall seemed to protrude into the lumen, mimicking intussusception and creating severe stenosis. One other feature that OFDI revealed was that the smooth lumen contour observed in the normal distal segments, crumpled progressively toward the segment where the accordion phenomenon was more obvious[7,8].

Conclusion:

It is very important to recognize such pseudo-lesions in order to avoid inappropriate interventions[9]. A number of factors may contribute to the appearance of this phenomenon, such as tortuous vessels, the of the guidewire (even soft shaft wire may cause the accordion phenomenon) and stent (as in the current case), and the small number of side branches[10]. Intravascular imaging tools like OCT, OFDI, and IVUS can be very useful to distinguish this phenomenon from other complications such as coronary dissection, spasm and thrombus.

References:

1. Muller O, Hamilos M, Ntalianis A, Sarno G, De Bruyne B. Images in cardiovascular medicine. The accordion phenomenon: lesson from a movie. Circulation 2008; 118:e677–e678.
2. Grewe K, Presti CF, Pe´rez JA. Torsion of internal mammary graft during percutaneous transluminal angioplasty: a

case report. Cathet Cardiovasc Diagn. 1990;19:195–197.

3. Rauh RA, Ninneman RW, Joseph D, Gupta VK, Senior DG, Miller WP. Accordion effect in tortuous right coronary arteries during percutaneous transluminal coronary angioplasty. Cathet Cardiovasc Diagn. 1991;23:107e110.
4. Nakabayashi K, Suzuki T, Okada H, Oka T . Different Intravascular Ultrasonograms Obtained from the Site of an Accordion Phenomenon before and after Distal Stenting. Int J Clin Med Imaging. 2016; 3: 478. doi:10.4172/2376-0249.1000478.
5. Goel PK, Agarwal A, Kapoor A. 'Concertina' effect during angioplasty of tortuous right and left coronary arteries and importance of using over-the wire system: a case report. Indian Heart J 2001; 53:87–90.
6. Manfrini O, Mont E, Leone O, et al. Sources of error and interpretation of plaque morphology by optical coherence tomography. Am J Cardiol. 2006; 15:156–159.
7. Prati F, Guagliumi G, Mintz GS, Costa M, Regar E, Akasaka T, Barlis P, Tearney GJ, Jang IK, Arbustini E, Bezerra HG, Ozaki Y, Bruining N, Dudek D, Radu M, Erglis A, Motreff P, Alfonso F, Toutouzas K, Gonzalo N, Tamburino C, Adriaenssens T, Pinto F, Serruys PW, Di Mario C; Expert's OCT Review Document. Expert review document part 2: methodology, terminology and clinical applications of optical coherence tomography for the assessment of interventional procedures. Eur Heart J. 2012;33:2513–2520. doi: 10.1093/eurheartj/ehs095.
8. Cuesta J, Bastante T, Rivero F, Antuña P, García-Guimaraes M, Benedicto A, Alfonso F. Coronary Pleating Mimicking Coronary Ruptures, Dissections, and Thrombi on Optical Coherence Tomography. Circ Cardiovasc Interv. 2016;9(5):e003654. doi: 10.1161/CIRCINTERVENTIONS.116.003654.
9. Davidavicius G, Manoharan G, De Bruyne B. The accordion phenomenon. Heart. 2005;91:471.
10. Doshi S, Shiu MF. Coronary pseudo-lesions induced in the left anterior descending and right coronary artery by the angioplasty guide-wire. Int J Cardiol. 1999;68:337–342.

作成日：2018年2月24日

Elucidation of the underlying mechanism by which prunella vulgaris exerts therapeutic effect on thyroiditis
夏枯草の抗甲状腺炎作用分子機構の解明

研究者氏名　陳　飛（第 39 期笹川医学研究者）
中国所属機関　南方医科大学珠江医院
日本研究機関　帝京大学医療技術学部臨床検査学科
指導責任者　鈴木　幸一
共同研究者名　川島　晃, 骆　予倩, 石藤　雄子、吉原　彩

Abstract:

Prunella vulgaris (PV) is a perennial herb. In Europe, it was used as food and tea. In China, this plant has been used to treat thyroid disease more than thousand years. Previously our team declared a relationship between immune response and autoimmune thyroid disease. We found that danger signal such as dsDNA or dsRNA can active innate immune response in thyrocytes to trigger autoimmune response, cell DNA fragments released from dying cells can stimulate thyrocytes. The Immune response continue and this circle will repeat. We tested whether Prunella vulgaris had effect on innate immune response in rat thyroid FRTL-5 cells. Firstly, we evaluate the aqueous extract of Prunella vulgaris (PVAE) action on thyroid hormone synthesis genes. We found that PVAE can suppressed the expression of sodium iodide symporter(*Nis*/*Slc5a5*) mRNA expression specifically in both concentration-and time-dependent manners. The highest decrease of *Nis*/*Slc5a5* mRNA expression reached to 5% of the control group. Secondly, we explored whether PVAE can inhibit the innate immune response stimulated by dsRNA and dsDNA in FRTL-5 cells. We found that PVAE can down-regulate mRNA expression of inflammatory cytokines interferon-beta(*Ifn-β*), tumor necrosis factor-α (*Tnf-α*) and *Il-6* significantly in response to dsRNA and dsDNA stimulation. And the *Ifn-β* and nuclear factor kappa–light-chain-enhancer of activated B cells(Nf-κb) signal activity also were suppressed by PVAE. These results suggest that PVAE is an active inhibiter to *Nis*/*Slc5a5* mRNA expression and innate immune response stimulated by dsRNA and dsDNA in FRTL-5 cells. We hypothesize that PVAE treating autoimmune thyroid disease(AITD) through Inhibiting innate immune activation and suppressing *Nis*/*Slc5a5* expression which maybe bring some inspiration for the treatment of AITD.

Keywords:

Prunella vulgaris, innate immune response, AITD, *Nis*/*Slc5a5*

Introduction:

AITD is the most common autoimmune disease [1], which developed by a combination of genetic susceptibility and environmental factors. Innate immune responses are associated with thyroid dysfunction, tissue destruction, and the likely development and perpetuation of AITD. The innate immune response is the major contributor of acute inflammation induced by infection or tissue damage which relate to the development of thyroiditis and trigger autoimmune thyroid disease. While, effective measures are still not founded to stop or delay the progression of Hashimoto's thyroiditis currently. Our team previous studies suggested that innate immune response relate to the development of thyroiditis [2], so inhibiting innate immune response may be an effective strategy.

Many data showed that PV has anti-inflammatory and immunomodulatory effects [3, 4]. Clinical trials declared that PV can treat Hashimoto's disease [5]. In the 2010 edition of Chinese Pharmacopoeia, the traditional Chinese patent medicines only made from PV that are listed including PV Cream and PV Oral Liquid. And the latter is permitted to treat thyroid goiter and some other diseases. These evidences illustrate that Prunella is a potential herb treating thyroid disease. However, the mechanism of PV on thyroid is seldom revealed. Therefore, in this study we explored the effect of PV on thyroid hormone function genes and its effect on thyroid cell innate immune response in FRTL-5 cells.

Method

Plant material

PVAE is the aqueous extract of P. vulgaris which were prepared and used as the method previously reported [6,7].

Cell culture and treatment

FRTL-5 rat thyroid cells were grown in Coon's modified Ham's F-12 medium. PVAE was used at various concentration (0, 31.25, 62.5,125,250,500 μg/mL).

Transfection of ds nucleic acids

One microgram of synthetic polynucleotides, poly (dA:dT) and poly(I:C) (GE Healthcare, Little Chalfont, United Kingdom).

RNA purification and real-time PCR

Total RNA was isolated using RNeasy Plus Mini Kit (Qiagen, Hilden, Germany), and cDNA was synthesized using the High-Capacity cDNA Reverse Transcription Kits (Applied Biosystems, Foster, USA).

Statistical analysis

All experiments were repeated at least three times and the mean ± SD of these experiments was calculated. The significance of the differences between experimental values was determined by an unpaired two-tailed t-test, wherein $p < 0.05$ was significant.

Result:

Suppressive effect of PVAE on expression of Nis/Slc5a5 gene regulating thyroid hormone

To evaluate the effects of PVAE on thyroid hormone secretion gene expression, we performed real-time PCR analysis using RNA purified from cells grown in the presence of TSH, insulin, and serum and with different PVAE concentrations for 24 hours. The mRNA expression of *Nis/Slc5a5*, thyroid peroxidase (*Tpo*), thyroglobulin(*Tg*), pendrin *(Pds/slc26a4)*, paired box gene 8 (*Pax8*) and dual oxidase maturation factor 2 (*Duox2*) were assayed. Only *Nis/Slc5a5* mRNA levels were specifically suppressed (Fig. 1). The inhibitive effect of PVAE is so stronger that the concentration 500 μg/mL PVAE decreased *Nis/Slc5a5* mRNA expression levels to 5% of the control group. The suppression of *Nis/Slc5a5* expression was evident at 24 hours after treatment with PVAE and existed after 72 hours (Fig. 1). These results indicated that PVAE suppressed the expression of *Nis/Slc5a5* in both concentration- and time-dependent manners. Gene expression level of *Tpo*, *Tg*, *Pds*, *Pax8*, *Duox2* were unreliable.

Protective effect of PVAE on dsDNA and dsRNA inducible inflammatory cytokine mRNA expression

Thyroid cells involve in the autoimmune response for expressing cytokines. We assessed the effect of PVAE on pro-inflammatory cytokine the production of thyroid innate immune activation using real-time PCR analysis. Results revealed that dsDNA and dsRNA (1μg/well) stimulation for 24 h remarkably increased inflammatory cytokine mRNA expression as compared with control group. The dsDNA induced expression of *Ifn-β* (20-fold) and *Il-6* (25-fold) (Fig. 3). The dsRNA induced (1ug/well) expression of *Ifn-β* (20-fold) and *Il-6* (25-fold) (Fig. 4). *Tnf-α* mRNA expression was not detected in control group by RT-PCR analysis. Expression of *Tnf-α* mRNA expression increased greatly after stimulation by dsDNA or dsRNA. Treatment with PVAE decrease dsDNA and dsRNA induced expression of *Ifn-β, Tnf-α* and *Il-6* to near the level of control group (Fig. 3.4). And the action of PVAE inhibit inflammatory cytokine

expression exit dose-dependent manner. All data indicate that PVAE suppresses inflammatory cytokine *Ifn-β, Tnf-α* and *Il-6* at mRNA expression level.

Discussion

Extraction PV can be divided into aqueous extraction and ethanol extraction mainly. The extraction all show bioactivity even though it is aqueous or ethanol [9,10]. In china clinical experience, this herb is provided to patients in a manner of aqueous extraction usually. So, we used aqueous extract of PV in the experiment.

Although PV has been used to treat thyroid disease in China for a long time, it has been researched in many cell lines except normal thyroid cell. For example, it shows anti-inflammatory effects on macrophages RAW 264.7 [11,12], anti-tumor effects on cancer cell [13,14]. Study on thyroid cells have been reported are seldom. So, on the reference of previous reports about PV, we determined the concentration range of PVAE on rat thyroid FRTL-5 cells, and found that the range from 1ug to 500μg/mL is an appropriate concentration. Secondly, we studied the effects of PVAE on genes expression relate to thyroid hormone synthesis

Thyroid hormone synthetic genes such as *Tpo*, *Tg*, *Pds*, *Pax8*, *Duox2* and *Nis/Slc5a5* were checked. *Nis/Slc5a5* mRNA levels were suppressed specifically and significantly. Results of other hormone synthesis gene *Tpo*, *Tg*, *Pds*, *Pax8* and *Duox2* expression are unreliable. *Nis/Slc5a5* is the plasma membrane glycoprotein mediating Iodine uptake that plays a key role as the first step in the biosynthesis of the thyroid hormones [15]. PVAE showed suppression effect on *Nis/Slc5a5* gene expression, whether it can regulate thyroid hormone synthesis is not known till now. Maybe animal experiment is required. According our clinical experience, PVAE treatment does not affect thyroid hormone levels of patients. It is well known that excessive amounts of iodide have been linked to the development of autoimmune thyroid disease in humans and animals [16]. Therefore, we hypothesize that one mechanism of Prunella vulgaris therapeutic effect probably related to reducing thyroid cells iodine uptake by inhibiting NIS gene expression.

Infection is an important etiological of AITD. According to pattern recognition receptors theory, the simulation to cell belong two types: damage-associated patterns(DAMP)and pathogen-associated molecular patterns (PAMP). PAMPs include lipopolysaccharides (LPS), peptidoglycans (PGN), and viral double-stranded RNAs (dsRNA) [17, 18], DAMP include genomic DNA fragments, heat shock proteins, uric acid et al [19]. From this perspective, the stimulation of double stranded DNA or RNA used in our study belong to two different modes respectively, different from the previous

research which selected only one stimulation lipopolysaccharide [11,12]. Double stranded DNA or RNA active thyroid cells innate immune responses successfully. It seemed that dsRNA stimulated thyroid cells produce more serious immune response. The same result had been reported by our group [2,20].

Infection can affect both thyroid and immune system. The reaction of thyroid innate immune response to infection in the occur and development of AITD should not be overlooked. In innate immune response, cytokines produced by thyroid cells recruit immune cells to the thyroid and thus accelerate the inflammation and development of AITD [23,24]. We chose rabbit thyroid cells to create innate immune responses which is not same as previous study focusing on immune cells. The treatment with PVAE significantly suppressed double stranded DNA or RNA induced *Ifn-β, Tnf-α* and *Il-6* mRNA expression. In previous studies about PV effect on macrophages RAW264.7, two laboratories got different conclusions. Eun et al found immune stimulatory activity of the extraction PV which can promote the expression of inflammatory cytokines expression and Nf-κb signal pathways activity in macrophages RAW264.7 [9]. Yu et al used extraction of PV treating lipopolysaccharide induced macrophages and found that extraction of PV can inhibit the expression of inflammatory cytokines and Nf-κb signal pathways activity [11]. We used rat thyroid FRTL-5 cells treated with PVAE and did not found that PVAE promote the expression of inflammatory cytokines and Nf-κb and Irf3 pathways activity. On the other side, clinical data showed that PV can reduce Hashimoto's disease patients the level of serum autoantibody [5].

In conclusion, these results indicate PV can affect thyroid function through inhibiting *Nis/Slc5a5* expression specifically and suppress innate immune response to DAMP and PAMP. The *in vitro* data partly illuminate it therapeutic mechanism on AITD. To investigate the overall effect of PVAE on thyroid, further studies in rabbit are needed.

References:

1. Hayter SM, Cook MC. Updated assessment of the prevalence, spectrum and case definition of autoimmune disease. Autoimmun Rev 2012; 11:754-765
2. Kawashima A, Yamazaki K, Hara T, Akama T, Yoshihara A, Sue M, Tanigawa K, Wu H, Ishido Y, Takeshita F, Ishii N, Sato K, Suzuki K. Demonstration of innate immune responses in the thyroid gland: potential to sense danger and a possible trigger for autoimmune reactions. Thyroid 2013; 23:477-487

3. Park SH, Koo HJ, Sung YY, Kim HK. The protective effect of Prunella vulgaris ethanol extract against vascular inflammation in TNF-α-stimulated human aortic smooth muscle cells. BMB Rep 2013; 46:352-357

4 Haarberg KM, Wymore Brand MJ, Overstreet AM, Hauck CC, Murphy PA, Hostetter JM, Ramer-Tait AE, Wannemuehler MJ. Orally administered extract from Prunella vulgaris attenuates spontaneous colitis in mdr1a(-/-) mice. World J Gastrointest Pharmacol Ther 2015; 6:223-237

5. Jingru liu, Qing wang, Prunella vulgaris capsule impact on Hashimoto's thyroiditis patients with autoantibodies and Th17 cells, Chinese Journal of Gerontology, 2012;24: 5413-5415.

6. Hwang SM, Lee YJ, Lee YP, Yoon JJ, Lee SM, Cha JD, Choi KM, Kang DG, Lee HS. Anti-Proliferative Effect of an Aqueous Extract of Prunella vulgaris in Vascular Smooth Muscle Cells. Evid Based Complement Alternat Med 2013; 2013:936463

7. Psotova J, Svobodova A, Kolarova H, Walterova D. Photoprotective properties of Prunella vulgaris and rosmarinic acid on human keratinocytes. J Photochem Photobiol B 2006; 84:167-174

8. Ishido Y, Luo Y, Yoshihara A, Hayashi M, Yoshida A, Hisatome I, Suzuki K. Follicular thyroglobulin enhances gene expression necessary for thyroid hormone secretion. Endocr J 2015; 62:1007-1015

9. Han EH, Choi JH, Hwang YP, Park HJ, Choi CY, Chung YC, Seo JK, Jeong HG. Immunostimulatory activity of aqueous extract isolated from Prunella vulgaris. Food Chem Toxicol 2009; 47:62-69

10. Hwang YJ, Lee EJ, Kim HR, Hwang KA. In vitro antioxidant and anticancer effects of solvent fractions from Prunella vulgaris var. lilacina. BMC Complement Altern Med 2013; 13:310

11. Hwang YJ, Lee EJ, Kim HR, Hwang KA. NF-κB-targeted anti-inflammatory activity of Prunella vulgaris var. lilacina in macrophages RAW 264.7. Int J Mol Sci 2013; 14:21489-21503

12. Li C, Huang Q, Fu X, Yue XJ, Liu RH, You LJ. Characterization, antioxidant and immunomodulatory activities of polysaccharides from Prunella vulgaris Linn. Int J Biol Macromol 2015; 75:298-305

13. Cho IH, Jang EH, Hong D, Jung B, Park MJ, Kim JH. Suppression of LPS-induced epithelial-mesenchymal transition by aqueous extracts of Prunella vulgaris through inhibition of the NF-κB/Snail signaling pathway and regulation of EMT-related protein expression. Oncol Rep 2015; 34:2445-2450

14. Yin DT, Lei M, Xu J, Li H, Wang Y, Liu Z, Ma R, Yu K, Li X. The Chinese herb Prunella vulgaris promotes apoptosis in human well-differentiated thyroid carcinoma cells via the B-cell lymphoma-2/Bcl-2-associated X protein/caspase-3 signaling pathway. Oncol Lett 2017; 14:1309-1314

15. Portulano C, Paroder-Belenitsky M, Carrasco N. The Na+/I- symporter (NIS): mechanism and medical impact. Endocr Rev 2014; 35:106-149

16. Luo Y, Kawashima A, Ishido Y, Yoshihara A, Oda K, Hiroi N, Ito T, Ishii N, Suzuki K. Iodine excess as an environmental risk factor for autoimmune thyroid disease. Int J Mol Sci 2014; 15:12895-12912

17. Takeuchi O, Akira S. Pattern recognition receptors and inflammation. Cell 2010; 140:805-820

18. Prantner D, Darville T, Nagarajan UM. Stimulator of IFN gene is critical for induction of IFN-beta during Chlamydia muridarum infection. J Immunol 2010; 184:2551-2560

19. Matzinger P. The danger model: a renewed sense of self. Science 2002; 296:301-305

20. Kawashima A, Tanigawa K, Akama T, Wu H, Sue M, Yoshihara A, Ishido Y, Kobiyama K, Takeshita F, Ishii KJ, Hirano H, Kimura H, Sakai T, Ishii N, Suzuki K. Fragments of genomic DNA released by injured cells activate innate immunity and suppress endocrine function in the thyroid. Endocrinology 2011; 152:1702-1712

Figure legends

Fig. 1. PVAE suppresses mRNA expression of *Nis/Slc5a5*. FRTL-5 cells were treated with various concentrations (0, 31.25, 62.5,125,250,500 μg/mL) PVAE 24 h or 350 μg/mL PVAE for the indicated time period for up to 48h. Total RNA was purified from the cells and subjected to real-time PCR analysis to determine the relative mRNA expression levels of *Nis/Slc5a5*, mRNA levels were normalized against *Gapdh* levels, and expressed as fold-change relative to the control. *** $p < 0.001$, compared to the control levels. Data are presented as mean ± SD relative to control levels (n = 3).

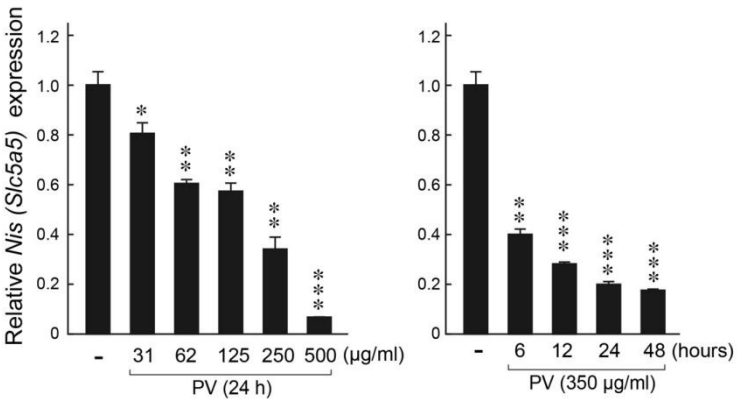

Fig. 2. **PVAE suppresses dsDNA induced inflammatory cytokine mRNA expression.** FRTL-5 cells were pretreated with various concentrations (0, 31.25, 62.5,125,250,500 μg/mL) PVAE 24 h then stimulated with dsDNA (1μg/well)

24h. Total RNA was purified from the cells and subjected to real-time PCR analysis to determine the relative mRNA expression levels of *Ifn-β, Tnf-α, Il-6* mRNA levels were normalized against *Gapdh* levels, and expressed as fold-change relative to the control. *** $p < 0.001$, compared to the control levels. Data are presented as mean ± SD relative to control levels (n = 3).

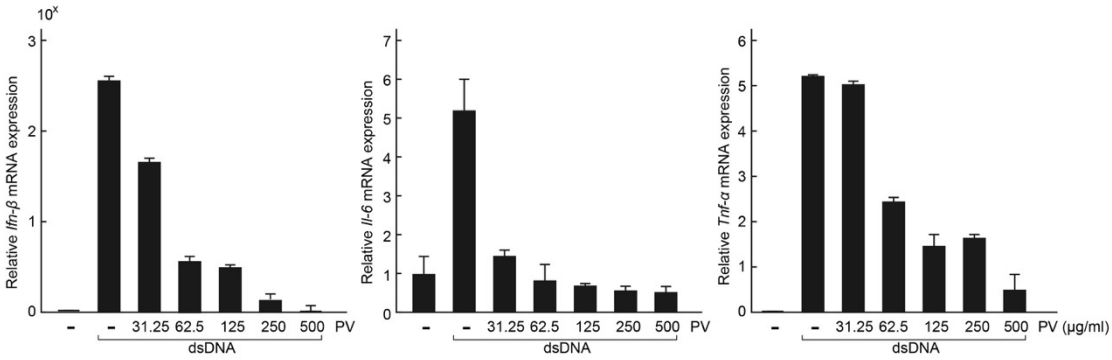

Fig. 3. **PVAE suppresses dsRNA induced inflammatory cytokine mRNA expression.** FRTL-5 cells were pretreated with various concentrations (0, 31.25, 62.5,125,250,500 μg/mL) PVAE 24 h then stimulated with dsRNA(1μg/well) 24h. Total RNA was purified from the cells and subjected to real-time PCR analysis to determine the relative mRNA expression levels of *Ifn-β, Tnf-α, Il-6* mRNA levels were normalized against *Gapdh* levels, and expressed as fold-change relative to the control. *** $p < 0.001$, compared to the control levels. Data are presented as mean ± SD relative to control levels (n = 3).

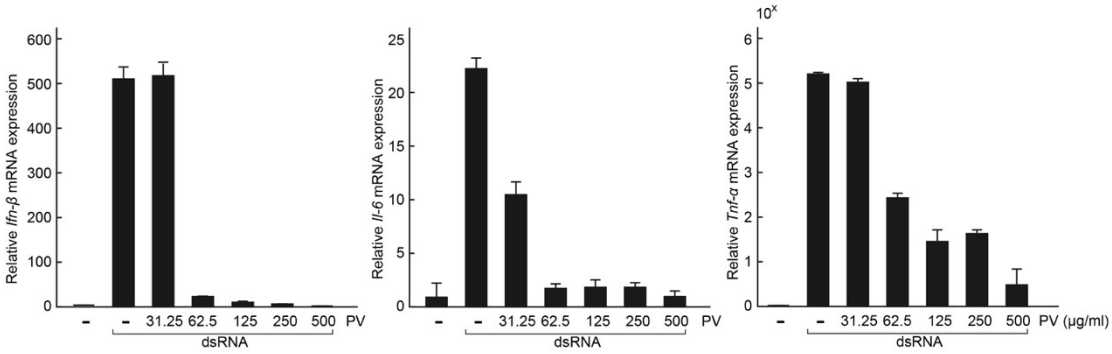

Fig. 4. PVAE suppresses Ifn-β and Nf-κb promoter activity. The effect of PVAE suppresses Ifn-β and Nf-κb promoter activity determined by using a luciferase reporter assay. FRTL-5 cells were transfected with Ifn-β or Nf-κb promoter luciferase chimeric plasmids. 6h later, Cells were treated with PVAE for 24h and then stimulated with dsDNA or dsRNA 24h which luciferase activity was measured. Values are expressed relative to those of cells cultured in a medium without PVAE. Data are the results from three different experiments, each performed in triplicate, and expressed as the mean±SD. *p < 0.001.

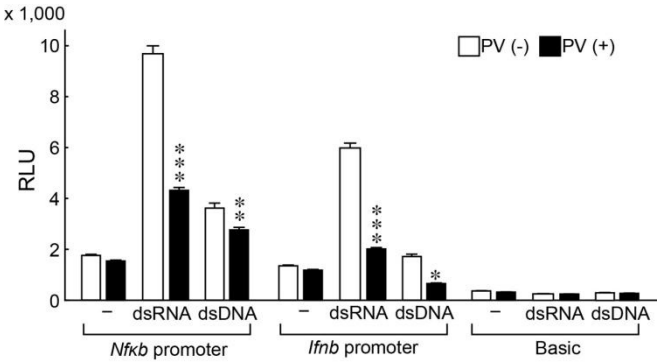

作成日：2018年 2月 20日

"A" elevation underlies the "X" overproduction in hydatidiform mole: an implication for the link between molar pregnancy and preeclampsia
胞状奇胎における“X”の過剰産生への“A”の関与について

研究者氏名　王　冠(第 39 期笹川医学研究者)
中国所属機関　天津市中心婦産科医院
日本研究機関　東京大学医学部附属病院女性診療科・産科
指導責任者　藤井　知行　教授
入山　高行　助教
共同研究者　吉川　美登利, 鈴木　研資, 永松　健, 大須　賀穣

Abstract:

Objective: The elevated levels of “A” induce “X” production in patients with hydatidiform mole(HM) which implicates the future development of preeclampsia(PE). Methods: The blood and placental samples were obtained from patients with HM(mole group) and normal pregnancy women(control group). The serum concentrations of "A" and "X" were measured by ELISA and the expression profiles of "A" in placental tissues were detected by immunohistochemistry(IHC). Then the human trophoblast cell line and primary cultured syncytiotrophoblasts were treated with “A" and the mRNA expression of "X" was detected by RT-PCR. Results: The serum concentrations of "A" and “X” were significantly elevated in mole group compared with the control group and the increased levels of “A” were positively correlated with the elevated "X". In molar placental tissues the higher expression of “A” mainly located on syncytiotrophoblasts. Meanwhile, the secretion of "X" was increased by "A" treatment in the HTR-8/SVneo cells and syncytiotrophoblasts. Conclusion: The increased levels of “A” lead “X” production which links the future development of PE in molar pregnancy.

Keywords: "A"; "X"; Hydatidiform mole; Preeclampsia.

Introduction:

Preeclampsia(PE) is a gestational syndrome of mainly characterized by hypertension and can increase the complications and mortality of gestation(1). The imbalance between angiogenic and anti-angiogenic factors has a important role in the development of PE(2). Especially, “X” due to induce hypertension and proteinuria which is a biomarker related to PE(3). Hydatidiform mole(HM) is a trophoblastic tumor and a risk for early-onset PE. Nearly 30-40% of untreated mole patients develop PE(4). Reports highlighted excess production of “X” contribute to the early-onset PE associated with HM(5). There was a report noted that the expression of “X” was increased in HM compared with the normal pregnancy women(6). So elevated levels of “X” are supposed to be involved in early-onset PE related with molar pregnancy.

“A" is a novel “T” superfamily cytokine which has been reported to link immune-associated diseases(7). There was a report showed “A” was excess expression in the serum of PE patients, about 24 folds higher than normal pregnancy(8). And then in pregnant mouse and human placental villous explant “A” can induce “B” production and elevated “B” stimulated “X” expression which contribute to PE(9). So we focus on “A” induced “X” which associated with the development of PE.

Here, we hypothesized that “A” elevation underlies the “X” overproduction in molar pregnancy, which implicates the future development of PE. In this study, we detected the levels of "A" in serum and placenta of molar patients and studied "A" induced "X" expression in cells to assess these hypotheses. These results reveal a previously unrecognized of "A" in HM which implicates the link between molar pregnancy and PE.

Materials and Methods:

Patients:

The experimental protocols were permitted by the IRB of Tokyo University and Nagoya University. The whole blood and placental samples were collected from patients with HM(mole group) and normal pregnancy women(control group) after signing informed consent form. Serum were separated and stored at −80°C. Tissues samples were randomly selected in all floating villi which mole group were diagnosed as complete HM and absence of a coexistent fetus, while there was no specific pathologic abnormalities in control group.

ELISA:

The levels of "A" and "X" in serum were measured separately by a sensitive ELISA Kits(R&D Systems, Tokyo, Japan). Serum "A" and "X" levels were separately compared between the two groups by T test. The correlation between "A" and "X" was analyzed by simple regression analysis.

Immunohistochemistry(IHC):

After deparaffinize and rehydrate, paraffin sections were incubated with citrate buffer(PH6.0) in microwave for 10 min. 0.3% H_2O_2 was used to block peroxidase. Slices were incubated with G-Block(Genostaff GB-01, Tokyo, Japan) for 10 min. Then 2 ug/ml "A" rabbit polyclonal antibody(Sigma:HPA012700-100, Tokyo, Japan) incubated overnight at 4°C. The anti-rabbit IgG biotin(Dako: E0432, Tokyo, Japan) was used for 30 min. Streptavidin-peroxidase label (Hamburger:426062, Tokyo, Japan) was used for 5 min. DAB/H_2O_2 reacted until color change. Slices were counterstained with Mayer's hematoxylin.

Cell Line:

Human trophoblast cell line HTR-8/SVneo were transferred to 24-wells plate and cultured with Dulbecco's Modified Eagle Medium(DMEM, Wako, Osaka), 10% fetal bovine serum(FBS) and antibiotic-antimycotic solution for 48 hours under 5% CO_2 at 37°C. And then 100 ng/ml recombinant human "A"(R&D Systems Inc, Tokyo, Japan) was used to co-culture for 18 hours.

Syncytiatization of Cytotrophoblast Cells In Vitro:

The methods of isolated and syncytialization of cytotrophoblast cells in vitro referenced the article of Dr. Tatsuya Fujii(10). Placental tissues were received from normal pregnant patients who chose to cesarean section in the full-term pregnancy and cytotrophoblast cells were isolated by a Mini MACS TM separator(Miltenyi Biotec). Purified cytotrophoblast cells were cultured with IMDM (GE Healthcare), 10% FBS, antibiotic-antimycotic solution, 200mM L-glutamine and 10ng/ml EGF and transferred to 24-well plates at a density of 2×10^6 cells/ml. After 96 hours, syncytiotrophoblasts were obtained and treated with 100 ng/ml recombinant human "A"(R&D Systems Inc, Tokyo, Japan) for 18 hours.

RT-PCR analysis:

After extracted total RNA and reverse transcribed cDNA, quantitative real-time PCR was completed by the Cycler thermal cycler system(Roche Diagnostics, Basel). Individual data were normalized against β-actin and calculated the mRNA expression of "X" gene by ΔΔCt method. The reaction of PCR: 1×(95°C, 15 min), 40×(95°C, 10s, 58°C, 8s, 72°C, 9s) and 1×(72°C, 10 min).

Statistical Analysis:

The differences of “A” and “X” expression between the two groups were analyzed by T test and the correlation was analyzed by simple regression analysis. All statistics and graphs were completed by GraphPad Prism 7 statistical software (GraphPad, San Diego, CA). *P* value <0.05 were considered to indicate statistical significance.

Results:

Circulating "A" and "X" Levels In HM and The Correlation Between "A" and "X".

We determined the levels of "A" and "X" in the circulation of normal pregnant women and patients with HM by ELISA. We found that circulating "A" levels were increased dramatically in mole group compared with control group($p<0.001$). "X" levels in mole group were also higher than control group($p<0.001$). Further, we analyzed the correlation between the levels of "A" and "X" in mole group. We observed the increased concentrations of "X" were positively correlated with elevated "A"($r =0.52$; $p<0.05$).

The Expression Profiles of "A" In The Placental Tissue of HM Patients and Normal Pregnant Women.

We examined the expression profiles of "A" in the placental tissues of HM and normal pregnancy women by IHC. Immunohistological studies demonstrated clearly that the expression of "A" was significantly increased in placental tissues of HM compare with normal pregnancy women. Additionally, "A" mainly stained on the surface and the cytoplasm of syncytiotrophoblasts.

"A" Promotes "X" Production In Human Trophoblast Cell Line and Primary Cultured Syncytiotrophoblasts.

To examine that "A" promotes "X" production, we treated the human trophoblast cell line HTR-8/SVneo cells and primary cultured syncytiotrophoblasts in vitro by"A" and PBS as a control. Compared with the control group, we demonstrated "X" production is significantly increased in the HTR-8/SVneo cells by "A" treatment($P<0.0001$). Simultaneously, in vitro primary cultured syncytiotrophoblasts, the expression of "X" was also increased after "A" treatment($P<0.05$).

Discussion:

The present study is the first to demonstrate the significantly elevated levels of "A" both in serum and placenta of molar pregnancy. And it is also noted that "A", mainly located on syncytiotrophoblasts, promotes the increased "X" levels in human trophoblast cell line and primary cultured syncytiotrophoblasts. Overall, our research results provided that elevated "A" induced "X" production which hints the relationship between HM and PE.

HM is a trophoblastic tumor due to over-proliferation of trophoblastic cells and more than 80% are benign(11). Molar pregnancy easily occur PE symptoms(12). Research proved that the imbalance between anti-angiogenic and angiogenic associated with the development of PE in molar pregnancy(5). In complete HM and partial HM, an anti-angiogenic factor "X" was excess production which contributes to PE and PE-like symptoms(5, 6, 13). "A", a homology with "T"", can mediate tumor regression via activating T cells and enhance tumor specific immunity, such as in the colon cancer, breast carcinoma, lymphoid malignancy and cervical cancer(7, 14). There was a report showed that "A" indirectly induced the secretion of "X" in pregnant mouse and human placental villi cells explant that promotes the development of PE symptoms(9). Our study showed that "A" present in molar pregnancy and significantly increased in the circulation and placentas of women with HM. Additionally, the increased "X" was significantly positively correlated with elevated "A" in serum of molar patients. Simultaneously, "A" stimulated the secretion of "X" in human trophoblast cell line and primary cultured syncytiotrophoblasts. Based on these results, elevated levels of "A" induced the production of "X" which may predict in the relationship of HM and PE.

Immunohistological analysis showed "A" protein were mainly located on the surface and cytoplasm of syncytiotrophoblasts in molar pregnancy. Syncytiotrophoblasts, the key part of the placenta links to maternal blood circulation, are the most important trophoblasts involved in material exchange, nutrient metabolism and immune regulation(15, 16). It contains synthesizers for transcribe and translate of "X" proteins. In PE, anti-angiogenic factor: excessive release of "X" by a disordered syncytiotrophoblasts involve the development of PE(17, 18). In our experiments "A" promotes the increased "X" levels in primary cultured syncytiotrophoblasts. Altogether, "A", located on syncytiotrophoblasts, may promote the overproduction of "X" which contributes to PE involved in molar pregnancy.

"A" can induce "X" production in pregnancy mouse and human placental villous explant. However, in molar pregnancy

the levels of “A" and it stimulates “X” production remain unclear. Here we provide both human serum and placentas evidence showed that the levels of “A" were significantly elevated and located on syncytiotrophoblasts in HM. Meanwhile, "A" is a effective factor that stimulates "X" production in human trophoblast cell line and primary cultured syncytiotrophoblasts. In conclusion, “A" elevation underlies “X” production in patients with HM which maybe a new biomarker implicates the future development of PE involved in molar pregnancy.

References:

1. Eric A P Steegers PvD, Johannes J Duvekot, Robert Pijnenborg. Pre-eclampsia. Lancet Oncol. 2010(July 1):376: 631–44.
2. Schrey-Petersen S SH. Anti-angiogenesis and preeclampsia in 2016. Curr hypertens rep. 2017:19: 6 Doi 0.1007/s 11906-017-0706-5.
3. Palei AC, Spradley FT, Warrington JP, George EM, Granger JP. Pathophysiology of hypertension in pre-eclampsia: a lesson in integrative physiology. Acta Physiol (Oxf). 2013;208(3):224-33.
4. Soto-Wright V, Bernstein M, Goldstein DP, Berkowitz RS. The changing clinical presentation of complete molar pregnancy. Obstet Gynecol. 1995;86(5):775-9.
5. Jimmy Espinoza JEU, Robert A. Starr, Robert P. Lorenz, Richard A. Bronsteen, Stanley M. Berry. Insights Into Angiogenic Imbalances During Pregnancy. 2009.
6. Kanter D, Lindheimer MD, Wang E, Borromeo RG, Bousfield E, Karumanchi SA, et al. Angiogenic dysfunction in molar pregnancy. Am J Obstet Gynecol. 2010;202(2):184 e1-5.
7. Johansson-Percival A, He B, Li ZJ, Kjellen A, Russell K, Li J, et al. De novo induction of intratumoral lymphoid structures and vessel normalization enhances immunotherapy in resistant tumors. Nat Immunol. 2017;18(11):1207-17.
8. Liu C, Luo R, Elliott SE, Wang W, Parchim NF, Iriyama T, et al. Elevated Transglutaminase Activity Triggers Angiotensin Receptor Activating Autoantibody Production and Pathophysiology of Preeclampsia. J Am Heart Assoc. 2015;4(12).
9. Iriyama T, Wang W, Parchim NF, Song A, Blackwell SC, Sibai BM, et al. Hypoxia-independent upregulation of placental hypoxia inducible factor-1alpha gene expression contributes to the pathogenesis of preeclampsia. Hypertension. 2015;65(6):1307-15.
10. Fujii T, Nagamatsu T, Morita K, Schust DJ, Iriyama T, Komatsu A, et al. Enhanced HIF2alpha expression during human trophoblast differentiation into syncytiotrophoblast suppresses transcription of placental growth factor. Sci Rep. 2017;7(1):12455.
11. Moein-Vaziri N, Fallahi J, Namavar-Jahromi B, Fardaei M, Momtahan M, Anvar Z. Clinical and genetic-epignetic aspects of recurrent hydatidiform mole: A review of literature. Taiwan J Obstet Gynecol. 2018;57(1):1-6.
12. Booth S, Eskandar O. A case of partial hydatidiform molar pregnancy with a placental diploid-triploid mosaicism associated with a euploid viable foetus complicated with severe pre-eclampsia. J Obstet Gynaecol. 2018:1-3.
13. N. Yoneda AS, K. Miura, R. Yonezawa, K. Takemura, S. Yoneda, H. Masuzaki, S. Saito. A triploid partial mole placenta from paternal isodisomy with a diploid fetus derived from one sperm and one oocyte may have caused angiogenic imbalance leading to preeclampsia-like symptoms at 19 weeks of gestation. 2013.
14. Galatola M, Cielo D, Panico C, Stellato P, Malamisura B, Carbone L, et al. Presymptomatic Diagnosis of Celiac Disease in Predisposed Children: The Role of Gene Expression Profile. J Pediatr Gastroenterol Nutr. 2017;65(3):314-20.
15. Gohner C, Plosch T, Faas MM. Immune-modulatory effects of syncytiotrophoblast extracellular vesicles in pregnancy and preeclampsia. Placenta. 2017.
16. Yue X, Sun Y, Zhong M, Ma Y, Wei Y, Sun F, et al. Decreased expression of fibroblast growth factor 13 in early-onset preeclampsia is associated with the increased trophoblast permeability. Placenta. 2018;62:43-9.

17. Redman CW, Staff AC. Preeclampsia, biomarkers, syncytiotrophoblast stress, and placental capacity. Am J Obstet Gynecol. 2015;213(4 Suppl):S9 e1, S9-11.

18. Cerdeira AS, Agrawal S, Staff AC, Redman CW, Vatish M. Angiogenic factors: Potential to change clinical practice in preeclampsia? BJOG. 2017.

作成日：2018 年 2 月 20 日

Comparison of Positioning for Preterm Infants between China and Japan
日中における早産児のポジショニングの比較

研究者氏名　夏　幸閣（第 39 期笹川医学研究者）
中国所属機関　広東省人民病院新生児科
日本研究機関　国立成育医療研究センター
指導責任者　丸山　秀彦　医師

Abstract

Background Positioning is an effective method of improving conditions and development of preterm infants. The aim of this study was to compare management and staffs' perceptions on positioning of preterm infants between China and Japan. **Methods** We surveyed 6 neonatal intensive care units (NICUs) in China and Japan with questionnaire. It had three parts: materials, carrying out and maintaining, and NICU staffs' perceptions on different diseases or symptoms. **Results** We found 3 major differences. First, a one-piece ready-made positioning mat in China was simply-operated and time-saving. But it might need detailed addition for each infant. Second, for intraventricular hemorrhage, head midline position, which was encouraged in China, would be supported by the reports: The head rotation would disturb the venous drainage from the head. Third, left lateral positioning, which was performed in China, would be better for gastro-esophageal reflux, although right lateral positioning would lead faster gastric emptying. **Conclusion** Investigating materials, management and staffs' perceptions on positioning of preterm infants could make us find some differences in 6 NICUs, especially between China and Japan. These differences would help us find the hints for improvement.

Key Words: Gastro-esophageal reflux, Intraventricular hemorrhage, Positioning, Preterm infant, Ready-made positioning mat

Introduction

Preterm infants are at increased risk of cognitive and motor impairment compared with term infants due to the immaturity of their organ systems[1,2]. Many researches have proved that positioning is an effective method for respiration[3,4], intraventricular hemorrhage (IVH)[5,6], apnea[7], gastro-esophageal reflux (GER)[8], stress[9], behavioral maturation[10,11], and sudden infant death syndrome (SIDS)[12].

In general, the posture in utero is ideal: trunk slightly bends forward and extremities are softly folded[13,14]. Neonatal Intensive Care Unit (NICU) staffs have attempted to make this positioning by nesting, swaddling or wrapping with commercial positioning aids[14,15], or rolled towels, rolled blankets, cotton gauze, and other particular materials made by the staff themselves.

Researches seldom reported how positioning was carried out in different NICUs. The aim of this study was to compare management and staffs' perceptions on positioning of preterm infants among 6 NICUs in China and Japan.

Methods

We performed the questionnaire survey. We chose 6 hospitals in China and Japan. Two of them were the author's hospitals: Guangdong General Hospital (GGH, the author's working hospital in Guangzhou, China) with 32 NICU beds, 28 Growing Care Unit (GCU) beds, 22 doctors and 70 nurses, and National Center for Child Health and Development (NCCHD, the author's studying hospital in Tokyo, Japan) with 21 NICU beds, 18 GCU beds, 17 doctors and 80 nurses.

Other 4 hospitals in Tokyo were: Tokyo Metropolitan Bokutoh Hospital (TMBH) with 15 NICU beds, 30 GCU beds, 13 doctors and 70 nurses; Tokyo Metropolitan Children's Medical Center (TMCMC) with 24 NICU beds, 48 GCU beds, 18 doctors and 128 nurses; Tokyo Women's Medical University Hospital (TWMUH) with 18 NICU beds, 21 GCU beds, 9 doctors and 54 nurses; and Japanese Red Cross Medical Center (JRCMC) with 15 NICU beds, 40 GCU beds, 9 doctors and 74 nurses.

The questionnaire has 3 sections. First section is about materials used for positioning. For example, materials placed under the infants, materials used as boundaries, assistant materials helped keeping the set positioning, and the usage of pillow and hat. Second section is about methods of carrying out and maintaining positioning. For example, steps of carrying out positioning, time taking, routinely change of positioning, staffs' opinions towards positioning and management of materials used. Last section is about staffs' perceptions of positioning on different diseases or symptoms. In this questionnaire, preterm infants were thought to be infants born at 25-27 gestational week, weighing 700-900g in acute phase.

We sent the questionnaire to the staffs of the 6 NICUs and then collected and analyzed the answers.

This study was approved by the ethical review board of NCCHD. And the staffs in each NICU agreed to participate this study.

Results

We summarized the answers about materials used for positioning in 6 NIC Us in Table 1. Hydro-cellular polyurethane dressings (HPD), cotton cushions, cotton sheets and silicon gauze were used to place straightly under preterm infants. As to boundaries, adjustable U-shaped metal covered by cushions (named as "bumper") were used in NCCHD and TMBH to surround the infants. Three or more rolled towels were used in TMCMC and JRCMC to make a nest for the infants. Ready-made positioning mats were used in GGH and TWMUH. In GGH, a ready-made positioning mat is a one-piece "preterm package." It consists of one piece normal thickness velvet cloth at bottom and 3 cm thickened overlapped velvet cloth (37cm x 14cm x 10cm) and two belts which cross or parallel in front of the baby (Figure 1). In TWMUH, a ready-made positioning mat is "positioning mat." This positioning mat is made by the soft cotton mats. The mats are folded to be like a box (Figure 2). The lower part of the body is covered by the mat. In order to keep the positioning, sand bags and rolled towels were used in the 5 Japanese NICUs, but nothing was used in GGH. Additionally, cotton cushions, cotton gauze, rolled rowels or cotton cushions were used in prone and lateral positioning in the 5 Japanese NICUs. Pillows were prepared in GGH with rolled towel and in TMCMC with folded cotton cushion. All of the 6 NICU used no hat, but 4 of them used some materials for surrounding the head.

Figure 1

Figure 2

Table 1. Materials used for positioning in 6 NICUs.

	GGH	NCCHD	TMBH	TMCMC	TWMUH	JRCMC
materials under the infant	cotton sheets and cotton cushion	HPD	silicon gauze and cotton sheets	silicon gauze	HPD and cotton sheets	cotton sheet
boundary	special designed positioning mat	U-shaped metal covered by cushion (bumper) or rolled towel	U-shaped metal covered by cushion (bumper)	rolled towel	special designed positioning mat	rolled towel

assistant materials keeping the positioning	nothing	sand bag and rolled towel	sand bag, rolled towel or seed bag	rolled towel	sand bags	sand bag and rolled towel
assistant materials for prone positioning	HPD on knees	cotton cushion and cotton gauze	cotton cushion, cotton gauze and rolled towel	rolled towel	rolled towel	sponge mat
assistant materials for lateral positioning	sometimes rolled towel, sometimes nothing	cotton cushion and cotton gauze	cotton cushion, cotton gauze and rolled towel	rolled towel	rolled towel	rolled towel
pillow	rolled towel	no	no	folded cotton cushion	no	no
hat	no particular hat, but sometimes use the upper part of positioning mat to cover the head	no, but they use rolled cotton cushion to surrounding the head	no, but they use rolled cotton sheet and cotton belt to surrounding the head	no	no, but they can use upper part of the positioning mat to surround the infant's head.	no

GGH: Guangdong General Hospital, NCCHD: National Center for Child Health and Development, TMBH: Tokyo Metropolitan Bokutoh Hospital, TMCMC: Tokyo Metropolitan Children's Medical Center, TWMUH: Tokyo Women's Medical University Hospital, JRCMC: Japanese Red Cross Medical Center, HPD: hydro-cellular polyurethane dressing

We summarized the answers about carrying out and maintaining of positioning in 6 NICUs (Table 2). The shortest time taken for preparing a suitable positioning was about 1-2 minutes in GGH, whereas the longest time was about 10-15 minutes in NCCHD. And 5-10 minutes in the other NICUs. NCCHD was the only unit, in which the staffs thought that it was quite difficult to prepare an ideal positioning; a little difficult in TWMUH and JRCMC, a little easy in TMBH and TMCMC, and quite easy in GGH. The answers from TWMUH showed that the staffs were not willing to use the materials in their NICU and that they thought the positioning was a little comfortable. After positioning was placed, 3 NICUs reported that the positioning could be kept for about 1-2 hours and 2 NICUs for 3 hours. Frequency of changing the positioning was every 2-3 hours in 5 NICUs. Positioning boundary itself was changed 1 or 2 times/week in 5 NICUs. Cotton sheets, towels, cover of the positioning boundaries were changed every day. Straightly-contracted materials were sterilized in 3 NICUs and were cleaned in 3 NICUs. Answers about the tube management were almost the same from the point of positioning.

Table 2. Carrying out and maintaining of positioning in 6 NICUs.

	GGH	NCCHD	TMBH	TMCMC	TWMUH	JRCMC
time taken	1-2 minutes	10-15 minutes	5 minutes	5-10 minutes	5 minutes	10 minutes
difficult or not	quite easy	quite difficult	a little easy	a little easy	a little difficult.	a little difficult
time of the settled positioning be kept	1-2 hours	it depends	3 hours	1-2 hours	3 hours	1-2 hours
frequency of reset or change of positioning	every 2-3 hours	it depends	every 3 hours	every 2-3 hours	every 2-3 hours	every 3 hours
nurse's willing	quite willing	quite willing	quite willing	quite willing	don't willing, just do as ordered	quite willing
infants with positioning	quite comfortable part	quite comfortable part	quite comfortable part	quite comfortable part	a little comfortable part	quite comfortable part
reuse of materials						
frequency of routinely exchange of materials	every day: cotton sheet. when dirty: cotton gauze, preterm mat.	every day: cotton sheet, rolled towel, cover of sand bags and bumper, cotton	every day from the second week: cotton sheets. once a week: bumper	every day: all materials	every day: towel. twice a week: positioning mat	every day: tower, cotton sheet once a week: sponge mat

		gauze and cotton cushion. first week: HPD				
deal with the changed materials	sterilize and reuse:_ positioning mat and cotton sheet. disposable: cotton gauze	clean and reuse: rolled towel, sand bags, bumper, cotton sheet. disposable: cotton gauze and cotton cushion	sterilize and reuse	clean and reuse	clean and reuse	sterilize and reuse: sponge mat, cotton sheet. clean and reuse: towel

GGH: Guangdong General Hospital, NCCHD: National Center for Child Health and Development, TMBH: Tokyo Metropolitan Bokutoh Hospital, TMCMC: Tokyo Metropolitan Children's Medical Center, TWMUH: Tokyo Women's Medical University Hospital, JRCMC: Japanese Red Cross Medical Center, HPD: hydro-cellular polyurethane dressing.

We summarized the answers about NICU staffs' perceptions of positioning on different diseases or symptoms (Table 3). As to IVH, GGH would make head position in midline. Other NICUs had their own ideas; head up or horizontal, supine or prone. 4 NICUs considered that prone and head up positioning is useful for apnea. 4 NICUs thought no particular methods for bradycardic and hypoxemic episodes and SIDS. All NICUs considered body prone with head up positioning useful for GER, TWCMC preferred right lateral with head up, GGH preferred left lateral with head titled up 30-45 degree. For energy expenditure, 2 NICUs took for no particular methods, 2 for prone positioning with head up, 1 for prone positioning with head naturally, and 1 for both body and head naturally. 1 NICU answered that nesting or swaddling could reduce energy expenditure. In sake of stress alleviating, 5 NICUs agreed with prone positioning. 1 NICU answered that holding by nurses worked in stress alleviating. 4 NICUs thought infants should be managed in prone positioning with head up after milk.

Table 3. NICU staffs' perceptions of positioning on different diseases or symptoms.

	GGH	NCCHD	TMBH	TMCMC	TWMUH	JRCMC
IVH	head midline	body naturally, head up or horizontal	body supine, head up	no particular method	body supine, head horizontal, minimal handing	body prone, head up
apnea	body prone, head up or horizontal	no particular method	body prone, head up	no particular method	body prone, head low	body prone, head up
SIDS	body supine, head up	no particular method	no particular method	no particular method	no particular method	body prone, head up
GER	body prone or left lateral, head titled up 30-45 degree	body prone, head up	body prone, head up	body prone or right lateral, head up	body prone, head up	body prone, head up
energy expenditure	body prone head up, nesting or swaddling	body prone, head naturally	naturally	no particular method	no particular method	body prone, head up
alleviating stress	body prone, head naturally	body prone, head naturally	body prone, head up	no particular method	body prone, head naturally, holding by nurse	body prone, head up
bradycardic and hypoxemic episodes	body prone, head up	no particular method	body prone, head up	body prone, head up	no particular method	body prone, head up
after milk	right side lateral, head up	no particular method	body prone, head up	body prone, head up	body prone, head up	body prone, head up

GGH: Guangdong General Hospital, NCCHD: National Center for Child Health and Development, TMBH: Tokyo Metropolitan Bokutoh Hospital, TMCMC: Tokyo Metropolitan Children's Medical Center, TWMUH: Tokyo Women's Medical University Hospital, JRCMC: Japanese Red Cross Medical Center, IVH: intraventricular hemorrhage, SIDS: sudden infant death syndrome, GER: gastro-esophageal reflux.

Discussion

Through this study, many things were different. Among them, we found 3 major differences.

First, we focused on a one-piece "Ready-made positioning mat." "Preterm package" was used in GGH, and "positioning mat" was used in TWMUH. GGH needed the shortest time for preparing a suitable positioning. The main reason might be Preterm package. In TWMUH, staffs considered their positioning a little difficult. On the opposite, the various materials and complex procedures made the longest time taken in NCCHD. Because of this way, the staffs in NCCHD thought that the positioning would be quite difficult. It is important to note: The TWMUH staffs thought that infants seemed a little comfortable, and that the staffs were not willing to do this positioning, but just did as ordered. GGH preferred to use a one-piece ready-made positioning mat for simple operation and time saving without any position-keeping materials. On the contrary, TWMUH did not feel satisfaction with a one-piece positioning mat. Other 4 Japanese NICUs also took some time for positioning in detail. So, it is quite important to find a simply-operated, time-saving, and infant-beneficial positioning for preterm infants.

As to IVH, GGH would make head position in midline. Other NICUs have their own ideas; head up or horizontal, supine or prone. Midline head position was enforced in GGH, based on the report that head rotation of infants could affect jugular venous drainage and cerebral blood volume and thus increase IVH[16,17]. From the report of term infants, turning the head occluded the jugular vein on the facial side and alteration in the superior sagittal sinus velocities were found[16]. Although head position would be related with respiratory management, including endotracheal tube, 5 Japanese NICUs might not take care of the head position.

All 6 NICUs agreed that prone positioning with head up was useful for GER. Staffs in GGH considered that left lateral positioning with head titled up 30-45 degree also useful because they considered less acidic esophageal exposure[8,18]. On the contrary, staffs in TMCMC thought right lateral positioning would be effective. Some reports showed that lower transient esophageal sphincter relaxation, which lead to GER, increased distension of proximal stomach in right lateral positioning compared to left lateral positioning[19,20]. Because right lateral position would be effective for gastric emptying[20,21], we should take care of position management for milk feeding.

We have several limitations. First, this study was conducted at 6 NICUs in Guangzhou, China and Tokyo, Japan. These NICUs might not represent the national characteristics. Second, questionnaires were answered by one staff of each NICU. Its answer might not represent other members' thoughts. Third, we have no outcome data. We could find the differences, but could not judge better or not.

In conclusion, investigating materials, management and staffs' perceptions on positioning of preterm infants could make us find some differences in 6 NICUs, especially between China and Japan. These differences would help us find the hints for improvement.

Acknowledgement

We really thank the staffs in 4 NICUs; Dr. Shimizu of TMBH, Dr. Kondo of TMCMC, Dr. Uchiyama of TWMUH and Dr. Nakao of JRCMC.

References

1. Symington AJ PJ. Developmental care for promoting development and preventing morbidity in preterm infants. *Cochrane Database Syst Rev.* 2006(2).

2. Spittle A OJ, Anderson PJ, Boyd R, Doyle LW. Early developmental intervention programmes provided post hospital discharge to prevent motor and cognitive impairment in preterm infants (Review). *Cochrane Database Syst Rev.* 2015(11).
3. Rivas Fernandez M RIFM, Diez-Izquierdo A, Escribano J, Balaguer A. Infant position in neonates receiving mechanical ventilation. *Cochrane Database Syst Rev.* 2016(11).
4. Rotschild A CD, Puterman ML, Phang MS, Ling E, Baldwin V. Optimal positioning of endotracheal tubes for ventilation of preterm infants. *Am J Dis Child* 1991;145(9):1007-1012.
5. Bijl-Marcus KA BA, de Vries LS, van Wezel-Meijler G. The Effect of Head Positioning and Head Tilting on the Incidence of Intraventricular Hemorrhage in Very Preterm Infants A Systematic Review. *Neonatology.* 2017;111(3):267-279.
6. Romantsik O CM, Bruschettini M. Head midline position for preventing the occurrence or extension of germinal matrix-intraventricular hemorrhage in preterm infants (Protocol). *Cochrane Database Syst Rev* 2016(9).
7. Ballout RA FJ, Kahale LA, Badr L. Body positioning for spontaneously breathing preterm infants with apnoea. *Cochrane Database Syst Rev.* 2017(1).
8. Corvaglia L RR, Ferlini M, Aceti A, Ancora G, Faldella G. The effect of body positioning on gastroesophageal reflux in premature infants evaluation by combined impedance and pH monitoring. *J Pediatr.* 2007;151(6):591-596.
9. Peng NH CL, Li TC, Smith M, Chang YS, Huang LC. . The effect of positioning on preterm infants' sleep wake states and stress behaviors during exposure to environmental stressors. *J Child Health Care.* 2014;18(4):314-325.
10. KA W. The importance of positioning in the near-term infant for sleep, play, and development. *NEWBORN & INFANT NUSNG REVIEWS.* 2007;7(2):76-81.
11. Aucott SD, PK;Atkins, E;Allen, MC. Neurodevelopmental care in the NICU. *Ment Retard Dev Disabil Res Rev.* 2002;8(4):298-308.
12. Pediatrics CoFaNAAo. Apnea, sudden infant death syndrome, and home monitoring. *Pediatrics* 2003;111(4 Pt 1):914-917.
13. Kenner.C MJM. Developmental Care of Newborns and Infants: A Guide for Health Professionals. 2nd ed. 2010:285-308.
14. Madlinger-Lewis L RL, Zarem C, Crapnell T, Inder T, Pineda R. The Effects of Alternative Positioning on Preterm Infants in the Neonatal Intensive Care Unit A Randomized Clinical Trial. *Res Dev Disabil.* 2014;35(2):490-497.
15. Picheansathian W WP, Baosoung C. Positioning of Preterm Infants for Optimal Physiological Development a systematic review. *JBI Libr Syst Rev.* 2009;7(7):224-259.
16. Cowan F TM. Changes in Superior Sagittal Sinus Blood Velocities Due to Postural Alterations and Pressure on the Head of the Newborn Infant. *Pediatrics* 1985;75(6):1038-1047.
17. Ancora G ME, Aceti A, Pierantoni L, Grandi S, Corvaglia L, Faldella G. Effect of Posture on Brain Hemodynamics in Preterm Newborns Not Mechanically Ventilated. *Neonatology.* 2010;97(3):212-217.
18. Corvaglia L MS, Aceti A, Arcuri S, Rossini R, Faldella G. Nonpharmacological management of gastroesophageal reflux in preterm infants. *Biomed Res Int* 2013:1-7.

19. Loots C KS, van Wijk M, McCall L, Peeters L, Lewindon P, Bijlmer R, Haslam R, Tobin J, Benninga M, Davidson G, Omari T. Body positioning and medical therapy for infantile gastroesophageal reflux symptoms. *J Pediatr Gastroenterol Nutr.* 2014;59(2):237-243.
20. Omari TI RN, Staunton E, Lontis R, Goodchild L, Haslam RR, Dent J, Davidson GP. Paradoxical impact of body positioning on gastroesophageal reflux and gastric emptying in the premature neonate. *J Pediatr* 2004;145(2):194-200.
21. Wijk MP BM, Dent J, Lontis R, Goodchild L, McCall LM, Haslam R, Davidson GP, Omari T. Effect of body position changes on postprandial gastroesophageal reflux and gastric emptying in the healthy premature neonate. *J Pediatr.* 2007;151(6):585-590.

作成日：2018 年 2 月 20 日

Improvements in Cuff Techniques in A Lung Transplantation Model in Rats: Device Improvement and Procedure Modification

ラットの肺移植モデルにおけるカフ技術の改善：装置の改善および処置の変更

研究者氏名　田　東（第 39 期笹川医学研究者）
中国所属機関　川北医学院附属医院
日本研究機関　京都大学附属病院
指導責任者　伊達　洋至 教授
共同研究者名　陳　豐史 講師

Abstract:

Background and objective: Rats are commonly used for modeling orthotopic lung transplantation, especially after Mizuta's cuff technique in rat lung transplantation was described in 1989. However, disadvantages and difficulties also exist due to the complexity of the procedure, especially for surgeons inexperienced in the technique. We aim to report the novel, innovative, simple processes and devices for a microsurgical lung transplantation model in rats with a high survival rate that can be easily performed by one surgeon alone. **Methods:** We performed 15 consecutive orthotopic unilateral lung transplantations in Lewis rats at Kyoto University with newly modified procedures and invented devices. The modified procedures were based on the traditional procedure and Kyoto University Hospital protocol, incorporating the following improvements: orotracheal intubation; a cuff with a tail; conservative dissection in the hilum; preservation of the left lung during anastomosis; successive anastomosis of the bronchus, the pulmonary vein, and the pulmonary artery; and one operator. **Results:** In our consecutive 15 pairs, both success rates and short-term (3 h) survival were 100% (15/15). The mean total operation time (from thoracotomy to transplant) was 39.01±1.06 minutes. The total transplant time (from flush to reperfusion) was 31.13±0.82 minutes. The donor thoracotomy lasted 7.88±0.56 minutes. Flush and harvest lasted 1.61±0.36 min. Dissection and cuffing preparation lasted 12.56±0.74 min. Recipient thoracotomy and hilum detection required 8.5±0.52 min. The implant time was 8.45±0.54 min. All anastomoses were completed in one attempt without vessel laceration, twisting or angulation. There were no deaths in our study 3 hours post-operation. **Conclusion:** We developed a modified orthotopic LT technique with cuff, and we invented some devices that can be easily used to shorten operative time while overcoming major drawbacks. The modified technique and invented devices have many advantages, including easy graft implantation, shortened operation time, fewer complications and a high degree of reproducibility. This improved technique can provide a more precise assessment of the rat LT model.

Keywords:

Cuff Techniques; Rats; Lung Transplantation; Devices Invention; Procedures Improvement

Introduction:

In recent years, with increases in lung disease, lung transplantation (LT) has become the most effective and most commonly used way to rescue patients with end-stage pulmonary diseases[1]. Orthotopic LT in an animal model is a necessary procedure that simulates human LT, including rejection, infection, ischemia/reperfusion processes, and chronic rejection that can offer much important information for LT research. An appropriate and stable animal model for LT is the basis of LT research[2, 3]. Rats were used as the representative rodent transplant models, first in 1971 by Asimacopoulos et

al. [4, 5]. In 1989, the use of a cuff technique in rat LT by Mizuta et al.[6] improved microsurgical rat LT techniques, facilitating anastomoses of the pulmonary artery and vein. In 1995, Reis et al.[7] described a non-suture external cuff technique that did not require microscopic suturing of the vessels or bronchus. They used a Teflon cuff instead of a cuff made of polyvinyl chloride or polyethylene that often leads to foreign-body reaction and fibrous tissue formation[1, 8, 9]. Recently, we attempted to modify the previously cuff model with invented devices and improved procedures. Our improvements permit easy handling, shortened operation time, fewer complications and high reproducibility.

Methods and Materials

1. Animals and Anesthesia

The Animal Care Committee of Kyoto University approved all procedures. Specific pathogen-free inbred male Lewis rats, age 12 weeks (weight, 290 to 310 g), were used both as donors and recipients. A total of 15 consecutive orthotopic LTs were performed in the study. Anesthesia was performed the same protocol as Kyoto University Hospital[10].

2. Left lung dissection and cuff placement

Cuffs were placed by the same protocol as Kyoto University Hospital[10]. The cuff consisted of a body of 1.5 mm, 2 mm, and 2 mm in length for pulmonary vein, artery and bronchus, respectively. There was a 1 mm cuff extension (cuff tail) for all three structures. A running knot was prepared for the pulmonary vein, and surgical knots (two rounds) were prepared for the pulmonary artery and bronchus before ligation.

Cuff making were performed in a dish which we invented in this study (Fig.1). The left main bronchus was the first structure dissected, owing to its anterior-most position. Then, the phrenic nerve was removed if visible. After phrenic nerve excision, the pulmonary artery was dissected easily because of clear exposure. The pulmonary vein with part of the atrial tissue was carefully dissected and cut after the abovementioned procedures.

3 Implantation (Fig. 2)

In the right lateral decubitus position, a 50ml plastic cylinder was placed under the right chest before left 5th intercostal space thoracotomy. Other procedures were performed as previous study[10]. The pulmonary artery, pulmonary vein, and left main bronchus were isolated. Curved incisions were sculptured from the inferior segmental vein, inferior segmental bronchus to superior segmental vein, inferior segmental bronchus. Regarding the pulmonary artery, a one-third circumference incision at the bifurcation of the pulmonary artery was performed for implantation.

4. Assessment of the graft lung

The outcomes of the transplanted rats and relevant times in orthotopic lung transplantation were assessed. After transplantation, we macroscopically checked the anastomotic structures for air or blood leakage. Atelectasis, lung inflation, and the color of the lung were evaluated 3 hours after closing the chest skin. The recipient rat was placed in a supine position, and the chest and abdomen were opened for donor lung harvest assessment 3 hours post-operation. All animals were euthanized on the day of our predetermined endpoint of the study.

5. Statistics

Statistical analysis was performed with SPSS version 25.0 software (Chicago, IL, USA). Data were reported as the means ± SD and were compared with paired t tests. P values less than 0.05 were considered statistically significant.

Results:

We performed 15 consecutive transplants with a success rate of 100%. All anastomoses were completed in one attempt without vessel laceration, twisting or angulation. Common complications such as vessel laceration, twisting and

angulation that occurred in previous studies were not observed. No atelectasis was found, and lung inflation and color were normal 3 hours after closing the chest skin. The average weights of donor and recipient rats were 289.80 ±5.24 and 290.27 ± 6.18 g, respectively. The mean duration for the total operation time (from thoracotomy to transplant) was 39.01±1.06 minutes. The total transplant time (from flush to transplant) was 31.13±0.82 minutes. The donor thoracotomy required 7.88±0.56 minutes. Flush and harvest lasted 1.61±0.36 min. Dissection and cuffing preparation required 12.56±0.74 min. Recipient thoracotomy and hilum detection required 8.5±0.52 min. The implant time was 8.45±0.54 min

Discussion:

Rat is the best model for lung transplantation because of its single-lobe left lung and because it is less expensive than larger animals. However, it is very difficult to master the procedure[11]. Therefore, a stable, simple and easy-to-perform model with high reproducibility would be of great importance. We reported an improved model of orthotopic left lung transplantation in rats based on Mizuta and colleagues' cuff technique[6] and considered the procedures from Kyoto University Hospital[10]. In our study, we made some important improvements both in devices and procedures that can complete the transplant with a high success rate in a short time.

1 Cuff (Fig. 3)

A previous study showed that the cuff consisted body 1.5 mm and tail 1 mm in length for all three structures[6]. In our study, the cuffs were produced from 14/16-gauge intravenous catheters for different structures. The cuff consisted of a body of 1.5 mm, 2 mm, and 2 mm in length for pulmonary vein, artery and bronchus, respectively. There was a 1 mm cuff extension (cuff tail) for all three structures. The body of the cuff for the pulmonary vein was shorter because the trunk of the pulmonary vein is shorter than the pulmonary artery and bronchus. Importantly, the cuff tail should be made smoothly at the end to prevent vessel damage.

2 Donor lung dissection and cuff making dish

Cuffing the three structures of donor lung was the most difficult and important procedure. In previous studies, many devices to prepare the cuffing were described[1, 8, 9]. We invented a useful device for donor lung dissection and cuff making that can make the dissection and cuffing easier, even for a new performer (Fig. 7, 8, 9). In our study, there was no failure in these procedures, and the mean time was (12.56±0.74 min) min. This was also the shortest time compared with other studies[1, 6, 8].

3. Technological improvement and advantages of the new procedure

We used a single order for cuffing: pulmonary vein first, then bronchus, and pulmonary artery last. This order was different from previous studies, having the advantages of a lower structure twist rate and easier cuffing [1]. In our study, we prepared a running knot for the pulmonary vein and surgical knots (two rounds) for the pulmonary artery and bronchus before ligation because the trunk of the pulmonary vein is very short due to its anatomic characteristics, even with part of the atrial tissue used to lengthen it[11]. It tends to slip out when circumferentially everted over the cuffs. Therefore, the performer should hold the everted cuff with one micro-clipper and tighten the knot with another micro-clipper. In our study, we put a tube under the right side of rat during thoracotomy of the left 5th intercostal space. This was just the same procedure as in human surgery to make the left hilum more superficial. These modifications allowed for better visualization that made hilum dissection and implantation easier. Regarding the recipient pulmonary vein, several possibilities are as follows: 1. If branches were far away from the proximal segment, we made the incision on the initial part of the segmental pulmonary vein; 2. If branches were near the proximal segment with significantly different size of veins, we made the incision on the larger branch and ligated the smaller one; 3. If branches near the proximal segment

had similar size of veins, we often made the curve incision from the inferior to superior segmental of the pulmonary vein.

Conclusion

We developed a modified orthotopic LT technique with cuff and invented some devices that can be easily used and that shorten operative time while overcoming major drawbacks. The modified technique and invented devices have many advantages, including easy graft implanting, shortened operation time, fewer complications and a high degree of reproducibility. This detailed procedure and improved technique can provide a more precise assessment in the rat LT model and can reduce the recurrent lung injury, which may affect research results.

References:

1 Zhai W, Ge J, Inci I, et al. Simplified rat lung transplantation by using a modified cuff technique. J Invest Surg 2008; 21(1): 33-7.

2 Christie JD, Edwards LB, Kucheryavaya AY, et al. The Registry of the International Society for Heart and Lung Transplantation: twenty-seventh official adult lung and heart-lung transplant report--2010. J Heart Lung Transplant 2010; 29(10): 1104-18.

3 Okazaki M, Krupnick AS, Kornfeld CG, et al. A mouse model of orthotopic vascularized aerated lung transplantation. Am J Transplant 2007; 7(6): 1672-9.

4 Asimacopoulos PJ, Molokhia FA, Pegg CA, Norman JC. Lung transplantation in the rat. Transplant Proc 1971; 3(1): 583-5.

5 Marck KW, Wildevuur CR. Lung transplantation in the rat: I. Technique and survival. Ann Thorac Surg 1982; 34(1): 74-80.

6 Mizuta T, Kawaguchi A, Nakahara K, Kawashima Y. Simplified rat lung transplantation using a cuff technique. J Thorac Cardiovasc Surg 1989; 97(4): 578-81.

7 Reis A, Giaid A, Serrick C, Shennib H. Improved outcome of rat lung transplantation with modification of the nonsuture external cuff technique. J Heart Lung Transplant 1995; 14(2): 274-9.

8 Habertheuer A, Kocher A, Laufer G, et al. Innovative, simplified orthotopic lung transplantation in rats. J Surg Res 2013; 185(1): 419-25.

9 Guo H, Nie J, Fan K, et al. Improvements of surgical techniques in a rat model of an orthotopic single lung transplant. Eur J Med Res 2013; 18: 1.

10 Tanaka S, Chen-Yoshikawa TF, Miyamoto E, et al. Vascular Endothelial-Cadherin Expression After Reperfusion Correlates With Lung Injury in Rat Lung Transplantation. Ann Thorac Surg 2016; 101(6): 2161-7.

11 Jungraithmayr WM, Korom S, Hillinger S, Weder W. A mouse model of orthotopic, single-lung transplantation. J Thorac Cardiovasc Surg 2009; 137(2): 486-91.

Figures:

Fig. 1 Cuff making dish

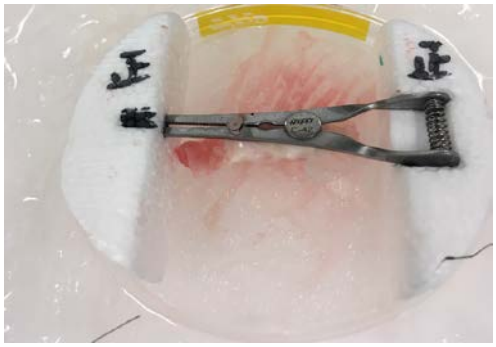

Fig. 2 Implantation

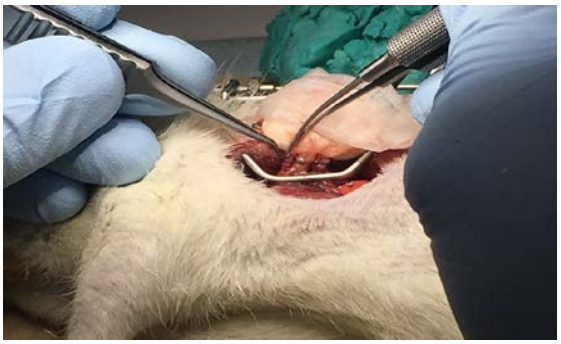

Fig. 3 Cuff

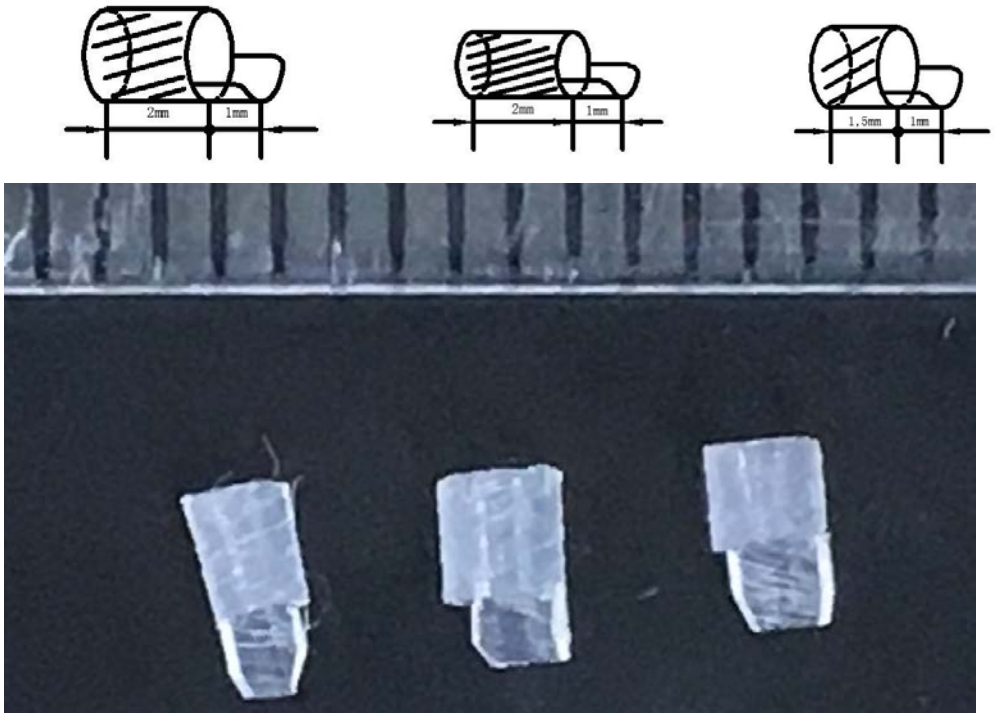

作成日：2018 年 2 月 26 日

Long-term effects of antihypertensive therapy on cardiovascular events and new onset diabetes mellitus in high-risk hypertensive patients in Japan
カンデサルタンとアムロジピンが日本人ハイリスク高血圧患者の 10 年超の予後に及ぼす影響：CASE-J 10

研究者氏名	劉　金梁（第 39 期笹川医学研究者）
中国所属機関	浙江大学医学部第二付属病院
日本研究機関	京都大学病院臨床研究センターEBM 推進部
指導責任者	上嶋　健治　教授
共同研究者	桑原　佳宏，加藤　恵理，誉田　真子

Abstract

To confirm the long-term effects of candesartan and amlodipine, we conducted a 10-year follow-up study in 4,703 high-risk hypertension patients. In general, blood pressure was well controlled (<140/90 mmHg) in both arms. The 10-year Kaplan-Meier rates for cardiovascular events were 14.7% for candesartan and 14.8% for amlodipine, and no significant difference was observed after adjustment for baseline characteristics (HRadj=0.97, 95% CI 0.80-1.18, P=0.770). However, candesartan showed lower rate of new onset diabetes as compared to amlodipine (8.3% vs 11.1%) over 10 year follow-up, and candesartan remained as an independent predictor for new onset diabetes reduction after adjustment (HRadj=0.72, 95% CI 0.52-0.99; P=0.040).

Keywords: Candesartan, Amlodipine, Cardiovascular events, New onset diabetes, Hypertension.

Introduction

Hypertension is the most prevalent and independent promoter of cardiovascular (CV) disease. Recently, some of the antihypertensive treatment are reported to have additional benefit in reducing these individual CV risk factors, particularly in new onset diabetes (NOD). For example, we have previously demonstrated in the Candesartan Antihypertensive Survival Evaluation in Japan (CASE-J) trial and its extension study[1], the Candesartan Antihypertensive Survival Evaluation in Japan Extension Study (CASE-J Ex)[2], that an angiotensin II receptor blocker (ARB), candesartan (CA), reduces NOD by 36% when compared with a calcium channel blocker (CCB), amlodipine (AM).

On contrary, the CASE-J and CASE-J Ex showed no statistical differences in prevention of CV events in patients taking CA or AM. However, considering that both the occurrence of NOD and development of CV events are relatively lengthy process, a longer follow-up may be needed to compare the true benefit of antihypertensive agents. In this study, we sought to evaluate 10-year results of antihypertensive treatment using CASE-J cohort.

Method

The Candesartan Antihypertensive Survival Evaluation in Japan, 10-year follow-up (CASE-J 10) combined prospective data from the CASE-J and CASE-J Ex and retrospectively collected data of the same cohort. The design and results of the CASE-J and CASE-J Ex trial are reported elsewhere [3,4]. Briefly, a total of 4,703 high-risk hypertensive patients were randomly and equally assigned to candesartan or amlodipine group in CASE-J. After 4 years of follow-up,

participants were invited to be followed for another 3 years (CASE-J Ex). Based on the results of the CASE-J and the CASE-J Ex, the CASE-J 10 was designed to assess long-term efficacy of CA and AM on blood pressure, CV events, and NOD by extending the follow-up to 10 years of the same cohort (Figure 1).

Figure 1. Flow chart of the CASE-J 10 study.

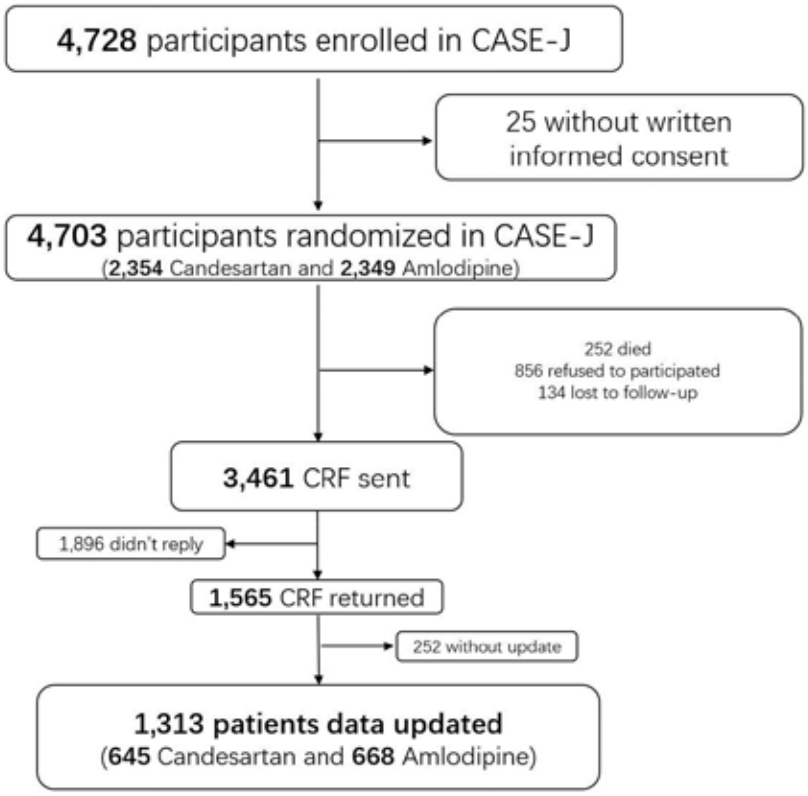

The primary endpoint was the time to first CV event, defined as composite of cerebrovascular, cardiac, renal, vascular events and sudden death. The secondary endpoints were each component of CV events (cerebrovascular, cardiac, renal, vascular events and sudden death), CV mortality, all-cause mortality and NOD. The study was approved by the Ethics Committee at the Kyoto University Graduate School of Medicine (R1115) in accordance with the principles of the Helsinki Declaration.

Results

A total of 1,313 patients' data was retrospectively updated in CASE-J 10, which extended the mean follow-up to 6.0 years (6.04 years for CA and 6.03 years for AM, p=0.918, Figure1). The baseline of CASE-J 10 trial was well balanced between the CA and AM group, except for the gender ratio (P=0.004) and current alcoholic (P=0.014), and it was not significantly different from 4,703 patients who enrolled in the CASE-J trial (Table 1).

Table 1. Characteristics of CASE-J and CASE-J 10.

Characteristics	CASE-J		CASE-J 10		
	CA (N=2354)	AM (N=2349)	CA (N=645)	AM (N=668)	P value
Female, n (%)	1092 (46.4)	1014 (43.2)	311 (48.2)	375 (56.1)	0.004
Age, years (SD)	63.8 (10.5)	63.9 (10.6)	62.8 (10.0)	62.9 (10.2	0.901
BMI, kg/m2 (SD)	24.6 (3.7)	24.5 (3.6)	24.7 (3.7)	24.6 (3.5)	0.374
SBP at enrollment, mmHg (SD)	162.5 (14.2)	163.2 (14.2)	162.8 (15.0)	163.6 (14.9)	0.343
DBP at enrollment, mmHg (SD)	91.6 (11.0)	91.8 (11.4)	91.8 (10.9)	92.1 (11.6)	0.714
Antihypertensive drug use at randomization, n (%)	1612 (68.5)	1553 (66.1)	409 (63.4)	406 (60.8)	0.326
Severe hypertension, n (%)	454 (19.3)	493 (21.0)	150 (23.3)	168 (25.1)	0.423
Current smokers, n (%)	489 (20.8)	536 (22.8)	127 (19.7)	160 (24.0)	0.062
Current alcoholic, n (%)	1239 (52.6)	1229 (52.3)	374 (58.0)	342 (51.2)	0.014
Type 2 diabetes mellitus, n (%)	1011 (42.9)	1007 (42.9)	280 (43.4)	277 (41.5)	0.476
History of cerebrovascular events, n (%)	248 (10.5)	225 (9.6)	66 (10.2)	71 (10.6)	0.814
History of cardiac events, n (%)	1007 (42.8)	1023 (43.6)	258 (40.0)	268 (40.1)	0.965
History of renal events, n (%)	572 (24.3)	543 (23.1)	130 (20.2)	125 (18.7)	0.509
Peripheral artery disease, n (%)	29 (1.2)	24 (1.4)	4 (0.6)	5 (0.7)	0.778
Hyperlipidemia, n (%)	608 (46.3)	930 (43.3)	311 (48.2)	297 (44.5)	0.172

The P-value indicates the results of comparison between the candesartan and amlodipine group in CASE-J 10 patients.

Blood pressure

After the treatment with allocated regimen, the mean systolic/diastolic BP was 136.9/77.1 (SD: 15.2/10.6) mmHg in the CA group and 136.7/76.9 (SD: 15.0/10.5) mmHg in the AM group. No significant treatment difference was observed for the absolute systolic BP reduction (25.6mmHg for CA and 26.6 mmHg for AM, P=0.080) or diastolic BP reduction (14.5mmHg for CA and 15.0 mmHg for AM, P=0.161).

CV events

The primary composite outcome of cerebrovascular, cardiac, renal, vascular events and sudden death occurred in 448 participants (225 for CA and 223 for AM) during the whole follow-up. The 10-year cumulative CV event rate was 14.7% for CA and 14.8% for AM overall. There was no significant between-group difference for primary composite endpoint after adjusting for baseline characteristics (HRadj=0.97, 95% CI 0.80-1.18, P=0.770, Figure 2).

Figure 2. 10-year Kaplan–Meier curves for CV events.

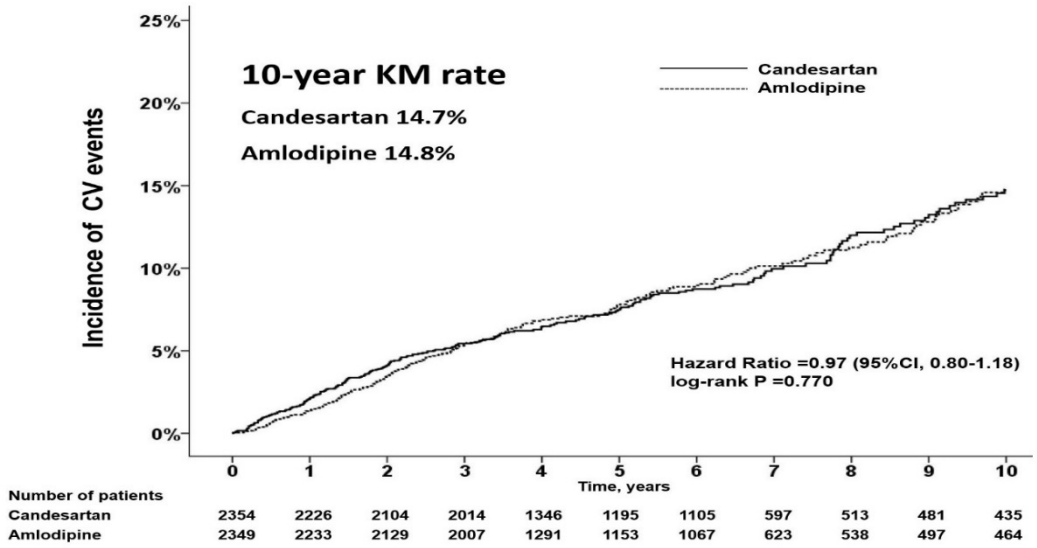

New onset diabetes

A total of 164 NODs (68 for CA and 96 for AM) occurred during the whole follow-up in 2,685 patients who did not have diabetes mellitus at enrollment. The 10-year cumulative event rate was 8.3% for CA and 11.1% for AM. After adjustment, CA reduced NOD by 30% compared to AM independent of other baseline factors throughout the whole follow-up (HRadj=0.72, 95% CI 0.52-0.99; P=0.040, Figure 3).

Figure 3. 10-year Kaplan–Meier curves for new onset diabetes mellitus.

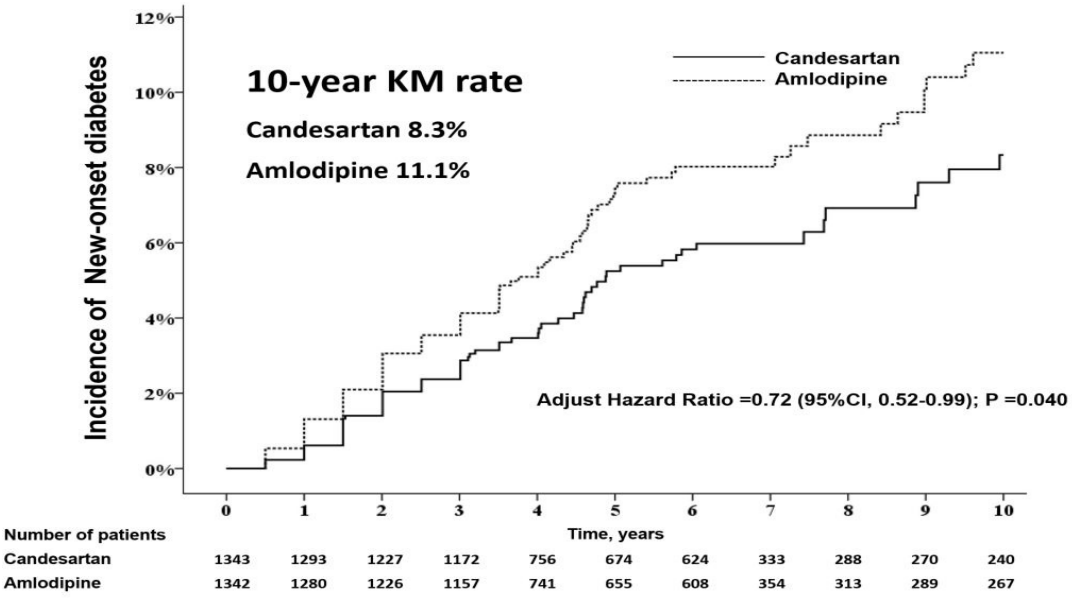

Discussion

The CASE-J 10 demonstrated no significant difference between the CA treatment group and AM treatment group on BP reduction throughout the long-term follow-up. More importantly, the incidence of CV events did not differ between the CA and AM arms even after adjusting for baseline characteristics. Nevertheless, the CA arm appeared to be associated with a lower incidence of NOD.

There are several reasonable hypotheses. First, more patients and a longer follow-up duration may be needed to adequately show any CV outcome difference in patients with NOD. A previous study with 25 years of follow-up shows that the mean observation time from NOD to first event is 9.1 years for myocardial infarction and 9.3 years for stroke [5]. However, the mean follow-up duration from NOD to the last visit was only 4.2 years in the CASE-J 10. Second, a well-managed BP may have helped to prevent or delay the onset of microvascular and macrovascular complications [6,7]. In our study, the BP was well controlled in both the CA-based and AM-based treatments. Lastly, for numerical comparison, CA had fewer renal events than AM, but it was more favorable with AM for cerebrovascular events and neutral for cardiac events. These heterogeneous results may explain why there was no difference in the primary endpoint or mortality. Nevertheless, given the current DM pandemic state and higher CV risks in patients with diabetes, reducing NOD has a strong clinical effect worldwide.

Limitations

There are several limitations to the CASE-J 10 that warrant consideration. First, unlike the CASE-J and CASE-J Ex, patient information was retrospectively collected in the CASE-J 10. As such, the analysis consisted of prospective and retrospective data. Second, as with any study with a long-term follow-up, considerable patients were censored. However, we have demonstrated that the baseline characteristics of the CASE-J 10 were similar to those of the CASE-J, and IPCW analysis showed that this influence was considered minimum. Third, the study population only included Japanese patients with high-risk hypertension, and generalizability of our data needs to be tested in different races with various lifestyles. Finally, in the CASE-J and CASE-J Ex, patients with NOD were defined as patients who reported a newly diagnosed DM on the adverse event form or those who initiated anti-diabetic agents after enrollment. However, in the CASE-J 10, only the latter was collected due to feasibility. However, only six patients (3 in the AM arm and 3 in the CA arm) who did not initiate anti-diabetic agents but had DM reported on adverse events in the CASE-J and CASE-J Ex. We have performed sensitivity analysis that excludes the six patients defined as NOD but did not initiate anti-diabetic agents, and the results were similar (Appendix 2). Although there are some limitations, we had an opportunity to study 28,385 patient-years of high-risk hypertension, which may serve as an important future reference.

Conclusion

In conclusion, the CASE-J 10 study was a unique and valuable opportunity to evaluate candesartan and amlodipine for a long-term efficacy on CV events and NOD. The CASE-J 10 demonstrated no significant difference between CA treatment group and AM treatment group on blood pressure reduction throughout the long follow-up. More importantly, the incidence of CV events did not differ between the CA and AM arms even after adjusting for baseline characteristics. Nevertheless, the CA arm appeared to be associated with a lower incidence of NOD.

References:

1. Ogihara T, Nakao K, Fukui T, et al. Effects of candesartan compared with amlodipine in hypertensive patients with high cardiovascular risks: candesartan antihypertensive survival evaluation in Japan trial. Hypertens Dallas Tex 1979 2008;51(2):393–8.

2. Ogihara T, Ueshima K, Nakao K, et al. Long-term effects of candesartan and amlodipine on cardiovascular morbidity and mortality in Japanese high-risk hypertensive patients: the Candesartan Antihypertensive Survival Evaluation in

Japan Extension Study (CASE-J Ex). Hypertens Res Off J Jpn Soc Hypertens 2011;34(12):1295–301.

3. Fukui T, Rahman M, Hayashi K, Takeda K, Higaki J, Sato T, *et al.* Candesartan Antihypertensive Survival Evaluation in Japan (CASE-J) trial of cardiovascular events in high-risk hypertensive patients: rationale, design, and methods. *Hypertens Res Off J Jpn Soc Hypertens* 2003; 26:979–990.

4. Ueshima K, Oba K, Yasuno S, Fujimoto A, Sato T, Fukiyama K, *et al.* Long-term effects of candesartan and amlodipine on cardiovascular mortality and morbidity in Japanese high-risk hypertensive patients: rationale, design, and characteristics of candesartan antihypertensive survival evaluation in Japan extension (CASE-J Ex). *Contemp Clin Trials* 2009; 30:97–101.

5. Almgren T, Wilhelmsen L, Samuelsson O, Himmelmann A, Rosengren A, Andersson OK. Diabetes in treated hypertension is common and carries a high cardiovascular risk: results from a 28-year follow-up. *J Hypertens* 2007; 25:1311–1317.

6. American Diabetes Association. 8. Cardiovascular Disease and Risk Management. *Diabetes Care* 2016; 39 Suppl 1:S60-71.

7. Dunder K, Lind L, Zethelius B, Berglund L, Lithell H. Increase in blood glucose concentration during antihypertensive treatment as a predictor of myocardial infarction: population based cohort study. *BMJ* 2003; 326:681.

作成日：2018 年 2 月 23 日

The Influence of Storage Temperature and Time Before Freeze Processing on Stem Cells Quality of Cord Blood Products
凍結処理前の貯蔵温度及び時間による臍帯血幹細胞の品質への影響

研究者氏名　葉　盛（第 39 期笹川医学研究者）
中国所属機関　南京赤十字血液センター機採科
日本所属機関　日本赤十字社近畿ブロック血液センター製剤部
指導責任者　木村　貴文　部長
共同研究者　下垣　一成，原田　博道，寺田　あかね，
渕崎　晶弘，越智　洋輔

Abstract:

Background. The potency and quality of hematopoietic stem cells (HSCs) in cord blood (CB) products is crucial for successful transplantations and other clinical applications. But the optimum condition for maintaining CB stem cells viability prior cryopreservation remains controversial. This study investigated the impact of storage temperature and time delay prior to further processing on stem cells quality of cord blood products.

Methods. 6 CB products preserved at 4℃ and other 6 products were at six different temperatures. Samples were collected daily until Day3 or Day4. Cell viabilities were evaluated by antibody co-staining with 7-amino actinomycin D (7-AAD) detecting nonviable cells and the following flow cytometry.

Results. Flow cytometric analysis showed the highest viabilities were obtained for samples preserved at low temperatures groups (4℃, 10℃ and 15℃) and the data achieved from 4℃ had no significance as compared with those from 10℃ and 15℃ groups.

Conclusion. Our data suggest that CB products are better preserved at low temperature such like 4℃ before further processing and cryopreservation to retain the potency of stem cells, and the prefreeze delay over 3 days should be avoided as much as possible.

Key Words:

Cord blood, temperature, cryopreservation, stem cell enumeration, CFU

Introduction:

Allogeneic hematopoietic stem cell transplantation (HSCT) is widely used for the treatment of various severe disorders, such like malignant hematologic diseases, bone marrow failure and genetic deficiencies [1-2]. Compared to bone marrow and mobilized peripheral blood stem cells, umbilical cord blood (UCB) has increasingly become a new candidate source of stem cells for HSCT with several advantages including low risk of acute or chronic graft-versus-host disease(GVHD), low requirement of human leukocyte antigen(HLA)-matching and reduced possibility of pathogen contagion [3]. In addition, the collection of UCB is fast and convenient for most hospitals with different technical condition and culture backgrounds [4]. Since the first utilization with UCB to treat a Fanconi anemia patient in France [5], more than 30,000 UCB transplants have performed in the past 3 decades [6]. However, due to the low numbers of nucleated cells (NCs) and $CD34^+$ cells in a single UCB unit for the HSCT in adult recipients, ex vivo expansion of hematopoietic stem cells (HSCs) and transplantation of multiple UCB units has been attempted to overcome these graft cell dose limitations [7-8].

During the application of UCB, one crucial factor for successful clinical outcome is the quality of hematopoietic stem

cells in UCB units. As published data mentioned before, the potency of UCB-derived hematopoietic stem cells and progenitor cells could be affected by many elements after collection such like time interval or storage temperature before processing and cryopreservation [9-10]. Hence, it is essential to determine the optimal conditions for preserving viability of stem cells in UCB units. Time delay prior to advanced procedure has limited firstly. According to current NetCord-FACT standards, cryopreservation of unrelated UCB units shall be initiated in 48 hours of collection and related ones in 72 hours for guaranteeing the quality of UCB products provided by over 50 UCB banks worldwide [11]. In China, this time interval has been narrowed down to 24 hours for all kinds of UCB products, while that is 36 hours in Japan. But the optimum fresh storage temperature has not been elucidated in these guidelines. For this reason, the storage temperature before cryopreservation varies in countries. For example, in Japan, UCB products is usually kept at 10℃ temporarily and this specification in China is nearly the same which is 4-10℃. On the other hand, in Europe, UCB units must be maintained at 22±4℃ during that period with indispensable solid validation [12-15].

The colony-forming unit (CFU) and $CD34^+$ cell contents have been proved to have association with engraftment potential of UCB units significantly [16-18]. Therefore, by using the stem cell enumeration (SCE) kit and CFU, many investigations have evaluated the impact of different storage temperatures and processing delays on cord blood quality before cryopreservation, and disputed results have published. From them, although the unsuitability of UCB units kept over 30℃ for engraftment has been revealed, depending on the study strategy and research design of different studies, either 4℃ or room temperature (RT; 22±4℃) could be thought most qualified to maintain the UCB potency according to various reports [19-23]. In this paper, we investigated the influence of storage temperature and time prior to further processing on stem cells quality of UCB products by SCE kits.

Materials and methods:

Fresh cord blood collection and selection

CB was collected from the umbilical vein into a 400-ml sterile blood bag containing 35 ml citrate-phosphate-dextrose-adenine (CPD-A) solution as anticoagulant in cooperating hospitals. The use of UCB products for research was allowed by the donor informed consent if the products are not qualified for clinical application. After that UCB products were shipped to Kinki Cord Blood Bank (KCBB) at room temperature with monitoring. According to the KCBB standard operating procedures (SOPs), UCB products which did not only meet the selection criteria (at least total NCs over 12.0×10^8, total viable $CD34^+$ cells over 3.0×10^6), but also collected within 24hours before, were selected for this study.

Fresh cord blood storage and sampling

Total 12 UCB products were analyzed without further deep freezing. The UCB age prior to initiating the experiments was 19.9±6.6 hrs, and the net volume was 78.0±12.4 mL. The experimental setup was consisting of two parts. One was 4°C storage experiment that 6 fresh UCB products (age 23.3±2.2 hrs, net volume 74.1±6.7 mL) were firstly tested before the storage as the baseline when they were just arrived at the KCBB lab on Day1. All the products then were preserved in a refrigerator at 4°C with temperature monitor (MPR-312D; SANYO). Six ml samples were collected to analyze every 24 hours until Day 3. Another part was the experiment by six different temperatures storage. Unlike the protocol of the first part, other 6 fresh UCB products (age 16.5±8.0 hrs, volume 81.9±14.6 mL) were selected and then each of them was divided into six equal-volume aliquots by use of Polyvinyl chloride split bags on Day1. One aliquot was placed in a refrigerator at 4°C (MPR-312D; SANYO), second one was placed at 10°C in another refrigerator (MPR-311PR; SANYO). And third one was placed in an incubator at 15°C (DRL-4BP; DAIDO INDUSTRIES.INC). The fourth and fifth aliquots were kept in two platelet shakers at 20°C and 25°C respectively but without shaking (DRL-3BP; DAIDO INDUSTRIES.INC). The last aliquot was put into an incubator with 30°C setting (IC802; YAMATO SCIENTIFIC CO,

LTD). At set time points (24, 48, and 72 hours after split as Day2, Day3 and Day4 respectively), 2ml samples were taken from each aliquot at six storage conditions and assessed the viability of $CD34^+$ cell s in whole blood.

Cell enumeration and viability assays

A 100 µL sample of UCB was added into BD Trucount tubes using reverse pipetting techniques and stained for 20 min in the dark at room temperature with 20 µL CD45–FITC clone 2D1, CD34–PE clone 8G12 and 20 µL 7-AAD (BD Biosciences). BD Trucount tubes contain an assayed quantity of freeze-dried fluorescent counting beads. The sample was then lysed with 2 mL 1×NH_4Cl lysing buffer (freshly prepared from 10× stock solution) for 10 min in the dark at room temperature. Flow cytometric (FCM) analysis was performed using a flow cytometer (BD FACSCanto Ⅱ, BD Biosciences), and data was acquired and analyzed by BD FACSCanto Version 2.4 software. Fig 1 represents the modified gating strategy developed based on the ISHAGE methods.

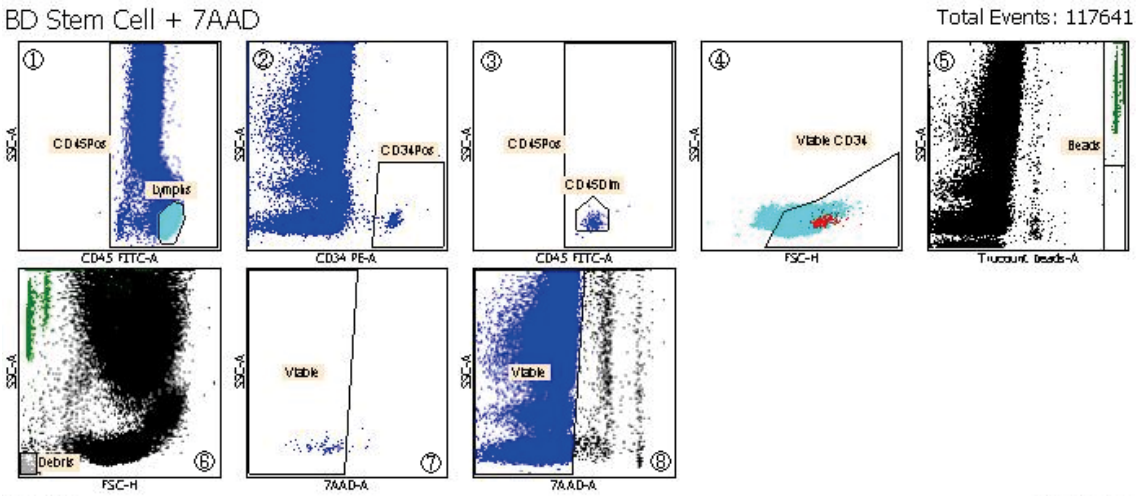

Plot No.	Gate(s)		Plot No.	Gate(s)
①	CD45Pos, Lymphs		⑤	Beads
②	CD34Pos		⑥	Debris
③	CD45Pos, CD45Dim		⑦	Viable
④	Viable CD34		⑧	Viable

Fig .1. The dot plots illustrate the ISHAGE modified gating strategy. Plot 1:CD45- positive lymphocyte gate; plot 2:CD34-postive; plot 3: CD45-positive and CD45-dim gates; plot 4: viable CD34-positive gate; plot 5: bead gate; plot 6: debris gate; plot 7: viable total CD34-positive ; plot 8: 7AAD-negative (viable) cells.

Statistical analysis

Results are presented as mean ± standard deviation (SD), One-way analysis of variance (ANOVA) techniques with post hoc analysis by Dunnett method were used to establish statistical significance between groups and p-values less than 0.05 were considered as showing the statistical significance. All statistical analyses and graphical demonstrations were performed using a GraphPad Prism 6.0c software (GraphPad Software Inc.).

Results:

Impact of storage time on $CD34^+$ cell viabilities in UCB products kept at 4 ℃

To clarify whether the processing delay may affect UCB quality, we selected 6 UCB products (age 23.3±2.2 hrs) to investigate their $CD34^+$ cell viability by FCM over 3 days. As shown in Table 1, cell viabilities were constantly stable at a high level in UCB stored at 4℃ for at least 72 hrs after collection.

n=6	$CD34^+$ cell viability in UCB products (%)		
	Day1	Day2	Day3
4℃	97.66±1.14	97.49±1.06	96.00±1.33

Table 1. The mean $CD34^+$ cell viabilities in whole blood samples kept at 4℃ until Day3 assessed by FCM.

Impact of storage temperature and time on $CD34^+$ cell viabilities in UCB products

The viability of $CD34^+$ cells had been little jeopardized when stored at 4℃, while other temperatures were found not to have the same effect. For elucidating this issue, another 6 CB products (age 16.5±8.0 hrs) were used for FCM analysis during this step to evaluate the cell viabilities of fresh UCB samples stored at 6 different temperatures (4℃, 10℃, 15℃, 20℃, 25℃ and 30℃) every 24 hrs until 72 hrs (Day4) after split from the original products. Temperature- and time-dependent alteration of $CD34^+$ cell viabilities in UCB samples are shown in Fig.2 and Fig.3, respectively. As Fig.2 shows below, compared with 4℃ values in each time interval group, $CD34^+$ cell viabilities show a significant decrease for increasing temperatures since Day3. On Day4, the $CD34^+$ cell viability, however, was significantly higher in samples from UCB products stored at 4℃ (98.25±1.21%) than those stored at 20℃, 25℃ and 30℃ (88.62±5.22, 85.03±4.58 and 53.34±14.41, P=0.0111, 0.0028 and 0.0018, respectively). Only a gradual petty decline was found between 4℃ and 10℃ and 15℃ throughout the storage period. Furthermore, Fig.3 demonstrates a minor decrease in $CD34^+$ viabilities with time past at 4℃, 10℃ and 15℃ groups during the whole storage period, compared with Day2 values in each temperature groups. In contrast, $CD34^+$ cell viability of other three temperature groups were declined rapidly from Day3, especially at 30℃. And significances were also found between Day2 (97.84±1.92%) and Day4 (88.62±5.22%, P=0.0138) at 20℃, and between Day2 (25℃:97.54±1.75%; 30℃:94.78±2.42%) and Day3 (25℃: 91.11±2.48%, P=0.0027; 30℃: 85.00±6.86%, P=0.0286) and Day4 (25℃: 85.03±4.58%, P=0.0028; 30℃: 53.34±14.41%, P=0.0010) at 25℃ and 30℃.

In summary, the highest viabilities were obtained in samples preserved at refrigerated temperatures (4℃, 10℃ and 15℃) , suggesting the suitable condition to maintain the potency of hematopoietic stem cells in UCB products.

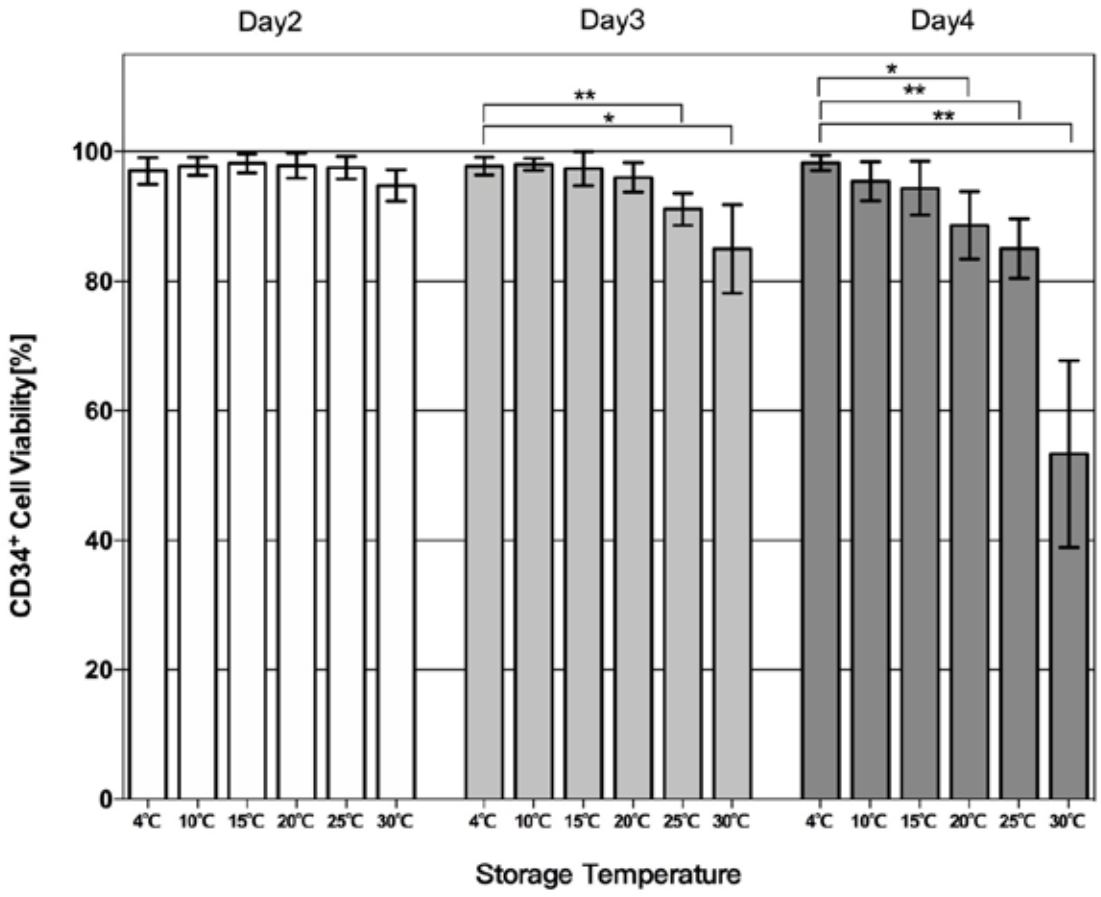

Fig.2. Temperature-dependent alteration in $CD34^+$ cell viabilities of CB samples before cryopreservation. Whiskers represent the SD. Only significant *P* values are shown.

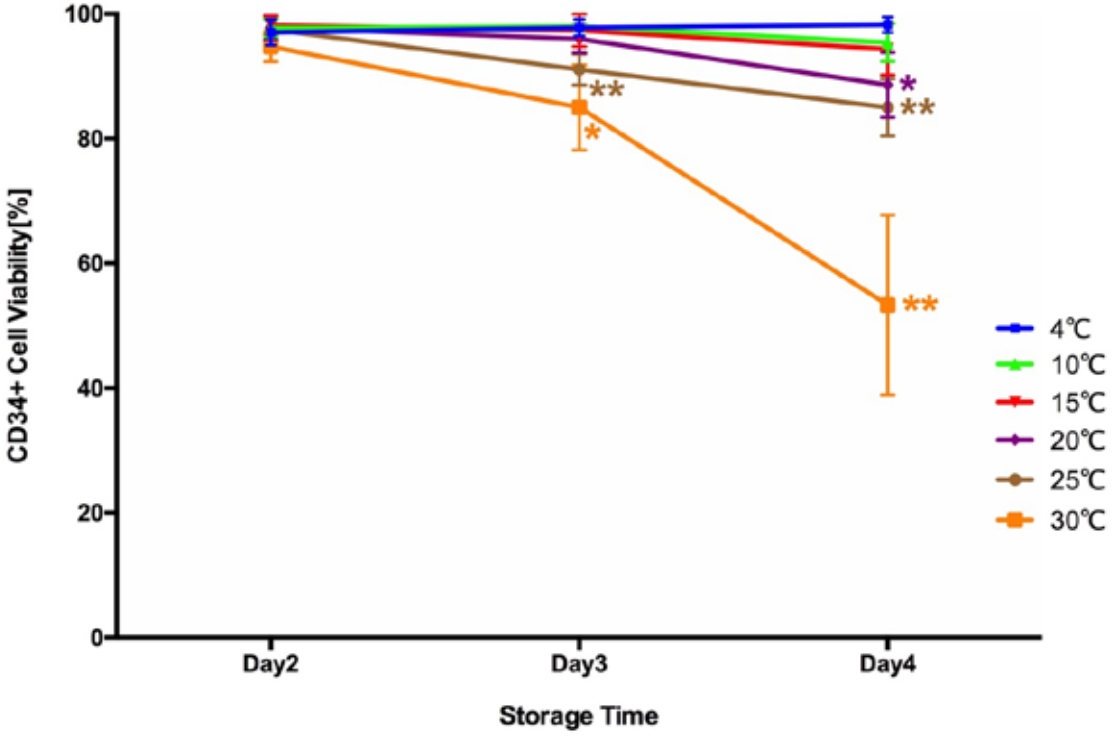

Fig.3. Time-dependent alteration in $CD34^+$ cell viabilities of CB samples before cryopreservation. Whiskers represent the SD. Only significant *P* values are shown.

Discussion:

As one crucial factor for UCB transplantation to achieve the engraftment of hematopoietic stem cells (HSCs) and progenitor cells in recipients, the physiological potency of stem cells must be maintained persistently as much as possible before clinical application. Although the fact that storage temperature and time delay before freezing could affect such potency such as the viability of $CD34^+$ cells has been proven in various previous studies, the exact suitable temperature and time for UCB temporary storage has not been determined. In attempt to understand the temperature- and time-dependent alteration of stem cell quality in CB samples before cryopreservation and to find out the best condition to preserve UCB products, this study investigated the $CD34^+$ cell viability in samples from UCB products via SCE kit by FCM.

As we mentioned before, UCB products are usually preserved at 4-10℃ for less than 36 hrs before freezing in Japan and China. We firstly evaluate the validity of 4℃ for maintaining the UCB quality in 400 mL-bags with CPD-A solution. According the data shown in Table 1, $CD34^+$ cell viability consistently stabilized at over 96% for at least 72 hrs after collection. To exclude the influence of anticoagulant solution, we also do the same tests with a few UCB products in 200 mL-bags with CPD solution. No significant difference was found in the $CD34^+$ cell viability (data not shown). Then, considering that room temperature (RT) is widely used for shipping and temporary storage in Europe, we divided each UCB products in 400-mL bags into 6 aliquots and treated them with same condition besides temperature. As shown in Fig.2 and.3, even the small bag at 4℃ can also keep the $CD34^+$ cell viability for up to 72hrs after split, which verified the results from 400mL-bags. The similar trend was also seen in 10℃ and 15℃ groups with a slight (not significant) reduction from Day3. Contrary to the Europe practice, the temperatures over 15℃ (especially 30℃) were proven to be unsuitable for retaining the potency of HSC in UCB products. It is interesting that 30℃, which is close to the physiological body temperature 37℃, was worst for HSC survival, because the $CD34^+$ cell viability declined shapely at 30℃ compared with other five groups.

This result could be explained by the fact that HSC in UCB are maintained in low oxygen and flow condition in vivo [24]. In stem cell physiology, a “hypoxic niche” hypothesis is now widely accepted to describe the microenvironment of HSCs in bone marrows (BM). Unlike peripheral blood cells, HSCs always likely localize in a distinct niche in bone marrow close to endosteum with low oxygen below 21% and HSCs can communicate there with the supportive cells by many ways such like cell-bound and cell-cell interactions and so on [25]. This hypoxic environment also has been proven to be helpful to maintain the self-renewal ability, quiescence and engraftment potential of HSCs from BM as well as UCB and to protect them from detrimental accumulation of reactive oxygen species (ROS) derived from mitochondrial respiration by using the glycolysis as main energy source [26-27]. But unlike the hypoxic “sweet home” in niches, UCB HSCs storage ex vivo are surrounded by numerous erythrocytes instead of stromal cells. This unfavorable condition may severely harm the potency of HSCs. During red cells storage, glycolysis is inhibited by lactate accumulation and ATP decline in medium and compromises the red cell membrane integrity. In addition, elevated levels of free hemoglobin and iron in supernatant would contribute to oxidative stress with incredibly high ROS level. Moreover, at 25℃ the metabolic rate of red cells is ten times higher than at 4℃ [28]. We think these findings could explain the inacceptable viability changes in $CD34^+$ HSCs in UCB products at high temperatures during 72 hrs storage periods, because HSC function could be better preserved with partially arrested and less susceptible metabolism at 4-15℃, but additional tests are needed to substantiate our deductions.

Our results are in great agreement with the findings of some studies that HSCs in UCB products at 4℃ are demonstrating persistently higher $CD34^+$ cell viability than cells from 24℃ and 37℃ [9, 19-20]. But it is not quite

accordant with other studies which concluded the RT was also suitable for preserving UCB products as well as 4℃ [21-23]. We propose the reason may be owing to the containers we used for the storage during the entire study. We did not choose tubes but PVC bags with same material of 400-ml blood bag, which stimulated the actual procedure with the feasibility for air exchange between cells and atmosphere. This air exchange may bring extra oxidative stress to stem cells.

In conclusion, our data challenged current UCB practice by using RT for shipping and storage and suggested that UCB products are better preserved at low temperature such like 4-15℃ before further processing and cryopreservation to retain the potency of HSCs, and that prefreezing delay over 3 days after collection should be avoided as much as possible.

References:

1. Grosso DA, Hess RC, Weiss MA. Immunotherapy in acute myeloid leukemia. Cancer. 2015 Aug 15; 121(16):2689-704.
2. Soysal T, Salihoğlu A, Esatoğlu SN, et al. Bone marrow transplantation for Behçet's disease: a case report and systematic review of the literature. Rheumatology (Oxford). 2014 Jun; 53(6):1136-41.
3. Wu S, Xie G, Wu J, et al. Influence of maternal, infant, and collection characteristics on high-quality cord blood units in Guangzhou Cord Blood Bank. Transfusion. 2015 Sep; 55(9):2158-67.
4. Kindwall-Keller T. Peripheral stem cell collection: from leukocyte growth factor to removal of catheter. J Clin Apher. 2014 Aug; 29(4):199-205.
5. Gluckman E, Broxmeyer HA, Auerbach AD, et al. Hematopoietic reconstitution in a patient with Fanconi's anemia by means of umbilical-cord blood from an HLA-identical sibling.N Engl J Med 1989;321:1174-8.
6. Ballen KK, Gluckman E, Broxmeyer HE. Umbilical cord blood transplantation: the first 25 years and beyond. Blood 2013; 122:491-8.
7. Lee JW, Kang HJ, Kim EK, et al. Successful salvage unrelated umbilical cord blood transplantation with two units after engraftment failure with single unit in severe aplastic anemia. J Korean Med Sci. 2009 Aug; 24(4):744-6.
8. Kindwall-Keller TL, Hegerfeldt Y, Meyerson HJ, et al. Prospective study of one- vs two-unit umbilical cord blood transplantation following reduced intensity conditioning in adults with hematological malignancies. Bone Marrow Transplant. 2012 Jul; 47(7):924-33.
9. Solomon M, Wofford J, Johnson C, et al. Factors influencing cord blood viability assessment before cryopreservation. Transfusion. 2010 Apr; 50(4):820-30.
10. Moldenhauer A, Wolf J, Habermann G, et al. Optimum storage conditions for cord blood-derived hematopoietic progenitor cells prior to isolation. Bone Marrow Transplant. 2007 Nov; 40(9):837-42.
11. FACT. Sixth edition NetCord-FACT international standards for cord blood collection, banking, and release for administration. 2016. Available from: http://www.factwebsite.org. [Accessed 3 October 2017].
12. Liu J, He J, Chen S, et al. Cord Blood Banking and Transplantation in China: A Ten Years Experience of a Single Public Bank. Transfus Med Hemother. 2012 Feb; 39(1):23-27.
13. Wu S, Xie G, Wu J, et al. Influence of maternal, infant, and collection characteristics on high-quality cord blood units in Guangzhou Cord Blood Bank. Transfusion. 2015 Sep; 55(9):2158-67.
14. German Medical Association. Directive on the manufacture and use of hematopoietic stem cell preparations. Dtsch Arztebl 2014, 111: [in German]. doi: 10.3238 / arztebl.2014.rl_haematop_sz01.
15. Guttridge MG, Soh TG, Belfield H, et al. Storage time affects umbilical cord blood viability. Transfusion. 2014 May; 54(5):1278-85.

16. Wagner JE, Barker JN, DeFor TE, et al. Transplantation of unrelated donor umbilical cord blood in 102 patients with malignant and nonmalignant diseases: influence of CD34 cell dose and HLA disparity on treatment-related mortality and survival. Blood 2002; 100:1611–18.
17. Page KM, Zhang L, Mendizabal A, et al. Total colony-forming units are a strong, independent predictor of neutrophil and platelet engraftment after unrelated umbilical cord blood transplantation: a single-center analysis of 435 cord blood transplants. Biol Blood MarrowTransplant 2011; 17:1362–74.
18. Rodrigues CA, Sanz G, Brunstein CG, et al. Analysis of risk factors for outcomes after unrelated cord blood transplantation in adults with lymphoid malignancies: a study by the Eurocord-Netcord and LymphomaWorking Party of the European Group for Blood and MarrowTransplantation. J Clin Oncol 2009; 27:256–63.
19. Louis I, Wagner E, Dieng MM, et al. Impact of storage temperature and processing delays on cord blood quality: discrepancy between functional in vitro and in vivo assays. Transfusion. 2012 Nov; 52(11):2401-5.
20. Fry LJ, Giner SQ, Gomez SG, et al. Avoiding room temperature storage and delayed cryopreservation provide better postthaw potency in hematopoietic progenitor cell grafts. Transfusion. 2013 Aug; 53(8):1834-42.
21. Radke TF, Barbosa D, Duggleby RC, et al. The Assessment of Parameters Affecting the Quality of Cord Blood by the Appliance of the Annexin V Staining Method and Correlation with CFU Assays. Stem Cells Int. 2013; 2013:823912.
22. Pereira-Cunha FG, Duarte AS, Reis-Alves SC, et al. Umbilical cord blood CD34(+) stem cells and other mononuclear cell subtypes processed up to 96 h from collection and stored at room temperature maintain a satisfactory functionality for cell therapy. Vox Sang. 2015 Jan; 108(1):72-81.
23. Schwandt S, Liedtke S, Kogler G. The influence of temperature treatment before cryopreservation on the viability and potency of cryopreserved and thawed CD34+ and CD45+ cord blood cells. Cytotherapy. 2017 Aug; 19(8):962-977.
24. Broxmeyer HE. Proliferative, self-renewal, and survival characteristics of cord blood hematopoietic stem and progenitor cells. In: Broxmeyer HE, editor. Cord blood: biology, immunology, banking, and clinical transplantation. Bethesda (MD): AABB Press; 2004. p. 1-21.
25. Jež M, Rožman P, Ivanović Z, et al. Concise review: the role of oxygen in hematopoietic stem cell physiology. J Cell Physiol. 2015 Sep;230(9):1999-2005.
26. Eliasson P, Jönsson JI. The hematopoietic stem cell niche: low in oxygen but a nice place to be. J Cell Physiol. 2010 Jan;222(1):17-22.
27. Ivanovic Z, Hermitte F, Brunet de la Grange P, et al. Simultaneous Maintenance of Human Cord Blood SCID-Repopulating Cells and Expansion of Committed Progenitors at Low O2 Concentration (3%). Stem Cells. 2004;22(5):716-24.
28. Orlov D, Karkouti K. The pathophysiology and consequences of red blood cell storage. Anaesthesia. 2015 Jan;70 Suppl 1:29-37, e9-12.

作成日：2018 年 2 月 22 日

Direct reprogramming of patients' fibroblasts to neurons to understand neurodegenerative diseases
患者の線維芽細胞をニューロンに直接再プログラムした神経変性疾患の理解

研究者氏名　金　銀実（第 39 期笹川医学研究者）
中国所属機関　吉林大学中日聯誼病院
日本研究機関　大阪大学附属病院
指導責任者　望月　秀樹　教授
共同研究者　長野　清一 准教授，池中　建介 助教

Key Words:
Neurodegenerative diseases, reprogramming, Direct conversion, Fibroblasts, Neuronal intranuclear inclusion disease

Abstract

Transplantation of exogenous neurons is a promising approach for treating neurodegenerative diseases. However, a major stumbling block has been the lack of a reliable source of donor neurons. Recent progress in tissue engineering research led to the generation of different types of cells from a handful of skin tissue. Lineage reprogramming is a nascent field, which holds great potential to expand its use in regenerative medicine and disease modeling. Reprogramming technology offers the ability to untangle the answer ability contributing risk factors for neurodegenerative diseases. In this study, we show human fibroblasts can be reprogrammed into neurons by reducing the expression of a single RNA binding protein PTB. Neuronal intranuclear inclusion disease (NIID) is a rare neurodegenerative disorder characterized pathologically by presence of eosinophilic intranuclear inclusions in neuronal and glial cells. Here, we show the direct conversion of a patient's fibroblasts into neurons using the same method, to explore whether the converted neurons have the original pathological features.

Introduction

A major barrier to research neurodegenerative diseases is inaccessibility to live diseased tissue for study. One solution is to derive induced pluripotent stem cells (iPSc) from patients and differentiate them into neurons. In 2006, Takahashi et al. directly reprogrammed somatic cells into iPSc, thereby opening a novel approach to disease modeling and drug discovery [1,2]. A new era in *in vitro* modeling of neurodegenerative diseases recently began when iPSc technology was established. iPSc from patients of neurodegenerative diseases with no universally satisfactory treatment strategy are currently available. This so-called reprogramming technology has provided a unique and unprecedented opportunity to model human conditions with disease-relevant cell types. However, a major hurdle for this approach is carcinogenic risk of iPSc [3,4]. The other important aspect with reprogramming to be concerned with is the genetic integrity of the established iPSC lines. As human iPSC generation is usually a clonal process from an adult cell type, there are many opportunities mutations or chromosomal aberrations to occur de novo, or be expanded from the somatic cell starting material. Whole genome sequencing of a large collection of iPSc lines demonstrated that an average of six coding mutations occur during reprogramming [5]. Large chromosomal abnormalities are also a fairly common during reprogramming and subsequent expansion of cells, with over 20% of published iPSc lines harboring a karyotypic defect[6]. An alternative strategy to obtain neurons that may lower carcinogenic risk is the direct conversion approach where differentiated cells. Recently, it has been shown that terminally differentiated somatic cells can be directly reprogrammed to become functional neuronal cells, which not only demonstrated a much greater cell rate plasticity of terminally differentiated cells than previously thought, but also expanded the cell sources accessible for basic and translational neural

biology studies [7,8]. Cells generated via direct conversion do not pass through a pluripotent state, may serve as an interesting alternative to iPSc for generating patient and disease specific neurons, without the need for transgenic manipulation to express a disease-associated gene of interest. Yuanchao Xue et al. [9] reported that repression of a single RNA binding protein PTB, which occurs during normal brain development via the action of miR-124, is sufficient to induce trans-differentiation of fibroblasts into functional neurons. They observed conversion of diverse cell types into neuronal-like cells by PTB depletion, including HeLa cells, human embryonic carcinoma stem cells, mouse neural progenitor cells, human retinal epithelial cells, and primary mouse embryo fibroblasts. Previous analysis by Yuta Nakano et al [10]. suggested that inclusions in NIID originated from nuclear bodies, an important nuclear domain related to the uniquitin-p62 mediated protein degradation system.

Here, we show the direct conversion of fibroblasts into neurons using the same methods, to investigate the effects of different lentiviral titers on neuronal differentiation, and analyze neurons derived from skin samples of NIID and control case immunohistochemically.

Cell culture

All experiments on human dermal tissues followed the guideline approved by the ethics committee of Osaka University Graduate School of Medicine. The skin tissues were obtained from Osaka University Graduate School of Neurology. They were maintained at 4℃ in Dulbecco's Modified Eagle's Medium (sigma), infiltrated with 75% ethanol for 2 minutes and then washed with phosphate buffered saline (PBS) containing 1% penicillin streptomycin five or six times until clean. After resection of blood vessels and subcutaneous adipose tissue, skin tissue was cut into approximately 1 mm x 1 mm tissue pieces, gently affixed to a 6cm dish and dried for 15 minutes. After which 2 ml of culture medium was added, subsequently 2 ml of culture medium was added after 2 days, and then medium was changed every 3 days until the cells became 50% confluent of the entire plate。Control human fibroblast SF8546 cells (51 year) were purchased from the RIKEN (Japan), and obtained fibroblasts were cultured in Dulbecco's Modified Eagle's Medium (sigma) containing 10% fetal bovine serum, 1% penicilin and streptomycin.

Plasmid cloning and lentivirus production

The sequence of PTBP1 shRNA obtained from Sigma Aldrich (Japan) was sub cloned into the pLKO.1 vector, which holds a puromycin-resistant gene for selection of transduced cells, by Dr Nagano of Department of Neurology, Osaka University Graduate School of Medicine (Japan). Lentiviral packaging plasmids △8.9 and VSV-G, were from Dr Nagano of Department of Neurology, Osaka University Graduate School of Medicine (Japan). To produce lentiviral vectors, PTBP1 shRNA plasmid, △8.9 plasmid and VSV-G plasmid were co-transduced into HEK 293FT cells, and supernatants were collected 24h and 48h after transfection. The supernatants, which contain active recombinant lentiviral vectors, were then used for subsequent gene transduction experiments.

RT-qPCR

Cells were collected in RNeasy and total RNAs were extracted according to the manufacturer's manual. Total RNAs were reverse transcribed to cDNAs using SuperScirpt III (Thermo Fisher). qPCR primers were purchased from Sigma, and qPCR was carried out using the SYBR green I Master mix in the ABI 7400. GAPDH was used as an endogenous control. Gene expressions were normalized to internal control genes and were compared to the reference control sample using the △△ct method.

Immunofluorescence staining

Cells were grown in 24-well plates, washed twice with PBS and fixed with 4% paraformaldehyde for 30min. They were permeabilized with 0.5% Triton X-100 in PBS for 5min at room temperature, blocked in 3% BSA in PBS for 30min

at room temperature and then incubated with primary antibody in blocking buffer overnight at 4℃, with secondary antibody in blocking buffer for 1h at room temperature. The following primary antibodies with indicated dilution were used; mouse anti-βIII-tubulin (Tuj1; Covance, 1:1000), anti-ubiquitin (Sigma,1:1000), anti-P62 (1:500). After staining with secondary antibodies, cells were washed three times with each for 5min, stained with DAPI in PBS, and examined under BZ-X700 and FV-1000D fluorescence microscopies.

Calculation of transduction efficiency

To calculate the efficiency of neuronal conversion, the average number of Tuj1-positive cells present in 10 randomly selected x10 virtual fields was counted. The percentage of neurons present was calculated against the total number of cells which was determined as DAPI-positive cells.

Statistical analyses

All statistical analyses were done with the software SPSS 22.0. The data were expressed as mean ± s.e.m. Unpaired, two-tailed Student's *t*-test was performed to evaluate whether two groups were significantly different from each other. No sample was excluded in our analysis.

Results

Fibroblasts direct conversion to neuronal-like cells

Human skin fibroblast SF8546 cells are widely used in many reprogramming experiments [11]. To investigate whether direct conversion into neurons from human fibroblasts is possible, we attempted to use PTBP1 shRNA to knock down PTB stably. PTBP1 shRNA sequence was cloned into the lentiviral vector pLKO.1, and the vector was then packaged into replication-deficient lentiviruses following established procedures. Knockdown of PTBP1 mRNA was verified with quantitative RT-PCR (qRT-PCR) (Fig.1B), which was consistent with mean knockdown level published on Sigma's website. The cells were then used for conversion by delivering lentiviral vectors coding PTBP1 shRNA, the factor previously identified as efficiently converting primary mouse embryo fibroblasts (MEFs) to neurons [9]**.** They were cultured in neural induction media with the indicated protocol (Fig.1A), After the transduction with the conversion factor, the cells were subsequently grown in neural basal medium [12]. After the selection of transduced cells with puromycin, the cells gradually became to have a compact cell body with one or many long processes, reminiscent of neurons (Fig.1C). When the cells were immunostained at day 15 with the antibody against βIII-tubulin, the protein could be detected, indicating the cells have a neuronal property (Fig.1D). In parallel, control cultures were transduced with lentiviral vectors that contain non-targeted shRNA sequence, by which neurons were never observed (Fig.1E). We found that high titer of lentivirus significantly increased the generation of $Tuj1^{+}$cells (17.93 ± 4.55% of the whole cells), over the level by low titer lentivirus (12.21 ± 4.20% of the whole cells; $p<0.05$, unpaired two-tailed Student's t-test; Fig.1F), and significantly increased the neurite length per cell (240.37 ± 83.19um), over the level by low titer lentivirus (193.63 ± 75.67um; $p<0.005$, unpaired two-tailed Student's t-test; Fig.1F). On the other hand, the number of neurites per cell was significantly reduced ($p<0.005$, unpaired two-tailed Student's t-test; MOI 20 versus MOI 40, Fig.1F). It seems that an increase in virus titer promotes neuronal development and maturation, within the limits of toxicity.

Primary cell lines expanded from adult human skin

In order to test whether fibroblasts could be expanded from adult human skin, we obtained adult human skin tissues from patients at upper arms near shoulders, and applied the same culture protocol as for control human fibroblast lines. One of the skin tissues was derived from a NIID patient. After resection of blood vessels and subcutaneous adipose tissues, skin tissues were cut into approximately 1mm x 1mm tissue pieces (Fig.2A). Keratinocytes typically emerged around 4-6 days after plating (Fig. 2B), followed by a rapid expansion, and fibroblasts emerged around 10-14 days after plating

（Fig.2B）. There were also some fibroblasts that appeared directly from the skin in about 1-2 weeks (Fig.2C). This shows that fibroblasts were successfully obtained from human skin tissue.

Intranuclear structures in NIID case

Successful transformation of the patient's fibroblasts into neurons could be detected by the appearance of neuron-like neurites and the positive staining with Tuj1 antibody (Fig.2D). Despite detailed examination, activated nuclear bodies were not found in the NIID case.

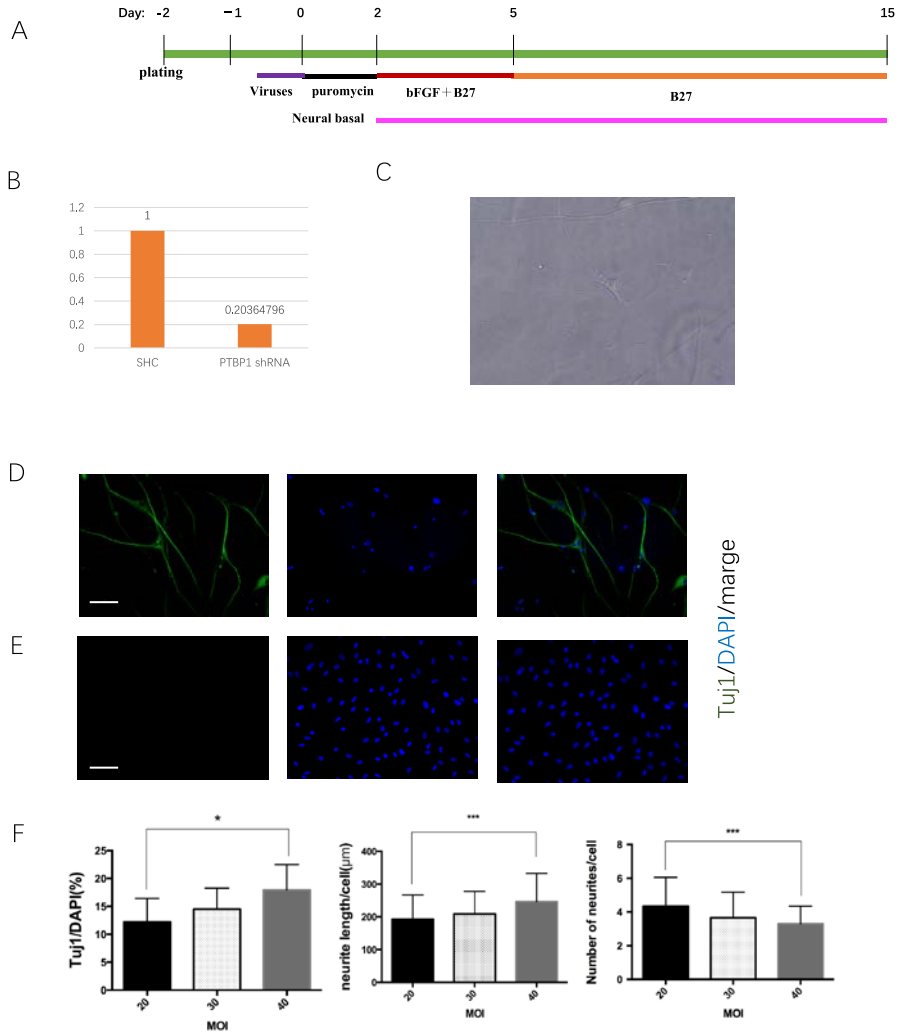

Figure 1. Differentiation of fibroblasts into neuronal-like cells in response to PTBP1 knockdown

(A) Protocol for the differentiation of fibroblasts. (B) Knockdown of PTBP1 mRNA in fibroblasts by a targeted shRNA. SHC: non-targeted control shRNA. (C) Morphology of differentiated cells with one or many long processes, reminiscent of neurons. (D, E) Induction of neuronal morphology and expression of the neuronal marker Tuj1 (green) in fibroblasts in response to depletion of PTB (D), but not in control (E). Nuclei are stained by DAPI (blue). Scale bar: 20um. (F) Reprogramming efficiency by the percentage of Tuj1 positive cells (left), neurite length per cell (middle) and the number of neurites per cell (right). *p<0.05 and ***p<0.005, unpaired, two tailed Student's t-test; n=3 wells from 3 independent experiments for each condition.

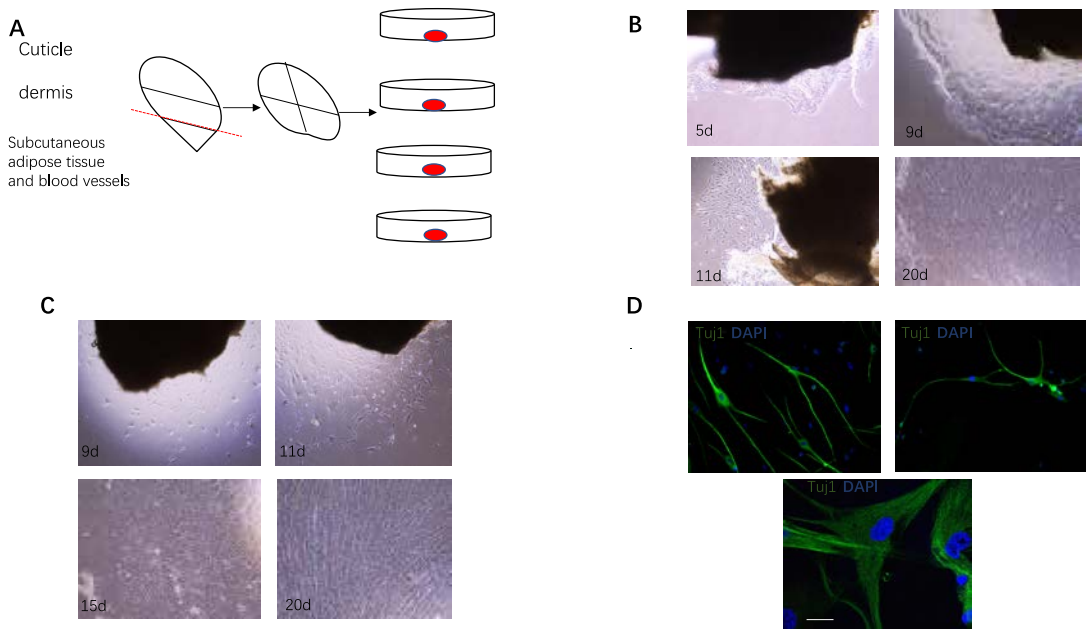

Figure 2. Establishment of human fibroblast cultures

(A) Skin tissues from patients were dissociated and plated under standard fibroblast conditions. After the fibroblasts were expanded and passaged once, they were frozen-stocked and subsequently used for experiments. (B, C) Keratinocytes (B) and fibroblasts (B, C) were cultured from skin tissues. (D) Fibroblast-derived neurons from a NIDD patient (upper left) and a control (upper right) were both negative for P62 and ubiquitin immunostaining. Scale bar: 20um.

Discussion

In this study, we used adult human skin tissues to generate fibroblast lines, and demonstrated that the PTBP1 knockdown was sufficient to reprogram the cells directly into neurons, which exhibited typical neuronal morphology and expressed neural marker. The expansion and culture of fibroblasts are fairly easy and efficient, marking it a reliable donor cell source for subsequent reprogramming. Direct reprogramming, or trans-differentiation, is the process of converting one differentiated cell type to another, without passing through a pluripotent or progenitor cell state. This process was described several decades before the derivation of iPS cells. In 1983, two studies demonstrated trans-differentiation by cellular fusion [13, 14]. In 1987 came the first demonstration that a single transcription factor, MYOD1, was capable of reprogramming mouse fibroblasts into myoblasts [15]. Trans-differentiation into neurons has been a recent development, first reported in 2010[16].

REST (also known as neuron-restrictive silencer factor, NRSF1) is a zinc finger transcription factor that was originally identified as a repressor of the SCG10[17], and sodium type II channel [18] genes. Data from in vitro experiments combined with the observed widespread distribution of REST in non-neuronal tissue led to the suggestion that the role of REST was to silence expression of specific neuronal genes in non-neuronal tissue [17,18]. Yuanchao Xue et al. [9], discovered a PTB-regulated microRNA program responsible for dismantling of multiple components of REST, and they provide further evidence that knockdown of REST itself is sufficient to trigger trans-differentiation of MEFs into neuronal-like cells. The REST complex is well known for its role in suppressing many neuronal gens, including miR-124, in non-neuronal cells, while miR-124 and other neuronal specific microRNAs target various REST components.

Neuronal intranuclear inclusion disease (NIID) is a neurodegenerative disorder characterized pathologically by the presence of eosinophilic nuclear inclusions (NIs) in neurons and glial cells. NIs are not restricted to the central nervous

system, but are also distributed in peripheral nerves and visceral organs. NIID has been considered to be a heterogeneous disease entity because of its highly variable clinical features. Recently, skin biopsies have been reported to be useful for the antemortem diagnosis of NIID, by which nuclear inclusions have been observed in adipocytes, fibroblasts and sweat gland cells in cutaneous tissues [19]. NIs in the biopsy specimens were immunopositive for ubiquitin and p62, as in the central nervous system [20, 21]. p62 is an adaptor molecule for the selective autophagic degradation of ubiquitinated proteins, and the colocalization of p62 and ubiquitin in cytoplasmic aggregates has been reported in various neurodegenerative disorders [22]. p62 is generally considered to be a cytosolic protein.

In this study, we studied neurons derived from human dermal fibroblasts and found no aggregates in the nucleus. We consider the following reasons: 1. After the transformation of fibroblasts into neurons, the original property to form aggregates disappeared. 2. Converting fibroblasts into neurons may have enhanced degradation of aggregates within the nucleus. 3. If stress is applied during the conversion of fibroblasts to neurons, it is possible to form aggregates in the nuclei of neurons.

Our results have several implications for the potential use of directly-differentiated neurons for neurodegenerative disease modeling, and the generation of neurons from abundant somatic cells such as fibroblasts. In conclusion, the field of reprogramming offers great promise for understanding and treating neurodegenerative diseases. Reprogramming offers a new tool where basic research into the mechanism of neurodegenerative pathology can be uncovered, where high throughput drug screening can be performed on the relevant cell type, as well as providing a new source of donor material for cell-based therapies. This is still a rapidly developing field, and given the advantages that direct reprogramming offers both for disease modelling and therapeutics, it will be interesting to see future developments in this arena. Future studies should aim to increase the efficiency of neuronal formation and to evaluate the converted neurons' ability to survive long term.

References

[1] Takahashi K, Tanabe K, Ohnuki m, Narita M, Ichisaka T, et al (2007). Induction of pluripotent stem cells from adult human fibroblasts by defined factors. Cell 131, 861-872

[2] Takahashi K, Yamanaka S, et al. (2006) Induction of pluripotent stem cells from mouse embryonic and adult fibroblasts cultures by defined factors. Cell 126, 663-676

[3] Nakagawa M, Koyanagi M, Tanabe K, et al. (2008) Generation of induced pluripotent stem cells without Myc from mouse and human fibroblasts. Nature Biotechnology 26, 101-106

[4] Miura K, Okada Y, Aoi T, et al. (2009) Variation in the safety of induced pluripotent stem cell lines. Nature Biotechnology biotechnol 27, 743-745

[5] Gore A, Li Z, Fung H-L, young JE, Agarwal S, Antosiewica-Bourget J et al. (2011) Somatic coding mutations in human induced pluripotent stem cells. Nature 471, 63-67

[6] Mayshar Y, Ben-David U, Lavon N, Biancotti J-C, Yakir B,Clark AT et al(2010) Identification and classification of chromosomal aberrations in human induced pluripotent stem cells. cell stem cell 7, 51-531

[7] Pang, Z., Yang, N.,Vierbuchen, T., et al(2011).Induction of human neuronal cells by defined transcription factors. Nature 476, 220-223

[8] Vierbuchen,T. ,Ostermeier A.,Pang,A.P.,Kokubu,Y.,Sudbof,T.C.,Werning,M., et al.(2010) Direct conversion of fibroblasts to functional neurons by defined factors, Nature 463, 1035-1041

[9] Yuanchao Xue, Kunfu Ouyang, Jie Huang, Yu Zhou et al (2013). Direct conversion of fibroblasts to neurons by reprogramming PTB-regulated microRNA circuits 17, 82-96

[10] Yuta Nakano, Junko Takahashi-Fujigasaki, Renpei Sengoku et al. (2017) PML nuclear bodies are altered in adult-onset neuronal intranuclear hyaline inclusion disease. Journal of Neuropathology Experimental Neurology 76, 585-594

[11] Park, I. H. et al. (2008) Reprogramming of human somatic cells to pluripotency with defined factors. Nature 451, 141-146

[12] Werning M, et al. (2002) Tau EGFP embryonic stem cells: An efficient tool for neuronal lineage selection and transplantation. J Neurosci Res 69, 918-924

[13] Blau, H. M., Chiu, C, P., Webster, C. (1983). Cytoplasmic activation of human nuclear genes in stable heterocaryons. Cell, 32, 1171-1180

[14] Takagi, N., Yoshida, M. A., Sugawara, O., & Sasaki, M. (1983). Reversal of X-inactivation in female mouse somatic cells hybridized with murine teratocarcinoma stem cells in vitro. Cell, 34, 1053-1062

[15] Davis, R.L., Weintraub, H., Lassar, A.B. (1987). Expression of a single transfected cDNA converts fibroblasts to myoblasts. Cell, 51, 987-1000

[16] Vierbuchen, T., Ostermeier, A., Pang, Z.P., Kokubu, Y., Sudbof, T. C., et al. (2010). Direct conversion of fibroblasts to functional neurons by defined factors. Nature, 463,1035-1041

[17] Schoenherr, C. Anderson, D. J. (1995). The neuron-restrictive silencer factor(NRSE): a coordinate repressor of multiple neuron-specific genes. Science, 267, 1360-1363

[18] Chong, J. A., Tapia-Ramirez, I., Kim, S., Toledo-Aral, J. J., et al. (1995). REST: a mammalian silencer protein that restricts sodium channel gene expression to neuros. Cell, 80, 949-957

[19] Sone J, Tanaka F, Koike H, et al. (2011). Skin biopsy is useful for the ante mortem diagnosis of neuronal intranuclear inclusion disease. Neurology, 76 ,1372-1376

[20] Sone J, Kitagawa N, Sugawara E, et al. (2014). Neuronal intranuclear inclusion disease cases with leukoencephalopathy diagnosed via skin biopsy. J Neurol Neurosurg Psychiatry, 85,354-356

[21] Mori F, Miki Y, Tanji K, et al. (2011). Incipient intranuclear inclusion body dis- ease in a 78-year-old woman. Neuropathology, 31,188-193

[22] Kuusisto E, Salminen A, Alafuzoff I.,et al .(2011). Ubiquitin-binding protein p62 is present in neuronal and glial inclusions in human tauopathies and synucleinopathies. Neuroreport, 12, 2085-2090

作成日：2018 年 3 月 5 日

Topographic distribution influences the prognostic impact of CD68 and CD204 positive macrophages in non-small cell lung cancer
非小細胞癌浸潤マクロファージの臨床病理学意義；浸潤部位別の検討

研 究 者 氏 名　　李　卓（第 39 期笹川医学研究者）
中 国 所 属 機 関　　西安医学院第一附属医院検査科
日 本 研 究 機 関　　秋田大学医学部器官病態学講座
指 導 責 任 者　　後藤　明輝 教授

Abstract:

Purpose: Tumor-associated macrophages(TAMs) are believed to influence tumor progression and the prognosis of patients. The purpose of this study was to clarify the correlation between TAMs density or location and the clinicopathological features of non-small-cell lung cancer(NSCLC), as well as explore the prognostic impact of TAMs in NSCLC.

Methods: CD68 and CD204 positive macrophages were detected in tumor cell nest, tumor stroma and alveolar air space in 297 patients with NSCLC using immunochemistry. The clinicopathological and genetic factors surveyed were the disease-free survival, age, gender, smoking status, histological type, disease stage, histological grade, pleural invasion, lymph node metastasis, EGFR gene mutations and ALK rearrangements.

Results: The number of $CD68^+$ macrophages was significantly more than $CD204^+$ macrophages in each location, and they were strongly correlated (P<0.0001 each). Factors such as male gender, being a smoker, advanced disease stage and histological grade, positive pleural invasion and node status and wild-type EGFR gene were significantly correlated with a higher density of $CD68^+/CD204^+$ TAMs in tumor stroma (P<0.05 each). While the age of patients or ALK rearrangement status in NSCLC was not correlated with $CD68^+/CD204^+$ TAMs (P>0.05 each). In tumor cell nest, a higher number of $CD68^+/CD204^+$ TAMs significantly correlated with smokers and EGFR gene mutations (P<0.05, respectively). Moreover, both of univariate and multivariate analyses revealed that a high number of $CD68^+/CD204^+$ TAMs in tumor stroma, but not in tumor cell nest or alveolar air space, was a significant prognostic factor for disease-free survival time of NSCLC (P<0.05, respectively). In adenocarcinoma, the lower density of $CD68^+/CD204^+$ TAMs in tumor stroma and the higher density of $CD68^+/CD204^+$ TAMs in tumor cell nest were observed compared with non-adenocarcinomas (P<0.05, respectively). Furthermore, the survival analysis showed that a higher $CD204^+$ TAMs in tumor stroma was an independent worse prognostic predictor for adenocarcinoma.

Conclusion: This clinicopathological study clarified the relationship between prognosis and TAMs location in NSCLC, and confirmed the worse prognostic value of higher $CD68^+/CD204^+$ stromal TAMs in NSCLC.

Key Words:

Tumor-associated macrophages (TAMs), CD68, CD204, non-small cell lung cancer, prognosis

Introduction:

Macrophage in tumors, generally known as tumor-associated macrophage (TAM), is one of key components of the cancer microenvironment, which influences tumor growth and progression. The novel concept of macrophages classified them into M1 macrophages, which act in a tumor-inhibiting manner, and M2 macrophages, which act in a tumor-promoting manner [1]. TAMs, especially M2-TAMs, are reportedly linked to poor prognosis in several cancers, such as breast cancer, pancreatic cancer, renal cell carcinoma, endometrial cancer, epithelial ovarian cancers and esophageal cancer [2]. For the immunohistochemical evaluation of TAMs, CD68 (a pan-macrophage marker) and CD204 (M2 macrophage marker) have been mainly utilized to date .

Lung cancer is the most common cause of cancer-related death worldwide and non-small cell lung cancer (NSCLC) is the major type of the cases. Previous studies demonstrated a positive correlation between TAMs density and worse prognosis in the advanced NSCLC treated with an EGFR-TKI [3]. Studies using CD204 as an M2 marker indicated a significant association of CD204 positive TAMs density and poor outcome of patients with lung adenocarcinoma [4] and lung squamous cell carcinoma [5]. Interestingly, some previous studies revealed that the histological features of tumors and location sites of macrophages could influences the role of TAMs [6]. So far, a few reports had compared the positive stromal TAMs and tumor cell nest TAMs in lung cancer, but most of them were smaller sample study or focused on a single subtype of disease [7]. In this study, in order to confirm whether TAMs can be used as a diagnosis or prognosis marker of surgically resected NSCLC cases, and find the relationship between prognosis and TAMs location in lung cancer, CD68 and CD204 immunohistochemistry was carried out in NSCLC specimens from 297 cases.

Methods:

Cases collection

A total of 297 patients with non-small cell lung cancer (NSCLC) were included in this study. These cases were between 2005 and 2013 at Akita University Hospital (Akita, Japan). The subtypes of the NSCLC included 226 adenocarcinomas, 61 squamous cell carcinomas, 4 adenosquamous carcinomas and 6 large cell carcinomas. None of the patients had received preoperative chemotherapy. The relative clinicopathological characteristics were obtained from clinical records. The disease-free survival time was measured from the date of surgery to the date of recurrence or death due to NSCLC or the date when the patients were last known to be disease free. Ethical approval was obtained from Akita University, Faculty of Medicine, Ethics Committee.

Immunohistochemistry (IHC)

4 μm thick tissue sections were cut and stained by a Ventana Discovery XT autostainer (Ventana Medical Systems, Tucson, AZ, USA) using a mouse anti-human CD68 monoclonal antibody (Clone PG-M1, 1:100; Dako, Japan) and mouse anti-human CD204 monoclonal antibody (Clone SRA-E5, 1:500; Trans Genic Inc, Japan). All IHC slides were scanned at an absolute magnification of 20× using a pathology digital imaging system (Nanozoomer virtual slide system, Hamamatsu Photonics, Shizuoka, Japan). For each slide, five representative 0.1mm2 fields of the tumor cell nests, tumor stroma and alveolar air space per tissue section were separately selected and counted for numbers of positive cells. Tumor cell nest was defined as areas where tumor cells accounted for more than 80% of total cells and tumor stroma as area where tumor stromal cells more than 80%. Alveolar air space was air space inside the main tumor or outside within three alveoli. The average number of these five fields represented the CD68 or CD204-positive cell number for each component of the tumor. The average number of these five fields represented the CD68 or

CD204-positive cell number for each component of the tumor.

Analyses of EGFR gene mutations and ALK rearrangements

For EGFR mutation analysis, DNA was extracted from 10-μm-thick FFPE or frozen tumor tissue from each case, and then screened for somatic mutations in EGFR exons 19 and 21 by a high-resolution melting (HRM) analysis, as described elsewhere [8]. The ALK rearrangement was analyzed by Reverse transcription-PCR using SuperScript III Reverse Transcriptase (Thermo Fisher Scientific, Waltham, MA, USA).

Statistical analysis

Statistical analysis was performed with the GraphPad Prism 6 software program for windows (GraphPad Software, San Diego, CA, USA) except for the multivariate survival analysis, which was performed using SPSS 18.0 software (IBM Corp, Armonk, NY, USA). Spearman rank correlation coefficients, Wilcoxon matched pairs test, one-way ANOVA and chi square test were used in this study. For the survival analysis, survival curves were estimated by the Kaplan-Meier method, and the differences in the disease-related survival were compared by the log-rank test. Cox proportional hazards regression model was used for the multivariate survival analysis. $P<0.05$ was considered statistically significant.

Results:

Distribution of $CD68^+$ TAMs and $CD204^+$ TAMs in NSCLC

A series of 297 NSCLC specimens were examined for CD68 and CD204 in tumor cell nest, tumor stroma and alveolar air space at the same time (Figure 1). The numbers of $CD68^+$ TAMs and $CD204^+$ TAMs were highest in alveolar air space, and lowest in the tumor cell nest sites ($P<0.001$). The distributions of $CD68^+$ TAMs and $CD204^+$ TAMs in each subtype of tissue were strongly correlated (tumor cell nest: r2=0.8490; tumor stroma: r2=0.7169; alveolar air space: r2=0.7416; $P<0.001$ each). However, the mean numbers of $CD68^+$ TAMs were significantly higher than the $CD204^+$ TAMs ($P<0.001$).

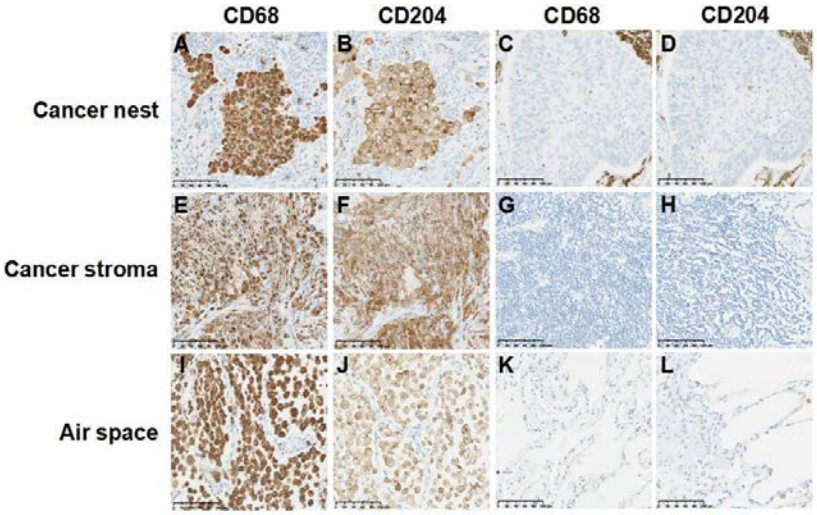

Figure1. Immunostaining of NSCLC with CD68 and CD204 antibody for TAMs

A. Cases with a high number of $CD68^+$ TAMs in cancer nest; B. Cases with a high number of $CD204^+$ TAMs in cancer nest;.C. Cases with a low number of $CD68^+$ TAMs in cancer nest; D. Cases with a low number of $CD204^+$ TAMs in cancer nest;.E. Cases with a high number of $CD68^+$ TAMs in cancer stroma; F. Cases with a high number of $CD204^+$ TAMs in cancer stroma; G. Cases with a low number of $CD68^+$ TAMs in cancer stroma; H. Cases with a low number of $CD204^+$ TAMs in cancer stroma; I. Cases with a high number of $CD68^+$ TAMs in air space; J. Cases with a high number of $CD204^+$ TAMs in air space; K. Cases witha low number of $CD68^+$ TAMs in air space; L. Cases with a low number of $CD204^+$ TAMs in air space.

Correlations between the CD68$^+$/CD204$^+$ TAMs and clinicopathological factors in NSCLC

All the patients were classified into two groups according to the median values of CD68$^+$ TAMs and CD204$^+$ TAMs in each subtype of location. Overall, a high numbers of CD68$^+$ TAMs and CD204$^+$ TAMs in tumor stroma were significantly correlated with the pathological factors in NSCLC, such as male gender; smokers; stage IB, II, III and IV disease; histological grade of G2, G3 and G4; pleural invasion; lymph node metastasis and wild-type EGFR gene. While high numbers of CD68$^+$ TAMs and CD204$^+$ TAMs in tumor cell nest were significantly correlated with smokers and EGFR gene mutation (Table 1). In contrast, the age of patients or ALK rearrangement status in NSCLC was not correlated with CD68$^+$/CD204$^+$ TAMs. No significant correlation was found between the CD68$^+$/CD204$^+$ TAMs in alveolar air space and all these clinicopathological factors in NSCLC. Moreover, in adenocarcinoma, the lower density of CD68$^+$/CD204$^+$ TAMs in tumor stroma and higher in tumor cell nest were found compared with non-adenocarcinomas.

Table 1. Relationship between CD68$^+$/CD204$^+$ TAMs and clinical features of non-small cell lung carcinoma.

			CD68$^+$ TAMs					CD204$^+$ TAMs				
		N	Low		High		*P*-value†	Low		Hig		*P*-value†
Age(year)	>65	201	100	49.75%	101	50.25%	0.7674	99	49.25%	102	50.75%	0.7732
	≤65	96	46	47.92%	50	52.08%		49	51.04%	47	48.96%	
Gender	F	113	79	69.91%	34	30.09%	< 0.0001*	76	67.26%	37	32.74%	< 0.0001*
	M	184	67	36.41%	117	63.59%		72	39.13%	112	60.87%	
Smoking status	Never-smoker	132	87	65.91%	45	34.09%	< 0.0001*	85	64.39%	47	35.61%	< 0.0001*
	Smoker	165	59	35.76%	106	64.24%		63	38.18%	102	61.82%	
Histology	Adenocarcinoma	226	139	61.50%	87	38.50%	< 0.0001*	138	60.00%	92	40.00%	< 0.0001*
	Non-adenocarcinoma	71	7	9.86%	64	90.14%		10	14.93%	57	85.07%	
Stage	Ia	111	74	66.67%	37	33.33%	< 0.0001*	71	63.96%	40	36.04%	< 0.05*
	Ib-IV	186	72	38.71%	114	61.29%		77	41.40%	109	58.60%	
Grade	G1	101	71	70.30%	30	29.70%	< 0.0001*	71	70.30%	30	29.70%	< 0.0001*
	G2-G4	196	75	38.27%	121	61.73%		77	39.29%	119	60.71%	
Pleural invasion	Absent	185	107	57.84%	78	42.16%	< 0.05*	107	57.84%	78	42.16%	< 0.05*
	Present	112	39	34.82%	73	65.18%		41	36.61%	71	63.39%	
Lymph node metastasis	Negative	231	126	54.55%	105	45.45%	< 0.05*	126	54.55%	105	45.45%	< 0.05*
	Positive	66	20	30.30%	46	69.70%		22	33.33%	44	66.67%	
ALK rearrangement	Negative	132	62	46.97%	70	53.03%	0.9048	59	44.70%	73	55.30%	0.4344
	Positive	4	2	50.00%	2	50.00%		1	25.00%	3	75.00%	
	Unknown	163	82	50.31%	81	49.69%		88	53.99%	75	46.01%	
EGFR status	Mutant	42	26	61.90%	16	38.10%	< 0.05*	29	69.05%	13	30.95%	< 0.05*
	Wild-type	127	45	35.43%	82	64.57%		50	39.37%	77	60.63%	
	Unknown	128	76	59.38%	52	40.63%		69	53.91%	59	46.09%	

†Chi-squared test, $^*P<0.05$.

Prognostic significance of the CD68$^+$/CD204$^+$ TAMs in NSCLC and lung adenocarcinoma

Kaplan-Meier analysis revealed that in NSCLC, both the high CD68$^+$ TAMs and CD204$^+$ TAMs in tumor stroma ($P<0.05$, respectively) (Figure 2-A), but not in the tumor cell nest or alveolar air space ($P>0.05$ each), showed a worse disease-free survival than the lower density groups. Furthermore, we also analyzed the prognostic value of other clinicopathological factors to identify the factors significantly influencing the survival. The pathological stage, histological grade, pleural invasion, and lymph node metastasis were confirmed as factors significantly correlated with

the prognosis in NSCLC (P<0.05, respectively). Multivariate survival analysis confirmed that the lymph node metastasis, high $CD68^+$ TAMs and $CD204^+$ TAMs in tumor stroma were statistically significant independent predictors of the worse prognosis in NSCLC (P<0.05, respectively) (Table 2).

Table 2. Univariate and multivariate analyses of clinicopathological factors for a disease-free survival in non- small cell lung cancer patients.

	Univariate analysis		Multivariate analysis	
	HR (95%CI)	***P* value**	**HR (95%CI)**	***P* value**
Age(>65 vs.≤65)	1.08 (0.72-1.61)	0.7115	/	/
Gender(Male vs.Female)	0.95 (0.65-1.40)	0.7997	/	/
Histological type(Adenocarcinoma vs.Non-adenocarcinoma)	1.12 (0.72-1.76)	0.611	/	/
Smoking status(Yes vs. No)	1.01 (0.69-1.47)	0.9573	/	/
EGFR gene status(Mutant vs. Wild-type)	1.28 (0.65-2.53)	0.4807	/	/
ALK rearrangement(Positive vs. Negative)	0.10 (0.01-1.25)	0.0734	/	/
$CD68^+$ TAMs in tumor cell nest(High vs. Low)	1.08 (0.74-1.58)	0.6857	/	/
$CD68^+$ TAMs in alveolar air space(High vs. Low)	0.96 (0.66-1.40)	0.8334	/	/
$CD204^+$ TAMs in tumor cell nest(High vs. Low)	1.21 (0.83-1.76)	0.3243	/	/
$CD204^+$ TAMs in alveolar air space(High vs. Low)	1.12 (0.77-1.63)	0.5605	/	/
Pathological stage(Ia vs Ib-IV)	0.61 (0.41-0.89)	< 0.05*	0.90 (0.52-1.55)	0.693
Histological grade(G1 vs.G2-G4)	0.63 (0.43-0.93)	< 0.05*	0.74 (0.46-1.20)	0.225
Pleural invasion(Present vs. Absent)	0.67 (0.45-0.99)	< 0.05*	1.05 (0.66-1.69)	0.827
Lymph node metastasis(Positive vs. Negative)	0.28 (0.17-0.45)	< 0.0001*	0.40 (0.26-0.63)	< 0.0001*
$CD68^+$ TAMs in tumor stroma(High vs. Low)	0.66 (0.45-0.96)	< 0.05*	1.76 (1.04-3.00)	< 0.05*
$CD204^+$ TAMs in tumor stroma(High vs. Low)	0.62 (0.43-0.91)	< 0.05*	0.55 (0.32-0.94)	< 0.05*

HR, hazard ratio; CI, confidence interval; *P<0.05.

Besides, we explored the association between $CD68^+/CD204^+$ stromal TAMs and clinical outcomes of lung adenocarcinoma and lung squamous cell carcinoma. Kaplan-Meier analysis revealed that the high $CD68^+$ TAMs and $CD204^+$ TAMs in tumor stroma were both significantly correlated with shorter disease-free survival time in lung adenocarcinoma patients (P<0.05, respectively) (Figure 2-B). But in lung squamous cell carcinoma patients, no significant association was found between the $CD68^+/CD204^+$ tumor stromal TAMs and the disease-free survival time (P>0.05, respectively). Furthermore, high $CD204^+$ stromal TAMs was confirmed to be a significant independent predictor of the disease-free survival time in lung adenocarcinoma by both univariate analysis and multivariate survival analysis (P<0.05) (Table 3).

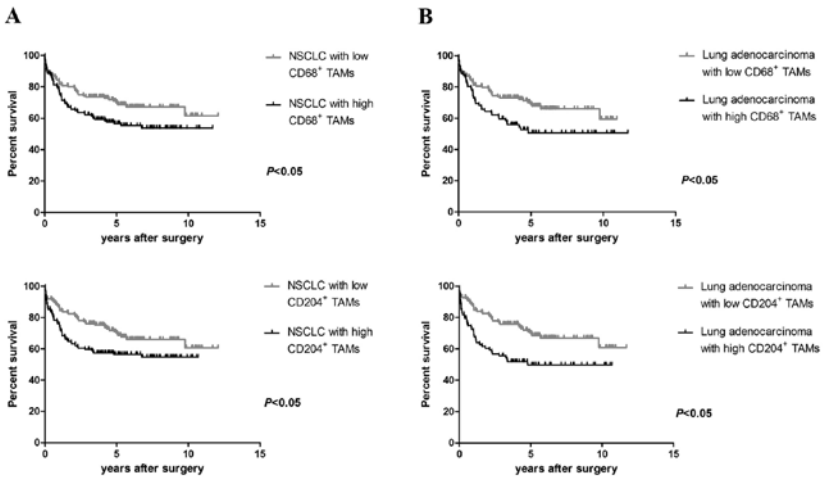

Figure 2. $CD68^+/CD204^+$ stromal TAMs and patients' disease-free survival in NSCLC (A) and lung adenocarcinoma (B)

Table 3. Univariate and multivariate analyses of clinicopathological factors for a disease-free survival in adenocarcinoma patients.

	Univariate analysis		Multivariate analysis	
	HR (95%CI)	***P* value**	**HR (95%CI)**	***P* value**
Adenocarcinoma progression(INV vs. AIS and MIA)	1.64 (0.89-3.01)	0.1141	/	/
Nuclear and mitotic grade risk stratisfication (High-grade vs. Low-grade)	1.82 (1.09-3.06)	< 0.05*	1.69 (1.03-2.78)	< 0.05*
Spread through air spaces(STAS) (Presnet vs. Absent)	0.51 (0.31-0.86)	< 0.05*	1.70 (1.06-2.73)	< 0.05*
$CD68^+$TAMs in tumor stroma(High vs. Low)	0.67 (0.46-0.98)	< 0.05*	0.83 (0.42-1.62)	0.578
$CD204^+$TAMs in tumor stroma(High vs. Low)	0.51 (0.33-0.81)	< 0.05*	2.34 (1.16-4.72)	< 0.05*

INV, invasive adenocarcinoma; AIS, adenocarcinoma in situ; MIA, minimally invasive adenocarcinoma; HR, hazard ratio; CI, confidence interval; *P<0.05.

Discussion:

To our best knowledge, the present study is the first to compare the TAMs distribution in three different topographical areas in NSCLC, including the tumor cell nest, tumor stroma and alveolar air space. Our analyses showed that numbers of $CD68^+$ TAMs and $CD204^+$ TAMs were highest in alveolar air space, and lowest in the tumor cell nest sites. In previous report, Dai et al. also compared the $CD68^+$ macrophages in both tumor stroma and tumor cell nest in NSCLC, and they indicated that the numbers of macrophages were significantly more in the tumor stroma than in the tumor islets , which is consistent to our findings. Furthermore, we found that the distributions of $CD68^+$ TAMs and $CD204^+$ TAMs were strongly correlated, respectively in the tumor cell nest, tumor stroma and alveolar air space. And the mean numbers of $CD68^+$ TAMs in each subtype of location were significantly higher than the $CD204^+$ TAMs. Ohtaki et al. previously compared the distribution of $CD68^+$ TAMs and $CD204^+$ TAMs in tumor stroma of lung adenocarcinoma and got the similar conclusion, which revealed that the mean number of $CD68^+$ macrophages is higher than the $CD204^+$ macrophages, and the distribution of them was strongly correlated [4]. These results indicated that the distribution and density of $CD68^+/CD204^+$ TAMs in each location are quite different, which maybe cause different clinical significance.

Accumulating evidence has revealed the positive correlation between TAMs density and a poor prognosis [1, 2, 9, 10]. Our clinicopathological observation of 297 cases also clearly illustrated that the high number of $CD68^+/CD204^+$ TAMs in tumor stroma were significantly correlated with multiple clinicopathological factors of NSCLC patients, which were related to a worse biological behavior of tumor. High numbers of $CD68^+$ TAMs and $CD204^+$ TAMs in tumor cell nest were significantly correlated with smoking habits and EGFR gene mutation. Whereas no significant correlation was found between the $CD68^+/CD204^+$ TAMs in alveolar air space and these relative clinicopathological factors in NSCLC. The survival analyses showed that the high numbers of $CD68^+/CD204^+$ TAMs in tumor stroma, rather than the tumor cell nest or alveolar air space, were significantly associated with shorter disease-free survival time in NSCLC. Furthermore, the similar effects were also illustrated in the lung adenocarcinoma group with 226 cases, where a univariate analysis showed the high expressions of $CD68^+$ TAMs and $CD204^+$ tumor stromal TAMs were correlated with shorter disease-free survival time. Especially the $CD204^+$ tumor stromal TAMs, which showed significantly correlated with the worse prognosis of lung adenocarcinoma in both univariate and multivariate survival analyses. It indicated that the CD204 could be a better marker than CD68 for the identification of TAMs in lung adenocarcinoma. All these results confirmed that the location of TAMs infiltration can influence different tumor progression [6, 7].

In conclusion, we analyzed 297 NSCLC cases in present study and found that the location of TAMs infiltration can influence different tumor progression. The high numbers of $CD68^{+}/CD204^{+}$ TAMs in tumor stroma were significantly associated with aggressive tumor behaviors and shorter disease-free survival time in NSCLC. These findings suggested that high tumor stromal TAMs density is an independent worse prognostic factor in NSCLC. Counting macrophages in the cancer stroma is more useful in predicting patients' disease-free survival time.

References:

[1] I. Rhee, Diverse macrophages polarization in tumor microenvironment, Archives of pharmacal research, 39 (2016) 1588-1596.

[2] M. Takeya, Y. Komohara, Role of tumor-associated macrophages in human malignancies: friend or foe?, Pathology international, 66 (2016) 491-505.

[3] F.T. Chung, K.Y. Lee, C.W. Wang, C.C. Heh, Y.F. Chan, H.W. Chen, C.H. Kuo, P.H. Feng, T.Y. Lin, C.H. Wang, C.L. Chou, H.C. Chen, S.M. Lin, H.P. Kuo, Tumor-associated macrophages correlate with response to epidermal growth factor receptor-tyrosine kinase inhibitors in advanced non-small cell lung cancer, International journal of cancer, 131 (2012) E227-235.

[4] Y. Ohtaki, G. Ishii, K. Nagai, S. Ashimine, T. Kuwata, T. Hishida, M. Nishimura, J. Yoshida, I. Takeyoshi, A. Ochiai, Stromal macrophage expressing CD204 is associated with tumor aggressiveness in lung adenocarcinoma, Journal of thoracic oncology : official publication of the International Association for the Study of Lung Cancer, 5 (2010) 1507-1515.

[5] S. Hirayama, G. Ishii, K. Nagai, S. Ono, M. Kojima, C. Yamauchi, K. Aokage, T. Hishida, J. Yoshida, K. Suzuki, A. Ochiai, Prognostic impact of CD204-positive macrophages in lung squamous cell carcinoma: possible contribution of Cd204-positive macrophages to the tumor-promoting microenvironment, Journal of thoracic oncology : official publication of the International Association for the Study of Lung Cancer, 7 (2012) 1790-1797.

[6] C. Medrek, F. Ponten, K. Jirstrom, K. Leandersson, The presence of tumor associated macrophages in tumor stroma as a prognostic marker for breast cancer patients, BMC cancer, 12 (2012) 306.

[7] F. Dai, L. Liu, G. Che, N. Yu, Q. Pu, S. Zhang, J. Ma, L. Ma, Z. You, The number and microlocalization of tumor-associated immune cells are associated with patient's survival time in non-small cell lung cancer, BMC cancer, 10 (2010) 220.

[8] K. Nomoto, K. Tsuta, T. Takano, T. Fukui, K. Yokozawa, H. Sakamoto, T. Yoshida, A.M. Maeshima, T. Shibata, K. Furuta, Y. Ohe, Y. Matsuno, Detection of EGFR mutations in archived cytologic specimens of non-small cell lung cancer using high-resolution melting analysis, American journal of clinical pathology, 126 (2006) 608-615.

[9] T. Yamaguchi, S. Fushida, Y. Yamamoto, T. Tsukada, J. Kinoshita, K. Oyama, T. Miyashita, H. Tajima, I. Ninomiya, S. Munesue, A. Harashima, S. Harada, H. Yamamoto, T. Ohta, Tumor-associated macrophages of the M2 phenotype contribute to progression in gastric cancer with peritoneal dissemination, Gastric cancer : official journal of the International Gastric Cancer Association and the Japanese Gastric Cancer Association, 19 (2016) 1052-1065.

[10] M. Shigeoka, N. Urakawa, T. Nakamura, M. Nishio, T. Watajima, D. Kuroda, T. Komori, Y. Kakeji, S. Semba, H. Yokozaki, Tumor associated macrophage expressing CD204 is associated with tumor aggressiveness of esophageal squamous cell carcinoma, Cancer science, 104 (2013) 1112-1119.

作成日：2018 年 2 月 20 日

^{18}F-Sodium Fluoride Dynamic PET/CT in patients with intracranial tumors
^{18}F- Sodium Fluoride ダイナミック PET/CT 検査を用いた脳腫瘍評価に関する後向き研究

研究者氏名　劉　恩濤（第 39 期笹川医学研究者）
中国所属機関　広東省人民病院 PET センター
日本研究機関　横浜市立大学大学院　放射線医学
指導責任者　井上　登美夫　教授
共同研究者名　金田　朋洋　准教授，日野　彩子　助教授

Abstract:

Purpose

The aim of this study was to compare the efficiency of ^{18}F-Sodium Fluoride and ^{18}F-FDG PET/CT in patients with intracranial tumors.

Methods

Checking the database from 2010 to 2017, found that the patient with brain tumors underwent ^{18}F-Sodium Fluoride PET/CT brain scan and ^{18}F-FDG PET/CT. And excluding the patient who without neurosurgical resection. Visual observation and semiquantitative analysis (SUVmax) were performed. The tumor metabolic morphology and intratumoral distribution of tracer were used to determine differential diagnosis between benign and malignant brain tumors. Cohen's kappa (κ), McNemar's test, and Bland–Altman plots were used to assess the repeatability and reproducibility of brain tumor detection. The Wilcoxon signed rank test was used to compare the performance by two tracers.

Results

A total of 24 patients underwent ^{18}F-Sodium Fluoride PET/CT and ^{18}F-FDG PET/CT. A total of 24 tumors was found in all patients. The malignant tumor type was glioblastoma (WHO grade III-IV) and astroblastoma (WHO grade III). And the benign tumor type was the meningioma, central neurocytoma, and pituitary adenoma. By visual analysis, Cohen's kappa (κ) values of routine MRI sequences, ^{18}F-Sodium Fluoride PET/CT, and ^{18}F-FDG PET/CT were 1.00, 0.791, and 0.739, respectively. And the McNemar's test found p-value > 0.05. Of the 24 patients, the median SUVmax of ^{18}F-FDG PET/CT and ^{18}F-Sodium Fluoride PET/CT was 4.40 (range 2.60-9.10) and 2.05 (range 0.20-14.20), respectively. There was a statistically significant difference between in SUVmax (Z = -3.26, P = 0.001).

Conclusions

This study demonstrates that ^{18}F-Sodium Fluoride PET/CT is better than ^{18}F-FDG PET/CT in detecting intracranial tumors and can provide additional diagnostic information, especially for meningiomas.

Key Words:

PET/CT, ^{18}F-sodium fluoride, ^{18}F-Fluorodeoxyglucose, Brain neoplasms

Introduction:

According to the latest CBTRUS Statistical Report: primary brain and other central nervous system tumors diagnosed in the United States, brain, and other central nervous system had an annual average incidence of 10.94 per 100,000 individuals in 15-39 years and of 40.82 per 100,000 individuals in older than 40 years[1]. And the annual incidence of gliomas, including glioblastoma, is around 6 cases per 100,000 individuals. Routine MRI sequences, including T2WI, FLAIR, and T1WI with contrast agents were recommended to assess the early diagnosis[2]. However, there were some

limitations of routine MRI in differentiating tumor tissues from the nonspecific tissue after radiotherapy, and assessments of tumor cellularity and differentiation. Molecular imaging using PET/CT could provide relevant additional information on tumor metabolism. The advantages of amino-acid PET/CT were well documented in above-mentioned features. In recent years, many research teams have found that some commonly used radiopharmaceuticals could be accumulated by some uncommon brain tumors. Moreover, we found that meningiomas could be demonstrated by ^{18}F-Sodium Fluoride PET/CT in our previous study[3-4]. So we want to observe ^{18}F-Sodium Fluoride PET/CT in other brain tumors.

Methods:

a) The Institutional Review Board sanction was obtained and the informed consent requirement was waived for this retrospective study.

b) Patients: Checking the database from 2010 to 2017, found that the patient with brain tumors underwent ^{18}F-Sodium Fluoride PET/CT brain scan and ^{18}F-FDG PET/CT. And excluding the patient who without neurosurgical resection.

c) The procedure of data acquisition: PET/CT protocol according to our previous studies.[4,8]

d) Imaging analysis: MRI images were reviewed by two board-certified radiologists. PET/CT images were assessed by two observers who received standard training and expertise in PET/CT diagnosis.

   1) Visual observation: On ^{18}F-sodium fluoride PET images, the tumor metabolic morphology and intratumoral distribution of tracer were described and assessed. ①"The malignant tumor" was defined as if the tumor was lobulated or irregular shaped, ill-defined serrated margin and ring-like increased uptake. If the tumor with central necrosis, which could be demonstrated as ring-like uptake on the PET images. ②In contrast, "the benign tumor " was defined as if the tumor was round shape, smooth margin, and diffusely homogeneously increased uptake on PET images. If the tumor was contiguous to skull and had a broad base, which was defined as the benign tumor.

   2) Semiquantitative analysis: SUVmax was used and defined as the ratio of the tumor uptake (kBq/ml) divided by the injected activity (kBq) normalized by the dilution volume (ml) at the time of imaging. Postulating the tissues in the body have a density of about 1 g/ml, SUV was calculated according to the following equation:

$$SUV = \frac{tumor\ \ uptake\ \ (kBq/ml)}{injected\ \ dose\ \ (kBq)/patient\ \ weight\ \ (g)} \cdot \frac{ml}{g}$$

e) Statistical analysis: Quantitative variables were expressed as mean ± standard deviation (SD) and categorical variables as frequencies or percentages. Normal distribution of variables was evaluated by using the Shapiro-Wilk test.The inter-rater reliability of MRI and PET/CT readings was evaluated by using Cohen's kappa (κ) and McNemar's test, which was based on following criteria: almost perfect if $\kappa > 0.80$, substantial if $0.80 \geq \kappa \geq 0.61$, moderate if $0.60 \geq \kappa \geq 0.41$, fair if $0.40 \geq \kappa \geq 0.21$, and slight if $0.20 \geq \kappa \geq 0.00$. Evaluation the repeatability and reproducibility for brain tumor detection by ^{18}F-Sodium Fluoride PET/CT by Bland-Altman plot. Comparisons of numerical data between two independent groups were performed by the Student's t test or the Mann-Whitney U test (two-tailed). The Wilcoxon signed ranks test was used to compare performance of ^{18}F-Sodium Fluoride PET/CT and ^{18}F-FDG PET/CT in detecting the brain tumor. Using non-parametric receiver operating characteristic (ROC) curves and comparing the areas under the curve (AUCs) to assess the parameters of ^{18}F-Sodium Fluoride PET/CT and ^{18}F-FDG PET/CT in detecting the brain tumor.

Results:

a) A total of 24 patients underwent ^{18}F-Sodium Fluoride PET/CT and ^{18}F-FDG PET/CT. A total of 24 tumors was found

in all patients. The malignant tumor type was glioblastoma (WHO grade III-IV) and astroblastoma (WHO grade III). And the benign tumor type was the meningioma, central neurocytoma, and pituitary adenoma.

b) By visual analysis, Cohen's kappa (κ) values of routine MRI sequences, ^{18}F-Sodium Fluoride PET/CT, and ^{18}F-FDG PET/CT were 1.00, 0.791, and 0.739, respectively. And the McNemar's test found p-value > 0.05.

c) For the 24 patients, the median SUVmax of ^{18}F-FDG PET/CT and ^{18}F-Sodium Fluoride PET/CT was 4.40 (range 2.60-9.10) and 2.05 (range 0.20-14.20), respectively. There was a statistically significant difference between in SUVmax (Z = -3.26, P = 0.001). Receiver operating characteristic (ROC) curves were performed and indicated that the SUVmax of ^{18}F-Sodium Fluoride had more value to diagnose intracranial tumors (Figure. 1-2).

d) For benign and malignant tumors, there was no statistically significant difference in SUVmax of ^{18}F-Sodium Fluoride and ^{18}F-FDG between benign and malignant tumors (Z = -0.534, P >0.05; Z = -0.604, P > 0.05, respectively) (Figure. 3-4).

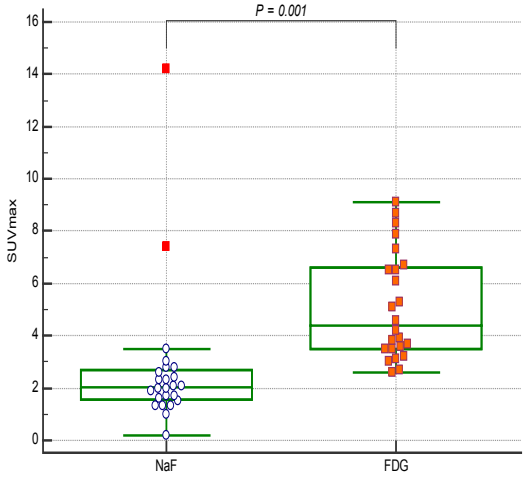

Fig 1. A comparison of SUVmax between 18F-NaF and 18F-FDG

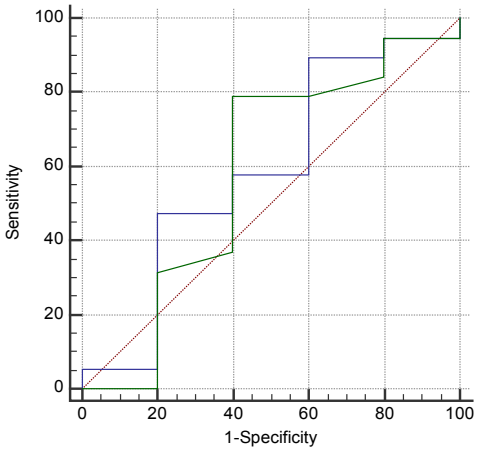

Fig 2. ROC curve analysis of 18F-NaF PET/CT and 18F-FDG PET/CT

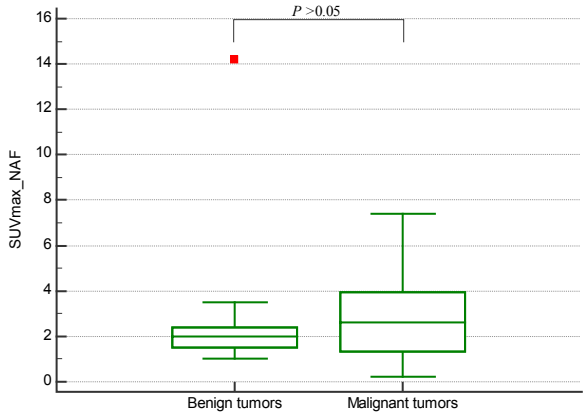

Fig 3. A comparison of SUVmax of 18F-Sodium Fluoride between benign and malignant tumors

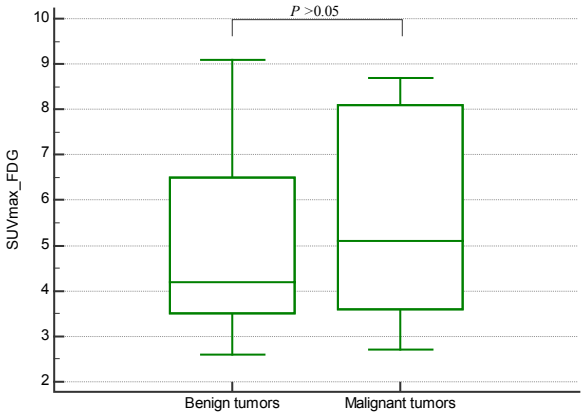

Fig 3. A comparison of SUVmax of 18F-FDG between benign and malignant tumors

Discussion:

Due to normal gray matter exhibited high ^{18}F-FDG uptake, which made the delineation of brain tumors challenging. The localization and differential diagnosis of brain tumors with ^{18}F-FDG PET/CT was difficult to narrow using PET/CT alone. ^{18}F-Sodium Fluoride was a common tracer used in bone scintigraphy. Considering the mechanism of ^{18}F-Sodium Fluoride and ^{99m}Tc-DP uptake in fluoroapatite of osseous lesions are similar. This trace could be accumulated by

bone lesions and calcified tissues. Osseous involvement was a common manifestation in meningiomas. And ^{18}F-Sodium Fluoride could be used to assess osseous involvement by meningiomas and already had documented in our previous study[3-21]. The blood-brain barrier (BBB) was damaged in intra-axial brain tumors. Therefore, we hypothesized that ^{18}F-Sodium Fluoride PET/CT brain scan could demonstrated the intra-axial lesions[22-36].

In this present study, all lesions were detected by ^{18}F-Sodium Fluoride PET/CT and 13 lesions by ^{18}F-FDG PET/CT. ROC curves demonstrated that the SUVmax of ^{18}F-Sodium Fluoride had more value to diagnose intracranial tumors. However, there is no significant valuable in the differential diagnosis of benign and malignant intracranial tumors.

The limitation of this study was the sample size (only 5 malignant tumors) and limited assessed parameters (only SUVmax). And in the present study, there was not including metastatic brain tumors, in the future research we will focus on this.

References:

1. Ostrom QT, Gittleman H, Liao P, et al. CBTRUS Statistical Report: Primary brain and other central nervous system tumors diagnosed in the United States in 2010-2014. *Neuro Oncol*. 2017;19:v1-v88.
2. Perkins A, Liu G. Primary Brain Tumors in Adults: Diagnosis and Treatment. *Am Fam Physician*. 2016;93:211-217.
3. Tateishi U, Tateishi K, Shizukuishi K, et al. 18F-Fluoride PET/CT allows detection of hyperostosis and osseous involvement in meningioma: initial experience. *Clin Nucl Med*. 2013;38:e125-31.
4. Tateishi U, Tateishi K, Hino-Shishikura A, Torii I, Inoue T, Kawahara N. Multimodal approach to detect osseous involvement in meningioma: additional value of (18)F-fluoride PET/CT for conventional imaging. *Radiology*. 2014;273:521-528.
5. Segall G, Delbeke D, Stabin MG, et al. SNM practice guideline for sodium 18F-fluoride PET/CT bone scans 1.0. *J Nucl Med*. 2010;51:1813-1820.
6. Freesmeyer M, Stecker FF, Schierz JH, Hofmann GO, Winkens T. First experience with early dynamic (18)F-NaF-PET/CT in patients with chronic osteomyelitis. *Ann Nucl Med*. 2014;28:314-321.
7. Sachpekidis C, Goldschmidt H, Hose D, et al. PET/CT studies of multiple myeloma using (18) F-FDG and (18) F-NaF: comparison of distribution patterns and tracers' pharmacokinetics. *Eur J Nucl Med Mol Imaging*. 2014;41:1343-1353.
8. Hino-Shishikura A, Tateishi U, Shibata H, et al. Tumor hypoxia and microscopic diffusion capacity in brain tumors: A comparison of62Cu-Diacetyl-Bis (N4-Methylthiosemicarbazone) PET/CT and diffusion-weighted MR imaging. *Eur J Nucl Med Mol Imaging*. 2014;41:1419-1427.
9. Oldan JD, Turkington TG, Choudhury K, Chin BB. Quantitative differences in [(18)F] NaF PET/CT: TOF versus non-TOF measurements. *Am J Nucl Med Mol Imaging*. 2015;5:504-514.
10. Grant FD, Fahey FH, Packard AB, Davis RT, Alavi A, Treves ST. Skeletal PET with 18F-fluoride: applying new technology to an old tracer. *J Nucl Med*. 2008;49:68-78.
11. Jadvar H, Desai B, Conti PS. Sodium 18F-fluoride PET/CT of bone, joint, and other disorders. *Semin Nucl Med*. 2015;45:58-65.
12. Wong KK, Piert M. Dynamic bone imaging with 99mTc-labeled diphosphonates and 18F-NaF: mechanisms and applications. *J Nucl Med*. 2013;54:590-599.

13. Hawkins RA, Choi Y, Huang SC, et al. Evaluation of the skeletal kinetics of fluorine-18-fluoride ion with PET. *J Nucl Med*. 1992;33:633-642.
14. Valdes-Martinez A, Kraft SL, Brundage CM, Arceneaux BK, Stewart JA, Gibbons DS. Assessment of blood pool, soft tissue, and skeletal uptake of sodium fluoride F 18 with positron emission tomography-computed tomography in four clinically normal dogs. *Am J Vet Res*. 2012;73:1589-1595.
15. Salgarello M, Lunardi G, Inno A, et al. 18F-NaF PET/CT Imaging of Brain Metastases. *Clin Nucl Med*. 2016;41:564-565.
16. Thenkondar A, Jafari L, Sooriash R, Hajsadeghi F, Berenji GR, Li Y. 18F-NaF PET Demonstrating Unusual Focal Tracer Activity in the Brain. *Clin Nucl Med*. 2017;42:127-128.
17. Tripathi M, Jaimini A, Singh N, et al. F-18 flurodeoxyglucose negative, F-18 fluoride accumulating in a brain metastasis in a treated case of carcinoma of the breast. *Clin Nucl Med*. 2009;34:287-289.
18. Peller PJ, Ho VB, Kransdorf MJ. Extraosseous Tc-99m MDP uptake: a pathophysiologic approach. *Radiographics*. 1993;13:715-734.
19. Vesey AT, Jenkins WS, Irkle A, et al. (18)F-Fluoride and (18)F-Fluorodeoxyglucose Positron Emission Tomography After Transient Ischemic Attack or Minor Ischemic Stroke: Case-Control Study. *Circ Cardiovasc Imaging*. 2017;10.
20. Guo J, Hu S, Wang H, Kuang A. Cerebral infarction on 99mTc-MDP SPECT/CT imaging. *Clin Nucl Med*. 2013;38:925-927.
21. Daouk J, Bouzerar R, Chaarani B, Zmudka J, Meyer ME, Baledent O. Use of dynamic (18)F-fluorodeoxyglucose positron emission tomography to investigate choroid plexus function in Alzheimer's disease. *Exp Gerontol*. 2016;77:62-68.
22. Alf MF, Wyss MT, Buck A, Weber B, Schibli R, Kramer SD. Quantification of brain glucose metabolism by 18F-FDG PET with real-time arterial and image-derived input function in mice. *J Nucl Med*. 2013;54:132-138.
23. Martirosyan NL, Georges J, Eschbacher JM, et al. Potential application of a handheld confocal endomicroscope imaging system using a variety of fluorophores in experimental gliomas and normal brain. *Neurosurg Focus*. 2014;36:E16.
24. Bruehlmeier M, Roelcke U, Schubiger PA, Ametamey SM. Assessment of hypoxia and perfusion in human brain tumors using PET with 18F-fluoromisonidazole and 15O-H2O. *J Nucl Med*. 2004;45:1851-1859.
25. Chen W, Dilsizian V. Targeted PET/CT imaging of vulnerable atherosclerotic plaques: microcalcification with sodium fluoride and inflammation with fluorodeoxyglucose. *Curr Cardiol Rep*. 2013;15:364.
26. Wilson 3rd GH, Gore JC, Yankeelov TE, et al. An Approach to Breast Cancer Diagnosis via PET Imaging of Microcalcifications Using (18)F-NaF. *J Nucl Med*. 2014;55:1138-1143.
27. Ordonez AA, DeMarco VP, Klunk MH, Pokkali S, Jain SK. Imaging Chronic Tuberculous Lesions Using Sodium [(18)F]Fluoride Positron Emission Tomography in Mice. *Mol Imaging Biol*. 2015;17:609-614.
28. Louis DN, Perry A, Reifenberger G, et al. The 2016 World Health Organization Classification of Tumors of the Central Nervous System: a summary. *Acta Neuropathol*. 2016;131:803-820.
29. Li Y, Tafti BA, Shaba W, Berenji GR. Extraosseus uptake of F-18 fluoride in the primary malignancy and cerebral metastasis in a case of non-small-cell lung cancer. *Clin Nucl Med*. 2011;36:609-611.
30. Sheth S, Colletti PM. Atlas of sodium fluoride PET bone scans: atlas of NaF PET bone scans. *Clin Nucl Med*.

2012;37:e110-6.

31. Jones RP, Iagaru A. 18F NaF brain metastasis uptake in a patient with melanoma. *Clin Nucl Med*. 2014;39:e448-50.
32. Gori S, Inno A, Lunardi G, et al. 18F-Sodium Fluoride PET-CT for the Assessment of Brain Metastasis from Lung Adenocarcinoma. *J Thorac Oncol*. 2015;10:e67-8.
33. Derlin T, Mester J, Klutmann S. Abnormal F-18 fluoride uptake in intracranial meningiomas on PET/CT. *Clin Nucl Med*. 2010;35:806-807.
34. Zacchi SR, Duarte PS, Coura Filho GB, Sapienza MT, Buchpiguel CA. Incidental finding of anterior cranial fossa meningioma on 18F-fluoride PET/CT. *Clin Nucl Med*. 2013;38:913-915.
35. Teo TY, Menda Y, McNeely P, Kahn D, Graham M. Incidental Meningioma Detected on 18F-Fluoride With PET/CT During Initial Staging for Prostate Cancer. *Clin Nucl Med*. 2015;40:596-597.
36. Priya RR, Manthri RG, Lakshmi AY, Kalawat T. Intracranial meningioma, mimicking brain metastasis on (18)F sodium fluoride bone scan in a case of carcinoma cervix. *Indian J Nucl Med*. 2016;31:295-297.

作成日：2018 年 2 月 26 日

Relationships between time pressure, relational coordination with nursing managers, and burnout in Japanese home-visiting nurses
日本人訪問看護師の時間圧力、看護管理者との関係調整、バーンアウトとの関係

研究者氏名　曹　暁翼（第 39 期笹川医学研究者）
中国所属機関　四川大学華西病院腎臓病科
日本研究機関　東京大学大学院医学系研究科 健康科学・看護学専攻
指導責任者　成瀬　昂　講師

Abstract:

Aim: To explore the reciprocal associations between time pressure, relational coordination with nursing managers and burnout, and to further examine the moderating effect of relational coordination with nursing managers on the time pressure and burnout relationship among home-visiting nurses in Japan.

Methods: This was a descriptive cross-sectional study with 93 Japanese home-visiting nurses included. A hierarchical moderated regression analysis with mean-centered predictor factors was conducted to explore the moderating role of relational coordination with nursing managers on the association between time pressure and burnout.

Results: The average score of time pressure was 2.80 ± 0.94, and the mean score for RC with nursing managers was 4.17 ± 0.71. The average scores on exhaustion and depersonalization were 2.46 ± 0.91 and 1.70 ± 0.70, respectively. Time pressure had a significant positive relationship with exhaustion and depersonalization ($r = 0.41$, $P < 0.001$; $r = 0.39$, $P < 0.001$). RC with nursing managers has a significant negative association with exhaustion and depersonalization *(*$r = -0.18$, $P < 0.05$; $r = -0.24$, $P < 0.05$). Time pressure predicted exhaustion and depersonalization significantly ($\beta = 0.41$, $P < 0.001$; $\beta = 0.43$, $P < 0.001$). Relational coordination with nursing managers was a significant negative contributor to depersonalization ($\beta = -0.21$, $P < 0.05$); however, its predictive effect on exhaustion was not significant ($\beta = -0.16$, $P > 0.05$). Significant interaction effects of time pressure and relational coordination with nursing managers on exhaustion and depersonalization were also identified ($\beta = -0.21$, $P < 0.05$; $\beta = -0.33$, $P < 0.001$). Time pressure was a strong significant predictor for exhaustion and depersonalization when home visiting nurses reported low relational coordination with nursing managers.

Conclusions: Relational coordination with nursing managers is an important resource for coping with high time pressure. Strategies such as establishing a skill-mix program to reduce nurses' time pressure, and developing a supportive work environment for the promotion of relational coordination with nursing managers may be effective strategies for burnout prevention and management in home-visiting nurses.

Key words: burnout, home nurses, moderating role, relational coordination, time pressure.

Introduction:

A dramatic growth of ageing population, an increase in early discharge from hospitals, and clients' preference for receiving care at home lead to increased demands for visiting nursing services in Japan [1]. On the other hand, the number of home-visiting nurses (HVNs) in Japan remains inadequate [2]. The disequilibrium between a rapid rise in demands for visiting nursing care and a severe shortage of HVNs promotes policymakers and nursing managers to develop a healthy work environment that encourages nurse retention and attracting new nurses.

Burnout is an important workplace health index. High burnout can lower job satisfaction and intent to stay in nurses

[3]. Unlike facility care, specific job characteristics may result in burnout in HVNs. Time pressure represents stress resulting from inadequate time to complete required tasks [4]. Time pressure is a specific stressor related to burnout in visiting nursing settings, as HVNs may experience stress reactions when the time allocated for care is inadequate [5]. In Japan, an HVN provides visiting care for an average of 3 or 4 clients per day [1]. He/she provide clients with medical and personal care in each visit. Then, the HVN moves to another client's home. If the previous client requires more time for care, or if the traffic or weather conditions are bad, the HVN may not arrive in the next client's home on time. Thereby, time pressure is a critical factor which may affect HVNs' well-being. Nevertheless, the association between time pressure and burnout in HVNs was not consistent [6-7].

Supervisor support is a heterogeneous structure which comprises emotional support, instrument support, and empathy with employees [8]. Although prior studies demonstrated that higher supervisor support resulted in lower burnout in HVNs, the evaluation measurements for supervisor support were different, which emphasized emotional support and supervisor-employee partnership, respectively [6, 9]. Relational coordination (RC) is defined as a mutual reinforcing process of interaction between communication and relationships conducted for the purpose of task integration [10]. It is composed of four communication items (frequency; timeliness; accuracy; and problem-solving, rather than blaming) and three relationship items (shared goals, shared knowledge, and mutual respect). Frequent communication keeps healthcare providers updated on patient progress, timely and accurate communication promotes information exchange, and communication on problem-solving facilitates problem solution. Moreover, effective coordination can be facilitated by shared goals for the work procedure and shared knowledge for each other's work. Mutual respect for the work can also help healthcare providers confirming their professional values and enhancing their inclination to collaborate [11].

The HVNs provide over 97% of visiting services on their own, without any assistance from colleagues in Japan [12]. As a result, it is necessary for nursing managers to make frequent, timely, and accurate communicate with HVNs. Contrasting supervisor support which previous studies focused on, RC with nursing managers emphasizes a combination of communication, information sharing, and respectful relationships between nurses and their nursing managers. Although earlier studies proposed that RC with nursing managers promoted work engagement in HVNs [12], the effect of RC with nursing managers on burnout has not been explored. In addition, no studies have explored the moderating effect of RC with nursing managers on the time pressure and burnout relationship in HVNs. Thereby, the aims of the study were to examine the reciprocal associations between time pressure, RC with nursing managers and burnout, and to further explore the moderating role of RC with nursing managers on the relationship between time pressure and burnout among home-visiting nurses in Japan.

Methods:

Study design and sample:

This was a cross-sectional study conducted in Miyazaki prefecture, Japan from November 2013 to February 2014. A convenience sampling method was used, and Internet and mail surveys were conducted to collect data. Nurses with a nurse license were recruited, with nursing managers or nurses who were not working during the investigation excluded. Of the 160 nurses in these 29 home visiting nursing agencies (HVNAs) who were eligible for the study, 93 nurses volunteered and successfully completed the surveys.

Measurement:

A single item (How often do you feel time pressure during home visits or when driving?) was used to evaluate the time pressure HVNs perceived, which was measured with a five-point Likert scale ranging from 1 ("not at all") to 5

("always") [7].

The Relational Coordination Scale (RCS) comprised seven items and two subscales (communication and relationships). A five-point Likert scale was used, and Cronbach's alpha for the overall scale was 0.85 [10]. Cronbach's alphas of each dimension of the Japanese version of the RCS (J-RCS) ranged from 0.77 to 0.86 and the test-retest reliabilities ranged from 0.67 to 0.83 [13]. In this study, Cronbach's alpha of the overall J-RCS was 0.88.

The Japanese Burnout Inventory (J-BI) is a 17-item scale with three subscales (exhaustion, depersonalization and personal achievement) [14]. Each item is scored on a five-point scale ranging from 1 ("no") to 5 ("always"). Cronbach's alphas of each subscale ranged from 0.84 to 0.86. Only exhaustion and depersonalization subscale were included for burnout evaluation in this study, Cronbach's alphas were 0.88 and 0.89 for exhaustion and depersonalization, respectively.

In addition, demographic data such as sex and age, and agency variable (e.g., the number of HVNs in each agency were also collected.

Data analyses:

The statistical analysis package used in the study was SPSS 23.0. Descriptive analyses were conducted using means and standard deviations (SD), and frequencies and percentages. Pearson correlation analyses were performed to explore the relationships between continuous variables. A hierarchical moderated regression analysis with mean-centered predictor factors was used to explore the moderating role of RC with nursing managers on the time pressure and burnout relationship. One SD above or below the mean was used to classify the subgroups with high or low RC with nursing managers, and the simple slope for the regression of time pressure on exhaustion and depersonalization was calculated, respectively [15]. $P < 0.05$ was considered statistically significant (two-tailed test).

Ethical approval:

Ethical approval was obtained from the Research Ethics Committee of The University of Tokyo.

Results:

Among the 93 respondents, 97.8% were female and 2.2% were male. The average age was 43.26 ± 7.98 ranging from 27 to 70 years. The mean years of nursing experience as a HVN were 6.12 ± 5.57 years, and the average years of job experience in the current position were 4.39 ± 4.22 years. Most of the respondents were full-time nurses (67.7%), and the majority of the respondents worked in a small agency (68.8%).

The average score of time pressure was 2.80 ± 0.94, and the mean score for RC with nursing managers was 4.17 ± 0.71. The average scores on exhaustion and depersonalization were 2.46 ± 0.91 and 1.70 ± 0.70, respectively. Time pressure had a significant positive relationship with exhaustion and depersonalization ($r = 0.41$, $P < 0.001$; $r = 0.39$, $P < 0.001$). RC with nursing managers has a significant negative association with exhaustion and depersonalization ($r = -0.18$, $P < 0.05$; $r = -0.24$, $P < 0.05$).

The findings of regression analysis showed that, in step 1, employment status predicted exhaustion significantly and negatively. Time pressure was a strong significant contributor to exhaustion in step 2. Nevertheless, the predictive effect of RC with nursing managers on exhaustion was insignificant. Finally, a significant interaction effect of time pressure and RC with nursing managers on exhaustion was identified (Table 1). Further analysis showed a strong significant association between time pressure and exhaustion in the subgroup with low RC with nursing managers ($\beta = 0.75$, $P < 0.001$).

The findings also showed that employment status was related to depersonalization significantly and negatively. The main effects of time pressure and RC with nursing managers on depersonalization were significant in step 2. In step 3,

the interaction term was a significant predictor for depersonalization (Table 2). Further analysis indicated that the relationship between time pressure and depersonalization was significantly strong in HVNs with low RC with nursing managers ($\beta = 0.79$, $P < 0.001$).

Discussion:

We found that time pressure was a significant contributor to exhaustion in HVNs, which is similar to previous studies [6-7]. This finding is also consistent with the JD-R model, pinpointing that exhaustion is the main result to job demands [9]. On the other hand, time pressure was also a significant predictor for depersonalization, which is not in parallel to an earlier study [6]. Based on the process model of burnout, job demands cause depersonalization through evoking exhaustion first. Job demands may affect employees' feeling of depersonalization, as they intend to obtain mental distance from their work and clients to reduce exhaustion related to stress [16]. In addition, time delays may cause interrupted job arrangements, nurses' anxiety, and complaints from clients, which may lead to HVNs feeling inadequate and exhausted, thus affecting their job satisfaction and feeling detached from work and clients.

Moreover, our study found a significant effect of RC with nursing managers on depersonalization, which is in consistence with the JD-R model, proposing that job resources can promote employee's attitudes toward work and clients [17]. The result is also in line with prior studies [6, 9]. As a result, it is critical for creating a frequent, timely and adequate nurse-supervisor communication mechanism, and developing goal-sharing, knowledge-sharing, and respectful job relationships with nursing managers. On the other hand, no significant and negative relationship between RC with nursing managers and exhaustion was found, which may be ascribed to the fact that exhaustion is mainly a health impairment process in response to job demands, but not a work motivation process in response to job resources.

In addition, we found a significant interaction effect between time pressure and RC with nursing managers on exhaustion and depersonalization. When the HVNs reported low RC with nursing managers, more time pressure led to more exhaustion and depersonalization. This can be explained by the JD-R model, which posits that increased job demands and reduced job resources adds to predicting burnout [18]. The results are also similar to previous studies, indicating that home healthcare workers with more job demands reported more burnout when they had less job resources [19-20].

Furthermore, our findings showed that the magnitude of interaction effects of time pressure and RC with nursing managers on exhaustion and depersonalization was stronger than earlier studies [9, 20], suggesting that strategies for encouraging information sharing and mutual respects between HVNs and nursing managers may reduce the negative effects of time pressure. When the HVNs encounter time pressure, they may benefit from information support from nursing managers to cope with demanding situations, then preventing burnout. This mechanism may be a kind of proactive coping strategy [21]. This is an important result for clinical practice. Unlike facility care focusing on face-to-face communication, telephone-based contact is a critical communication model between HVNs and nursing managers [22]. HVNs typically feel isolated during working hours; as a result, developing a telephone-based contact platform to assist nurses in receiving frequent, timely, adequate, and problem-solving information support may be an effective burnout prevention and management intervention.

Some limitations were noted. First, a cross-sectional research design hinders the probability of identifying causality. A longitudinal design is recommended for future studies. Second, the sample size was small and the respondents were from one prefecture in Japan, which might limit generalizability of the findings. More HVNs working in more prefectures are required. Finally, although the item for time pressure assessment was established based on conceptual analysis and

expert consultation, its reliability and validity require more confirmation. Future studies are required to develop an HVN-sensitive time pressure scale with acceptable psychometric properties to accurately and effectively assess HVNs' work environment.

Conclusions:

Time pressure is a strong predictor for exhaustion and depersonalization, and RC with nursing managers has a significant moderating effect on the relationship between time pressure and burnout among HVNs in Japan. The findings imply that good RC with nursing managers is a critical resource for coping with high time pressure, and for burnout prevention and management.

References:

1. Japan Visiting Nursing Foundation. (2015). Visiting nursing system in Japan. [Cited 1 July 2015.] Available from URL: http://www.jvnf.or.jp/homon/english/vnj2015.pdf

2. Japan Nursing Association. (2015). Statistical data on nursing service in Japan: nurses and assistant nurses. [Cited 1 January 2015.] Available from URL: http://www.nurse.or.jp/home/statistics/pdf/toukei04.pdf

3. Labrague, L.J., McEnroe-Petitte, D.M., Gloe, D., *et al.* (2017). Organizational politics, nurses' stress, burnout levels, turnover intention and job satisfaction. *International Nursing Review, 64,* 109-116.

4. Thompson, C., Dalgleish, L., Bucknall, T., *et al.* (2008). The effects of time pressure and experience on nurses' risk assessment decisions: a signal detection analysis. *Nursing Research, 57,* 302-311.

5. Greggs-McQuilkin, D. (2004). The stressful world of nursing. *Medsurg Nursing, 13,* 141-189.

6. Jansen, P.G., Kerkstra, A., Abu-Saad, H.H., *et al.* (1996). The effects of job characteristics and individual characteristics on job satisfaction and burnout in community nursing. *International Journal of Nursing Studies, 33,* 407-421.

7. Naruse, T., Taguchi, A., Kuwahara, Y., *et al.* (2012). Relationship between perceived time pressure during visits and burnout among home visiting nurses in Japan. *Japan Journal of Nursing Science, 9,* 185-194.

8. Weigl, M., Stab, N., Herms, I., *et al.* (2016). The associations of supervisor support and work overload with burnout and depression: a cross-sectional study in two nursing settings. *Journal of Advanced Nursing, 72,* 1774-1788.

9. Bakker, A.B., Demerouti, E., Taris, T.W., *et al.* (2003). A multigroup analysis of the job resources model in four home organizations. *International Journal of Stress Management, 10*, 16-38.

10. Gittell, J.H., Fairfield, K.M., Bierbaum, B., *et al.* (2000). Impact of relational coordination on quality of care, postoperative pain and functioning, and length of stay: a nine-hospital study of surgical patients. *Medical Care, 38*, 807-819.

11. Havens, D.S., Vasey, J., Gittell, J.H., *et al.* (2010). Relational coordination among nurses and other providers: impact on the quality of patient care. *Journal of Nursing Management, 18,* 926-937.

12. Naruse, T., Sakai, M. & Nagata, S. (2016). Effects of relational coordination among colleagues and span of control on work engagement among home-visiting nurses. *Japan Journal of Nursing Science, 13,* 240-246.

13. Naruse, T., Sakai, M. & Nagata, S. (2014). Reliability and validity of the Japanese version of the Relational Coordination Scale. *Nihon Koshu Eisei Zasshi, 61,* 565-573 (in Japanese).

14. Kubo, M. & Tao, M. (1992). Measurement of burnout. *Psychological Review, 35,* 361-276 (in Japanese).

15. Aiken, L. & West, S.G. (1991). *Multiple Regression: Testing and Interpreting Interactions.* SAGE Publications,

New York.

16. Leiter, M.P. & Maslach, C. (1988). The impact of interpersonal environment of burnout and organizational commitment. *Journal of Organizational Behavior, 9,* 297-308.

17. Demerouti, E., Bakker, A.B., Nachreiner, F., *et al.* (2001). The job demands-resources model of burnout. *Journal of Applied Psychology, 86,* 499-512.

18. Bakker, A.B. & Demerouti, E. (2007). The job demands-resources model: state of the art. *Journal of Managerial Psychology 22,* 309-328.

19. Bakker, A.B., Demerouti, E. & Euwema, M.C. (2005). Job resources buffer the impact of job demands on burnout. *Journal of Occupational Health Psychology, 10,* 170-180.

20. Xanthopoulou, D., Bakker, A.B., Dollard, M.F., *et al.* (2007). When do job demands particularly predict burnout?: The moderating role of job resources. *Journal of Managerial Psychology, 22,* 766-786.

21. Aspinwall, L.G. & Taylor, S.G. (1997). A stitch in time: self-regulation and proactive coping. *Psychological Bulletin, 121*, 417-436.

22. Or, C.K., Valdez, R.S., Casper, G.R., *et al*. (2009). Human factors and ergonomics in home care: Current concerns and future considerations for health information technology. *Work, 33,* 201-209.

Tables:

Table 1

Results of hierarchical regression analyses on emotional exhaustion (n = 93)

Predictor variables	Emotional exhaustion								
	Model 1			Model 2			Model 3		
	B	SE	β	B	SE	β	B	SE	β
Step 1: Control variables									
Sex (female/male)	-0.20	0.66	-0.03	-0.55	0.60	-0.09	-0.60	0.59	-0.10
Age	-0.02	0.01	-0.15	-0.01	0.01	-0.06	-0.01	0.01	-0.05
Job experience as a home visiting nurse	0.03	0.02	0.17	0.02	0.02	0.10	0.02	0.02	0.09
Job experience in the current position	-0.03	0.03	-0.14	-0.02	0.03	-0.09	-0.02	0.03	-0.08
Employment status (full-time/part time)	-0.45	0.21	-0.23*	-0.49	0.20	-0.25*	-0.50	0.19	-0.26*
Span of control (small/large)	-0.01	0.21	-0.01	0.01	0.19	0.03	0.19	0.18	0.02
Step 2: Main effects									
Time pressure				0.40	0.10	0.41***	0.39	0.09	0.40***
RC with nursing managers				-0.21	0.13	-0.16	-0.29	0.13	-0.22*
Step 3: Interaction effect									
Time pressure × RC with nursing managers							-0.24	0.11	-0.21*
ΔR^2	0.112			0.186			0.040		

R^2	0.112	0.288	0.328
F	1.790	4.197***	4.445***

*** $P < 0.001$; ** $P < 0.01$; * $P < 0.05$.

B, unstandardized regression coefficient; SE, standardized error; β, standardized regression coefficient; RC, relational coordination.

Table 2

Results of hierarchical regression analyses on depersonalization (n = 93)

Predictor variables	Depersonalization								
	Model 1			Model 2			Model 3		
	B	SE	β	B	SE	β	B	SE	β
Step 1: Control variables									
Sex (female/male)	-0.42	0.50	-0.09	-0.71	0.45	-0.15	-0.78	0.42	-0.16
Age	-0.02	0.01	-0.21	-0.01	0.01	-0.11	-0.01	0.01	-0.09
Job experience as a home visiting nurse	0.01	0.02	0.02	0.03	0.02	0.16	-0.01	0.01	-0.07
Job experience in the current position	0.02	0.02	0.11	-0.02	0.03	-0.09	0.03	0.03	0.17
Employment status (full-time/part time)	-0.33	0.16	-0.23*	-0.36	0.15	-0.24*	-0.37	0.14	-0.25**
Span of control (small/large)	0.11	0.16	0.07	0.12	0.14	0.08	0.15	0.13	0.10
Step 2: Main effects									
Time pressure				0.32	0.07	0.43***	0.31	0.07	0.42***
RC with nursing managers				-0.21	0.09	-0.21*	-0.31	0.09	-0.31**
Step 3: Interaction effect									
Time pressure × RC with nursing managers							-0.28	0.08	-0.33***
Δ R^2	0.099			0.212			0.099		
R^2	0.099			0.311			0.410		
F	1.560			4.688***			6.328***		

*** $P < 0.001$; ** $P < 0.01$; * $P < 0.05$.

B, unstandardized regression coefficient; SE, standardized error; β, standardized regression coefficient; RC, relational coordination.

作成日：2018年2月22日

日中笹川医学奨学金制度第39期研究者名簿

NO.	氏名	中国所属機関	研究先研究先部署	指導責任者
3901	李　君鵬	吉林省人民医院 救急外科 主治医師	東北大学大学院医学系研究科 消化器外科学分野	亀井　　尚　　教授
3902	李　　卓	西安医学院第一附属医院 検験科 主治医師	秋田大学大学院医学系研究科 器官病態学	後藤　明輝　　教授
3903	石　筝筝	首都医科大学附属北京中医医院 救急及び重症医学科 主治医師	千葉大学大学院医学研究院 救急集中治療医学	織田　成人　　教授
3904	王　　冠	天津市中心婦産科医院 婦産科 医師	東京大学医学部附属病院 女性診療科・産科	藤井　知行　　教授
3905	王　黎明	中国医科大学附属第一医院 胸外科 主治医師	東京大学医学部附属病院 呼吸器外科	中島　　淳　　教授
3906	曹　暁翼	四川大学華西医院 腎内科 講師	東京大学大学院医学系研究科 健康科学・看護学専攻地域看護学分野	成瀬　　昴　　講師
3907	童　方麗	広東省口腔医院 牙体牙髄科 副主任医師	東京医科歯科大学 大学院医歯学総合研究科 歯髄生物学分野	興地　隆史　　教授
3908	夏　幸閣	広東省人民医院 新生児重症監護室 主管護師	国立成育医療研究センター 周産期・母性診療センター　新生児科	丸山　秀彦　　医員
3909	董　文武	中国医科大学附属第一医院 甲状腺総合外科 講師	東京女子医科大学 内分泌外科	岡本　高宏　　教授
3910	陳　　飛	広州南方医科大学珠江医院 普通外科 主治医師	帝京大学 医療技術学部臨床検査学科	鈴木　幸一　　教授
3911	劉　恩涛	広東省人民医院 核医学科 主治医師	横浜市立大学大学院医学研究科 放射線医学	井上　登美夫 教授
3912	朱　舜明	陝西省人民医院 循環器科 副主任医師	湘南鎌倉総合病院心臓センター 循環器内科	齋藤　　滋　　総長・部長
3913	黄　　勇	江西中医薬大学附属医院 腎内科 医師	山梨大学大学院医学工学総合研究部 先端応用医学	姚　　建　　准教授
3914	趙　　瑩	嘉応学院医学院 薬学系 講師	名古屋市立大学大学院薬学研究科 薬物送達学	尾関　哲也　　教授
3915	田　　東	川北医学院附属医院 胸心外科 医師	京都大学大学院医学研究科 呼吸器外科学	伊達　洋至　　教授
3916	顧　世忠	中国医科大学附属第一医院 運動医学、関節外科 主治医師	京都大学大学院医学研究科 整形外科学	松田　秀一　　教授
3917	戴　映雪	成都市疾病予防控制中心 伝染病防治科 医師	京都大学大学院医学研究科 社会疫学	木原　正博　　教授
3918	劉　林林	天津市安定医院 心理門診 主治医師	京都大学大学院医学研究科 健康増進・行動学	古川　壽亮　　教授
3919	劉　金梁	浙江大学医学院附属第二医院 感染症疾病科 住院医師	京都大学大学院医学研究科 内科学	上嶋　健治　　特定教授
3920	金　銀実	吉林大学中日聯誼医院 神経内二科 主治医師	大阪大学医学部附属病院 神経内科学	望月　秀樹　　教授
3921	黎　顕莉	南方医科大学深圳医院 眼科 主治医師	大阪大学大学院医学系研究科 眼科学	西田　幸二　　教授
3922	葉　　盛	南京紅十字血液中心 機採科 主治医師	日本赤十字社 近畿ブロック血液センター	木村　貴文　　製剤部長
3923	焦　丹丹	河南科技大学第一附属医院 呼吸科 護師	兵庫県立大学地域ケア開発研究所	増野　園惠　　所長・教授
3924	徐　妍妍	中日友好医院 放射科 住院医師	琉球大学大学院医学研究科 放射線診断治療学講座	村山　貞之　　教授